

Inaugural Dissertation  
for  
obtaining the Doctoral Degree  
of the  
Combined Faculty of Mathematics, Engineering and Natural Sciences  
of the  
Ruprecht-Karls-University  
Heidelberg

Presented by

**M.Sc. Sarah Jane Neuberth**

Born in Speyer

Oral examination: 03.06.2022



SPDEF Regulates Fatty Acid Metabolism Driving Tumor  
Growth in Androgen Receptor-Positive Breast Cancer

Referees: Prof Dr. Andreas Trumpp  
Prof. Dr. Holger Sultmann



*'Nothing in life is to be feared, it is only to be understood.'*

*Marie Curie*



## Declaration

The work presented in this dissertation was performed from June 2017 until December 2021 at the German Cancer Research Center (Deutsches Krebsforschungszentrum, DKFZ, Heidelberg) and the Heidelberg Institute for Stem Cell Technology and Experimental Medicine (HI-STEM gGmbH, Heidelberg) under the supervision of Prof. Dr. Andreas Trumpp and Dr. Martin Sprick.

Declarations according to § 8 (3) c), d) and h) of the Doctoral Degree Regulations:

- c) I hereby declare that I have written the submitted dissertation myself and, in this process, have used no other sources or materials than those explicitly indicated.
- d) I hereby declare that I have not applied to be examined at any other institution, nor have I used the dissertation in this way or any other form at any other institution as an examination paper nor submitted it to any other faculty as dissertation.
- h) I hereby consent to the verification of the dissertation by means of electronic data processing programs against standing scientific standards.

---

Date, Place

---

Signature





## Summary

Despite advances in the treatment of breast cancer, it is still the second leading cause of cancer-related death in women worldwide. A large number of patients develop recurrence and die of advanced metastatic disease. More than 70% of metastatic breast cancers express androgen receptor (AR) representing a potential target for anti-hormone therapies. AR is suggested to directly interact with the lineage-specific transcription factor, SAM pointed domain-containing ETS transcription factor (SPDEF) in breast cancer however, the functional role of SPDEF and its interaction with AR remains to be elucidated. I found that AR expression highly correlates with SPDEF expression in breast cancer patients. To study its functional role in tumorigenesis and metastatic outgrowth, I utilized patient-derived xenograft (PDX) derived cell lines from liquid biopsies of metastatic breast cancer patients. Using genetically manipulated PDX cell models, I demonstrated that repression of SPDEF significantly reduced tumor growth of AR<sup>+</sup> breast cancer cells *in vivo*. Downregulation of SPDEF prevented metastasis formation in the brain whereas lung metastatic lesions were not affected by SPDEF silencing. Reduced tumor growth upon downregulation of SPDEF was also observed in estrogen receptor (ER)-positive breast cancer cells. Notably, I observed enhanced tumor growth in an AR negative breast cancer model suggesting a tumor suppressive function when AR is not present. Overexpression of SPDEF in AR<sup>-</sup> breast cancer cells significantly inhibited *in vivo* tumor growth. To investigate the underlying mechanism on the molecular level, I established transcriptional profiles by performing tumor tissue and cell line microarray analysis in SPDEF-overexpressing and knockdown models. Mechanistically, I found that SPDEF regulates key metabolic processes: (1) Pharmacological inhibition of AR or silencing of SPDEF restricted mitochondrial respiration activity resulting in decreased energy production. AR activation by testosterone treatment enhanced basal and maximal oxygen consumption rates, as did SPDEF overexpression. However, testosterone treatment did not restore decrease in mitochondrial respiration when SPDEF was downregulated. (2) Further, I found that SPDEF regulates genes encoding enzymes involved in glucose and fatty acid metabolism in AR<sup>+</sup> breast cancer cells. FBP1, the rate-limiting enzyme in gluconeogenesis was identified as a direct target gene of SPDEF. However, FBP1 deletion did not impair *in vivo* tumor growth. Enzymes involved in *de novo* fatty acid biosynthesis were downregulated in SPDEF knockdown SPDEF-deficient cells. The fatty acid transporter CD36 was upregulated upon downregulation of SPDEF as validated

by RT-qPCR and western blot analysis. Flow cytometry analysis revealed increased plasma-membrane localized CD36 expression in shSPDEF cells and vice versa, cell surface CD36 expression was decreased in SPDEF-overexpressing cells. I performed isotope tracing experiments using  $^{13}\text{C}$ -glucose,  $^{13}\text{C}$ -glutamine and  $^{13}\text{C}$ -acetate to functionally assess fatty acid metabolism upon deregulation of SPDEF. SPDEF knockdown cells showed decreased biosynthesis of specific fatty acids, however, they restored their cellular fatty acid pool by increased uptake of exogenous fatty acids. Abolishing CD36 expression in AR<sup>+</sup> breast cancer cells suggested that fatty acid uptake is critically required for cell growth of SPDEF knockdown cells. Pharmacological inhibition of CD36 induced a significant cytostatic effect in SPDEF knockdown cells. These data suggest that CD36 mediates exogenous fatty acid uptake as compensatory pathway when *de novo* fatty acid biosynthesis is decreased by SPDEF downregulation. In agreement, SPDEF knockdown cells did not have a significant growth disadvantage *in vitro* under saturated culture conditions. Usual cell culture media contain saturated levels of carbon sources and nutrients which do not reflect the physiological conditions found in the patient, making it difficult to study the metabolic profiles of cancer cells *in vitro*. However, when cells were cultured under physiological conditions resembling the natural cellular environment found in the patient, cells showed a significantly decreased growth rate when SPDEF was downregulated. These findings suggest that lipid and energy metabolism are transcriptionally regulated by SPDEF facilitating cell survival in nutrient-depleted environments and hence, tumor and metastatic outgrowth of AR<sup>+</sup> breast cancer cells. Since initial data suggested that pharmacological inhibition of AR mimics the effect of SPDEF downregulation, targeting AR and CD36 simultaneously may be a treatment strategy for AR<sup>+</sup> breast cancer patients.

## Zusammenfassung

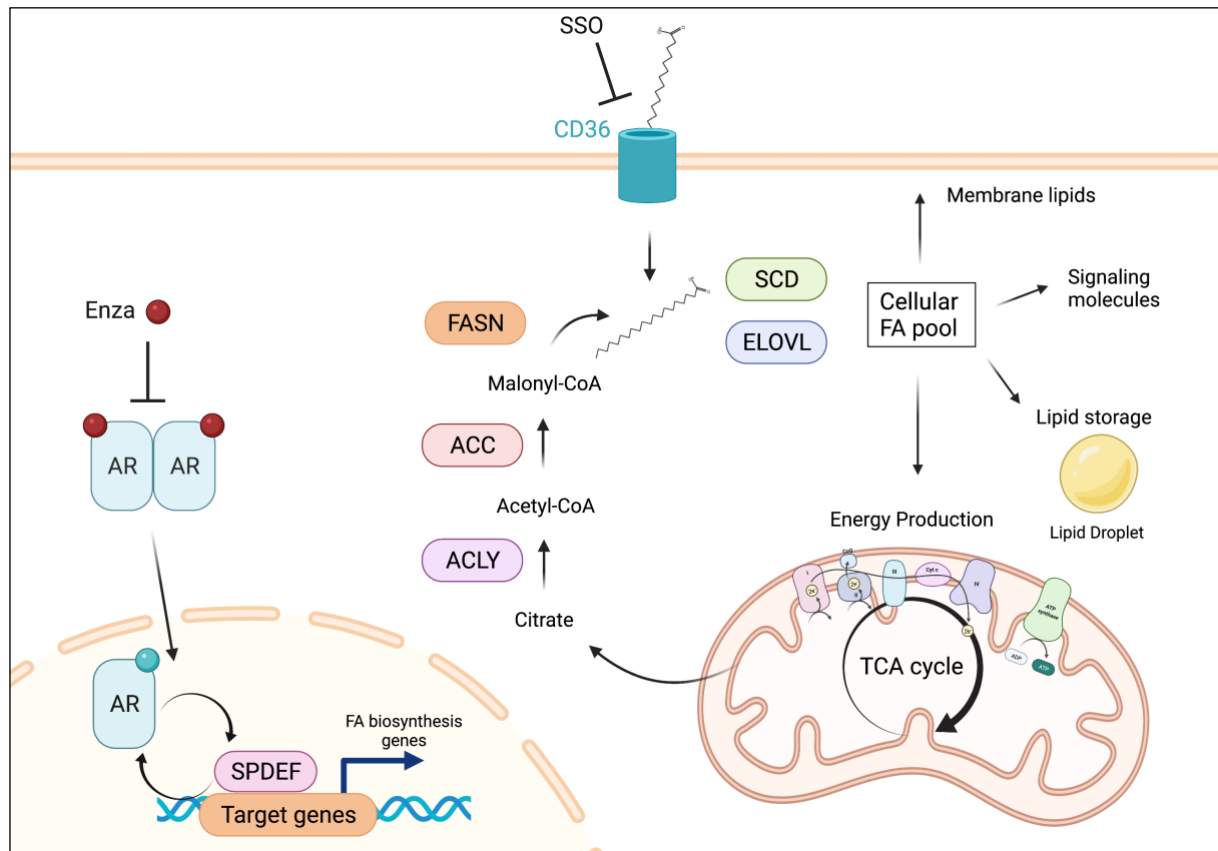
Trotz Fortschritten in der Behandlung von Brustkrebs, ist er immer noch die zweithäufigste krebsbedingte Todesursache bei Frauen weltweit. Eine große Zahl von Patientinnen entwickelt ein Rezidiv und stirbt an einer fortgeschrittenen metastasierten Erkrankung. Mehr als 70 % der metastasierenden Brusttumore exprimieren den Androgenrezeptor (AR), der ein potenzielles Ziel für Anti-Hormontherapien darstellt. Es wird vermutet, dass AR bei Brustkrebs direkt mit dem linienspezifischen Transkriptionsfaktor SPDEF (SAM pointed domain-containing ETS transcription factor) interagiert. Die funktionelle Rolle von SPDEF und seine Interaktion mit AR in Brustkrebs ist noch weitgehend unbekannt. Ich habe festgestellt, dass die AR-Expression bei Brustkrebspatientinnen stark mit der SPDEF-Expression korreliert. Um die funktionelle Rolle von SPDEF bei der Tumorentstehung und dem Wachstum von Metastasen zu untersuchen, habe ich aus Flüssigbiopsien von metastasierenden Brustkrebspatientinnen abgeleitete PDX-Zelllinien (patient-derived xenograft) verwendet. Mit Hilfe von genetisch manipulierten PDX-Zellmodellen konnte ich zeigen, dass die Unterdrückung von SPDEF das Tumorstadium von AR-positiven Brustkrebszellen *in vivo* deutlich reduziert. Die Herunterregulierung von SPDEF verhinderte die Bildung von Metastasen im Gehirn, während Lungenmetastasen durch das Ausschalten von SPDEF nicht beeinflusst wurden. Eine Verringerung des Tumorstadiums nach Herunterregulieren von SPDEF wurde auch bei Östrogenrezeptor (ER)-positiven Brustkrebszellen beobachtet. Bemerkenswerterweise habe ich in einem AR-negativen Brustkrebsmodell ein verstärktes Tumorstadium beobachtet, was auf eine tumorsuppressive Funktion bei fehlendem AR schließen lässt. Die Überexpression von SPDEF in AR-positiven Brustkrebszellen hemmte das Tumorstadium *in vivo* deutlich. Um den zugrundeliegenden Mechanismus auf molekularer Ebene zu untersuchen, erstellte ich Transkriptionsprofile durch die Durchführung von Microarray-Analysen von Tumorgewebe und Zelllinien in SPDEF-überexprimierenden und Knockdown-Modellen. Mechanistisch gesehen habe ich herausgefunden, dass SPDEF wichtige Stoffwechselprozesse reguliert: (1) Die pharmakologische Hemmung von AR oder das Herunterregulieren von SPDEF schränkte die mitochondriale Atmungsaktivität ein, was zu einer verminderten Energieproduktion führte. Die AR-Aktivierung durch Testosteron-Behandlung steigerte die basale und maximale Sauerstoffverbrauchsrate, ebenso wie die Überexpression von SPDEF. Die Testosteronbehandlung führte jedoch nicht zu einer Wiederherstellung des Rückgangs der mitochondrialen Atmung, wenn SPDEF herunterreguliert war. (2) Außerdem fand ich heraus,

dass SPDEF Gene reguliert, die für Enzyme kodieren, die am Glukose- und Fettsäurestoffwechsel in AR-positiven Brustkrebszellen beteiligt sind. FBP1 ist ein ratenlimitierendes Enzym in der Glukoneogenese und wurde als direktes Zielgen von SPDEF identifiziert. Das Ausschalten von FBP1 führte jedoch nicht zu einer Beeinträchtigung des Tumorwachstums *in vivo*. Enzyme, die an der Fettsäurebiosynthese beteiligt sind, wurden in SPDEF-Knockdown-Zellen und Knock-out-Zellen herunterreguliert. Der Fettsäuretransporter CD36 wurde durch die Herunterregulierung von SPDEF hochreguliert, was durch RT-qPCR und Western Blot-Analyse bestätigt wurde. Durchflusszytometrische Analysen ergaben eine erhöhte Expression von CD36 an der Plasmamembran in SPDEF-Knockdown-Zellen und umgekehrt eine verringerte Expression von CD36 an der Zelloberfläche in SPDEF-überexprimierenden Zellen. Um den Fettsäurestoffwechsel bei Deregulierung von SPDEF funktionell zu bewerten, führte ich Experimente durch bei welchen die Isotopenmarkierung von Glucose, Glutamin und Acetat in Fettsäuren gemessen wird. Zellen, bei denen SPDEF ausgeschaltet wurde, zeigten eine verringerte Biosynthese spezifischer Fettsäuren, stellten jedoch ihren zellulären Fettsäurepool durch erhöhte Aufnahme exogener Fettsäuren wieder her. Die Unterdrückung der CD36-Expression in AR-positiven Brustkrebszellen deutet darauf hin, dass die Aufnahme von Fettsäuren für das Zellwachstum von SPDEF-Knockdown-Zellen von entscheidender Bedeutung ist. Die pharmakologische Hemmung von CD36 führte zu einer signifikanten zytostatischen Wirkung in SPDEF-Knockdown-Zellen. Diese Daten deuten darauf hin, dass CD36 die Aufnahme exogener Fettsäuren als kompensatorischen Weg vermittelt, wenn die Fettsäurebiosynthese durch die Herunterregulierung von SPDEF verringert ist. In Übereinstimmung damit wiesen SPDEF-Knockdown-Zellen unter gesättigten Kulturbedingungen *in vitro* keinen signifikanten Wachstumsnachteil auf. Übliche Zellkulturmedien enthalten gesättigte Mengen an Kohlenstoffquellen und Nährstoffen, die nicht die physiologischen Bedingungen im Patienten widerspiegeln, was es schwierig macht, die Stoffwechselprofile von Krebszellen *in vitro* zu untersuchen. Wurden die Zellen jedoch unter physiologischen Bedingungen kultiviert, die dem natürlichen zellulären Umfeld des Patienten ähneln, zeigten die Zellen eine deutlich verringerte Wachstumsrate, wenn SPDEF herunterreguliert wurde. Diese Ergebnisse deuten darauf hin, dass der Lipid- und Energiestoffwechsel durch SPDEF transkriptionell reguliert wird, was das Überleben der Zellen in nährstoffarmen Umgebungen und damit das Tumor- und Metastasierungswachstum von AR-positiven Brustkrebszellen erleichtert. Da erste Daten darauf hindeuten, dass die pharmakologische Hemmung von AR die Wirkung der Herunterregulierung von SPDEF

nachahmt, könnte die gleichzeitige Inhibierung von AR und CD36 eine Behandlungsstrategie für AR-positive Brustkrebspatientinnen darstellen.



## Graphical abstract



## Highlights

- SPDEF inhibits *in vivo* tumor growth of AR<sup>+</sup> breast cancer cells
- SPDEF regulates expression of *de novo* fatty acid biosynthesis genes in AR<sup>+</sup> breast cancer cells
- Downregulation of SPDEF results in upregulation of cell surface CD36 expression and creates vulnerability on CD36
- Targeting SPDEF and CD36 simultaneously affects *in vitro* cancer cell growth
- SPDEF controls mitochondrial respiration activity
- Pharmacological inhibition of AR mimics repression of mitochondrial respiration activity by SPDEF downregulation





## Table of contents

<b>Declaration</b> .....	<b>I</b>
<b>Summary</b> .....	<b>II</b>
<b>Zusammenfassung</b> .....	<b>IV</b>
<b>Graphical abstract</b> .....	<b>VIII</b>
<b>1 Introduction</b> .....	<b>1</b>
<b>1.1 Epidemiology and molecular subtypes of breast cancer</b> .....	<b>1</b>
<b>1.2 Hormone receptor signaling in breast cancer</b> .....	<b>5</b>
1.2.1 Estrogen receptor signaling and anti-estrogen therapies in breast cancer .....	5
1.2.2 Androgen receptor expression and anti-androgen therapies in breast cancer .....	7
1.2.3 SPDEF in breast cancer .....	11
<b>1.3 Cancer cell metabolism</b> .....	<b>14</b>
1.3.1 Glucose metabolism in cancer cells.....	14
1.3.2 Fatty acid metabolism in cancer cells.....	17
<b>2 Aim of this study</b> .....	<b>21</b>
<b>3 Results</b> .....	<b>22</b>
<b>3.1 SPDEF and AR expression in breast cancer</b> .....	<b>22</b>
3.1.1 <i>SPDEF</i> and <i>AR</i> are heterogeneously expressed in distinct breast cancer subtypes.....	22
3.1.2 <i>SPDEF</i> and <i>AR</i> predict survival probability in breast cancer.....	24
3.1.3 <i>SPDEF</i> and <i>AR</i> expression correlate in patient-derived xenograft cell models.....	25
<b>3.2 Generation of SPDEF overexpression and knockdown cell models</b> .....	<b>28</b>
<b>3.3 SPDEF impacts tumor growth <i>in vivo</i></b> .....	<b>31</b>
3.3.1 <i>SPDEF</i> downregulation inhibits <i>in vivo</i> tumor growth in AR <sup>+</sup> breast cancer models.....	31
3.3.2 <i>SPDEF</i> knock-out inhibits <i>in vivo</i> tumor growth in AR <sup>+</sup> breast cancer model .....	34
3.3.3 <i>SPDEF</i> downregulation inhibits <i>in vivo</i> brain metastasis formation in AR <sup>+</sup> breast cancer model.....	35
3.3.4 <i>SPDEF</i> downregulation enhances <i>in vivo</i> tumor growth in AR <sup>-</sup> triple negative breast cancer model .....	37
<b>3.4 Transcriptional profiling of SPDEF overexpression and knockdown breast cancer cell models</b> .....	<b>38</b>
3.4.1 Gene expression-based analysis of AR <sup>+</sup> ER <sup>-</sup> BPE8 <i>SPDEF</i> overexpression and knockdown cell models .....	39
3.4.2 Gene expression-based analysis of AR <sup>+</sup> ER <sup>+</sup> CTC223 <i>SPDEF</i> overexpression and knockdown cell models .....	43

3.4.3	Gene expression-based analysis of AR <sup>-</sup> ER <sup>+</sup> CTC288 SPDEF overexpression and knockdown cell models .....	46
3.4.4	Gene-expression based analysis of luminal (like) – HR <sup>+</sup> SPDEF overexpression and knockdown cell models .....	47
3.4.5	Gene expression-based analysis of AR <sup>-</sup> TNBC BPE7 SPDEF overexpression and knockdown cell models .....	51
<b>3.5</b>	<b>Transcriptional profiling of AR<sup>+</sup> and AR<sup>-</sup> PDX tumors upon SPDEF downregulation ..</b> .....	<b>54</b>
<b>3.6</b>	<b>SPDEF and AR signaling .....</b>	<b>57</b>
3.6.1	SPDEF regulates <i>AR</i> and its target genes in AR <sup>+</sup> breast cancer cells.....	58
3.6.2	Pharmacological activation of AR regulates <i>AR</i> and <i>SPDEF</i> gene expression in AR <sup>+</sup> breast cancer cells .....	60
3.6.3	AR knock-out impairs SPDEF expression .....	61
3.6.4	AR knock-out does not impair <i>in vivo</i> tumor growth.....	63
<b>3.7</b>	<b>SPDEF regulates <i>FBP1</i> expression in AR<sup>+</sup> breast cancer cells.....</b>	<b>64</b>
3.7.1	SPDEF regulates gene expression of the rate-limiting enzymes in gluconeogenesis <i>FBP1</i> and <i>PCK2</i> in AR <sup>+</sup> breast cancer cells .....	64
3.7.2	Glycolysis genes are upregulated in AR <sup>-</sup> breast tumors upon SPDEF downregulation .....	66
3.7.3	SPDEF and <i>FBP1</i> are co-expressed in AR <sup>+</sup> breast cancer models.....	67
3.7.4	<i>FBP1</i> is a direct target gene of SPDEF .....	68
3.7.5	<i>FBP1</i> knock-out impairs glycolytic genes' expression .....	69
3.7.6	<i>FBP1</i> knock-out does not impair <i>in vivo</i> tumor growth .....	70
3.7.7	<i>SPDEF</i> and <i>FBP1</i> are co-expressed in breast cancer patients.....	71
<b>3.8</b>	<b>SPDEF regulates fatty acid metabolism in AR<sup>+</sup> breast cancer cells .....</b>	<b>73</b>
3.8.1	SPDEF regulates gene expression of the rate-limiting enzymes in <i>de novo</i> fatty acid biosynthesis in AR <sup>+</sup> breast cancer cells .....	73
3.8.2	Fatty acid synthesis genes are downregulated in AR <sup>+</sup> breast tumors upon SPDEF downregulation . .....	75
3.8.3	SPDEF regulates fatty acid biosynthesis enzymes and CD36 protein expression .....	76
3.8.4	SPDEF knockdown cells decrease <i>de novo</i> fatty acid synthesis but increase exogenous fatty acid uptake of specific fatty acids .....	78
3.8.5	Abolishing CD36 expression in SPDEF knockdown cells impairs <i>in vitro</i> cell growth.....	82
3.8.6	SPDEF knockdown cells have a growth disadvantage in lipid-depleted environment .....	85
3.8.7	SPDEF and <i>FASN</i> are co-expressed in PDX-derived cell models and breast cancer patients .....	87
<b>3.9</b>	<b>SPDEF regulates mitochondrial metabolism .....</b>	<b>90</b>
3.9.1	SPDEF regulates mitochondrial respiration activity in AR <sup>+</sup> breast cancer cell models.....	90
3.9.2	Pharmacological activation or inhibition of AR impairs mitochondrial respiration activity .....	93
3.9.3	SPDEF regulates mitochondrial proteins .....	95

---

<b>4</b>	<b>Discussion</b> .....	<b>98</b>
4.1	SPDEF regulates AR signaling in breast cancer.....	98
4.2	SPDEF regulates FBP1 and glucose metabolism in AR <sup>+</sup> breast cancer .....	101
4.3	SPDEF regulates fatty acid metabolism in AR <sup>+</sup> breast cancer.....	103
4.4	SPDEF regulates mitochondrial metabolism in AR <sup>+</sup> breast cancer.....	109
<b>5</b>	<b>Material and Methods</b> .....	<b>113</b>
5.1	Cell lines and cell culture .....	113
5.2	Cell growth assay .....	116
5.3	Immunohistochemistry.....	117
5.4	Western blot analysis.....	117
5.5	Quantitative real-time PCR analysis .....	120
5.6	Transcriptional profiling by microarray analysis .....	122
5.7	In vitro drug treatment assays.....	123
5.8	siRNA transfection of HEK293T cells .....	124
5.9	SPDEF overexpression and knockdown vector constructs.....	125
5.10	Virus production.....	127
5.11	Transduction of cell lines .....	128
5.12	Flow cytometry.....	129
5.13	Microscope image acquisition.....	129
5.14	CRISPR/Cas9-mediated knock-out .....	130
5.15	Sanger sequencing .....	131
5.16	Animal experiments.....	131
5.17	Seahorse assays .....	133
5.18	Isotope tracing experiments.....	135
5.19	Patient data analysis .....	136
5.20	Graphics software.....	136
<b>6</b>	<b>Supplements</b> .....	<b>137</b>
<b>7</b>	<b>References</b> .....	<b>161</b>

---

<b>8</b>	<b>List of Abbreviations.....</b>	<b>183</b>
<b>9</b>	<b>List of Figures .....</b>	<b>191</b>
<b>10</b>	<b>List of Tables.....</b>	<b>195</b>
<b>11</b>	<b>List of Supplement.....</b>	<b>196</b>
<b>12</b>	<b>Contributions .....</b>	<b>198</b>
<b>13</b>	<b>Acknowledgements.....</b>	<b>200</b>

# 1 Introduction

## 1.1 Epidemiology and molecular subtypes of breast cancer

Cancer is a major public health issue worldwide and the second leading cause of death after heart diseases<sup>1</sup>. In women, breast cancer accounts for 30% of female cancers and displays a mortality rate of 15%<sup>1,2</sup> (Figure 2A). 287,850 new cases of female breast cancer are estimated in the United States in 2022<sup>3</sup>. The global incidence of breast cancer has been increasing by 3.1% annually<sup>4,5</sup>. All breast cancers arise from cells in the terminal duct lobular units of the collecting duct<sup>4</sup> (Figure 1). The most common breast cancer type by about 70-75% is invasive carcinoma of no special type (previously called invasive ductal carcinoma) arising from epithelial cells in the mammary ducts<sup>6,7</sup>. 10-14% of breast cancers are lobular carcinomas and remaining other carcinomas are classified as special type. Ductal carcinoma in situ (DCIS) is non-invasive and locally restricted to the ducts. However, often it develops into invasive or even metastatic breast cancer.

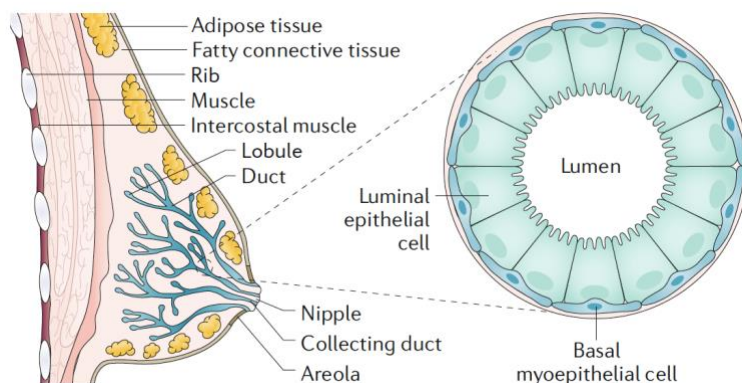


**Figure 1: Breast cancer.** The majority of breast cancers arise from epithelial cells in the mammary ducts referred to as invasive carcinoma of no special type. Lobular carcinomas arise from basal myoepithelial cells. Figure taken from Harbeck *et al.*, 2019.<sup>4</sup>

Once a patient has been diagnosed with a malignant tumor, breast cancer stage is determined based on size and location of the primary tumor, and spread to nearby lymph nodes or secondary sites. Metastatic breast cancer (mBC) is classified as stage IV and the most advanced stage of breast cancer. It is characterized by spreading into secondary tissues beyond the breast and nearby lymph nodes<sup>2,4,6,7</sup>. Metastatic breast cancer cells mainly spread to and invade the lungs, liver, brain and bones, however different molecular subtypes show tropism for distinct metastatic sites<sup>4,8</sup>. The majority of breast cancers are diagnosed at early stage and show a 5-year relative survival rate of 90.3%<sup>1,3</sup>. However, about 30% of patients eventually develop relapse and die of advanced metastatic disease. Tumor features that result in metastases in breast

cancer are largely unknown<sup>4</sup>. If the cancer has spread to distant organs, the 5-year survival rate decreases to 29% only<sup>1,3</sup>.

Breast cancer is a highly heterogeneous disease and clinically divided into four molecular subtypes determined by hormone receptor (HR) expression including estrogen receptor (ER), progesterone receptor (PR), and expression of the tyrosine kinase human epidermal growth factor receptor 2 (HER2)<sup>9</sup> (Figure 2C, D). International standardized diagnostic evaluation of these markers is essential for breast cancer classification and therapy decision-making<sup>10,11</sup>. At diagnosis, marker expression is routinely tested by immunohistochemistry on pre-surgical biopsy samples. ER and PR nuclear staining in >1% of tumor cells is considered as HR-positive (HR<sup>+</sup>)<sup>11</sup>. Luminal ER<sup>+</sup> and PR<sup>+</sup> tumors make up the majority of breast cancers (78%) and are further subdivided into Luminal A and B based on histochemical staining for the proliferation marker protein human Ki-67 (hKi67)<sup>3,9</sup> (Figure 2C, D). However, hKi67 staining has not been standardized or recommended yet<sup>12</sup>. A cut-off value of 20% has been widely used whereas >30% of stained nuclei is considered as highly proliferative and ascribed as luminal B tumor (Figure 2D). Luminal B tumors are either HER2<sup>-</sup> or HER2<sup>+</sup>. 4% of breast cancers are HR<sup>-</sup>/HER2<sup>+</sup> characterized by overexpression or amplification of HER2 receptor in > 10% of invasive tumor cells<sup>3,10</sup> (Figure 2C). Triple negative breast cancers (TNBC) are negative for ER, PR and HER2, and account for 10% of all breast cancers. TNBC presents the poorest prognosis of all subtypes and 5-year survival rate decreases to 12.2% for distant disease<sup>1,3</sup> (Figure 2B).



However, female breast cancer mortality showed its peak in 1989 and since then has decreased by 42% due to increased awareness, mammography screening allowing earlier detection and improvements in therapies<sup>3</sup>. Treatment strategies differ according to molecular subtype and tumor stage.

Early breast cancer is locally restricted to the breast or has only spread to the axillary lymph nodes. It is considered to be curable in 70-80% of patients<sup>4</sup>. Often locoregional therapy including surgery of primary tumor and radiation therapy is sufficient. Systemic treatment can be given in the neoadjuvant setting for patients with large tumors to reduce tumor burden or pathological complete response (pCR) prognostic value, especially of HER2<sup>+</sup> or TNBC subtypes<sup>13</sup> (Figure 2D). Adjuvant therapy is applied in most cases, in particular when increased risk of recurrence is indicated<sup>2,4</sup>. Luminal HR<sup>+</sup> breast cancers are treated with endocrine therapy targeting ER activity using tamoxifen or aromatase inhibitors in first line. In addition, chemotherapy with anthracycline followed by taxanes is given to luminal patients with high proliferation rate or high grade tumors. In HER2<sup>+</sup> breast cancer, dual blockade of HER2 using

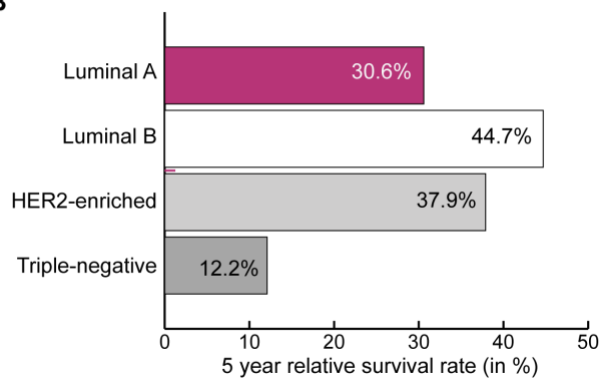
anti-HER2 antibodies trastuzumab plus pertuzumab has become (neoadjuvant) standard of care in combination with chemotherapy<sup>2,4</sup>. In contrast, no targeted therapies exist yet for TNBC. Hence, standard of care treatment includes chemotherapy only. Advanced breast cancer with distant organ metastases remains to be incurable with a median survival time of 2-3 years<sup>14</sup>. Thus, therapeutic treatment of mBC aims to alleviate symptoms, improve quality of life and prolong survival time. At this stage, TNBC patients undergo complete testing for germline *BRCA* mutation and PD-L1 expression<sup>2</sup>. The immune checkpoint inhibitor, atezolizumab, plus nab-paclitaxel improved progression-free survival by about 2.5 months in TNBC tumors expressing more than 1% PD-L1<sup>15,16</sup>. However, there is still controversy about using checkpoint inhibitors in breast cancer because checkpoint inhibitor monotherapy is not promising<sup>17,18</sup>. Patients harboring *BRAC1* or *BRAC2* mutation are treated with PARP inhibitor, often in combination with paclitaxel plus carboplatin<sup>19-21</sup>. Furthermore, future therapeutic approaches in breast cancer aim to individualize therapy for patients and personalized medicine.

A

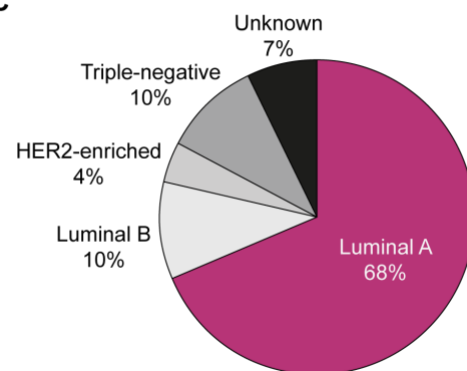
## Estimated New Cases

			Males	Females			
Prostate	268,490	27%			Breast	287,850	31%
Lung & bronchus	117,910	12%			Lung & bronchus	118,830	13%
Colon & rectum	80,690	8%			Colon & rectum	70,340	8%
Urinary bladder	61,700	6%			Uterine corpus	65,950	7%
Melanoma of the skin	57,180	6%			Melanoma of the skin	42,600	5%
Kidney & renal pelvis	50,290	5%			Non-Hodgkin lymphoma	36,350	4%
Non-Hodgkin lymphoma	44,120	4%			Thyroid	31,940	3%
Oral cavity & pharynx	38,700	4%			Pancreas	29,240	3%
Leukemia	35,810	4%			Kidney & renal pelvis	28,710	3%
Pancreas	32,970	3%			Leukemia	24,840	3%
<b>All Sites</b>	<b>983,160</b>	<b>100%</b>			<b>All Sites</b>	<b>934,870</b>	<b>100%</b>

B



C



D

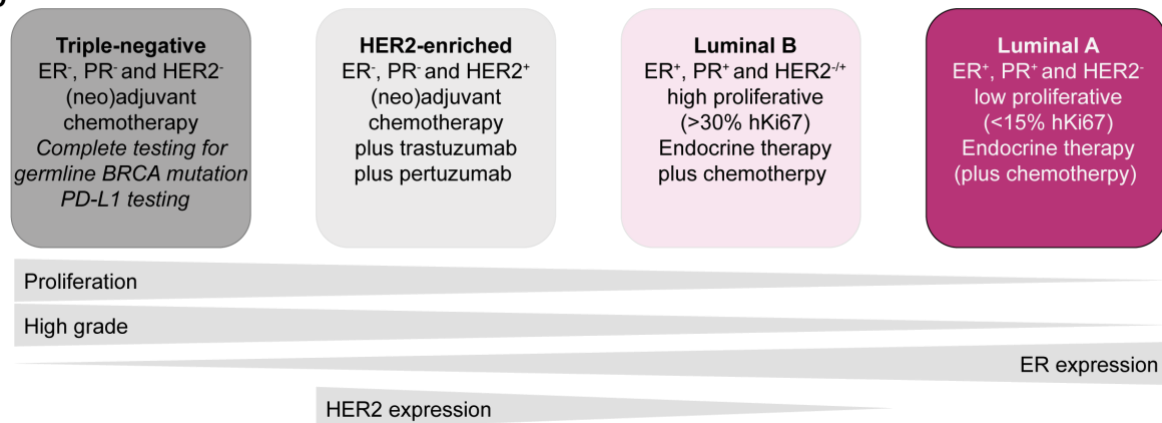


**Figure 2: Breast cancer subtypes and statistics.** (A) Top ten cancer types for the estimated new cases by sex in the United States in 2022 according to Siegel *et al.*, 2022. Breast cancer is the most frequent malignancy in women. Figure taken from Siegel *et al.*, 2022. (B) 5 year relative survival rate (in %) of female breast cancer subtypes according to Surveillance, Epidemiology, and End Results (SEER) program<sup>3</sup>. (C) Percent of female breast cancer cases by molecular subtypes according to SEER program<sup>3</sup>. (D) Surrogate intrinsic subtypes based on hormone receptor, HER2 expression, proliferation, and grade. ER, estrogen receptor; PR, progesterone receptor; HER2, human epidermal growth factor receptor 2; hKi67, proliferation marker human Ki67.



## 1.2 Hormone receptor signaling in breast cancer

### 1.2.1 Estrogen receptor signaling and anti-estrogen therapies in breast cancer

Estrogen receptor belongs to the superfamily of nuclear hormone receptors (NRs) which share common structures and unique features of being able to directly bind to DNA to function as transcription factors<sup>22-24</sup>. Within this superfamily, subfamily 3 comprises steroid hormone receptors including ER, PR, and androgen receptor (AR) among others<sup>24,25</sup>. They consist of six domains, A-F (Figure 3): The N-terminal domain (A-domain) contains the ligand-independent transactivation domain ‘Activation Function 1’ (AF1) which in combination with AF2 (F-domain) facilitates transcriptional activation of the receptor<sup>24,26</sup>. In addition, co-regulatory proteins interact with the N-terminal region of NR. AF2, located at the C-terminus, confers ligand-dependent transcriptional activation of NRs. The most highly conserved region is the DNA-binding domain (DBD) (C-domain) which facilitates binding of the NR to response elements (RE) on the DNA. These REs are located in the promoter region of NR-target genes, and at intronic and enhancer sites. Further, the DBD is also involved in the homodimerization of steroid hormone receptors. The C-domain is followed by the hinge region (domain D) which contains the nuclear localization signal (NLS). Domain E/F harbors the highly conserved ligand-binding domain (LBD) and dimerization site.



**Figure 3: Structure and domains of nuclear hormone receptors.** Nuclear hormone receptors (NRs) share a common structure and domains, A-F. The activation function 1 (AF-1) domain is located the N-terminal and contains the ligand-independent transactivation domain. Co-factors interact with the A/B domains. The DNA-binding domain (DBD) is localized within the C-domain that binds NR response elements on the DNA. The hinge region (HR) is located within the D-domain and contains the nuclear localization signal. This region is followed by the ligand-binding domain (LBD) within the E-domain. The F-domain harbors the AF-2 and promotes ligand-dependent NR activation.

The most potent endogenous ligand for ER is the hormone, 17 $\beta$ -estradiol (E2) which is highly selective for this receptor. Upon estrogen binding, the ER undergoes conformational changes into a homodimerized transcriptional activator<sup>27</sup>. The ER homodimer binds to estrogen-response elements (ERE) on the DNA and builds a transcriptional complex with co-regulatory

proteins. Those can be either activating (co-activators) or repressing (co-repressors) and thereby directly regulate ER target gene expression<sup>28</sup>. Many ER target genes have been identified being involved in cell proliferation and survival<sup>29,30</sup>. In agreement, estrogen is known to enhance proliferation of breast cancer cells<sup>31,32</sup>. However, in the past, estradiol was found to have inhibitory effects in post-menopausal advanced breast cancer patients at very high concentrations<sup>33,34</sup>. In contrast, selective ER modulators (SERMs) such as tamoxifen function as ER antagonists and have been used as endocrine therapy since the 1970s in the clinical management of breast cancer<sup>35,36</sup>. Tamoxifen is oxidized into its active metabolites 4-hydroxytamoxifen and endoxifen by cytochrome P450 (CYP) enzymes, not least involved in hormone biosynthesis and breakdown<sup>37</sup>. Tamoxifen competes with estradiol for the ligand-binding site of ER (Figure 4). Antagonistic conformational changes and recruitment of co-repressors form a silenced ER transcriptional complex blocking EREs on the DNA<sup>38-41</sup>. Importantly, differential expression of co-regulators is highly dependent on tissue types and impacts ER transcriptional control and drug efficiency<sup>42,43</sup>. Tamoxifen has remained a standard of care treatment for ER<sup>+</sup> breast cancers. However, several intrinsic or acquired resistance mechanisms allow cancer cells to escape tamoxifen treatment and remain to rely on active ligand-independent ER signaling for cell growth. In contrast to SERMs, selective estrogen receptor degraders (SERDs) such as fulvestrant bind to ER resulting in its destabilization and degradation<sup>44-47</sup> (Figure 4). Fulvestrant prevents ER homodimerization and thereby represses ER activation. Further, fulvestrant accelerates ER turnover rate through its degradation by the ubiquitin-proteasome pathway. Another class of inhibitors of the ER pathways applied in the clinical management of breast cancer are aromatase inhibitors (AIs). Aromatase (CYP19A1) is a key enzyme in the biosynthesis of estrogen. It is a member of the cytochrome P450 superfamily and catalyzes the conversion of androstenedione to estrone, and testosterone to estradiol. AIs inhibit endogenous estrogen biosynthesis resulting in decreased estradiol levels and ER activation<sup>26,48</sup>. In post-menopausal women, AIs are the preferred given endocrine therapy for patients with advanced ER<sup>+</sup> breast cancers – often in combination with CDK4/6 inhibitors<sup>2,49,50</sup>. In pre-menopausal women with advanced ER<sup>+</sup> disease, ovarian ablation or suppression is recommended combined with tamoxifen treatment<sup>2,51</sup>. However, endocrine therapy resistance is near-universal and attributed to several resistance mechanism including ESR1 mutations<sup>52</sup>. Of high interest, recent studies suggest that high AR expression correlates with endocrine therapy resistance. In tamoxifen-resistant MCF-7 cells, downregulation of AR, but not pharmacological inhibition of AR upon antiandrogen treatment, restored sensitivity to

antiestrogen treatment<sup>53</sup>. These results suggest AR activation as a resistance mechanism to endocrine therapy in ER<sup>+</sup> breast cancers.

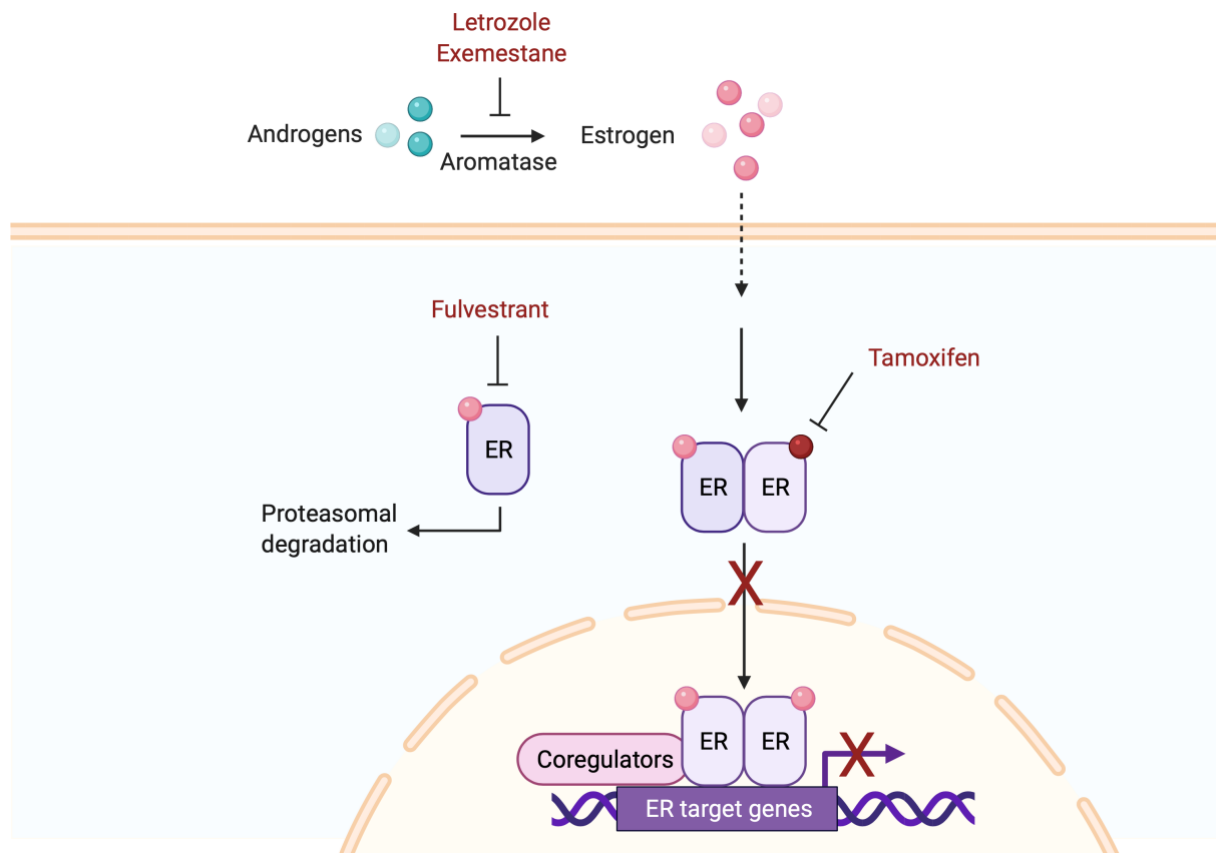


**Figure 4: Activation and pharmacological inhibition of estrogen receptor in breast cancer.** Scheme illustrates agonist activation of estrogen receptor (ER) by estrogens, and pharmacological inhibition upon treatment with anti-estrogen compounds (red). Androgens are converted to estrogens by the enzyme aromatase. Letrozole and exemestane are aromatase inhibitors targeting the conversion from androgen to estrogen. Estrogen binds to ER inducing its homodimerization and translocation into the nucleus. Activated ER binds to estrogen response elements (EREs) on the DNA at the promoter regions of ER target genes. Subsequently, ER target genes are transcribed upon co-activator recruitment to ER. Tamoxifen is an anti-estrogen compound that directly binds to the ligand binding domain (LBD) of ER. Blocking the LBD for estrogen binding prevents the activation of ER and transcription of ER target genes. Fulvestrant is an ER degrader preventing its homodimerization and promoting the proteasomal degradation of ER.

### 1.2.2 Androgen receptor expression and anti-androgen therapies in breast cancer

The majority of breast cancers express androgen receptor (AR). Up to 90% of primary breast tumors are AR<sup>+</sup> and 75% of metastases exhibit AR expression<sup>54–57</sup>. Furthermore, it has been shown that AR expression is conserved during the metastatic process<sup>58</sup>. 90% of ER<sup>+</sup> tumors and 31.8% of ER<sup>-</sup> tumors express AR as assessed within a meta-analysis of 19 studies including a total number of 7693 patients<sup>59</sup>.

AR belongs to the type I NRs along with ER as mentioned earlier (Chapter 1.2)<sup>24,60</sup>. Its inactive form is located in the cytoplasm bound to heat-shock proteins (HSPs) (Figure 5). Upon androgen binding to its LBD, AR is activated and forms homodimers similar to other steroid hormone receptors (1.2). Testosterone can be converted to 5 $\alpha$ -dihydrotestosterone (DHT) by the enzyme 5 $\alpha$ -reductase, which is the most potent natural androgen binding to and activating AR<sup>61,62</sup>. Subsequently, AR is translocated into the nucleus where it binds to androgen-response elements (AREs) on the DNA and regulates transcription of AR target genes<sup>24</sup>. In addition, AR has been demonstrated to activate signal transduction by non-genomic signaling. In contrast to its transcriptional function, non-genomic actions of AR might be much faster and observed within minutes after androgen exposure. Upon androgen activation, AR associates with the non-receptor tyrosine kinase Src in the cytosol, resulting in enhanced prostate cancer cell proliferation by activating the MAPK/ERK cascade<sup>63-65</sup>. Among others, AR activates PI3K/AKT signaling pathway by non-genomic action. Ligand-activated AR directly interacts with PI3K in the cytoplasm. Subsequently, p110 catalytic subunit is activated and phosphatidylinositol-3,4,5-triphosphate (PIP<sub>3</sub>) lipids are generated in order to induce activation of AKT kinase<sup>66,67</sup>. The latter is known to regulate transcription factors, inhibit apoptosis and promote cell survival<sup>68,69</sup>. Moreover, PI3K/AKT and MAPK/ERK signaling pathways are able to constitutively transactivate AR signaling - in the absence of androgens<sup>69-72</sup>.

Given that AR expression is high in ER<sup>+</sup> tumors relative to ER<sup>-</sup> breast cancers suggests that AR and ER cooperate with each other in breast cancer. Functionally, AR and ER share many similarities in their mechanism of action and signaling pathways<sup>66</sup>. Further, they recognize similar DNA sequences (ER binds to 5'AGGTCA-3' and AR binds to 5'AGAACA-3' sequences) and recruit identical co-regulatory proteins for their activation<sup>24,73</sup>. Previous studies have shown that AR competes with ER for shared binding sites and that AR activation represses ER transcriptional activity<sup>73-75</sup>. In addition, these studies show that AR- and ER-binding sites significantly overlapped suggesting that AR regulates a subset of ER target genes in ER<sup>+</sup> breast cancer. Besides, AR was found to regulate gene expression of targets exclusive to AR in ER<sup>+</sup> breast cancer cells upon androgen-activation<sup>75-77</sup>. Importantly, most of the ER<sup>+</sup> tumors are found in post-menopausal patients who have very low levels of 17 $\beta$ -estradiol but high androgen levels<sup>75,77</sup>. Further, testosterone levels in patients are thought to increase upon AI treatment<sup>78</sup>.

The prognostic role of AR has been extensively studied in ER<sup>+</sup> breast cancer. Patients with luminal tumors displaying an AR:ER ratio >2 showed decreased disease-free survival and more aggressive biological features in comparison to patients with lower AR:ER ratios<sup>79,80</sup>. Additional studies found AR to be associated with breast cancer progression and endocrine

therapy resistance in ER<sup>+</sup> tumors<sup>81</sup>. In contrast, several others have reported that AR expression would be associated with better outcome in luminal breast cancer patients<sup>53,58,82</sup>. However, defining positive expression of AR seems to be highly variable with cut-off levels ranging from 1-75%<sup>83-86</sup>. A recent study has stated that >78% of tumor cells are required to express AR protein in order to accurately assess its prognostic value in ER<sup>+</sup> tumors<sup>59,87</sup>. Further, luminal breast cancer patients with >78% AR expression defined as AR<sup>+</sup> had better prognosis. Taken together, the prognostic role of AR in luminal ER<sup>+</sup> tumors remains unclear.

These data suggest that AR functions differ in the presence or absence of ER. In comparison to ER<sup>+</sup> tumors, AR is less expressed in TNBC tumors. However, AR is found to be expressed in up to one third of TNBC samples. This is of special interest since no targeted therapies exist yet for TNBC. Transcriptional profiling of TNBC patient samples by tissue microarray analysis identified a subset of ER<sup>-</sup> tumors expressing a hormonally regulated gene signature<sup>88</sup>. Differential gene expression analysis revealed *AR*, *CYP5*, *XBPI*, *FOXA1*, *SPDEF* and AR target genes, *APOD* and *PIP*, to be among the top 50 significantly overexpressed genes in the luminal-like ER<sup>-</sup> tumors. Additional studies have shown that a subset of TNBCs exist which express AR making them more luminal-like<sup>89</sup>. This group of breast tumors has been referred to as ‘molecular apocrine’ breast cancers and featured by increased androgen signaling<sup>90</sup>. In contrast, quadruple negative breast cancer (QNBC) are negative for steroid hormone receptor expression of ER, PR, HER2 and AR. Luminal-associated genes including *XBPI*, *FOXA1* and *SPDEF* were found to be enriched in AR<sup>+</sup> TNBC samples, which clustered with ER<sup>+</sup> tumors<sup>90,91</sup>. Two independent studies classified the MDA-MB-453 TNBC cell line as molecular apocrine cell model characterized by high expression of AR mRNA and protein, AR co-regulatory proteins and luminal markers<sup>90</sup>. AR expression constitutes a clinically relevant target which is not least studied using MDA-MB-453 cells. However, AR<sup>+</sup> breast cancer cells showed both, proliferative and inhibitory effects when treated with androgens *in vitro*<sup>92</sup>. Yet, a subset of the TNBC cohort might benefit from hormonal therapies targeting AR.

AR is known to drive the majority of prostate carcinoma (PCa) in men<sup>89,91</sup>. Thus, the role of AR activation and expression has been well characterized in this context. AR has been demonstrated to be involved in cell proliferation, survival and metastases. Several anti-AR therapy strategies have been applied in the clinical management of PCa. Androgen deprivation therapy (ADT) and castration are first-line treatment options for men with metastatic prostate cancer (mPC)<sup>93-95</sup>. Both treatments attempt to decrease plasma testosterone levels in men in order to reduce tumor growth. In addition, 5 $\alpha$ -DHT production from testosterone in the prostate can be inhibited by targeting the 5 $\alpha$ -reductase enzyme<sup>96,97</sup>. While androgen levels are known

to increase in post-menopausal women, they are still low in comparison to testosterone levels found in men. Thus, above mentioned pharmacological agents are rather effective in male than female patients. Anti-androgens are a class of non-steroidal competitive inhibitors of the AR such as bicalutamide<sup>98–100</sup>. It blocks androgen binding and thus impairs nuclear AR signaling. In a phase II trial in mBC patients, bicalutamide showed a clinical benefit rate (CBR) of 19% in patients with AR<sup>+</sup> ER<sup>-</sup> tumors<sup>101</sup>. Additional clinical trials are assessing the combination of bicalutamide and AIs in the treatment of AR<sup>+</sup> ER<sup>+</sup> BC patients<sup>102</sup>. Enzalutamide is a second generation anti-androgen which has been used in the clinical management of prostate cancer as well<sup>103</sup>. It blocks the binding site of testosterone and thereby inhibits the homodimerization of the receptor (Figure 5). Subsequently, AR translocation into the nucleus is inhibited resulting in repression of AR target genes' transcription. Enzalutamide treatment has been found to be synergistic with anti-estrogen treatment *in vitro* in MCF7 cells<sup>104–107</sup>. In addition, enzalutamide and tamoxifen co-treatment significantly reduced *in vivo* tumor growth of AR<sup>+</sup> ER<sup>+</sup> patient-derived xenografts. These results suggest that targeting AR and ER simultaneously might be an effective treatment strategy for AR<sup>+</sup> ER<sup>+</sup> BC patients. Further, enzalutamide has been also shown to inhibit *in vivo* tumor growth of MDA-MB-453 AR<sup>+</sup> ER<sup>-</sup> breast tumors<sup>108</sup>. However, androgen treatment showed contradicting effects in AR<sup>+</sup> TNBC cell lines<sup>108</sup>. In a phase II trial (NCT01889238) in advanced AR<sup>+</sup> TNBC patients, 47% of patients exhibited an AR-associated gene signature and improved clinical outcomes upon enzalutamide treatment<sup>109</sup>. The ENDEAR trial (NCT02929576) which assessed combination treatment of chemotherapy +/- enzalutamide was withdrawn due to limited information about AR signaling in TNBC<sup>110</sup>. Currently, feasibility of enzalutamide is investigated in AR<sup>+</sup> TNBC patients reporting disease-free survival (DFS) and overall survival (OS). Recent data of this trial (NCT02750358) has demonstrated that enzalutamide is a feasible treatment option in this patient cohort and well-tolerated in women. However, AR expression > 10% determined by IHC might not be sufficient to predict anti-androgen treatment response<sup>111–113</sup>. Instead Lehmann and colleagues have identified that molecular apocrine breast cancer patients with tumors >80% AR<sup>+</sup> cells were associated with better treatment response. RNA-sequencing analyses of pre- and posttreatment biopsies derived from patients showing response towards enzalutamide revealed decrease in cell cycle and AR target genes expression including *TFF3*, *SPDEF*; *FOXAI*, *PIP*, *APOD MYBPC1*, *CLDN8* and *PGC*. Consequently, this gene expression signature might be applied in order to identify patients who could benefit from anti-androgen treatment<sup>113</sup>.

Despite having identified the presence of AR in breast cancer, the role of AR signaling in BC seems quite controversial and remains to be fully elucidated. In addition, AR represents a

potential effective therapeutic target also in BC which has been increasingly appreciated within clinical trials.

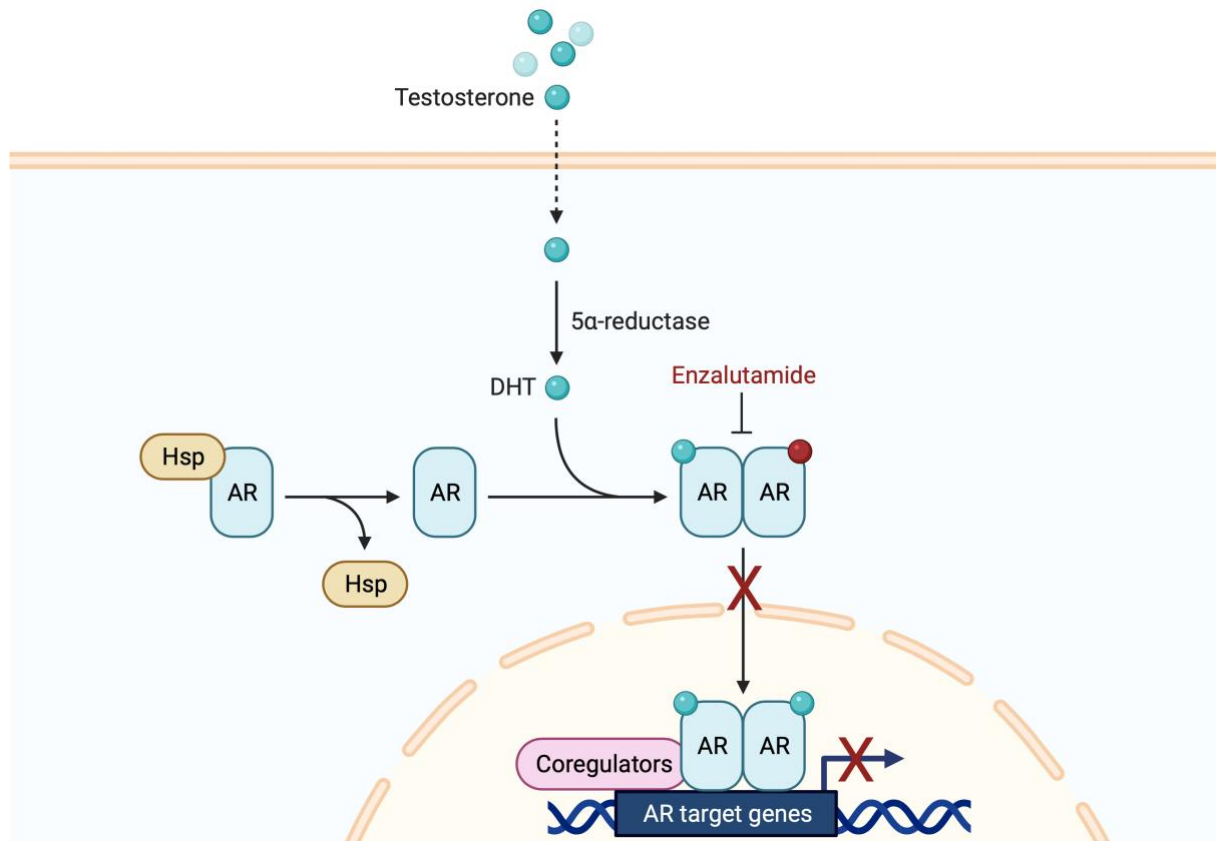


**Figure 5: Activation and pharmacological inhibition of androgen receptor.** Scheme illustrates androgen receptor (AR) agonist activation by dihydrotestosterone (DHT) and pharmacological inhibition by enzalutamide treatment. In its inactive form, AR is located in the cytosol bound to heat-shock proteins (Hsp). Testosterone is converted to DHT by the enzyme 5 $\alpha$ -reductase in the cytosol of the cell. DHT binds to AR at ligand binding domain and activates AR which is subsequently translocated into the nucleus. AR binds to androgen response elements (AREs) on the DNA in the promoter region of AR target genes. Co-regulatory proteins are recruited to AREs resulting in transcription of AR target genes. Enzalutamide binds to the ligand binding domain of AR and thus inhibits binding of androgens and homodimerization. As a result, AR cannot be activated and translocate into the nucleus. AR target gene transcription is repressed.

### 1.2.3 SPDEF in breast cancer

The E-twenty-six-specific sequence or E26 transforming sequence (ETS) family of transcription factors contains 28 members found to be expressed in humans<sup>114</sup>. The unifying feature of ETS transcription factors is an evolutionarily highly conserved 85 amino acid ETS DNA-binding domain (Figure 6). Yet, they retain individual sequence-specific DNA-binding properties<sup>115,116</sup>. A subset of ETS transcription factors contain an additional conserved 65-85 amino acid pointed domain (PNT) implemented in homo-oligomerization, hetero-dimerization

and transcriptional repression<sup>117–120</sup>. ETS transcription factor activity is highly regulated by transcriptional and post-transcriptional control, co-regulatory proteins and microRNAs<sup>114</sup>. Several post-transcriptional modifications such as phosphorylation and glycosylation among others tightly control DNA binding, transcriptional activation and repression, protein-protein interaction and subcellular localization of ETS transcription factors<sup>121,122</sup>. Most cell types express multiple transcription factors of the ETS family<sup>114</sup>. In normal development, ETS transcription factors are involved in the regulation of various biological processes including cell cycle, proliferation, differentiation, apoptosis and others. Aberrant ETS transcription factor signaling thus results in tumor initiation, progression and metastatic disease<sup>114</sup>. *Cis*-acting mutations within the regulatory region of a gene can lead to gain of ETS transcriptional activity. This phenomenon has been observed for telomerase reverse transcriptase in nearly 70% of melanomas<sup>123,124</sup>. Further, mutations generating ETS-binding sites are among the most frequent mutations found in solid tumors<sup>125</sup>. In addition, ETS transcription factor activity and stability can be increased by perturbed upstream signaling pathways that are involved in post-translational modifications of ETS members<sup>114</sup>. For example, ETS factors stability is increased through phosphorylation constituted by mutations in receptor tyrosine kinases<sup>126</sup>.

SAM pointed domain-containing ETS transcription factor (SPDEF) also known as prostate-derived ETS transcription factor (PDEF) is a special ETS member and recognizes ‘GGAT’ core sequence instead of ‘GGAA’ compared to other ETS transcription factors. *SPDEF* gene is located at chromosome 6p21.31 and encodes six exons with a length of 1005 nucleotides. Two isoforms have been discovered by alternative splicing, one skipping exon 4. SPDEF exhibits potential phosphorylation sites for protein kinase C, tyrosine kinase, AKT and MAPK. In addition, SPDEF protein was found to be glycosylated. However, the role of SPDEF phosphorylation and glycosylation in regard to its function needs to be further investigated<sup>127</sup>. Unlike the majority of ETS transcription factors, SPDEF is expressed exclusively in epithelial hormone-regulated tissues including prostate, breast, ovary and colon. This suggests that SPDEF plays an essential role in normal development and function in these tissues. SPDEF has been first described as novel ETS transcription factor in prostate cancer. In this context, SPDEF has been demonstrated to function as co-regulator of AR transcription factor. It directly interacts with the AR DNA binding domain thereby enhancing androgen-mediated transactivation of AR target genes’ promoters such as *prostate-specific antigen (PSA)*<sup>127</sup>.

In the mammary gland, SPDEF has been implicated in luminal differentiation of normal mammary epithelial cells<sup>128</sup>. In breast cancer, SPDEF was found to be highly expressed in luminal and HER2-enriched subtypes. In contrast, SPDEF expression is low in TNBC<sup>129</sup>. Tissue



microarray analysis of molecular apocrine patient samples has demonstrated that high SPDEF levels are associated with AR expression in these tumors<sup>89,90</sup>. Further, SPDEF is included in the gene signature predicting response towards enzalutamide<sup>91,113</sup>. Compared to healthy tissue, SPDEF mRNA and protein are found to be overexpressed in early-stage and low-grade breast cancers<sup>128,130–134</sup>. Along with tumor progression, SPDEF expression has been observed to decrease in highly malignant tumors and metastatic disease<sup>135</sup>. Based on these data, SPDEF has been suggested to have distinct functions in different stages of breast cancer development. Strikingly, the role of SPDEF in breast cancer is highly controversial and it has been described to have dual functions<sup>136</sup>. In ER<sup>+</sup> tumors, SPDEF has been stated to drive tumor growth. Its expression highly correlates with ER expression and ER is recruited to the *SPDEF* promoter region in an estrogen-dependent manner. ER co-regulatory proteins, FOXA1 and GATA3, have been shown to be implemented in the regulation of *SPDEF* gene expression. Downregulation of SPDEF inhibited *in vivo* tumor growth of luminal breast cancers<sup>128</sup>. Cao and colleagues found that SPDEF and AR are co-expressed in TNBC and that *SPDEF* gene expression is regulated by AR. Further, they found that SPDEF negatively regulates MAD1, a transcriptional repressor of the oncogene MYC, resulting in enhanced MYC-mediated gene transcription. As a consequence, MYC promotes proliferation, migration and invasion of TNBC cells *in vitro*<sup>137</sup>. Taken together, these data and additional studies have demonstrated that SPDEF has a pro-tumorigenic function in breast cancer<sup>128,131,136–139</sup>. In contrast, others have proposed SPDEF to act as tumor-suppressor gene inhibiting cell growth and proliferation in breast cancer. In ER<sup>+</sup> MCF-7 cells, silencing of SPDEF enhanced cell and tumor growth *in vitro* and *in vivo*<sup>140</sup>. Another study has stated that SPDEF directly regulates cyclin-dependent kinase (CDK) inhibitor p21 expression in a mouse mammary tumor cell line. Increased p21 levels lead to reduced CDK2 activity that ultimately results in reduced cell growth *in vitro* and *in vivo*<sup>141</sup>. Further, SPDEF has been shown to repress uPA ligand which bound to its receptor uPAR has been implemented in tumor development. Downregulation of uPA by SPDEF inhibits cell migration in basal-like invasive breast cancer cell lines<sup>142</sup>. These and other studies support the tumor-suppressive role of SPDEF in breast cancer<sup>128,140–143</sup>. Further studies are needed in order to better understand the function of SPDEF in distinct breast cancer subtypes and stages.



**Figure 6: SPDEF protein structure.** ETS transcription factors share a highly conserved ETS domain which harbors the DNA-binding domain. SPDEF binds to DNA sequences containing the core motif ‘GGAT’. The ETS domain also functions as protein-protein interaction site. SPDEF contains a pointed domain (PNT) functioning in homo- and heterodimerization and transcriptional repression.

## 1.3 Cancer cell metabolism

### 1.3.1 Glucose metabolism in cancer cells

Cellular metabolic reprogramming is a core hallmark of cancer<sup>144,145</sup>. Cancer cells have been observed to adjust their cellular energy metabolism in order to fuel cell growth and division. Normal cells process glucose to pyruvate during glycolysis in the cytosol (Figure 7). In the presence of oxygen, pyruvate is shuttled into the mitochondria where it becomes fully oxidized to carbon dioxide via oxidative phosphorylation (OxPhos). Glycolysis producing lactate as end product is favored under anaerobic conditions. Otto Warburg was the first to describe the abnormal phenomenon of cancer cells to largely rely on glycolysis even in the presence of oxygen. This state of aberrant glucose metabolism has been termed ‘aerobic glycolysis’<sup>146–148</sup>. This metabolic switch seemed to be counterintuitive when considering that cancer cells need to compensate for approx. 18-fold lower efficiency of ATP production through glycolysis relative to mitochondrial respiration. However, cancer cells have been shown to accomplish their cellular needs in part by increasing the import of nutrients from the microenvironment. Further, increased glycolytic activity leads to enhanced incorporation of glycolytic intermediates into various biosynthetic pathways. Carbon intermediates are utilized as building blocks for the assembly of macromolecules and organelles needed for cell division<sup>149,150</sup>.

A portion of carbon substrates are used for NADPH generation from NADP<sup>+</sup>, a reducing cofactor utilized within various biosynthetic reactions and maintaining cellular redox capacity. NADPH as electron donor is needed for *de novo* fatty acid and cholesterol synthesis among other anabolic pathways<sup>151</sup>. The pentose phosphate pathway is a branching pathway in glycolysis, in which glucose-6-phosphate is partially oxidized to generate NADPH and ribose-

5-phosphate. Pentose phosphate pathway activity is often elevated in tumor cells, not least because ribose-5-phosphate is utilized for nucleotide generation<sup>152</sup>.

Hexosamine biosynthesis is another branch of the glycolytic pathway using fructose-6-phosphate and glutamine as substrates in order to produce glucosamine-6-phosphate. N-acetylglucosamine (GlcNAc) is generated through the hexosamine pathway and serves as substrate for N- and O-linked glycosylation of various proteins and lipids. Fructose-6-phosphate can be either generated by oxidation of glucose catalyzed within the first two steps of glycolysis, by the enzymes hexokinase (HK) and phosphohexose isomerase (GPI), or within gluconeogenesis. Most steps in gluconeogenesis are the reverse reactions of glycolysis with exception of three irreversible steps in order to produce glucose from non-carbohydrate substrates. Fructose-1,6-bisphosphatase (FBP1), the rate-limiting enzyme in gluconeogenesis, catalyzes the hydrolysis of fructose-1,6-bisphosphate (F-1,6-BP) to fructose-6-phosphate and inorganic phosphate. In contrast to other rate-limiting enzymes catalyzing branching pathways of glycolysis which are frequently upregulated in cancer cells, loss of FBP1 has been demonstrated to drive tumorigenesis<sup>153-156</sup>. Low FBP1 expression has been stated as a prognostic factor associated with worse survival probability in breast cancer<sup>153</sup>. Two other glycolytic branched pathways are the biosynthesis of phospholipids using glycerol-3-phosphate that is a major structural component of cell membranes, and 3-phosphoglycerate as a precursor for serine and glycine biosynthesis<sup>152</sup>.

The last step of glycolysis is catalyzed by the enzyme pyruvate kinase (PK) that converts phosphoenolpyruvate to pyruvate. In highly glycolytic tumor cells, most of the resulting pyruvate is converted to lactate by lactate dehydrogenase A or B (LDHA/B). The rest of pyruvate is irreversibly decarboxylated to acetyl-CoA by pyruvate dehydrogenase (PDH) located in the mitochondrial matrix. Acetyl-CoA enters the citric acid cycle (tricarboxylic acid cycle, TCA cycle) in order to generate citrate. Citrate is secreted into the cytosol and converted into acetyl-CoA and oxaloacetate. The latter is converted to malate in order to be shuttled back into the mitochondria whereas acetyl-CoA serves as precursor for *de novo* fatty acid biosynthesis. Hence, not only glycolytic but also TCA cycle intermediates serve as substrates for anabolic pathways needed for cancer cell proliferation. To sustain TCA cycle activity facing citrate export for fatty acid and cholesterol biosynthesis, cancer cells re-supply intermediates into the TCA cycle in a process called 'anaplerosis'<sup>152</sup>. Glutamine serves as anaplerotic substrate incorporated into the TCA cycle and is an additional carbon source utilized in high amounts by cancer cells for energy production<sup>157,158</sup>. A high anaplerotic flux is an indicator for rapidly proliferating tumor cells. In addition, glutamine provides nitrogen for the *de novo*

synthesis of a number of nitrogen-containing compounds such as purine and pyrimidine nucleotides, glucosamine-6-phosphate and non-essential amino acids<sup>152</sup>.

While proliferating tumor cells have been thought to rely on glycolysis for energy production and biosynthesis of cell components, quiescent tumor cells have been demonstrated to preferentially utilize glucose for complete oxidation via OxPhos in the mitochondria<sup>159</sup>. Oxidation of carbon sources via the TCA cycle produces reducing equivalents in the form of NADH and FADH<sub>2</sub> which mediate the transfer of electrons to the mitochondrial electron transport chain in order to generate ATP. Elevated expression of mitochondrial respiratory components has been observed in a quiescent subpopulation of tumor cells<sup>160,161</sup>. However, the importance of OxPhos activity in cancer cells has long been underappreciated despite the evidence that some cancer types are markedly less glycolytic and exhibit higher dependence on mitochondrial respiration. Cancer cells often display distinct metabolic features which are characteristic of their tissue of origin<sup>162</sup>. While lung, liver and colorectal cancers are highly glycolytic, glioblastomas and melanomas have been stated to rely on OxPhos activity<sup>162,163</sup>. Breast cancer cells have been shown to generate more than 80% of their ATP by oxidative phosphorylation and the maintenance of the mitochondrial membrane potential is crucial for proliferation of tumor cells<sup>164,165</sup>. Targeting mitochondrial metabolism has become a potential strategy to treat ‘oxidative tumors’<sup>166</sup>. Metformin, a drug that has been used to treat type II diabetes, has been applied in clinical management of breast cancer patients and impaired cancer cell proliferation and tumor growth<sup>167-170</sup>. Although the precise mechanism of action of metformin remains partly unclear, recent studies have shown that mitochondrial complex I displays a key target of metformin<sup>170-172</sup>. Mutations in mitochondrial complex I are frequently observed in breast cancers and are associated with increased sensitivity towards metformin<sup>173</sup>. Recent studies have suggested that tumor cells adapt their metabolism along with tumor progression and metastatic disease in order to meet energetic and biosynthetic demands specific for tumor stage and microenvironment. Thus, metabolic profiles of primary tumor cells might differ from those found in metastatic lesions. Several studies have suggested that invasive and metastatic breast cancer cells shift their metabolism towards OxPhos. Engaging both, OxPhos and glycolysis may provide metabolic plasticity needed to survive and engraft at distinct organ sites<sup>161,174-177</sup>. Further studies addressing metabolic profile and plasticity of cancer cells are needed to implement cancer cell metabolism as an important variable in clinical management of metastatic breast cancer.

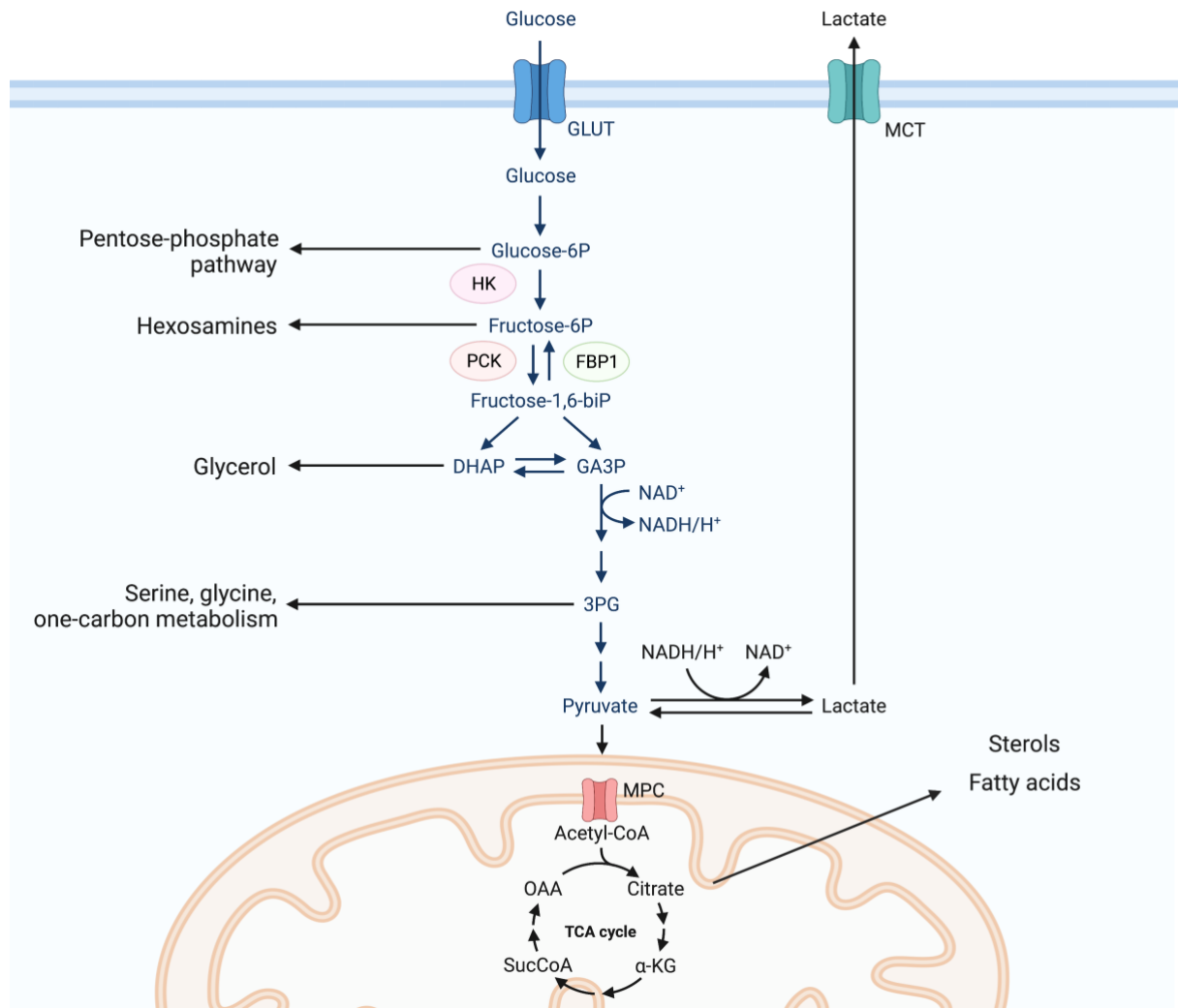


**Figure 7: Glucose metabolism in cancer cells.** Overview of glucose metabolism in cancer cells. Glucose is imported into the cell via glucose transporters (GLUT) and oxidized within glycolysis. Hexokinase (HK) is the rate-limiting enzyme catalyzing the first reaction in glycolysis. Fructose-1,6-bisphosphatase (FBP1) is the rate-limiting enzyme in gluconeogenesis and catalyzes the conversion from fructose-1,6-bisphosphate into fructose-6-phosphate and inorganic phosphate. During glycolysis, glucose is processed to pyruvate which can be imported into the mitochondria as a substrate for the TCA cycle. In proliferating cancer cells, the majority of pyruvate is converted to lactate.

### 1.3.2 Fatty acid metabolism in cancer cells

Fatty acids (FAs) play an essential role in a variety of biological processes including synthesis of biological membrane components, signal transduction pathways, and energy production and storage. Fatty acid metabolism encompasses (1) uptake of exogenous fatty acids from the microenvironment via the cell membrane constituted by fatty acid transporters (2) storage of fatty acids in the form of triacylglycerols (3) *de novo* biosynthesis of fatty acids in the cytosol, and (4) degradation via  $\beta$ -oxidation in the mitochondria of the cells<sup>178,179</sup>.

In normal adult tissues with exception of the liver, adipose tissue or mammary epithelium during lactation, *de novo* fatty acid synthesis rate is low<sup>180</sup>. In contrast, tumor cells generate almost all of their cellular FAs through *de novo* synthesis<sup>178,181</sup>. Three major enzymes are involved in fatty acid synthesis, namely ATP citrate lyase (ACLY), acetyl-CoA carboxylase- $\alpha$  (ACACA, also known as ACC1) and fatty acid synthase (FASN) (Figure 8). In the first step, cytosolic citrate is cleaved into acetyl-CoA and oxalacetate by ACLY<sup>182</sup>. Acetyl-CoA is carboxylated by ACC to produce malonyl-CoA which in turn is assembled into a 16-carbon long chain fatty acid palmitate (C16:0) by FASN<sup>183,184</sup>. Palmitate is then elongated and desaturated by several enzymes in order to generate long chain fatty acids of various lengths and degrees of saturation<sup>185–187</sup>. Inhibition of these enzymes involved in fatty acid biosynthesis has been observed to repress tumor cell growth *in vitro* and *in vivo*<sup>188–194</sup>. In addition, malonyl-CoA serves as precursor for cholesterol biosynthesis. Cholesterol is a major structural component of lipid bilayers and determines membrane fluidity being more rigid and packed when cholesterol concentration is high<sup>195</sup>. Further, cholesterol itself serves as a precursor for steroid hormone biosynthesis, essential for hormone-dependent breast cancer growth<sup>196</sup>.

Increased FA biosynthesis could be either an adaptation mechanism to high metabolic demands of rapidly growing cancer cells or to reduced availability of exogenous fatty acids and lipids in the tumor microenvironment<sup>178</sup>. The tumor microenvironment is frequently hypoxic which leads to repression of the TCA cycle and OxPhos<sup>197</sup>. Elevated expression of fatty acid transporter accompanied by enhanced uptake of exogenous fatty acids has been observed in cancer cells under hypoxic conditions<sup>198</sup>. In severe hypoxic and nutrient restricted tumor regions, cancer cells may completely be dependent on exogenous lipid uptake. Several studies have demonstrated that cancer cells increase lipid uptake upon hypoxia when there is low availability of substrates needed for FA synthesis. FA binding proteins are involved in the uptake of exogenous fatty acids and subcellular trafficking of FAs in breast and glioblastoma cells<sup>198,199</sup>. Hypoxia has been also shown to promote the storage of excess lipids within lipid droplets, which are specialized organelles storing neutral lipids, cholesterol and cholesteryl esters. Cancer cells use these stored lipids for energy production via  $\beta$ -oxidation in the mitochondria and antioxidation defense upon oxygen availability<sup>178,199</sup>. The flexibility to switch from FA synthesis to lipid uptake and degradation allows cancer cells to immediately adapt to their microenvironment and temporal fluctuations in oxygen availabilities<sup>200,201</sup>.

FAs have various functions in cancer cells including the generation of building blocks for biological membranes needed for cell division. Next to cholesterol, phospholipids are hydrophobic molecules and major structural components of cell membranes. They make up a

special class of lipids synthesized from fatty acids<sup>178</sup>. In addition, membrane phospholipids function as signaling molecules giving rise to second messengers such as diacylglycerol (DAG) and phosphatidylinositol-3,4,5-triphosphate (PIP<sub>3</sub>) upon extracellular signals<sup>202,203</sup>. Further, the structural composition and overall saturation level of cell membranes changes due to increased fatty acid synthesis in tumor cells. Levels of monounsaturated fatty acids increase by *de novo* synthesis while polyunsaturated fatty acids that are mainly derived from dietary lipids are reduced. The increase in saturated fatty acids lead to better protection of cancer cells from reactive oxygen species (ROS) since those are less susceptible to lipid peroxidation<sup>204,205</sup>.

Excess FAs are preferentially stored in the form of triacylglycerides (TAGs) within lipid droplets and can be used for energy production at later time points<sup>206</sup>. Lipids are energy-rich compounds and their oxidation results in more than twice the energy comparing degradation of palmitate with glucose. Free fatty acids are imported into the mitochondria where  $\beta$ -oxidation takes place. In several steps, one molecule of acetyl-CoA generates three molecules of NADH, one molecule of FADH<sub>2</sub> and one molecule GTP in the TCA cycle. Electrons from these reducing cofactors are transferred to the mitochondrial electron transport chain. In total, approx. 130 molecules of ATP are generated by degradation of the 16-carbon palmitic acid. Degradation of fatty acids and *de novo* biosynthesis are mutually exclusive processes which are compartmentally separated from each other and regulated by a negative feedback loop<sup>178</sup>. Although the role of newly synthesized fatty acids in cancer cells is quite well investigated, much less is known about the role of  $\beta$ -oxidation in cancer cells. However, several studies have suggested that cancer cells rely on fatty acid oxidation under stressed conditions<sup>207</sup>.

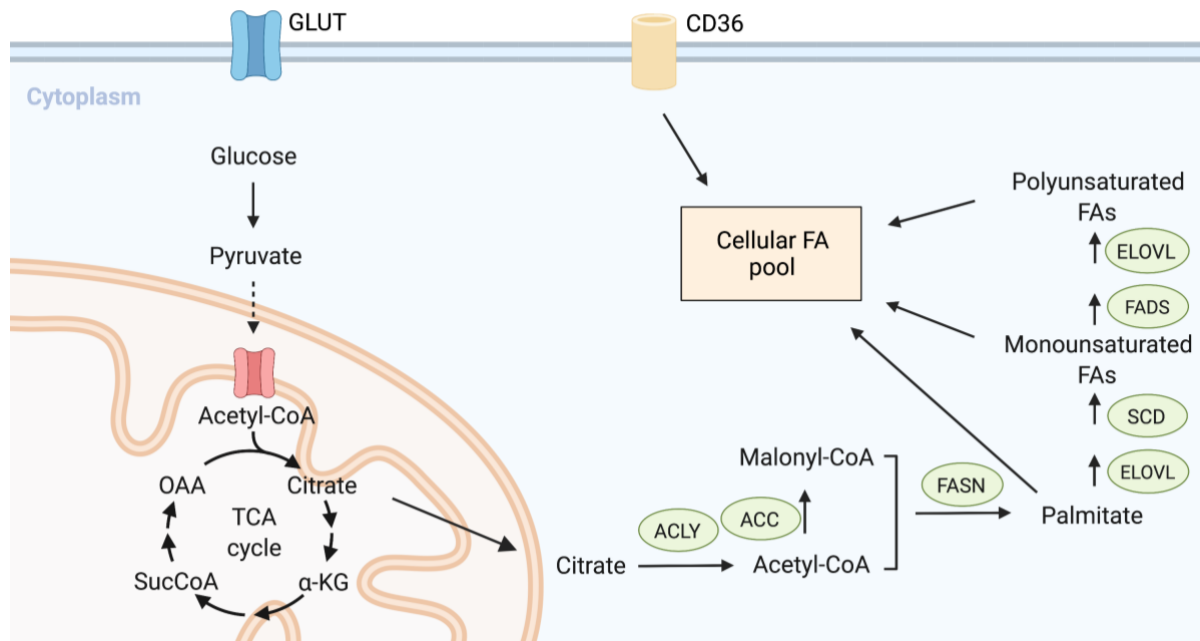


**Figure 8: Fatty acid synthesis and uptake.** Simplified overview of fatty acid biosynthesis and uptake from the microenvironment. Citrate derived from the TCA cycle is shuttled from the mitochondria into the cytosol where it is cleaved by ATP-citrate lyase (ACLY) to acetyl-CoA and oxalacetate. Acetyl-CoA is carboxylated to malonyl-CoA and repeatedly condensed by fatty acid synthase (FASN) generating palmitate (C16:0). Palmitate can be elongated by fatty acid elongases (ELOVL) and desaturated by stearoyl-CoA desaturase (SCD). Fatty acid desaturase (FADS) is an alternative enzyme introducing double bonds in long-chain fatty acids. CD36 is a main fatty acid transporter localized at the cell surface and facilitates exogenous fatty acid uptake from the microenvironment.



## 2 Aim of this study

Breast cancer is the second leading cause of cancer-related deaths in women worldwide. In most cases, primary breast cancer is diagnosed at early stage and well-curable. Eventually, more than 30% of patients develop recurrence and the advanced metastatic disease leads to death of the patients<sup>1</sup>. Understanding the metastatic process and elucidating molecular mechanisms driving tumor growth of advanced breast cancer cells will allow to develop new treatment strategies. The majority of breast cancer express androgen receptor (AR)<sup>59</sup>. Therefore, a cohort of breast cancer patients might benefit from anti-androgen hormone therapy. However, clinical trials have failed due to limited and contradicting knowledge about AR signaling in breast cancer<sup>111-113</sup>. A known co-factor of AR in prostate carcinoma, the transcription factor SPDEF is found to be highly expressed in breast cancer as well<sup>129</sup>. However, its interaction with AR and functional role in breast cancer remains to be elucidated. Recent studies have suggested that SPDEF drives tumor growth in luminal tumors but function as tumor suppressor in triple negative breast cancer<sup>136</sup>. Further, SPDEF has been included in a gene signature supposed to predict sensitivity towards anti-androgen treatment in breast cancer patients<sup>113</sup>.

The objective of this study was to investigate the functional role of SPDEF in breast cancer. I addressed the question whether this transcription factor is involved in tumorigenesis. Further, I asked whether SPDEF is associated with AR expression in breast cancer. Based on controversial literature<sup>136</sup>, I hypothesized that SPDEF might have different functions dependent on the co-expression of hormone receptors. To this end, I analyzed the role of SPDEF *in vitro* and *in vivo* in distinct breast cancer subtypes in the absence and presence of AR. PDX-derived cell lines were utilized in order to generate SPDEF overexpression, knockdown and knock-out models. Newly acquired knowledge about the controversial role of SPDEF and AR signaling in breast cancer might be helpful to better stratify which patients may benefit from anti-androgen treatments. In addition, SPDEF itself represents an interesting target for breast cancer therapy since it is specifically expressed in hormone-responsive tissues but not ubiquitously found in the body.

### 3 Results

#### 3.1 SPDEF and AR expression in breast cancer

##### 3.1.1 SPDEF and AR are heterogeneously expressed in distinct breast cancer subtypes

SPDEF is a known co-factor of the androgen receptor (AR) in prostate carcinoma (PCa)<sup>127</sup>. It has been previously shown to be also expressed in luminal breast tumors<sup>129</sup>. Therefore, I asked whether SPDEF is involved in breast cancer tumorigenesis and associated with AR signaling. To address this question, I accessed mRNA expression data from the METABRIC data set including 1904 breast cancer patients. Of those, 1459 patients are classified as ER positive and 445 as ER negative. *SPDEF* mRNA levels were found to be significantly higher in luminal breast cancers (including ER<sup>+</sup>/HER2<sup>+</sup>/high and low proliferative tumors) and HER2-enriched tumors (Figure 9A) relative to TNBC (ER<sup>-</sup>/HER2<sup>-</sup>). However, the range of *SPDEF* mRNA expression was larger within the cohort of ER<sup>-</sup>/HER2<sup>-</sup> patients suggesting high levels of heterogeneity within this subtype. In line with *SPDEF* levels, expression of *AR* was significantly higher in luminal and HER2-enriched tumors compared to ER<sup>-</sup>/HER2<sup>-</sup> breast cancers (Figure 9B).

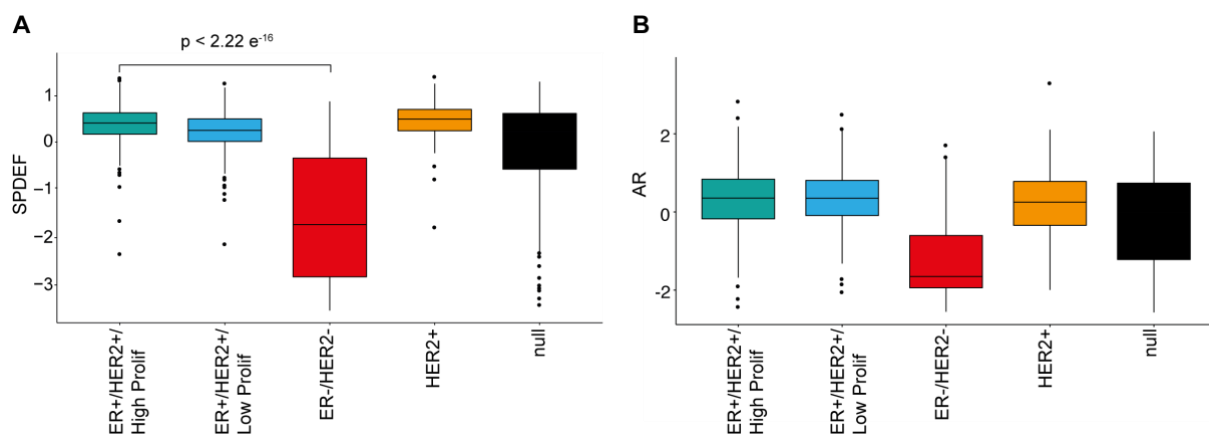


**Figure 9: *SPDEF* and *AR* mRNA expression in different breast cancer subtypes.** *SPDEF* (A) and *AR* (B) mRNA expression in ER positive (+)/HER2 positive (+)/High Proliferative (Prolif), ER<sup>+</sup>/HER2<sup>+</sup>/Low Prolif, ER<sup>-</sup>/HER2<sup>-</sup> and HER2<sup>+</sup> breast cancer patients derived from the METABRIC data set including 1904 patients.

To further determine whether *SPDEF* and *AR* expression correlate in breast cancer, I calculated the Pearson and Spearman scores for *AR* based on co-expression with *SPDEF* in ER<sup>-</sup> (Figure 10B, upper panel and Supplementary Table 1) and ER<sup>+</sup> BC patients (Figure 10B, lower panel

and Supplementary Table 1). I found that *SPDEF* and *AR* are highly co-expressed in breast cancer. Strikingly, the linear correlation of *SPDEF* and *AR* expression (Pearson correlation coefficient  $r$ ) was larger in ER<sup>-</sup> patients compared to ER<sup>+</sup> BC patients, despite the higher expression of both genes in ER<sup>+</sup> tumors.

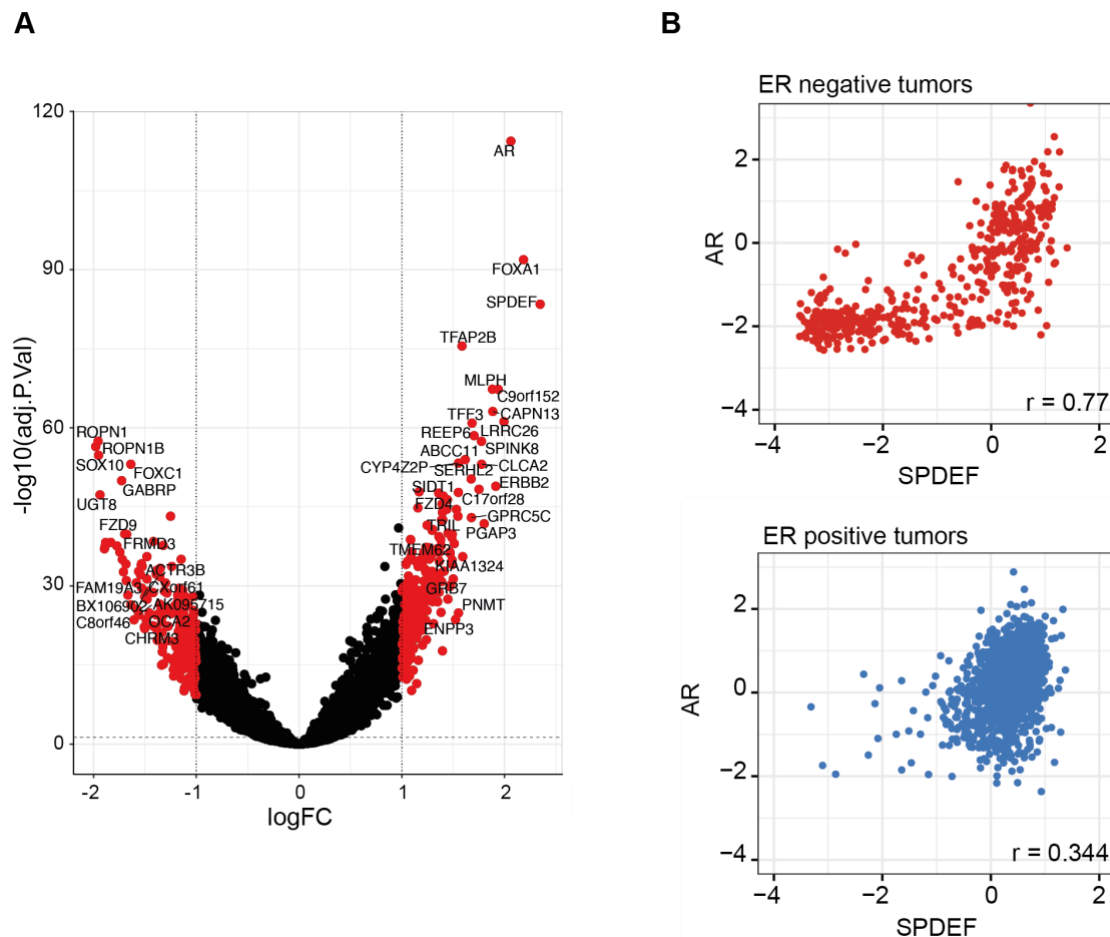


**Figure 10: *SPDEF* and *AR* are co-expressed in breast cancer patients.** (A) Differential gene expression analysis between AR<sup>high</sup> and AR<sup>low</sup> ER<sup>-</sup> breast cancer patients based on *AR* mRNA expression. Volcano plot represents all differentially expressed genes. Highlighted in red are all genes with an adjusted p-value < 0.05 and log-fold change (FC) > 1. Annotated are all genes with an adjusted p-value < 0.005 and logFC > 1.5. (B) Linear correlation of *SPDEF* and *AR* gene expression in ER negative (upper panel, red) and ER positive (lower panel, blue) breast cancer patients. Depicted is the Pearson correlation coefficient  $r$  calculated with R package ggpubr.

As *SPDEF* might interact with both hormone receptors, ER and AR<sup>127,128</sup>, I further explored the co-expression of *ESR1*, the gene encoding ER, and *SPDEF* in all BC patients. I found that expression of these genes highly correlated with each other, although the covariance was lower than for *SPDEF* and *AR* co-expression (Supplementary Figure 1A). *SPDEF* and *ESR1* expression especially correlated in ER<sup>+</sup> patients whereas *AR* mRNA levels were also high in most ER<sup>+</sup> patients (Supplementary Figure 2). In contrast, ER<sup>-</sup> patients showed either high levels for *SPDEF* and *AR* and low levels of *ESR1*, or low expression for all three genes (Supplementary Figure 2).

Due to more pronounced correlation between *AR* and *SPDEF* in ER<sup>-</sup> tumors, I focused on ER<sup>-</sup> breast cancer patients. I run differential gene expression analysis using the METABRIC data set for AR<sup>high</sup> and AR<sup>low</sup> ER<sup>-</sup> BC tumors based on *AR* mRNA expression. *SPDEF* was the most differentially expressed gene (with the highest fold change) associated with high *AR* mRNA expression, followed by *FOXA1* and *AR* gene itself (Figure 10A). Interestingly, the gene encoding for the HER2 receptor *ERBB2* was among the top six differentially expressed genes enriched in AR<sup>high</sup> tumors.

Taken together, these analyses suggest that *SPDEF* and *AR* are highly co-expressed in ER<sup>+</sup> and ER<sup>-</sup> breast cancers, and that a subpopulation of ER<sup>-</sup> patients exist which are either positive or negative for both genes of interest.

### 3.1.2 *SPDEF* and *AR* predict survival probability in breast cancer

In order to evaluate the impact of *SPDEF* and *AR* expression on patients' survival, I analyzed survival data from patients included in the METABRIC data set. ER<sup>-</sup> patients with high levels of *SPDEF* tumor mRNA expression showed a significant lower survival probability compared to patients with low levels of *SPDEF* (Figure 11B). In line with this finding, high *AR* tumor mRNA expression was associated with decreased survival probabilities in ER<sup>-</sup> patients (Figure 11A). Similar results were found for ER<sup>+</sup> patients (Supplementary Figure 1B, C).

Together, these findings demonstrate that *SPDEF* and *AR* are co-expressed in breast cancer tumors and increased *SPDEF/AR* mRNA expression is associated with poor prognosis in patients.

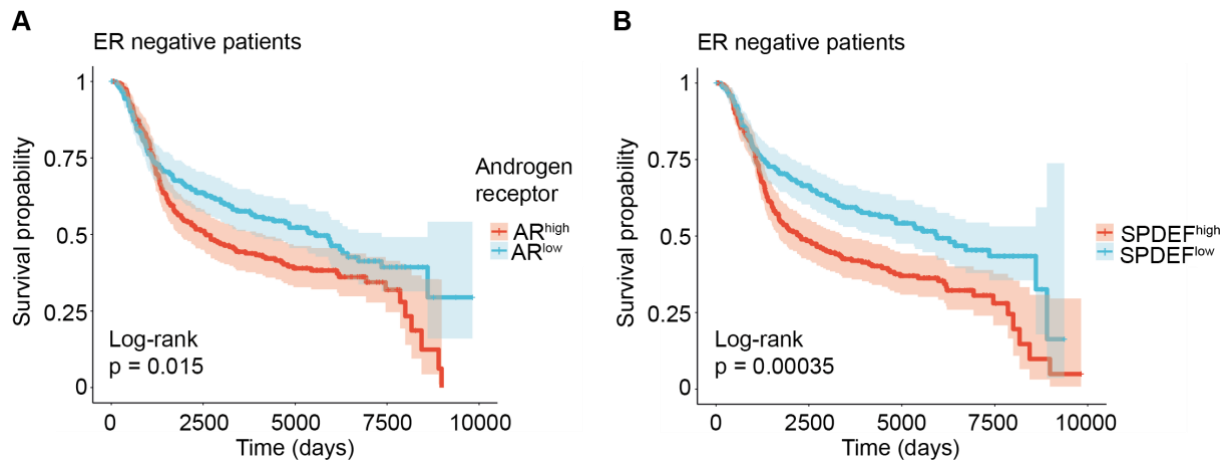


**Figure 11: High *AR* and *SPDEF* expression are associated with worse prognosis for ER<sup>-</sup> breast cancer patients.** (A, B) Kaplan-Meier estimator for survival probability of ER<sup>-</sup> breast cancer patients stratified based on *AR* (A) and *SPDEF* (B) gene expression. Data is extracted from METABRIC data set including 445 ER<sup>-</sup> breast cancer patients.

### 3.1.3 *SPDEF* and *AR* expression correlate in patient-derived xenograft cell models

Metastatic breast cancer cell lines derived from patient-derived xenografts (PDX) have been previously established in our lab by Dr. Massimo Saini, Dr. Roberto Würth and colleagues<sup>208</sup>. Those are originated from liquid biopsies derived from metastatic breast cancer (mBC) patients including blood (circulating tumor cells (CTCs)), ascites and breast pleural effusion (BPE) samples (Figure 12A). In brief, cells were injected orthotopically into the mammary fat pad of immunocompromised NSG mice. Successfully engrafted tumors were harvested and resembled histopathological features compared to patient samples. Subsequently, tumors were enzymatically digested and cell suspension was sorted for EpCAM<sup>+</sup> cells. Sorted cells were cultured in serum-low conditions in a defined cancer stem cell medium (Table 1). To study the functional role of *SPDEF* and its target genes in metastatic breast cancer, I utilized the following PDX cell lines: CTC288, CTC223, BPE8 and BPE7. Based on IHC staining of tumor biopsies, the patients from who CTC288 and CTC223 were derived, were classified as ER<sup>+</sup> luminal BC patients whereas BPE7 and BPE8 tumors were derived from TNBC patients (Supplementary Figure 3A and Supplementary Table 2). As it is known that the HR status of tumor cells can change during disease progression<sup>209</sup>, we performed IHC analysis of PDX tumors. While CTC288, BPE7 and BPE8 retained their preassigned HR status, ER expression was barely detectable in CTC223 PDX tumors (Supplementary Figure 3A, upper panel).

In order to determine the AR status in the PDX cell models, I performed immunohistochemistry (IHC) staining for AR in co-work with Vanessa Vogel (Figure 12B, upper panels). We found that the majority of CTC223 PDX tumor cells were positive for AR protein whereas BPE8 cells were highly heterogenous for AR expression. In contrast, CTC288 and BPE7 PDX tumors were negative for AR staining. Human Ki67 staining was applied to detect proliferating cells (Figure 12B, lower panels). We could not determine endogenous SPDEF expression by immunohistochemistry staining due to detection limit of the respective anti-SPDEF antibody (data not shown). Further, I assessed SPDEF and AR protein expression in PDX-derived cell lines by western blot analysis (Figure 12C). In line with IHC findings, BPE8 and CTC223 cell lines showed higher expression levels of AR protein compared to BPE7 cells (Figure 12C). In agreement with mRNA correlation in breast cancer patients, SPDEF protein was co-expressed with AR in BPE8 and CTC223 cells. In contrast, SPDEF levels were lower in BPE7 cells (Figure 12C). I validated the co-expression of SPDEF and AR in additional breast cancer cell lines using AR<sup>+</sup> and AR<sup>-</sup> PCa cell lines (LNCaP and PC3) as controls (Figure 12D and Supplementary Figure 3C). AR<sup>+</sup> LNCaP cells showed high AR and SPDEF protein levels whereas no signals could be detected in AR<sup>-</sup> PC3 cells using anti-AR and anti-SPDEF antibodies, respectively. Breast cancer MDA-MB-453 cells derived from TNBC showed high levels of AR and SPDEF protein. Although SK-BR-3 cells are known to be AR<sup>+210</sup>, I could not detect AR protein using the anti-AR antibody. However, SPDEF was found to be strongly expressed in SK-BR-3 cells. MDA-MB-231 cells derived from TNBC were negative for both, AR and SPDEF – similar to BPE7 cells.

Based on these findings, I referred BPE8 and CTC223 cell lines as AR<sup>+</sup> and BPE7 cells as AR<sup>-</sup> cell models. Since AR<sup>+</sup> PCa tumors are hormone-driven and in first line sensitive towards anti-androgen treatment, I hypothesized that AR<sup>+</sup> breast cancer cells might as well be responsive towards the AR inhibitor enzalutamide (Enza). Cell viability was remarkably reduced upon treatment with Enza for six days *in vitro* in AR<sup>+</sup> BPE8 and CTC223 cells whereas treatment did not show any significant effects in AR<sup>-</sup> BPE7 cells (Figure 12E).

Taken together, these data show that BPE8 and CTC223 PDX cell lines are AR<sup>+</sup> and sensitive towards anti-androgen treatment. Both, SPDEF and AR are highly expressed in these two cell models. In contrast, SPDEF levels were low in AR<sup>-</sup> BPE7 cells which did not respond to Enza treatment.

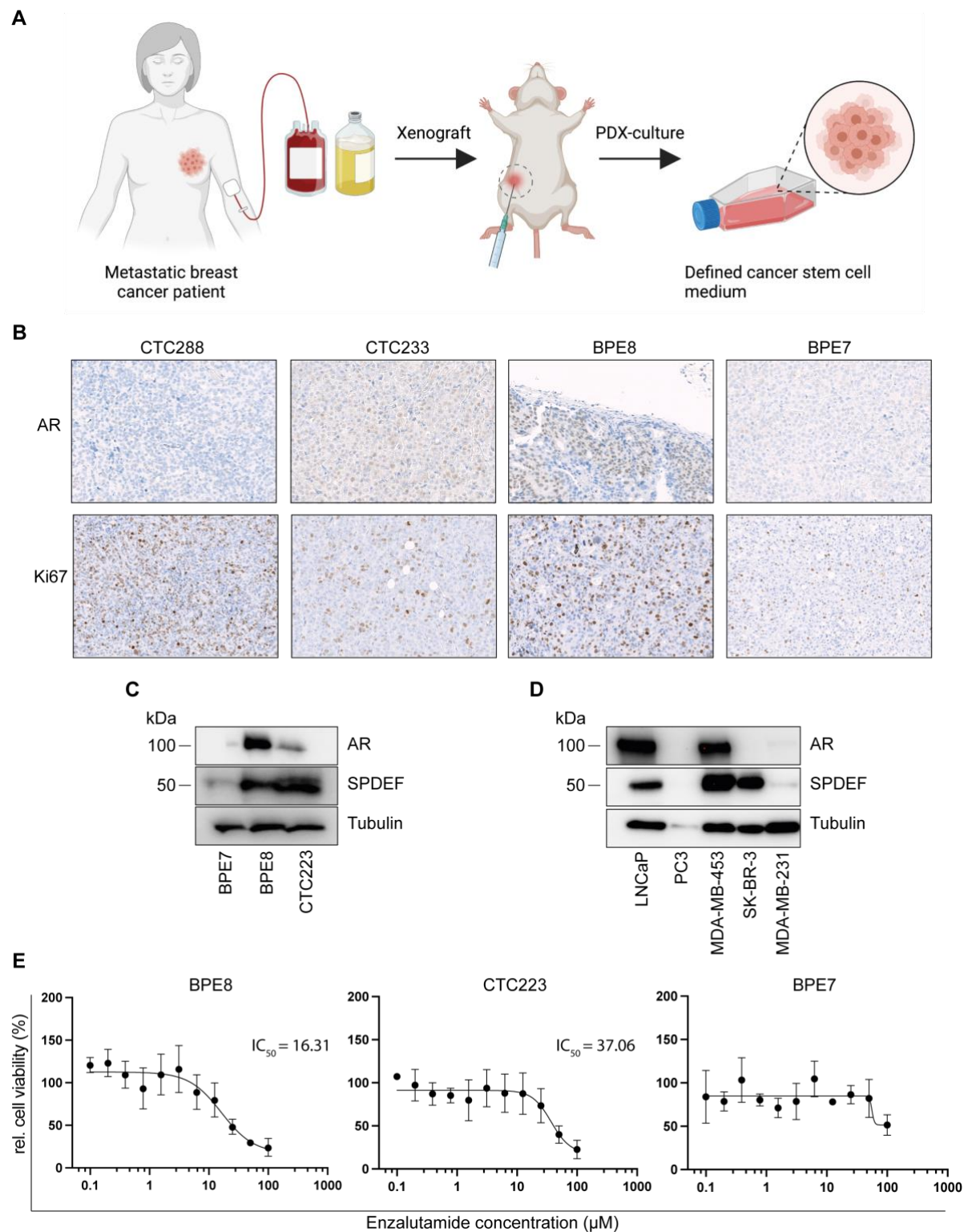


**Figure 12: SPDEF and AR expression in PDX cell models.** (A) Schematic diagram depicting the generation of patient-derived xenograft (PDX) cell models derived from liquid biopsies of metastatic breast cancer patients, cultured in defined breast cancer stem cell medium. (B) Androgen receptor (AR) expression in xenograft tumors by immunohistochemistry (IHC) staining (upper panels). Human Ki67 staining as proliferation marker in xenograft tumors (lower panels). IHC staining was performed by Vanessa Vogel. (C, D) Representative western blot analysis of AR and SPDEF protein expression in serum-free cultured PDX-derived cell lines (C) and commercially available prostate cancer (PCa) and breast cancer cell lines (D). AR<sup>+</sup> and AR<sup>-</sup> PCa cell lines were used as controls<sup>211,212</sup>. Tubulin serves as loading control; kDa, kilo Dalton. (legend continues on the next page).

### 3.2 Generation of SPDEF overexpression and knockdown cell models

To investigate the impact of SPDEF on tumor growth and the malignancy of breast cancer, I established stable SPDEF-overexpressing and doxycycline-inducible knockdown cell lines (Figure 14A). For this purpose, Dr. Franziska Zickgraf tested different shRNAs targeting SPDEF in PDX-derived ovarian cancer cell lines in order to downregulate SPDEF expression. In addition, she cloned the full-length SPDEF encoding cDNA sequence into a Lego iT2 vector to establish SPDEF-overexpressing cells<sup>213</sup>. A non-silencing (NS) shRNA or empty iT2 vector were used as controls. We produced lentivirus from both lentiviral vectors and I transduced different breast cancer cell lines including CTC288, CTC223, BPE8, BPE7 and MDA-MB-453. After transduction, cells were sorted for either tdTomato<sup>+</sup> (Lego iT2) or RFP<sup>+</sup> (pTRIPZ) fluorescence and expanded (Figure 14).

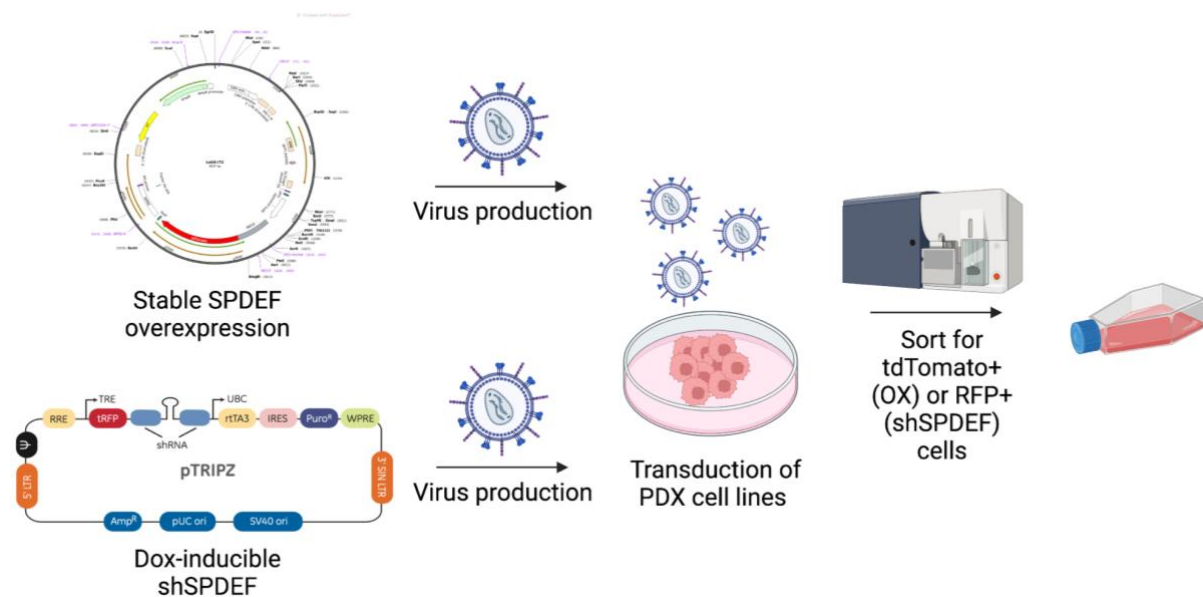


**Figure 13: Generation of SPDEF overexpression and knockdown cell models.** Schematic diagram depicts virus production and transduction of cell lines in order to establish SPDEF overexpression (OX) and knockdown (shSPDEF) cell models. Dox, doxycycline; PDX, patient-derived xenograft; RFP, red fluorescent protein.

Subsequently, I validated SPDEF mRNA and protein expression levels in wildtype (WT), untransduced, iT2 control (iT2), SPDEF-overexpressing (OX), pTRIPZ non-silencing control (NS) and shSPDEF (knockdown, KD) cells (Figure 14A-H). Untransduced cells were treated as transduced cells with the exception of adding virus to cells. BPE8- and CTC288-transduced

(E) Cell viability after treatment with enzalutamide for six days *in vitro* analyzed by CellTiter-Blue<sup>®</sup> (Promega) measurements. Representative experiment for each cell line. Error bars depict standard deviation of technical replicates (n= 4).



cells were sorted into high and low SPDEF populations based on the fluorescence intensities of the reporters, tdTomato (LeGo iT2) and RFP (pTRIPZ). SPDEF mRNA and protein expression increased with higher tdTomato fluorescence intensity in SPDEF OX cells of BPE8 and CTC288 (Figure 14A, B, D, E). In BPE8 cells, SPDEF knockdown efficiency was stronger in low-intensity sorted cells based on mRNA expression (Figure 14A), although protein levels were quite similar in both knockdown cell lines (BPE8 low and high) (Figure 14D). In CTC288 cells, SPDEF knockdown efficiency was in line with increased RFP fluorescence intensity (Figure 14B, E). All following experiments were performed using ‘high-intensity’-sorted cells, unless stated otherwise. In general, the SPDEF overexpression efficiency varied between the different cell lines. Although *SPDEF* mRNA levels were high in BPE8 WT cells, the increase in SPDEF OX cells was 60-fold compared to approx. 5-fold increase in SPDEF low-expressing BPE7 cells. Variance in knockdown efficiency was also observed among the different cell lines resulting in an average reduction in SPDEF expression levels of 50-70%. The greatest reduction of 92.2% in SPDEF expression in CTC223 shSPDEF cells was reached upon doxycycline (Dox) treatment for seven days (Supplementary Figure 4B). Thus, all following experiments with Dox-induced pTRIPZ NS and shSPDEF cells were used, were performed after treatment with Dox for seven days, unless stated otherwise. Downregulation of SPDEF in BPE7 cells upon Dox treatment was quite heterogeneous *in vitro*. To test the knockdown efficiency of SPDEF in BPE7 cells, RNA was extracted of five cell passages and RT-qPCR was repeatedly performed (Supplementary Figure 4A). *SPDEF* gene expression was roughly 30% reduced. To conclude, I established four different stable SPDEF-overexpressing cell lines and five Dox-inducible shSPDEF cell lines of different breast cancer subtypes including appropriate control cells.

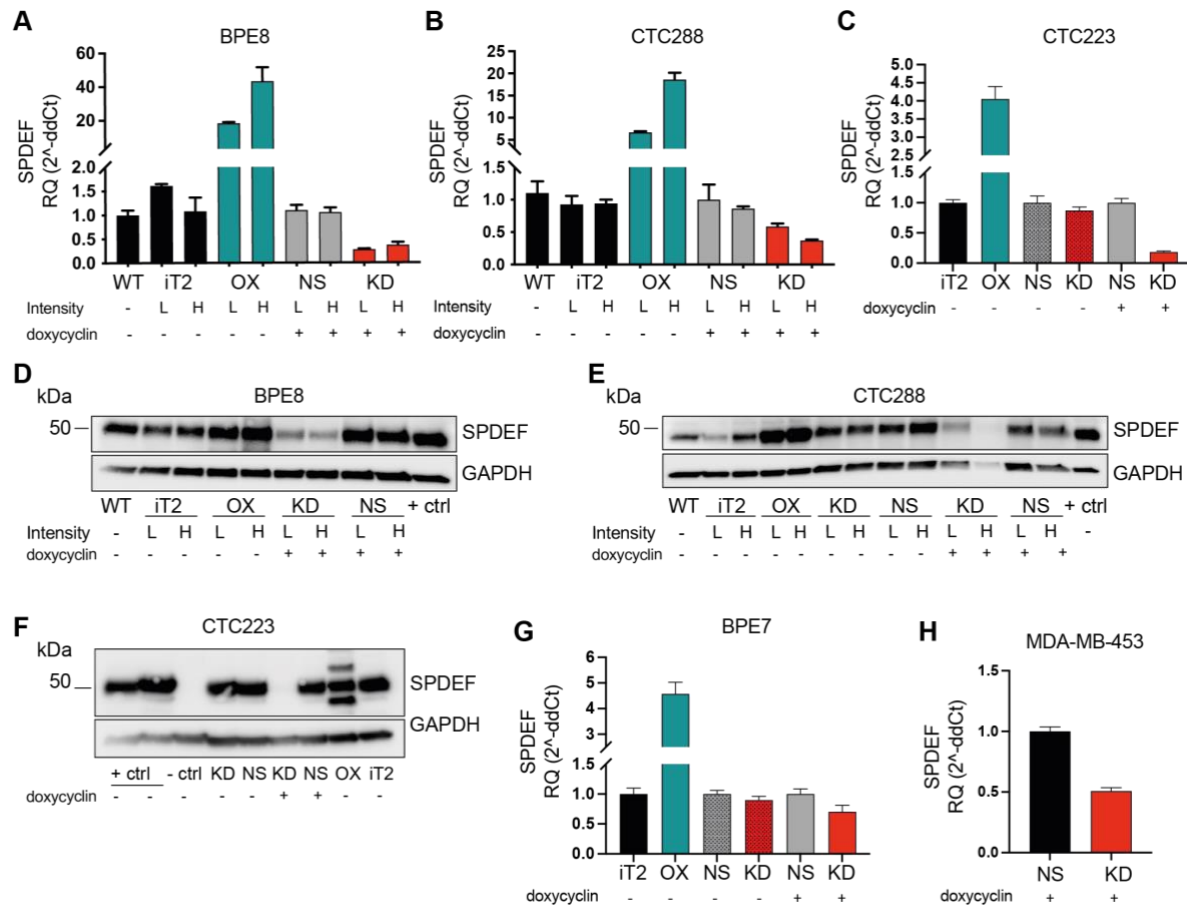


**Figure 14: Generation and validation of SPDEF overexpression and knockdown cell models.** (A-C, G-H) Validation of SPDEF gene expression by RT-qPCR analysis in BPE8 (A), CTC288 (B), CTC223 (C), BPE7 (G), MDA-MB-453 (H) wild type (WT), iT2 empty vector control (iT2), SPDEF overexpression (OX), pTRIPZ non-silencing control (NS), and SPDEF knockdown (KD) cells. Representative blots are shown. Error bars depict mean  $\pm$  SD of technical replicates (n=3). RNA extraction, cDNA synthesis and RT-qPCR were partially performed by Ornella Kossi. (E-G) Representative western blot analysis for SPDEF protein expression in BPE8 (D), CTC288 (E) and CTC223 (F) cells. MCF-7, SPDEF-transfected HEK293 and HEK293 WT cells served as positive and negative controls, respectively in (F). GAPDH as loading control; kDa, kilo Dalton. Intensity depicts sorting strategy based on high (H) and low (L) fluorescent signal intensity. Cells were treated with doxycycline for at least one week before RNA or protein was extracted (+ doxycycline).

### 3.3 SPDEF impacts tumor growth *in vivo*

#### 3.3.1 SPDEF downregulation inhibits *in vivo* tumor growth in AR<sup>+</sup> breast cancer models

To investigate the role of SPDEF in tumorigenesis of AR<sup>+</sup> breast cancer, I utilized the stable SPDEF-overexpressing (OX) and shSPDEF cell models of BPE8, CTC223 and MDA-MB-453 cell lines (3.2) which were injected orthotopically into the mammary fat pad of immunocompromised mice (Figure 15A).

First, I addressed the clonogenic potential of BPE8 cells upon SPDEF overexpression or downregulation by performing an *in vivo* limiting dilution assay. For this purpose, 1,000, 10,000 or 100,000 cells of either experimental cell lines, SPDEF OX or shSPDEF cells, or appropriate controls were orthotopically injected into the mammary fat pad of NSG mice. Tumor cell engraftment was significantly reduced upon downregulation of SPDEF relative to non-silencing control when either 1,000 or 10,000 cells were injected (Figure 15B). No significant difference was observed when a high cell number of 100,000 cells were implanted. This data suggests that SPDEF regulates the tumor-initiating capacity of BPE8 cells. In contrast, overexpression of SPDEF did not affect tumor cell engraftment compared to iT2 empty vector control cells irrespective of the starting cell number (Figure 15C). This indicates that cells with high endogenous SPDEF levels do not need further upregulation to affect tumor growth (Figure 12C).

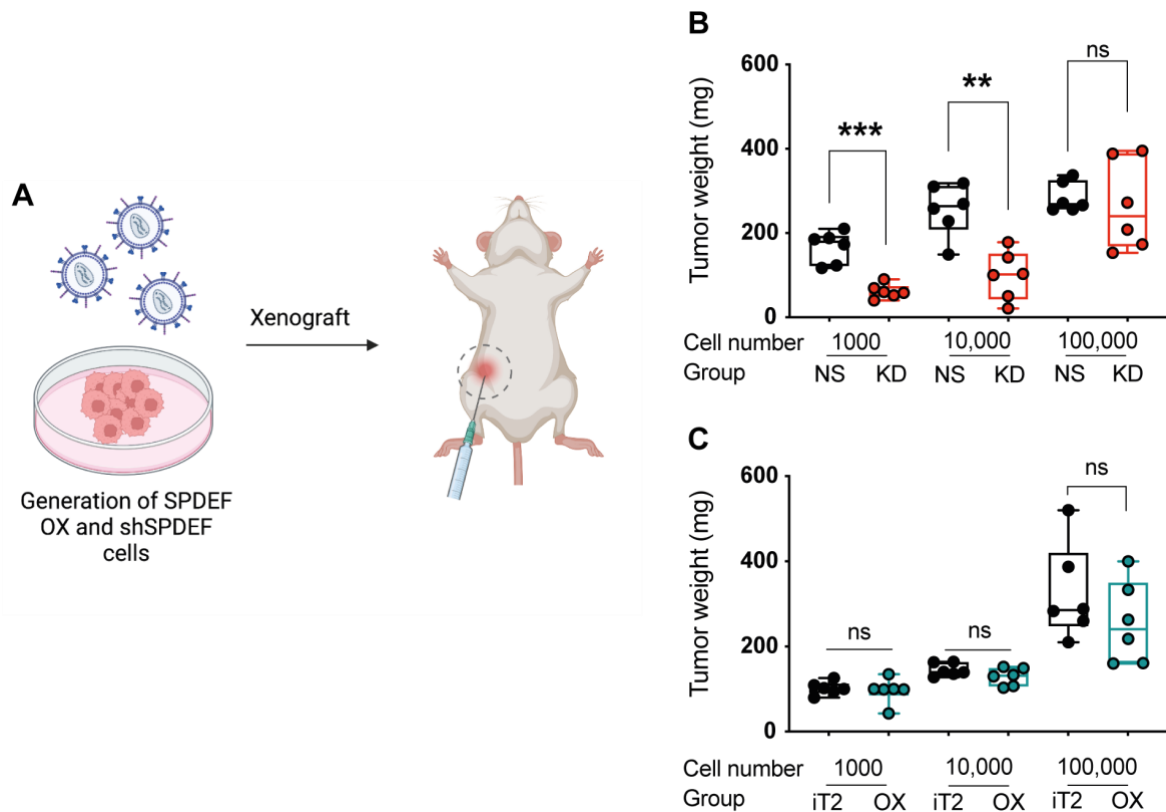


**Figure 15: SPDEF downregulation reduces *in vivo* tumor-initiating capacity of AR<sup>+</sup> breast cancer cells.** (A) Schematic figure illustrates the experimental design of orthotopic tumor models in the mammary fat pad (mfp) of NSG mice. Mice injected with doxycycline (Dox)-inducible vector constructed cells, pTRIPZ non-silencing (NS) or shSPDEF (SPDEF knockdown, KD) were pretreated with doxycycline in drinking water up to one week before cells were injected. pTRIPZ NS and shSPDEF cells were pretreated with Dox *in vitro* one week before the experiment was started. (B, C) Tumor weight was measured *ex vivo* when endpoint was reached. Either 1000, 10,000 or 100,000 cells of pTRIPZ NS or KD cells (B), or iT2 empty vector or SPDEF-overexpressing (OX) cells, were injected into mfp of mice (n= 6 mice/group). Whisker plots show all individual mice through their quartiles. P-value was calculated using an unpaired two-tailed t-test; \* p < 0.05, \*\* p < 0.01, \*\*\* p < 0.001; ns, not significant. Orthotopic injections into mfp of NSG mice were performed by Corinna Klein.

Next, I assessed the impact of SPDEF on growth of primary tumors in mice. Cells were injected into the mammary fat pad and tumor growth was followed by caliper measurements. SPDEF downregulation significantly impaired primary tumor growth compared to non-silencing control in BPE8 cells (Figure 16A, B). The experiment was terminated after 18 weeks when the pTRIPZ NS control group reached maximal tumor volume (Figure 16A). At this time point, shSPDEF tumor growth was reduced by 91.3%. Tumor weight was measured *ex vivo* and was 73.8% lower when SPDEF was downregulated relative to control tumor weights (Figure 16B, right). This observation could be validated using an additional AR<sup>+</sup> breast cancer cell model CTC223 (Figure 16C, D). Tumor growth was significantly reduced in mice injected with CTC223 shSPDEF cells compared to pTRIPZ NS control group (Figure 16C, D left). Final tumor volume was approx. 50% reduced in shSPDEF tumors as depicted in Figure 16D. Tumor weight was also significantly higher in control tumors in comparison to SPDEF downregulated-

tumors (Figure 16D, right). Based on these data, SPDEF acts pro-tumorigenic in AR<sup>+</sup> breast cancer models and downregulation of SPDEF significantly inhibits tumor growth *in vivo*.

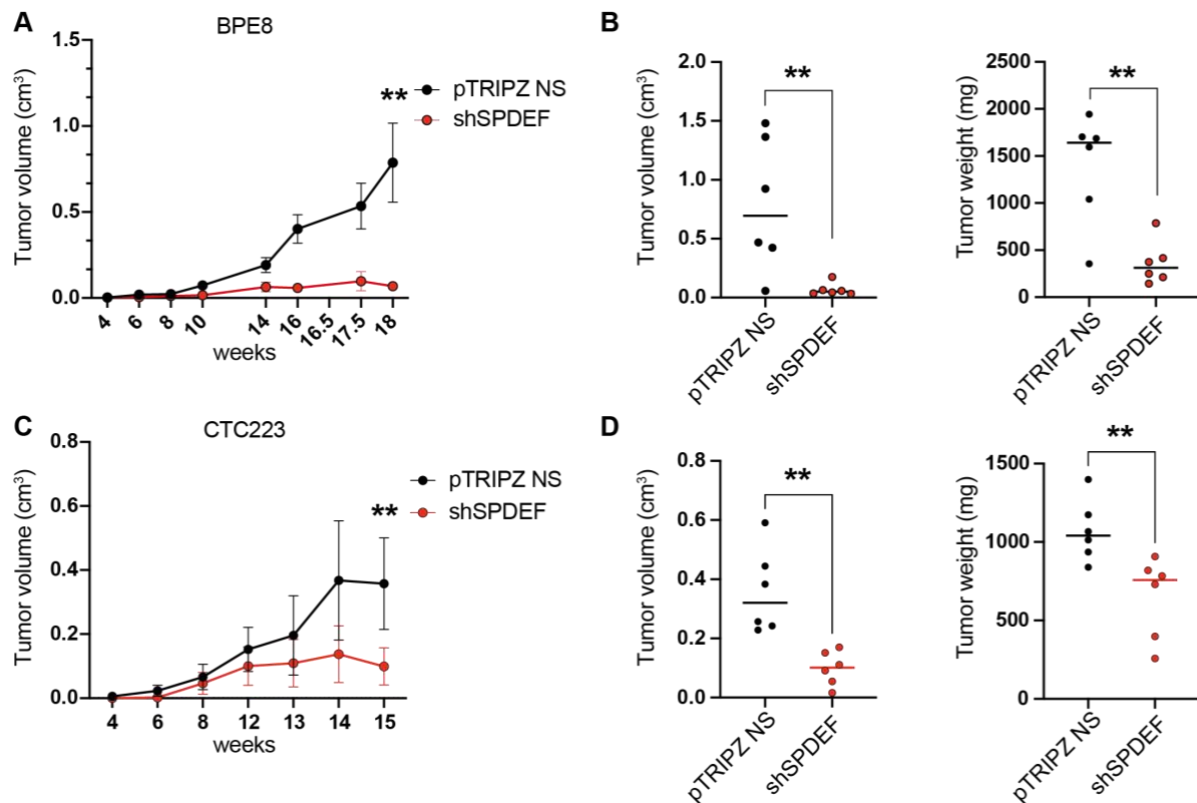


**Figure 16: SPDEF downregulation inhibits *in vivo* tumor growth in AR<sup>+</sup> breast cancer models.** (A) Growth followed over time of mammary fat pad (MFP) tumors generated from shSPDEF BPE8 and pTRIPZ non-silencing (NS) control BPE8 cells in NSG mice (n= 6 mice/group; 10,000 cells/mouse). Tumor volumes were measured by caliper. Error bars depict mean  $\pm$  SEM. Mann-Whitney U-test was used to calculate p-value as appropriate. (B) Bar chart depicts median of tumor volume at last time point of (A) (left). Tumor weight was measured *ex vivo* at endpoint; median is depicted (right). (C) Growth followed over time of MFP tumors generated from shSPDEF CTC223 and pTRIPZ NS CTC223 control cells in NSG mice (n= 6 mice/group). Error bars depict mean  $\pm$  SD. (D) Bar chart depicts median of tumor volume at last time point of (C) (left). Tumor weight was measured *ex vivo* at endpoint; median is depicted (right). P-value was calculated for the last time point using an unpaired two-tailed t-test; \* p < 0.05, \*\* p < 0.01, \*\*\* p < 0.001; ns, not significant.

Although overexpression of SPDEF did not affect tumor-initiation capacity and final tumor weight in TNBC AR<sup>+</sup> BPE8 cells (Figure 15C), primary tumor growth in the AR<sup>+</sup>, ER<sup>+</sup> CTC223 cell model was assessed upon SPDEF upregulation. Surprisingly, tumor growth was reduced when SPDEF was overexpressed compared to iT2 controls (Supplementary Figure 5A). In line, tumor volume and weight were significantly lower in the experimental group relative to control tumors (Supplementary Figure 5B). The same phenotype was observed in ER<sup>+</sup> CTC288 cells (Supplementary Figure 6). Whereas SPDEF downregulation significantly reduced tumor-initiation capacity within an *in vivo* limiting dilution assay (Supplementary Figure 6A), overexpression of SPDEF seemed to have similar impacts (Supplementary Figure 6B). Based

on these findings, I argue that balanced expression levels of SPDEF are critical in ER<sup>+</sup>/AR<sup>+/-</sup> breast cancer. Further, SPDEF functions might be different in the presence of ER<sup>75,136,214</sup>.

### 3.3.2 SPDEF knock-out inhibits *in vivo* tumor growth in AR<sup>+</sup> breast cancer model

SPDEF drives *in vivo* tumor growth of AR<sup>+</sup> breast cancer cells based on an Dox-inducible shRNA-mediated knockdown model. Since only one shRNA targeting *SPDEF* was used in previous *in vivo* experiments, I utilized CRISPR/Cas9 based gene editing to completely abolish SPDEF expression and assessed tumor growth upon SPDEF knock-out (KO). To this end, I used two guide RNAs (gRNAs) targeting *SPDEF* and a non-targeting (NT) control to electroporate AR<sup>+</sup> BPE8 cells. SPDEF protein expression was dramatically reduced in SPDEF KO#1 cells and completely abolished in SPDEF KO#2 cells relative to NT control which showed high endogenous expression levels (Figure 17A). Cells were injected orthotopically into the mammary fat pad of NSG mice and tumor growth was followed by caliper measurements. Figure 17B illustrates tumor growth over time in NT control and SPDEF KO#2 groups. Tumor growth was significantly inhibited upon abolishment of SPDEF expression. The experiment was terminated after 22 weeks when the NT control group reached maximal tumor volume. At this time point, very small tumors were palpable within the experimental group. Interestingly, SPDEF KO cells were lethal *in vitro* and could not be expanded. Over two passages, cells harboring SPDEF KO were lost (data not shown). Nonetheless, SPDEF KO cells formed tumors *in vivo* at a late time point. Cells injected into mice could not be sorted for SPDEF KO due to the lack of a reporter gene. A possible explanation for delayed tumor growth in the experimental group would be that few SPDEF wild-type cells grew out and formed tumors finally. Tumor volume and tumor weight were assessed *ex vivo* at the endpoint of the experiment. Both parameters were significantly decreased in SPDEF KO tumors compared to NT controls (Figure 17C, D). To conclude, I confirmed previous findings that SPDEF acts pro-tumorigenic in AR<sup>+</sup> breast cancer models utilizing an additional gene editing tool. CRISPR/Cas9-mediated SPDEF KO significantly inhibited *in vivo* tumor growth in AR<sup>+</sup> breast cancer cells.

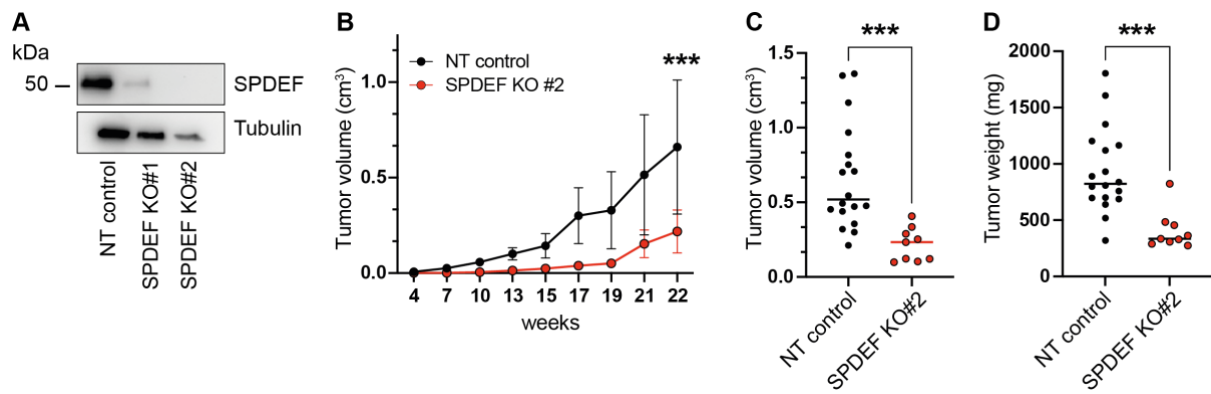


**Figure 17: SPDEF knock-out inhibits *in vivo* tumor growth in AR<sup>+</sup> breast cancer model.** (A) Representative western blot displays SPDEF protein expression in BPE8 non-targeting (NT) control, SPDEF knock-out (KO)#1 and SPDEF KO#2 cells. (B) Growth followed over time of MFP tumors generated from BPE8 SPDEF KO#2 and NT control cells in NSG mice (NT control, n= 20 mice/group; SPDEF KO#2, n= 10 mice/group; 10,000 cells/mouse). Error bars depict mean  $\pm$  SD. (C) Bar chart depicts median of tumor volume at last time point of (B). (D) Tumor weight was measured *ex vivo* at endpoint; median is depicted. P-value was calculated for the endpoint using a Mann-Whitney U-test; \* p < 0.05, \*\* p < 0.01, \*\*\* p < 0.001; ns, not significant.

### 3.3.3 SPDEF downregulation inhibits *in vivo* brain metastasis formation in AR<sup>+</sup> breast cancer model

To test whether SPDEF is involved in AR<sup>+</sup> breast cancer metastatic outgrowth into secondary tissues, pTRIPZ NS and shSPDEF BPE8 cells were implanted orthotopically into the mammary fat pad (mfp) of NSG mice, respectively. Tumor growth was followed by caliper measurements. In order to mimic the clinical setting realistically, primary tumors grown in mfp were resected once tumors reached volumes of 0.1-0.5 cm<sup>3</sup>. Tumor cell spread to secondary tissues was detected by *in vivo* bioluminescence measurements. At experimental endpoint, lungs and brains were resected and analyzed *ex vivo* by measuring total flux (photons/second). Downregulation of SPDEF impaired frequency of brain metastasis formation compared to pTRIPZ NS control cells. Whereas total flux was roughly 4.85 x 10<sup>6</sup> photons/s in brains from mice harboring tumors generated from pTRIPZ NS control cells, total flux was 94.65% reduced in brains from shSPDEF mfp tumor bearing mice. Due to loss of animals throughout the experiment, group size was limited and decreased statistical power (p-value = 0.0564).

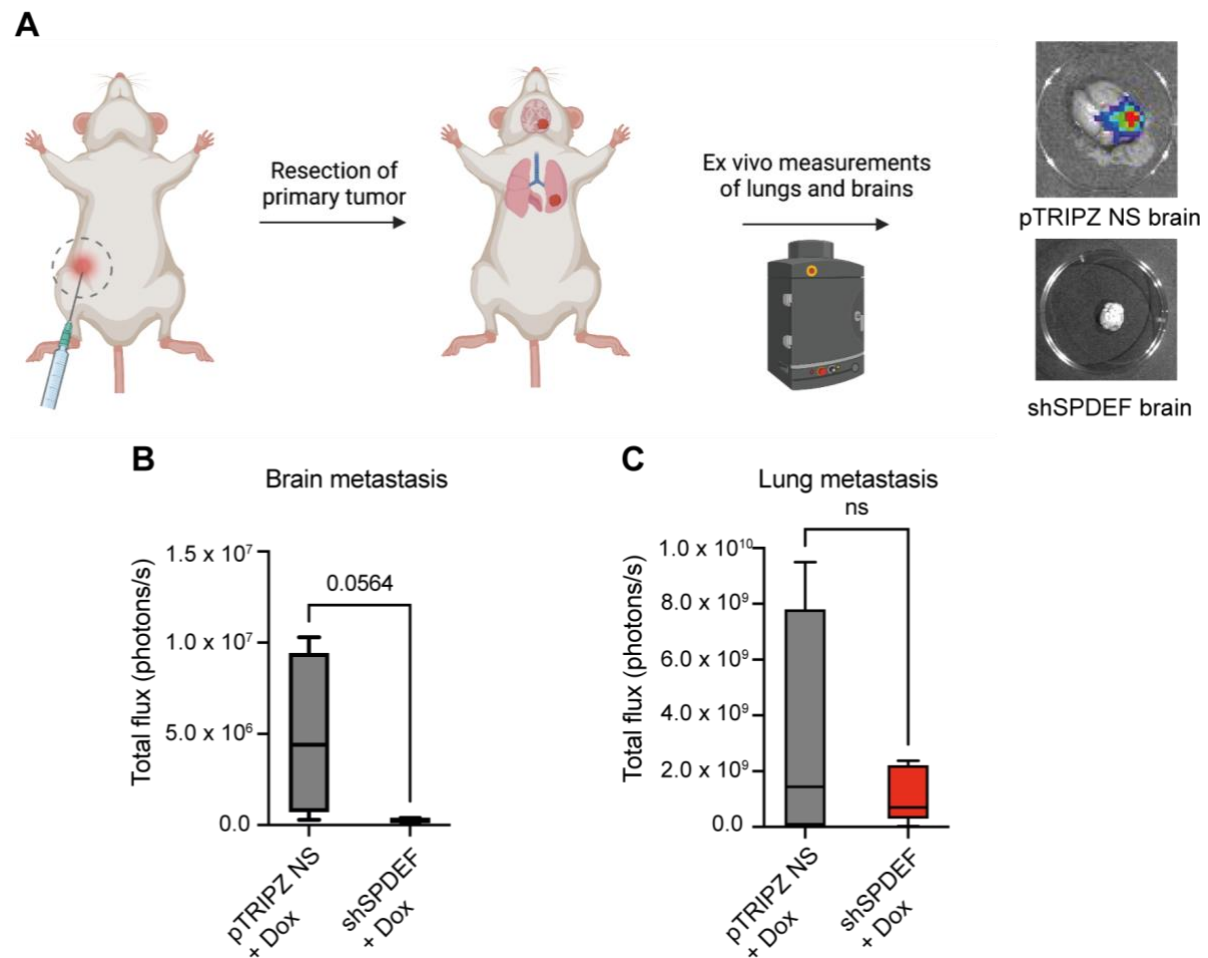


**Figure 18: SPDEF downregulation inhibits *in vivo* brain metastasis formation in AR<sup>+</sup> breast cancer model.**

(A) Schematic figure illustrates the experimental design of orthotopic tumor growth in the mammary fat pad (mfp) of NSG mice followed by primary tumor resection (n= 10 mice/group; 100,000 cells/mouse). Primary tumors were resected once volumes of 0.1-0.5 cm<sup>3</sup> were reached. Dissemination of breast cancer cells into secondary organs was assessed by bioluminescence measurements. At the experimental endpoint, lungs and brains of mice were harvested and measured *ex vivo* (pTRIPZ NS, n= 5; shSPDEF, n= 4). Illustrated is one representative brain from each group. Mice were pretreated with doxycycline in drinking water up to one week before cells were injected. pTRIPZ NS and shSPDEF cells were pretreated with Dox *in vitro* one week before the experiment was started. Brain (B) and lung (C) metastases were measured *ex vivo* when endpoint was reached given as total flux in photons/seconds (s). Whisker plots show min and max values through their quartiles. P-value was calculated using an unpaired two-tailed t-test; \* p < 0.05, \*\* p < 0.01, \*\*\* p < 0.001; ns, not significant.

In contrast, lungs of mice of both groups harbored breast cancer cells displaying a high total flux of 3.10 x 10<sup>9</sup> photons/s (in control lungs) and 1.15x10<sup>9</sup> photons/s (in shSPDEF lungs), respectively. Taken together, these data suggest that brain metastasis formation is impaired upon SPDEF downregulation whereas shSPDEF breast cancer cells are able to colonize the lungs.



### 3.3.4 SPDEF downregulation enhances *in vivo* tumor growth in AR<sup>-</sup> triple negative breast cancer model

Next, I asked whether SPDEF would have similar impact on *in vivo* tumor growth of AR<sup>-</sup> breast cancer cells. For this purpose, either BPE7 pTRIPZ NS or shSPDEF cells were injected into the mammary fat pad and tumor growth was followed by caliper and bioluminescence measurements. Strikingly, SPDEF downregulation significantly enhanced primary tumor growth compared to non-silencing control cells (Figure 19A). The experiment was terminated after 14.5 weeks when the experimental group reached maximal tumor volume of 1.5 cm<sup>3</sup>. Tumor growth was ~ 6.5-fold increased upon SPDEF knockdown (Figure 19B, left). Further, tumor weight was measured *ex vivo* and 79.4 % lower in the control group relative to shSPDEF tumors (Figure 19B, right).

This data suggests that SPDEF acts tumor-suppressive in the absence of AR expression. To validate this hypothesis, I assessed BPE7 tumor growth *in vivo* upon overexpression of SPDEF. Therefore, BPE7 SPDEF-overexpressing (OX) and respective iT2 empty vector control cells were implanted into mfp of NSG mice and tumor growth was followed by caliper measurements. In agreement with the prior experiment, tumor growth was significantly inhibited when SPDEF was overexpressed (Figure 19C). Tumor size was 90.5% decreased in the SPDEF OX group and tumor weight was significantly lower in those mice (Figure 19D). Taken together, these data show that SPDEF is a tumor suppressor in AR<sup>-</sup> TNBC cells and that the function of SPDEF might differ in dependence of the hormone receptors' status in breast cancer.

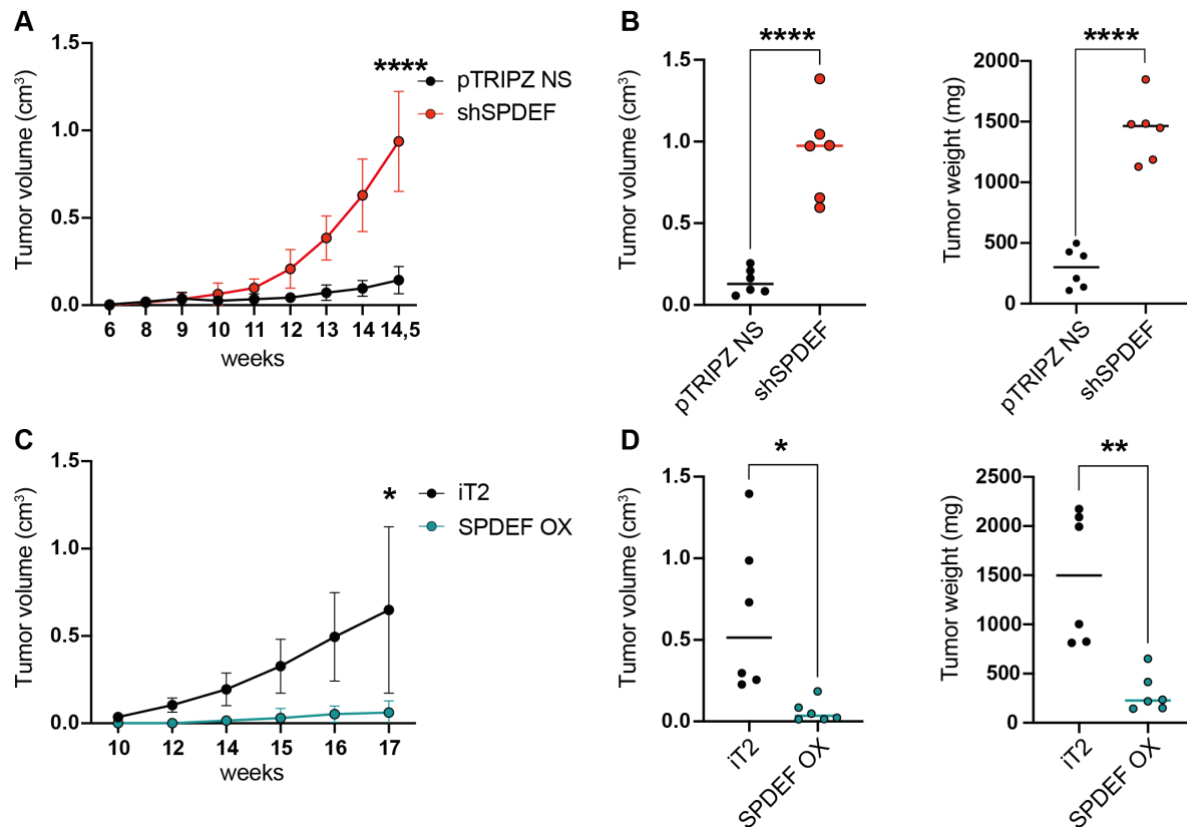


**Figure 19: SPDEF acts tumor-suppressive in AR<sup>+</sup> triple negative breast cancer BPE7 cells.** (A) Growth followed over time of mammary fat pad (MFP) tumors generated from shSPDEF BPE7 and pTRIPZ non-silencing (NS) control BPE7 cells in NSG mice (n= 6 mice/group; 10,000 cells/mouse). Tumor volumes were measured by caliper. Error bars depict mean  $\pm$  SD. (B) Bar chart depicts median of tumor volume at last time point of (A) (left). Tumor weight was measured *ex vivo* at endpoint; median is depicted (right). (C) Growth followed over time of MFP tumors generated from SPDEF-overexpressing (OX) BPE7 and iT2 empty vector control (iT2) BPE7 cells in NSG mice (n= 6 mice/group). Error bars depict mean  $\pm$  SD. (D) Bar chart depicts median of tumor volume at last time point of (C) (left). Tumor weight was measured *ex vivo* at endpoint; median is depicted (right). P-value was calculated for the last time point using an unpaired two-tailed t-test. (D, left) Mann-Whitney U-test was used to calculate p-value as appropriate; \* p < 0.05, \*\* p < 0.01, \*\*\* p < 0.001, \*\*\*\* p < 0.0001; ns, not significant.

### 3.4 Transcriptional profiling of SPDEF overexpression and knockdown breast cancer cell models

I aimed to identify the underlying mechanism how SPDEF drives tumor growth in AR<sup>+</sup> breast cancer, and the contradicting function of SPDEF in the absence of AR expression. To this end, I established transcriptional profiles of the SPDEF-overexpressing and shSPDEF PDX cell lines and respective controls using human-specific microarrays. I performed microarray-based gene expression analysis of at least three *in vitro* cell passages of each cell line including: SPDEF OX, iT2 control, shSPDEF and pTRIPZ NS cells of the lines BPE8, CTC288, CTC223 and

BPE7, respectively. For BPE8 and CTC288 cell lines, transcriptional profile analysis was extensively performed for ‘high’- and ‘low-intensity’ sorted cells for three cell passages each.

### 3.4.1 Gene expression-based analysis of AR<sup>+</sup> ER<sup>-</sup> BPE8 SPDEF overexpression and knockdown cell models

Principal component (PC) analysis separated BPE8 pTRIPZ NS control and shSPDEF cells from each other in PC2 by 26.9% (Figure 20A). Noticeably, RNA1 of each cell line was separated from RNA2 and RNA3 samples -irrespective whether SPDEF was downregulated. Hierarchical clustering did not separate samples into control and shSPDEF groups (data not shown). Differential gene expression analysis was applied to identify differentially regulated genes between the two groups and top variant genes are represented in volcano plot Figure 20B. Overall, roughly 280 genes were significantly ( $p$ -value < 0.05) deregulated upon SPDEF knockdown. The majority of differentially expressed genes were downregulated in shSPDEF cells. Interestingly, the fatty acid transporter *CD36* was the most upregulated gene displaying the highest positive fold change upon SPDEF knockdown (Figure 20B). In contrast, the glucose transporter encoded by the *SLC2A10* gene was downregulated in line with SPDEF expression. *SPDEF* gene itself was among the top 15 downregulated genes and served as internal control. Further, I identified several genes associated with hormone receptor (HR) signaling to be downregulated in shSPDEF cells including *SRARP*, *FGFR4*, *CREB3L1*, *CREB3L4* and *TFF3* among others (Figure 20B).

Principal component analysis in BPE8 SPDEF OX and iT2 control cell lines nicely separated the two groups from each other in PC2 (78.4%) (Figure 20C). Differential gene expression analysis clustered samples according to their groups but sort intensity (‘high’ and ‘low’) did not influence gene expression-based stratification (Supplementary Figure 7). Remarkably, many more genes were differentially regulated upon overexpression of SPDEF compared to the number of total variant genes in SPDEF knockdown cells relative to controls (Figure 20D). This might be due to the smaller variance between shSPDEF and control samples, in comparison to the variance between SPDEF OX and iT2 control. Nonetheless, many differentially regulated genes overlapped between the samples.

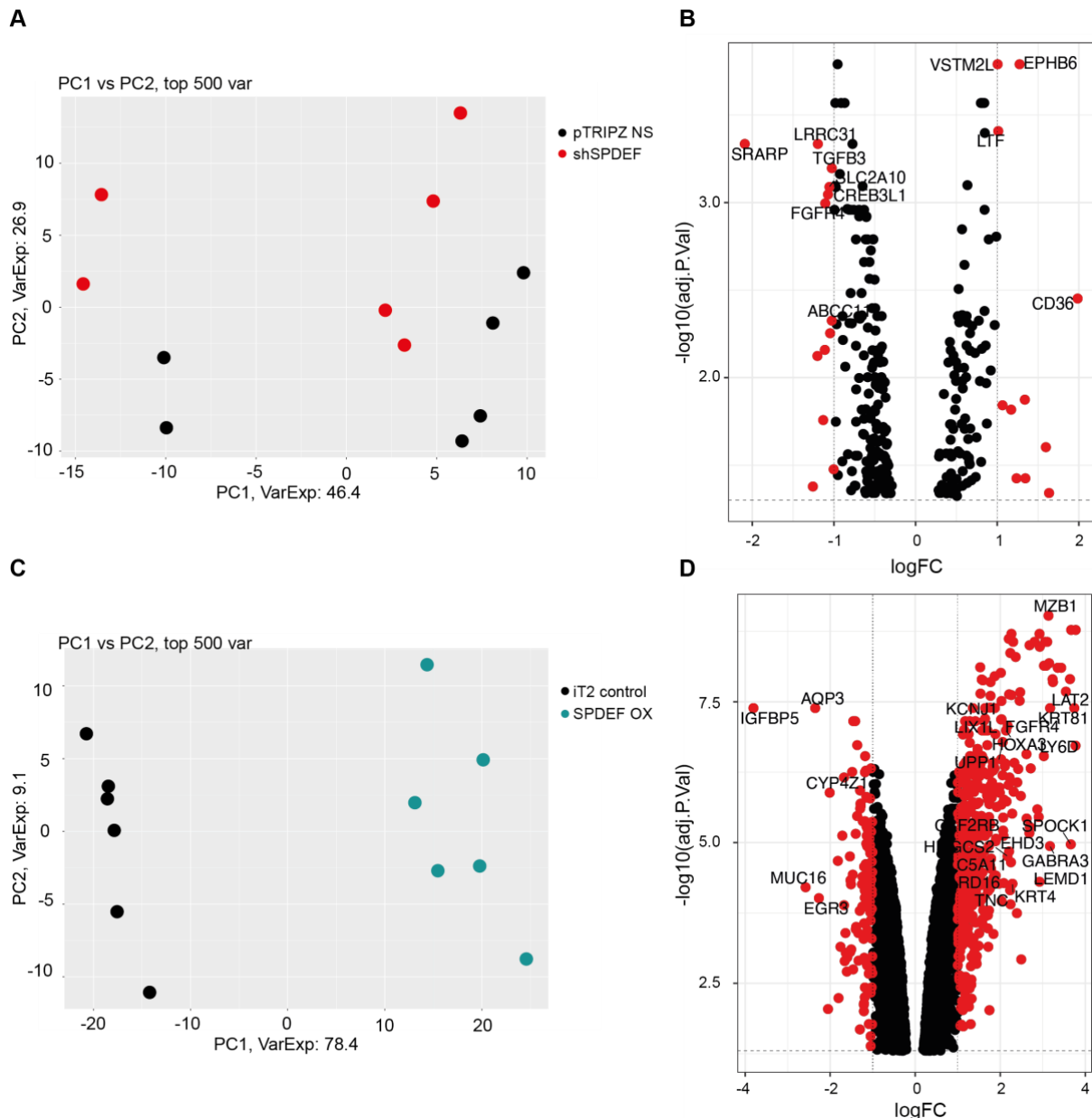


**Figure 20: Gene expression-based stratification of BPE8 SPDEF cell lines.** (A) Principal component (PC) analysis of BPE8 pTRIPZ non-silencing (NS) control and shSPDEF cells ( $n=6$  samples/group). Cells were treated with doxycycline for at least one week before RNA was extracted. Four samples on the left represent RNA1 ‘high/low’-intensity sorted of each sample. Percentage indicates proportion of variance explained by each component. (B) Volcano plot represents all significant differentially expressed genes between BPE8 pTRIPZ NS control and shSPDEF cells. Highlighted in red are all genes with an adjusted p-value  $< 0.05$  and log-fold change (FC)  $> 1$ . Annotated are all genes with an adjusted p-value  $< 0.005$ . (C) PCA of BPE8 iT2 empty vector control (iT2) and SPDEF-overexpressing (OX) cells ( $n=6$  samples/group). (D) Volcano plot represents all significant differentially expressed genes between BPE8 iT2 control and SPDEF OX cells. Highlighted in red are all genes with an adjusted p-value  $< 0.05$  and log-fold change (FC)  $> 1$ . Annotated are all genes with an adjusted p-value  $< 0.005$ .

In order to get an overview which genes and subsequent pathways were deregulated upon overexpression or downregulation of SPDEF, I performed Gene Set Enrichment Analysis (GSEA) of the two experimental and respective control groups (Figure 21). GSEA revealed genes involved in fatty acid and glycerolipid metabolism to be enriched upon SPDEF OX

(Figure 21A). Vice versa, hallmark of glycolysis was negatively associated in shSPDEF cells relative to the control (Figure 21C). Overall, I found many metabolic pathways and associated signaling pathways regulating cell metabolism to be deregulated in SPDEF OX and knockdown cell lines (Supplementary Figure 10). ‘PI3K/AKT/mTOR Signaling’ and ‘mTORC1 Signaling’ both, were significantly downregulated in shSPDEF cells relative to the control (Supplementary Figure 10A). In addition, ‘Purine and Pyrimidine Metabolism’ was downregulated in shSPDEF cells (Supplementary Figure 10B).

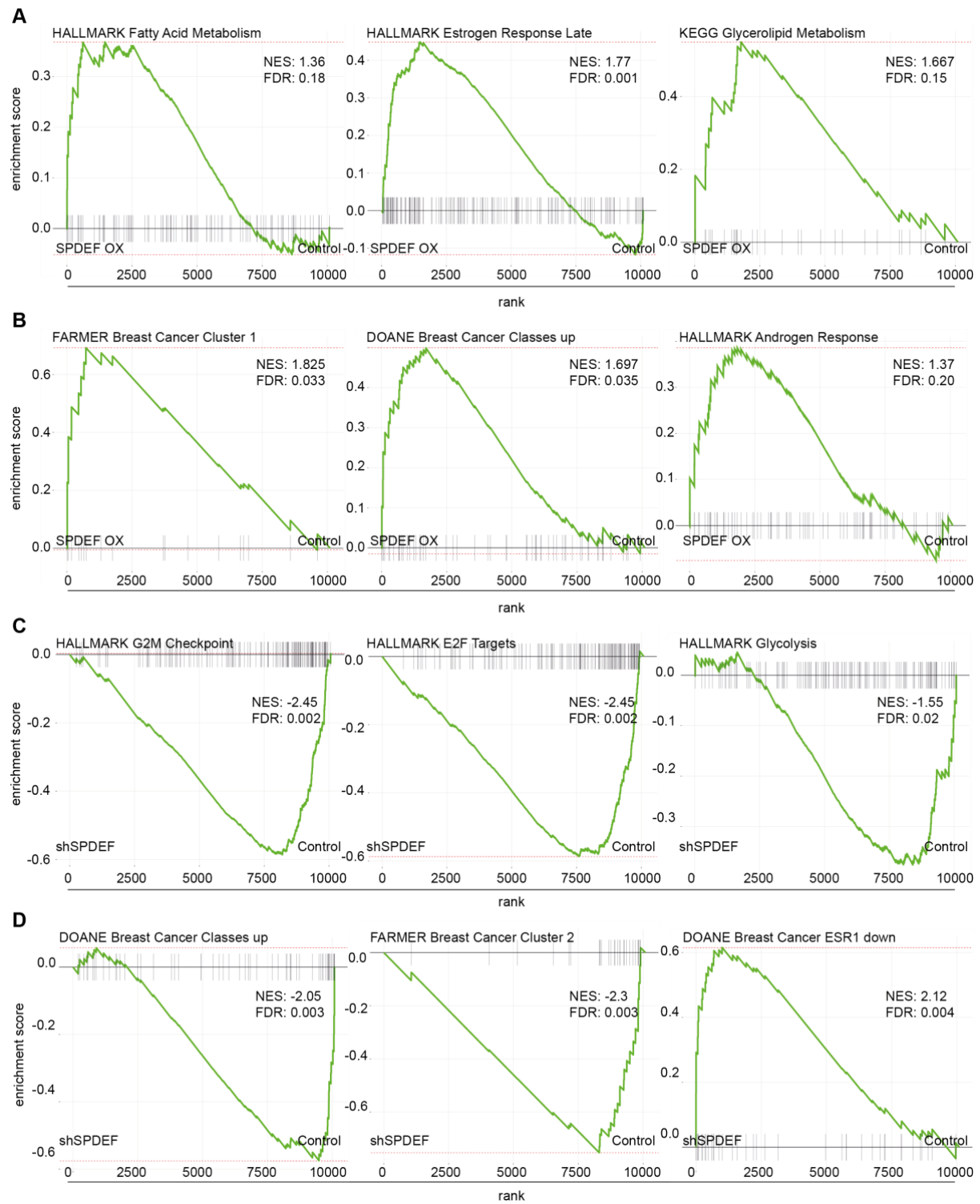


**Figure 21: Gene Set Enrichment Analysis of BPE8 SPDEF-overexpressing and shSPDEF cells compared to respective controls.** (A, B) Gene Set Enrichment Analysis (GSEA) of BPE8 SPDEF-overexpression (OX) and iT2 empty vector control (Control) samples (n= 3/group). (C, D) GSEA of BPE8 shSPDEF and pTRIPZ non-silencing control (Control) samples (n= 3/group). Statistical significance was assessed using 10,000 permutations on the phenotype. All differentially expressed genes were pre-ranked based on t-value. NES, normalized enrichment score; FDR, false discovery rate.

Strikingly, previously curated gene sets (C2) ‘FARMER Breast Cancer Cluster’ and ‘DOANE Breast Cancer Classes up’ were enriched in SPDEF-overexpressing cells (Figure 21B). In

contrast, enrichment scores of these gene sets were significantly decreased upon downregulation of SPDEF (Figure 21D). These gene sets encompass genes upregulated in a subset of ER<sup>-</sup> PR<sup>-</sup> breast tumors that display molecular similarity to luminal tumors, relative to the rest of ER<sup>-</sup> PR<sup>-</sup> samples. In addition, this gene signature significantly overlaps with the androgen-induced transcriptional program in AR<sup>+</sup> MDA-MB-453 cells. Contra vise, genes downregulated in *ESR1*-expressing breast tumors relative to *ESR1* negative tumors are included in the gene set ‘DOANE Breast Cancer ESR1 down’ that is enriched in shSPDEF cells. These data validate that SPDEF regulates gene sets associated with the molecular apocrine subtype of breast cancer. In agreement, ‘Hallmark Androgen Response’ was found to be decreased in shSPDEF cells relative to control (Supplementary Figure 10A, left panel).

### 3.4.2 Gene expression-based analysis of AR<sup>+</sup> ER<sup>+</sup> CTC223 SPDEF overexpression and knockdown cell models

Similar to previously described SPDEF OX samples, principal component analysis (PCA) separated CTC223 SPDEF OX models from control samples in PC2 (62.2%) (Figure 22A). Differentially expressed genes between SPDEF OX and iT2 control cells are illustrated in Figure 22B. Similar genes as found in the BPE8 cell line were differentially regulated upon overexpression of SPDEF including AR-associated genes *SRARP* and *TFF3*, and the glucose transporter *SLC2A10*. Further, *ERBB4* encoding the HER4 receptor and mammaglobin marker genes *SCGB1D2* and *SCGB2A2* were among the top targets upregulated in SPDEF OX cells. Of high interest, I found that the fatty acid transporter *CD36* was among the top ten downregulated genes in agreement with previous findings in BPE8 cells. In addition to *CD36*, expression of other genes encoding metabolic enzymes and proteins, namely *KYNU*, *CYP4Z1* and *RARRES1* among others, was significantly deregulated. SPDEF knockdown samples were separated from the control group in PC2 (58%) within PCA (Figure 22C). Differentially expressed gene analysis in CTC223 shSPDEF cells confirmed *SLC2A10* and *SCGB2A2* genes’ expression to be decreased upon downregulation of SPDEF (Figure 22D). Again, detection of decrease in *SPDEF* gene expression served as internal control.

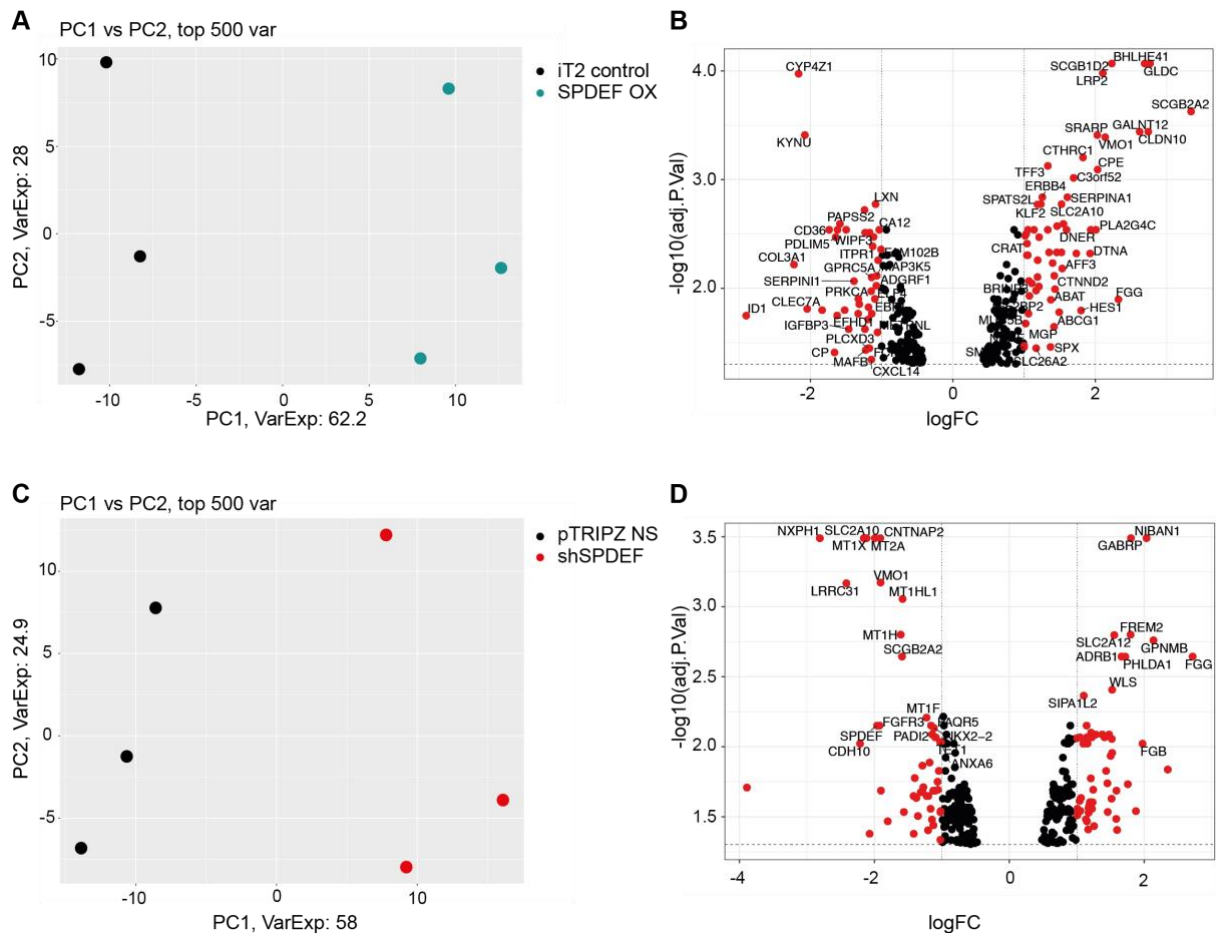


**Figure 22: Gene expression-based stratification of CTC223 SPDEF cell lines.** (A) Principal component (PC) analysis of CTC223 iT2 empty vector (iT2) control and SPDEF-overexpressing (OX) cells ( $n=3$  samples/group). Percentage indicates proportion of variance explained by each component. (B) Volcano plot represents all significant differentially expressed genes between CTC223 iT2 control and SPDEF OX cells. Highlighted in red are all genes with an adjusted  $p$ -value  $< 0.05$  and log-fold change (FC)  $> 1$ . Annotated are all genes with an adjusted  $p$ -value  $< 0.005$ . (C) PCA of CTC223 pTRIPZ non-silencing (NS) control and shSPDEF cells ( $n=3$  samples/group). Cells were treated with doxycycline for one week before RNA was harvested. (D) Volcano plot represents all significant differentially expressed genes between CTC223 pTRIPZ NS control and shSPDEF cells. Highlighted in red are all genes with an adjusted  $p$ -value  $< 0.05$  and log-fold change (FC)  $> 1$ . Annotated are all genes with an adjusted  $p$ -value  $< 0.005$ .

Similar differentially expressed genes as in BPE8 cells suggested that similar pathways would be deregulated. GSEA confirmed that metabolic pathways including gluconeogenesis and glycolysis, and oxidative phosphorylation (OxPhos) were enriched in shSPDEF CTC223 cells (Figure 23A and Supplementary Figure 11C). Further, I observed that energy production pathways such as ATP and NADH production were negatively enriched upon SPDEF downregulation (Figure 23B). In line with increased OxPhos gene set enrichment, ‘Myc Targets V1’ were enriched upon downregulation of SPDEF (Supplementary Figure 11C). Vice versa, ‘Hallmark Glycolysis’ was increased in SPDEF OX cells relative to iT2 control (Supplementary Figure 11A). AR-associated curated gene sets namely ‘FARMER Breast Cancer’ and ‘DOANE



Breast Cancer' were found to be highly enriched in agreement with previous findings (Figure 23C and Supplementary Figure 11B)<sup>89,90</sup>.

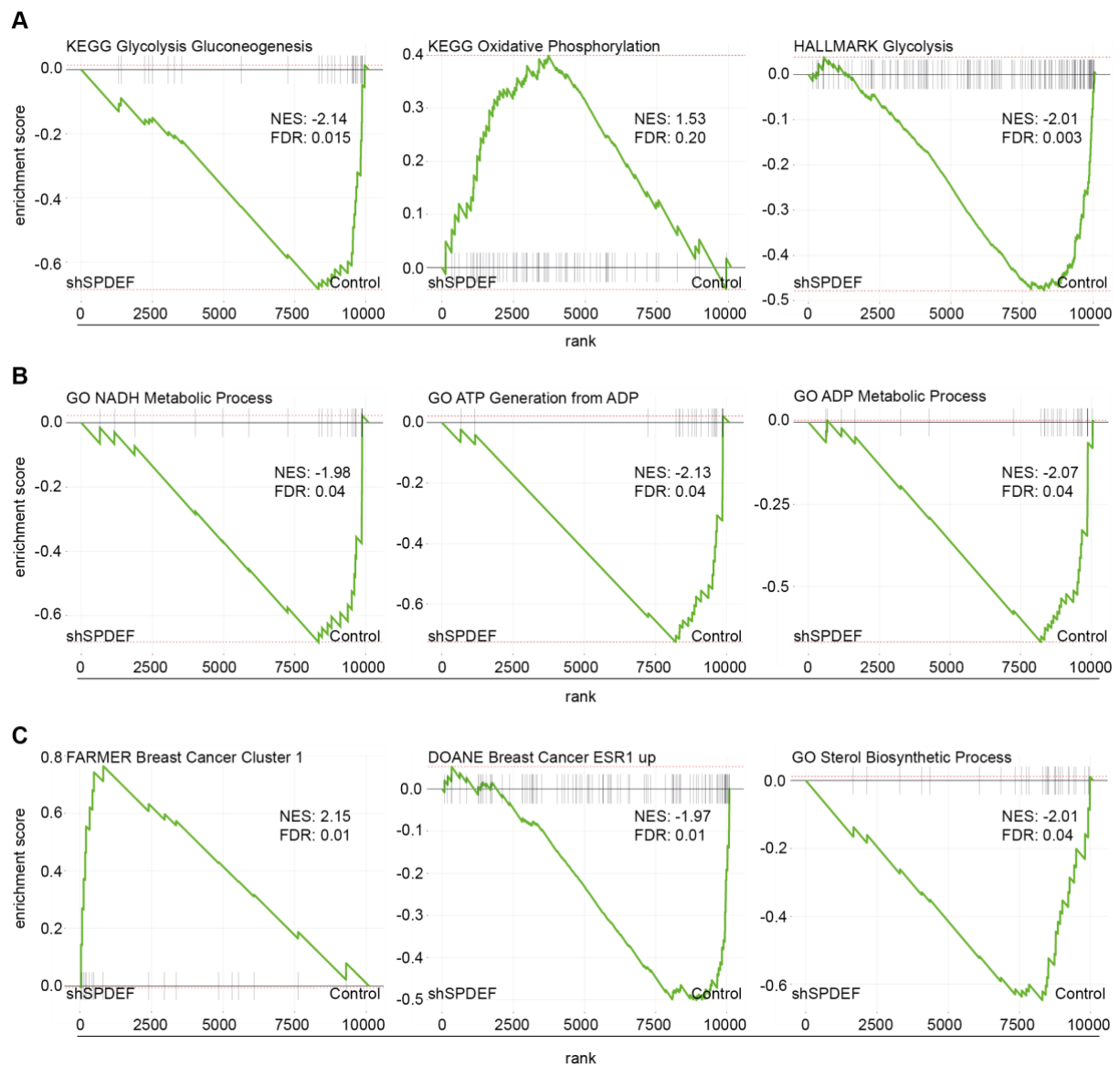


**Figure 23: Gene Set Enrichment Analysis of CTC223 shSPDEF cells compared to pTRIPZ non-silencing control.** Gene Set Enrichment Analysis (GSEA) between two groups: CTC223 shSPDEF and pTRIPZ non-silencing (Control) (n= 3/group). (A) KEGG and Hallmark pathways. (B) Gene Ontology (GO) gene sets. (C) C2 curated gene sets. Statistical significance was assessed using 10,000 permutations on the phenotype. All differentially expressed genes were pre-ranked based on t-value. NES, normalized enrichment score; FDR, false discovery rate.

### 3.4.3 Gene expression-based analysis of AR<sup>-</sup> ER<sup>+</sup> CTC288 SPDEF overexpression and knockdown cell models

PCA highly separated SPDEF-overexpressing samples from controls in CTC288 cells in PC2 (82.9%) (Supplementary Figure 8A). Hierarchical clustering also separated the samples into SPDEF OX and iT2 control groups based on top 100 variant genes (data not shown). Performing differential gene expression analysis, this was accompanied by many significant differentially expressed genes upon overexpression of SPDEF (data not shown). On first sight, top target genes were quite different from targets found in AR<sup>+</sup> BPE8 and CTC223 cell models.

In shSPDEF samples, RNA extracted from ‘low-intensity’ sorted cells clustered closer to pTRIPZ non-silencing control samples in PCA (Supplementary Figure 8C, left panel). For this reason, ‘low-intensity’ sorted samples were removed from analysis and PCA was re-analyzed separating shSPDEF cells from controls in PC2 (64%) (Supplementary Figure 8C, right panel). Differential gene expression analysis revealed more genes to be differentially expressed in CTC288 cells upon downregulation of SPDEF in comparison to BPE8 and CTC223 cell lines (Supplementary Figure 8B). Furthermore, similar SPDEF target genes were identified as in AR<sup>+</sup> cell models.

Running GSEA, I noticed that similar pathways were also enriched in luminal CTC288 cells as found in the molecular apocrine models (Supplementary Figure 14). OxPhos gene sets were positively enriched upon SPDEF downregulation as previously observed for the CTC223 cell model as well (Supplementary Figure 14B). Several cell metabolism-regulating signaling pathways were negatively enriched in shSPDEF cells relative to control. In line with reduced *in vivo* tumor growth upon SPDEF overexpression but also knockdown, same pathways were negatively enriched in both experimental groups relative to respective controls. Namely those were ‘Myc Targets’ and ‘mTORC1 signaling’ both, which are implemented in regulating cell metabolism (Supplementary Figure 12 and Supplementary Figure 14). Moreover, gene sets describing the molecular apocrine phenotype were negatively enriched in SPDEF knockdown cells compared to non-silencing control, although CTC228 cells are negative for AR expression (Supplementary Figure 13).

### 3.4.4 Gene-expression based analysis of luminal (like) – HR<sup>+</sup> SPDEF overexpression and knockdown cell models

BPE8 and CTC223 are both AR<sup>+</sup> cell lines making them more luminal-like compared to quadruple negative or basal-like breast cancer<sup>89–91</sup>. CTC288 are AR<sup>-</sup> but ER<sup>+</sup> and thus derived from luminal breast cancer. I found similarities in their transcriptional profiles between all three afore-mentioned cell lines and subsequent GSEA revealed similar pathways to be deregulated upon SPDEF overexpression or knockdown, respectively. Also, *in vivo* tumor growth was significantly inhibited when SPDEF was downregulated in all three cell lines. I aimed to identify their common features leading to the pro-tumorigenic function observed *in vivo*. For this reason, I performed an overall differential gene expression analysis including all ('high-sorted') shSPDEF and pTRIPZ NS samples of BPE8, CTC223 and CTC288 models. As expected, hierarchical clustering separated the samples based on their origin according to cell lines (Figure 24A). Variance expression in sPC1 and sPC2 was quite similar and separated CTC288, CTC223 and BPE8 in a comparable distance to each other. Hierarchical clustering based on top 100 variant genes separated samples also according to cell lines' background (Figure 24B). Within the cell line groups, RNA samples of pTRIPZ NS control cells clustered apart from shSPDEF cells, with exception of BPE8 cells. For the latter, no stratification could be observed based on SPDEF expression applying unsupervised clustering analysis – as stated in previous analysis for single cell lines.

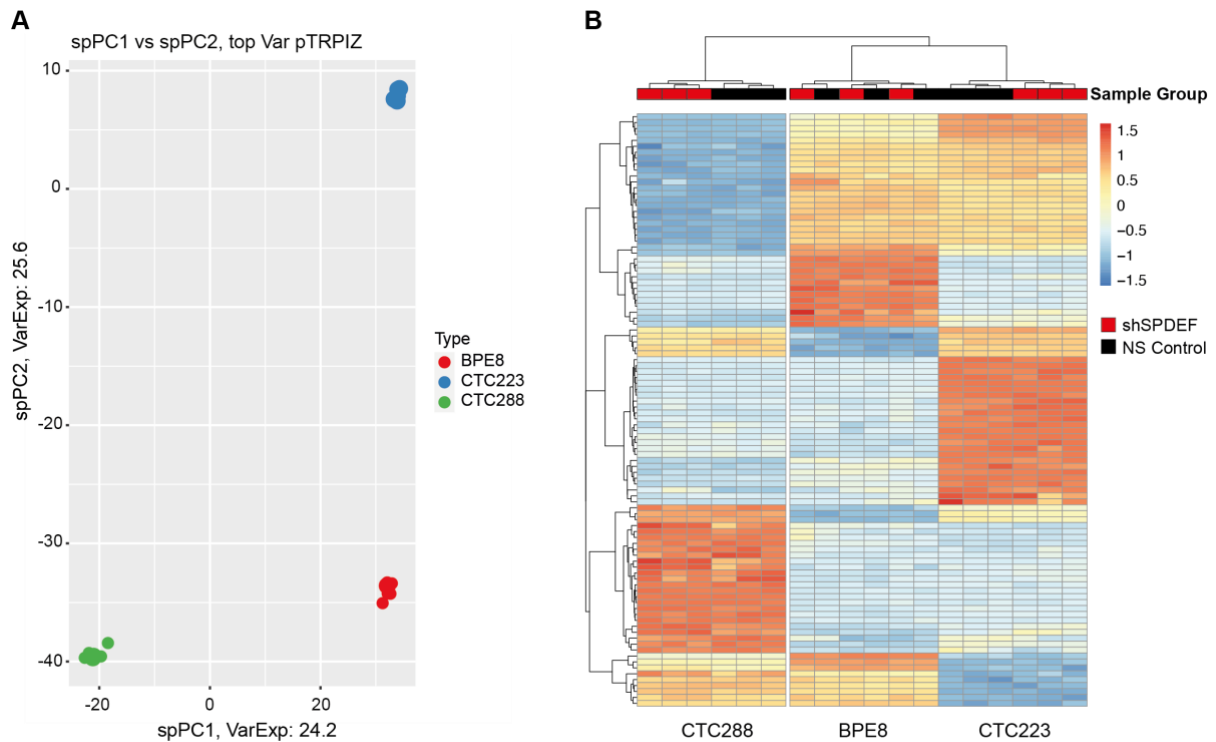


**Figure 24: Top variant gene stratification of pTRIPZ non-silencing and shSPDEF samples of CTC288, CTC223 and BPE8 cell lines.** (A) Principal component (PC) analysis of pTRIPZ non-silencing (NS) and shSPDEF samples of CTC288, CTC223 and BPE8 cell lines separates cells based on cell lines' origin (n=3 samples/group/cell line). Percentage indicates proportion of variance explained by each component. (B) Unsupervised, hierarchical clustering separated samples based on cell line background and SPDEF expression with exception of BPE8 samples. Same samples as in (A).

With the help of Dr. Felix Geist, we applied background correction such that we could analyze differences based on downregulation of SPDEF and identified differentially regulated genes in all three cell lines (Figure 25A). As observed in previous analysis, AR-associated targets such as *CREB3L4* were significantly downregulated in line with SPDEF expression (Figure 25A). The glucose transporter gene *SLC2A10* was among the top three significant differentially regulated genes whereas the fatty acid transporter *CD36* was one of the top three upregulated genes displaying the highest fold change.

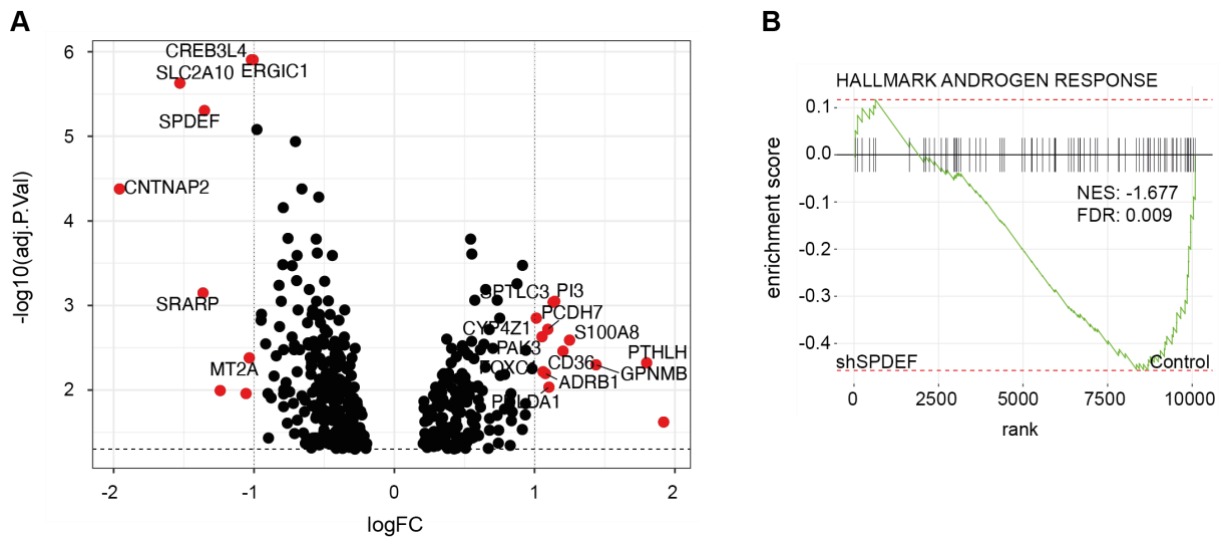


**Figure 25: Differentially expressed genes between shSPDEF and control cells of BPE8, CTC223 and CTC288 models.** (A) Volcano plot represents all significant differentially expressed genes (DEG) between pTRIPZ NS control and shSPDEF cells performing DEG analysis for BPE8, CTC223 and CTC288 cell lines applying background correction. Highlighted in red are all genes with an adjusted p-value < 0.05 and log-fold change (FC) > 1. Annotated are all genes with an adjusted p-value < 0.005. (B) Gene set enrichment analysis was performed detecting ‘Hallmark Androgen Response’ to be negatively enriched in shSPDEF cells relative to pTRIPZ NS (Control). Statistical significance was assessed using 10,000 permutations on the phenotype. All differentially expressed genes were pre-ranked based on t-value. NES, normalized enrichment score; FDR, false discovery rate.

Subsequent GSEA revealed ‘Androgen Response’ (Figure 25B) and AR-associated curated gene sets ‘FARMER Breast Cancer Cluster 2’ and ‘DOANE Breast Cancer ESR1 up’ among others to be downregulated in SPDEF knockdown (shSPDEF) cells relative to pTRIPZ NS control (Figure 26). This was in agreement with pathways found to be enriched in single cell line-analyses.

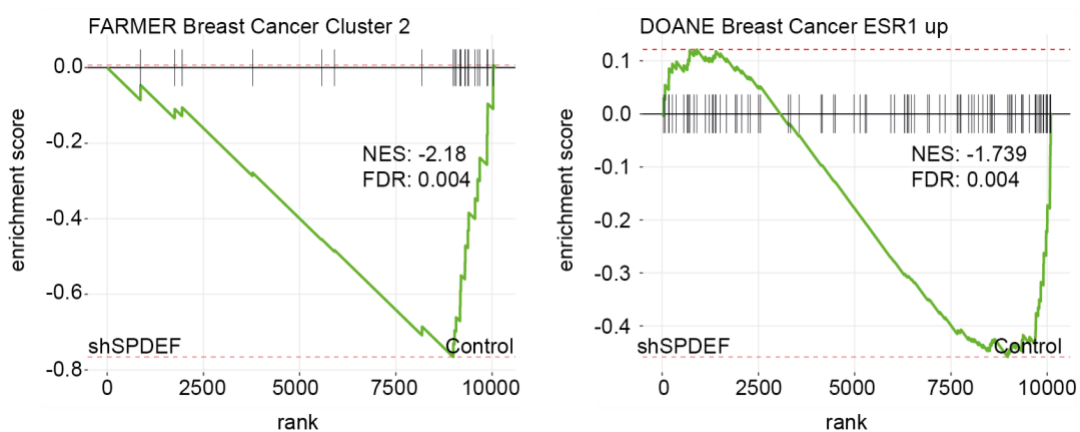


**Figure 26: AR-associated curated gene sets (C2) are negatively enriched in shSPDEF cells of BPE8, CTC223 and CTC288 relative to controls.** Gene Set Enrichment Analysis (GSEA) performed for shSPDEF cell lines of BPE8, CTC223 and CTC288 compared to pTRIPZ non-silencing controls revealed metabolic gene sets to be mainly negatively enriched upon SPDEF downregulation. Statistical significance was assessed using 10,000 permutations on the phenotype. All differentially expressed genes were pre-ranked based on t-value. NES, normalized enrichment score; FDR, false discovery rate.

In addition, plenty of metabolic gene sets namely ‘Carbohydrate Biosynthetic Process’, ‘Glucose Metabolic Process’, ‘Glycolysis and Gluconeogenesis’, ‘ATP Generation from ADP’ and ‘NADH Metabolic Process’ among others were found to be downregulated in shSPDEF cells (Figure 27 and Supplementary Figure 15). In contrast, ‘KEGG Tryptophan Metabolism’ was positively associated with low SPDEF levels which is in agreement with the previous finding that the *KYNU* gene encoding the enzyme kynureninase was significantly downregulated in SPDEF OX cells.

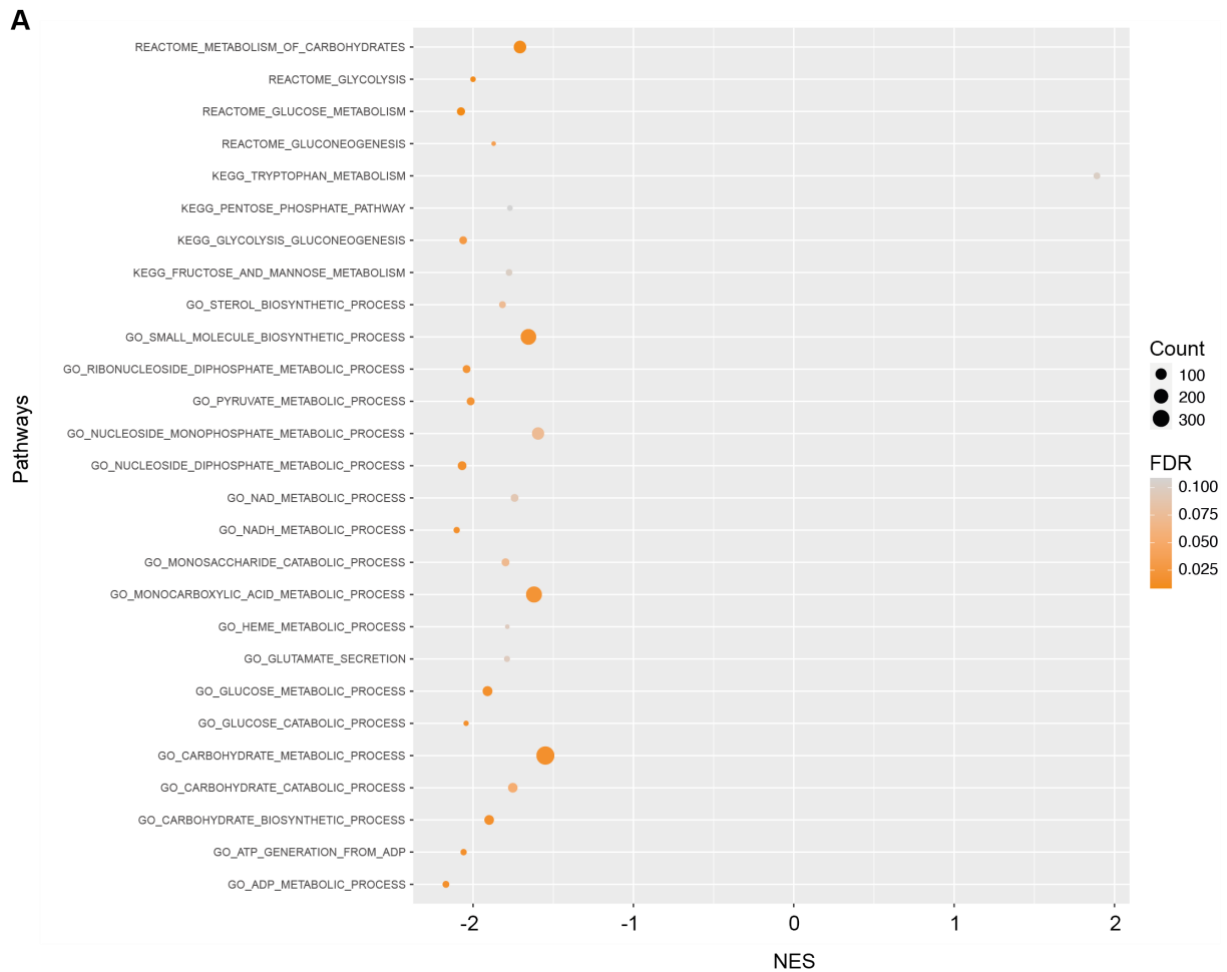


**Figure 27: Metabolic gene sets enriched in shSPDEF cells relative to control of BPE8, CTC223 and CTC288 cell models.** (A) Gene Set Enrichment Analysis (GSEA) performed for shSPDEF cell lines of BPE8, CTC223 and CTC288 compared to pTRIPZ non-silencing controls revealed metabolic gene sets to be mainly negatively enriched upon SPDEF downregulation. Statistical significance was assessed using 10,000 permutations on the phenotype. All differentially expressed genes were pre-ranked based on t-value. NES, normalized enrichment score; FDR, false discovery rate.

### 3.4.5 Gene expression-based analysis of AR<sup>-</sup> TNBC BPE7 SPDEF overexpression and knockdown cell models

In AR<sup>-</sup> TNBC BPE7 cells, endogenous SPDEF levels were rather low. Nonetheless, further downregulation of SPDEF by shRNA dramatically enhanced *in vivo* tumor growth in these cells. SPDEF OX significantly inhibited tumor growth of BPE7 cells. These data suggested that SPDEF would act as a tumor suppressor gene in the absence of AR and ER.

To investigate whether SPDEF has different roles in breast cancer dependent on its hormonal background, I established transcriptional profiles for both, AR<sup>+</sup> and AR<sup>-</sup> breast cancer models. In the PCA, SPDEF OX BPE7 cells were highly separated from control cells in PC2 (87.5%) (Figure 28A). Hierarchical clustering based on top 100 variant genes also separated the samples into the same two groups, SPDEF OX and controls, respectively (data not shown). I performed differential gene expression analysis for the two groups and found almost 1000 genes to be significantly deregulated (p-value < 0.05) (Figure 28B). As previously observed in CTC223 SPDEF OX cells, mammaglobin marker genes SCGB1D2 and SCGB2A1 were among the top targets upregulated upon overexpression of SPDEF (Figure 28B). In line with AR<sup>+</sup> cell lines, AR targets *TFF1* and *TFF3* were upregulated when SPDEF was high. However, I could not detect *CREB3L4* gene expression in BPE7 cells based on microarray analysis.

PCA of shSPDEF and pTRIPZ NS control samples separated shSPDEF RNA3 apart from RNA4 and RNA5 in PC2 (51.4%). RNA3 was more similar to pTRIPZ NS RNA samples (1-3) in PC1 (26.6%) than to the other shSPDEF replicates (Supplementary Figure 9A). Unsupervised, hierarchical clustering separated samples in similar manner: shSPDEF RNA3 clustered with pTRIPZ NS control RNA3-5 samples (Supplementary Figure 9B). This observation suggested that SPDEF was not properly downregulated in the cells of which RNA3 was extracted. As mentioned earlier, downregulation of SPDEF *in vitro* was quite heterogenous such that I decided to exclude RNA3 from the subsequent bioinformatical analysis. When RNA3 was removed from both groups, PCA highly separated the samples into two groups: shSPDEF and pTRIPZ NS in PC2 (93.9%) (Figure 28C). Hierarchical clustering according to the top 100 variant genes also separated the samples into the same clusters (data not shown). Of high interest, differential gene expression analysis between both groups identified the fatty acid transporter gene *CD36* to be opposingly regulated in BPE7 cells compared to the AR<sup>+</sup> cell lines, BPE8 and CTC223 (Figure 28D). *CD36* gene expression was significantly downregulated

upon SPDEF knockdown whereas *CD36* was upregulated in shSPDEF BPE8 and CTC223 cells relative to respective controls.

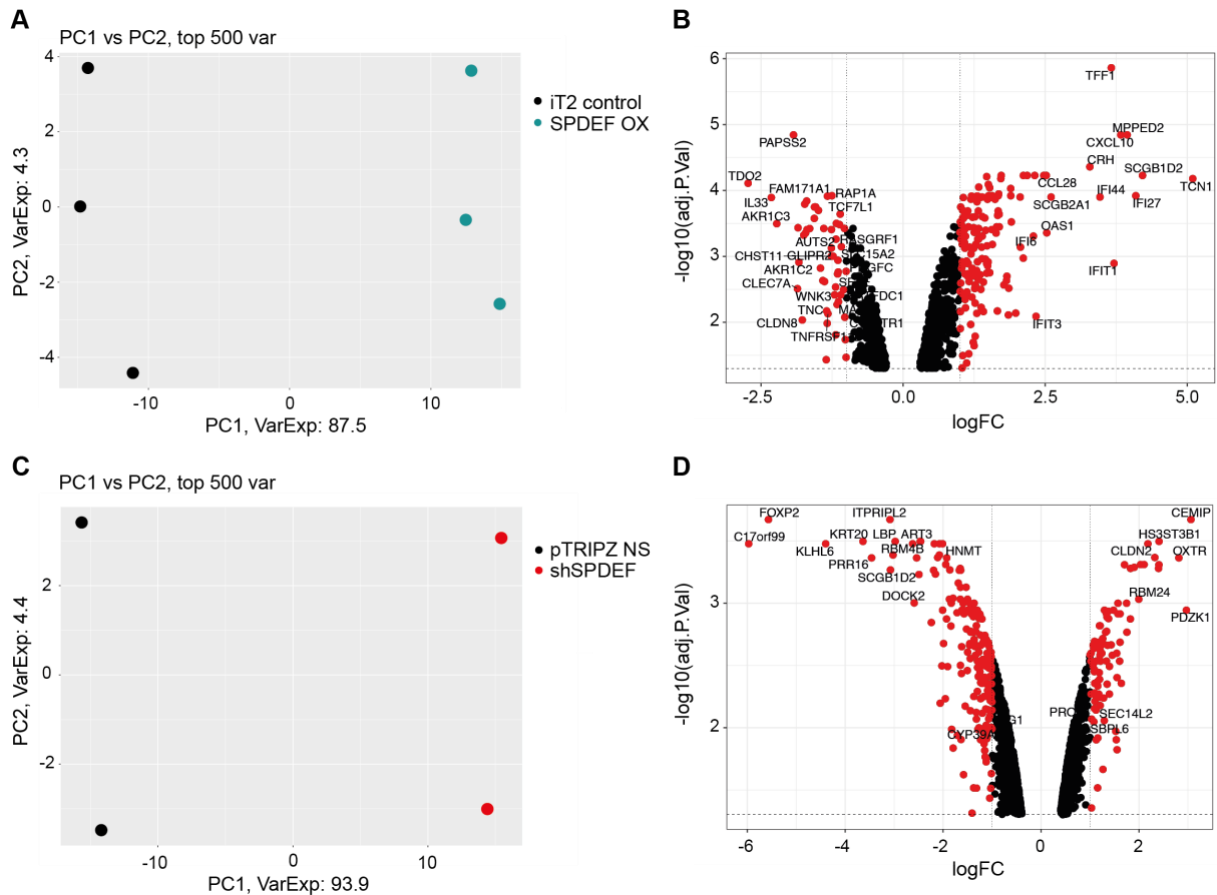


**Figure 28: Gene expression-based stratification of BPE7 SPDEF cell lines.** (A) Principal component (PC) analysis of BPE7 iT2 empty vector (iT2) control and SPDEF-overexpressing (OX) cells ( $n=3$  samples/group). Percentage indicates proportion of variance explained by each component. (B) Volcano plot represents all significant differentially expressed genes between BPE7 iT2 control and SPDEF OX cells. Highlighted in red are all genes with an adjusted p-value  $< 0.05$  and log-fold change (FC)  $> 1$ . Annotated are all genes with an adjusted p-value  $< 0.005$ . (C) PCA of BPE7 pTRIPZ non-silencing (NS) control and shSPDEF cells ( $n=2$  samples/group). Cells were treated with doxycycline for one week before RNA was harvested. (D) Volcano plot represents all significant differentially expressed genes between BPE7 pTRIPZ NS control and shSPDEF cells. Highlighted in red are all genes with an adjusted p-value  $< 0.05$  and log-fold change (FC)  $> 1$ . Annotated are all genes with an adjusted p-value  $< 0.005$ .

GSEA revealed that AR-associated gene sets ‘FARMER Breast Cancer Cluster 1’, ‘DOANE Breast Cancer Classes up’ and ‘FARMER Breast Cancer Apocrine vs Luminal’ were downregulated in SPDEF knockdown cells as observed for all cell models, irrespective of AR status (Figure 29). Vice versa, these gene sets’ expression levels were significantly decreased in SPDEF OX cells (Supplementary Figure 16C). This suggests that genes included in these gene sets are likely to be regulated by SPDEF independent of AR expression.



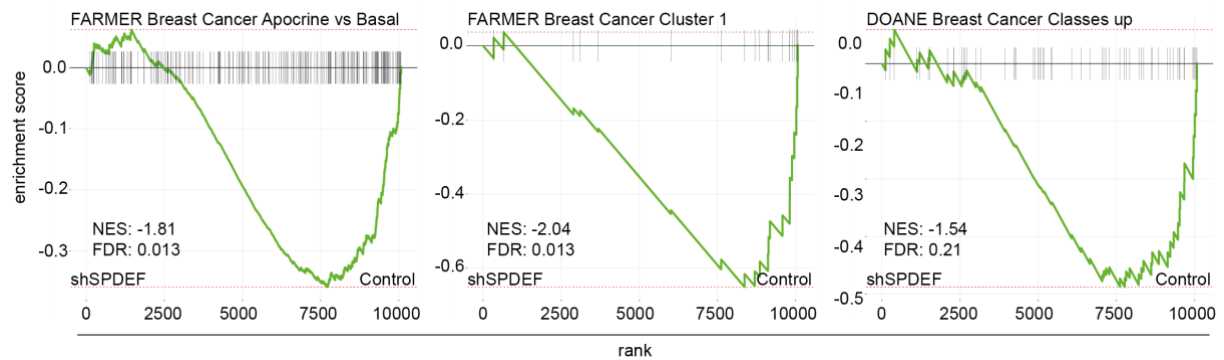


**Figure 29: AR-associated curated gene sets are negatively enriched in BPE7 shSPDEF cells relative to non-silencing control.** Gene Set Enrichment Analysis (GSEA) for C2 curated gene sets between BPE7 shSPDEF and pTRIPZ non-silencing control (Control) cells (n=3/group). Statistical significance was assessed using 10,000 permutations on the phenotype. All differentially expressed genes were pre-ranked based on t-value. NES, normalized enrichment score; FDR, false discovery rate.

In agreement with reduced tumor growth, SPDEF OX was associated with decreased levels in hallmark ‘E2F Targets’ and ‘G2M checkpoint’ (Supplementary Figure 16B). Further, I discovered that ‘Interferon Alpha Response’ and ‘Interferon Gamma Response’ were highly enriched upon SPDEF overexpression suggesting that also other pathways not found in AR<sup>+</sup> cell models might be associated with the observed phenotype of AR<sup>-</sup> BPE7 cells (Supplementary Figure 16A). Vice versa, interferon alpha and gamma signaling pathways were found to be negatively enriched in BPE7 SPDEF knockdown cells (Figure 30A). In BPE7 SPDEF knockdown cells, OxPhos gene sets were enriched when SPDEF was downregulated (Figure 30B). OxPhos gene set enrichment was accompanied by an increase of ‘Myc targets V1’ in BPE7 shSPDEF cells (Figure 30B, right panel). This was observed for CTC223 cells previously. However, in case of BPE7 cells, SPDEF knockdown significantly enhanced *in vivo* tumor formation suggesting that these cells may rely on *c-Myc* oncogenic-signaling. Furthermore, sugar metabolism-associated gene sets namely ‘KEGG Starch and Sucrose Metabolism’ and ‘KEGG Amino Sugar and Nucleotide Sugar Metabolism’ were decreased in SPDEF knockdown cells.

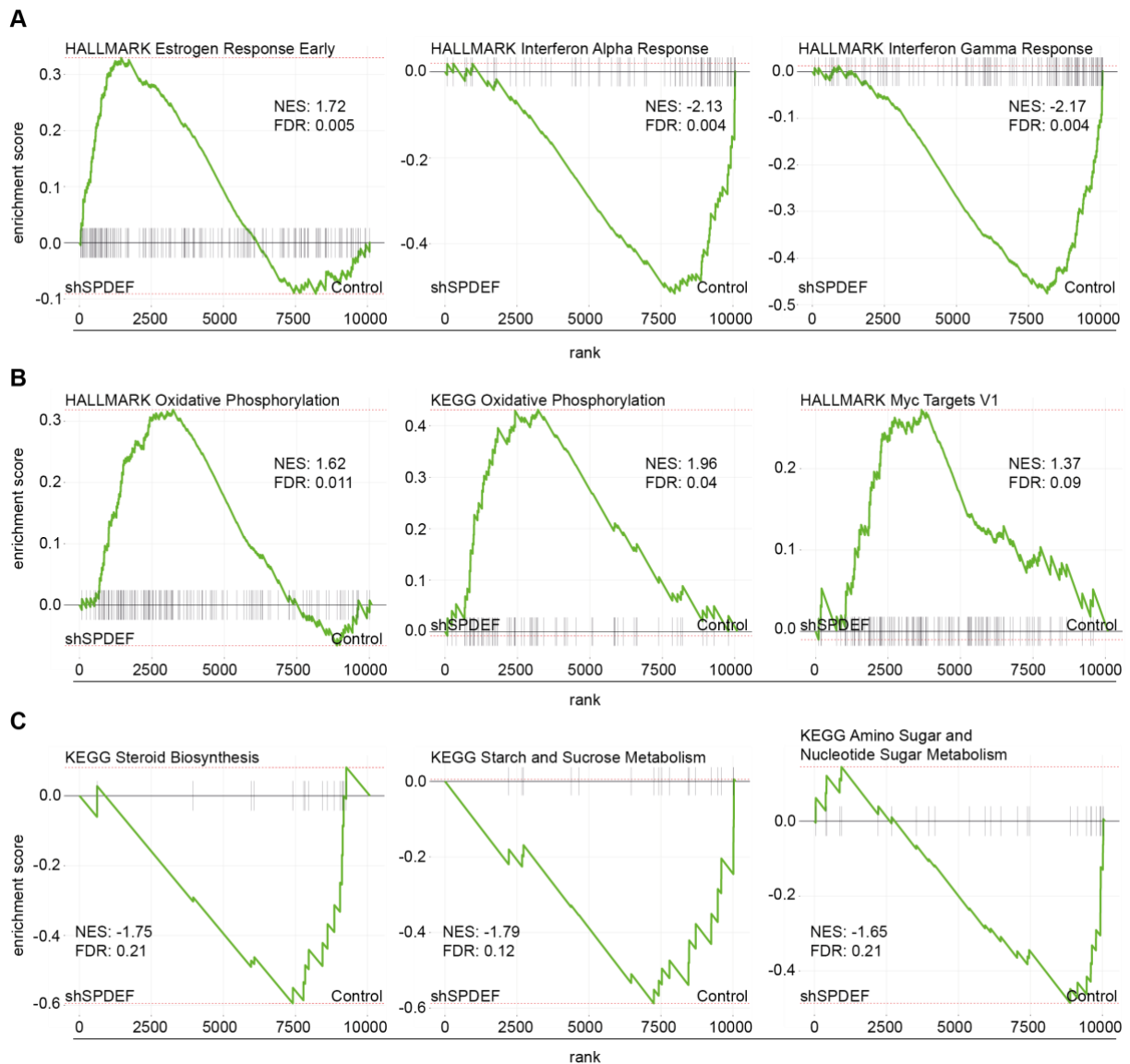


**Figure 30: Gene Set Enrichment Analysis of BPE7 shSPDEF cells relative to non-silencing control.** Gene Set Enrichment Analysis (GSEA) between BPE7 shSPDEF and pTRIPZ non-silencing control (Control) cells (n=3/group). Statistical significance was assessed using 10,000 permutations on the phenotype. All differentially expressed genes were pre-ranked based on t-value. (A, B) HALLMARKS gene sets. (C) KEGG pathways gene sets. NES, normalized enrichment score; FDR, false discovery rate.

### 3.5 Transcriptional profiling of AR<sup>+</sup> and AR<sup>-</sup> PDX tumors upon SPDEF downregulation

Transcriptional profiling of *in vitro* PDX cell models was performed to investigate the underlying mechanism of altered tumor growth upon SPDEF downregulation. Subsequent GSEA revealed that AR signaling and metabolic pathways were deregulated upon SPDEF overexpression and knockdown, respectively. However, cell culture *in vitro* conditions might

be different from the *in vivo* tumor microenvironment. Studying the metabolic profile of cancer cells might be difficult using artificial *in vitro* cell culture approaches. To investigate whether reprogramming of cell metabolism and/or disruption of AR signaling might be responsible for altered *in vivo* tumor growth in the mammary fat pad of NSG mice, I performed tissue microarray analysis of BPE8 AR<sup>+</sup> and BPE7 AR<sup>-</sup> PDX tumors upon SPDEF downregulation. In the PCA, BPE7 SPDEF knockdown samples were separated from control tumors in PC2 (51.8%) (Supplementary Figure 17A, left). Similar findings were noted for BPE8 shSPDEF tumors which were separated from controls in PC2 (52.8%) (Supplementary Figure 17A, right). Hierarchical clustering based on top 100 variant genes also separated the samples into shSPDEF and pTRIPZ NS tumors in both cell models, BPE7 and BPE8 (Supplementary Figure 17B). Differential gene expression analysis was performed comparing knockdown and control cells followed by GSEA. Downregulation of *SPDEF* was confirmed in BPE8 shSPDEF tumors relative to controls (data not shown). In BPE7 samples, *SPDEF* mRNA was not detected by tissue microarray analysis most likely because endogenous expression was already low. GSEA in AR<sup>+</sup> BPE8 tumors discovered similar gene sets to be enriched as previously found *in vitro*: fatty acid metabolism was decreased in shSPDEF tumors relative to controls (Figure 31B). In agreement, AR signaling-associated gene sets were downregulated in SPDEF knockdown models (Figure 31A). Contra vise, several signaling pathways known to regulate cell metabolism were enriched in shSPDEF tumors in comparison to controls, namely mTOR and PI3K/AKT signaling pathways and Myc V1 targets (data not shown).

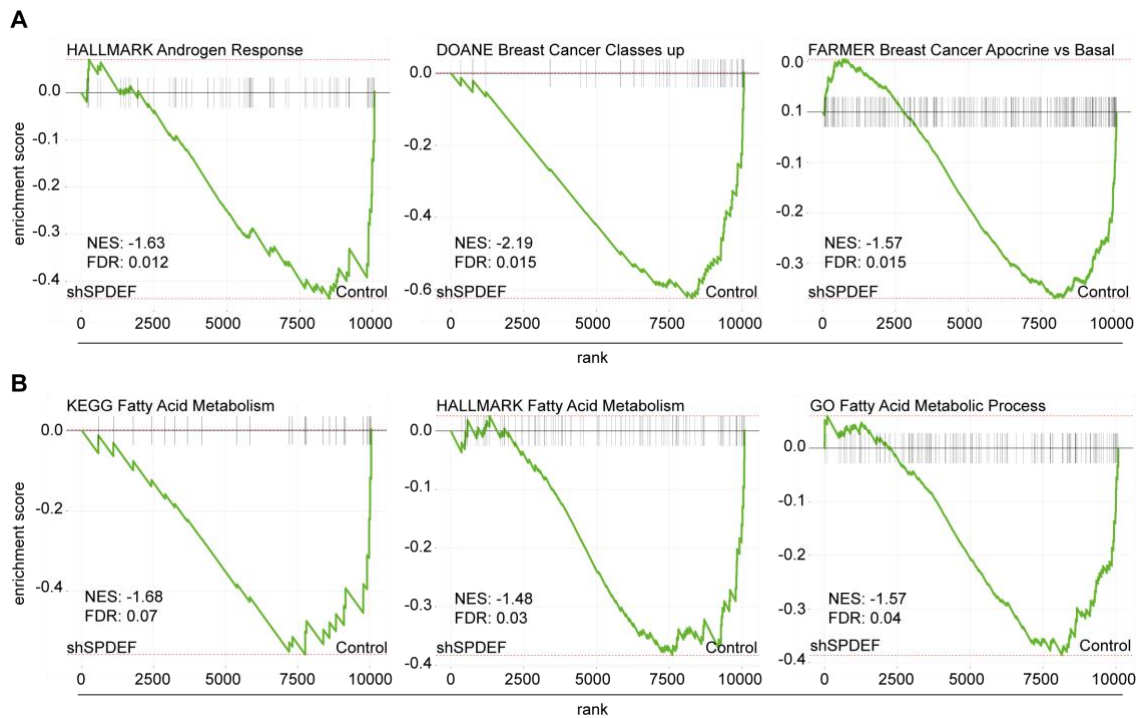


**Figure 31: Gene Set Enrichment Analysis of BPE8 shSPDEF tumors relative to controls.** Gene Set Enrichment Analysis (GSEA) between BPE8 shSPDEF and pTRIPZ non-silencing control (Control) tumors (n=4/group). Statistical significance was assessed using 10,000 permutations on the phenotype. All differentially expressed genes were pre-ranked based on t-value. (A) AR signaling-associated gene sets. (B) Fatty acid metabolism gene sets. NES, normalized enrichment score; FDR, false discovery rate.

GSEA in AR<sup>-</sup> BPE7 tumors revealed glycolysis, pentose phosphate pathway and fructose metabolism to be highly upregulated when SPDEF was downregulated enhancing tumor growth (data not shown). Of high interest, gene sets ‘glucose metabolic process’, ‘ATP generation from ADP’, and ‘NADH metabolic process’ among others were significantly increased in shSPDEF tumors relative to controls, opposing to what has been found for tumors derived from AR<sup>+</sup> BPE8 cells (Figure 32).

Taken together, these findings argue that fatty acid metabolism and AR signaling was significantly decreased *in vitro* and *in vivo* upon SPDEF downregulation in BPE8 AR<sup>+</sup> breast cancer model. BPE7 shSPDEF tumors were enriched for glucose and energy metabolic processes relative to controls. In addition, these data nicely show that *in vitro* cultures reflect *in vivo* transcriptional profiles.

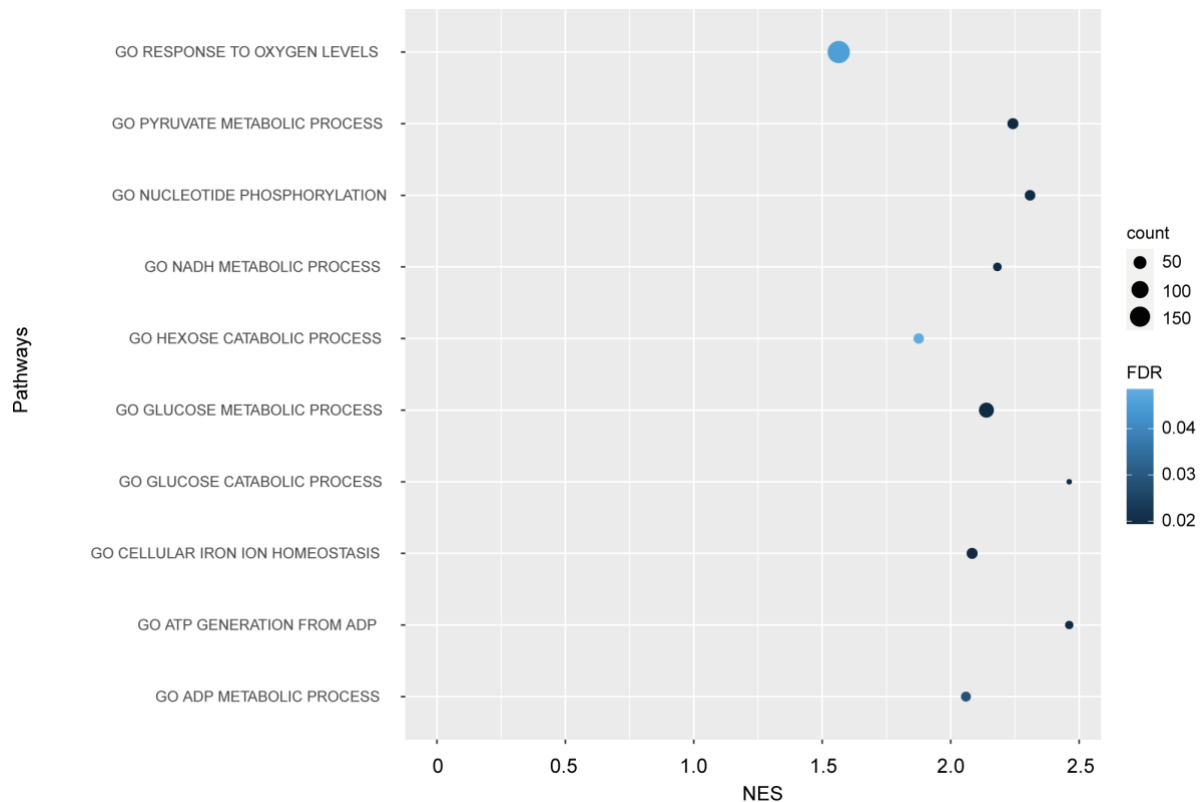


**Figure 32: Metabolic gene sets enriched in BPE7 shSPDEF tumors relative to controls.** (A) Gene Set Enrichment Analysis (GSEA) performed for BPE7 shSPDEF tumors compared to pTRIPZ non-silencing controls revealed metabolic gene sets to be positively enriched upon SPDEF downregulation. Statistical significance was assessed using 10,000 permutations on the phenotype. All differentially expressed genes were pre-ranked based on t-value. NES, normalized enrichment score; FDR, false discovery rate.

### 3.6 SPDEF and AR signaling

Gene expression analysis based on microarray data nominated AR target genes to be differentially expressed in SPDEF OX and shSPDEF cells relative to controls. Subsequent GSEA revealed that AR response and AR-associated curated gene sets (e.g. ‘FARMER Breast Cancer’ and ‘DOANE Breast Cancer’) were positively enriched in SPDEF OX and vice versa downregulated in knockdown cell lines. To further elucidate interaction of SPDEF and AR in AR<sup>+</sup> breast cancer cells, gene expression of AR and its targets was validated upon SPDEF overexpression, knockdown or CRISPR/Cas9-mediated knock-out, respectively. To analyze this interaction further from the side of the AR, I established transcriptional profiles for SPDEF and targets upon pharmacological activation or inhibition of AR, or genetic deletion of AR mediated by CRISPR/Cas9 gene editing.

### 3.6.1 SPDEF regulates AR and its target genes in AR<sup>+</sup> breast cancer cells

To further investigate the interaction of SPDEF and AR signaling, I analyzed the expression of AR target genes in SPDEF OX and shSPDEF cells by RT-qPCR analysis. Opposing to *SPDEF* expression, *AR* transcript levels were slightly downregulated upon overexpression of SPDEF relative to iT2 control in AR<sup>+</sup> BPE8 and CTC223 cells (Figure 33A, C). As expected, this was not observed in AR<sup>-</sup> BPE7 cells (Figure 33E). In agreement, *AR* expression was upregulated in shSPDEF cells in BPE8 and CTC223 cell models but also in BPE7 cells (Figure 33B, D, F). Surprisingly, this could not be validated in AR<sup>+</sup> MDA-MB-453 cells (Supplementary Figure 18A). Gene expression of AR targets *CREB3L4* and *TFF3* was decreased in shSPDEF cells and increased upon SPDEF overexpression in all cell lines, BPE8, CTC223, BPE7 and MDA-MB-453 (Figure 33 and Supplementary Figure 18A). *PIP* and *XBPI* expression were downregulated in shSPDEF AR<sup>+</sup> cell lines, BPE8, CTC223 and MDA-MB-453, but not in AR<sup>-</sup> BPE7 cells (Figure 33B, D, F and Supplementary Figure 18A). The hormone receptor-associated transcription factor *FOXAI* was only found to be downregulated in MDA-MB-453 cells in which *AR* gene expression was unchanged (Supplementary Figure 18A). *ERBB2* gene expression is often associated with AR expression in breast cancer<sup>89,90</sup>. In agreement, I also found high co-expression of *AR* and *ERBB2* mRNA in patients using the METABRIC data set (Figure 10A). For this reason, I assessed *ERBB2* transcript levels in shSPDEF and SPDEF OX cells. However, I could not observe major changes on RNA level in any cell line (Figure 33 and Supplementary Figure 18A).

Taken together, these data suggest that SPDEF reciprocally regulates *AR* gene expression in a negative manner. However, AR target genes were deregulated in line with SPDEF expression.

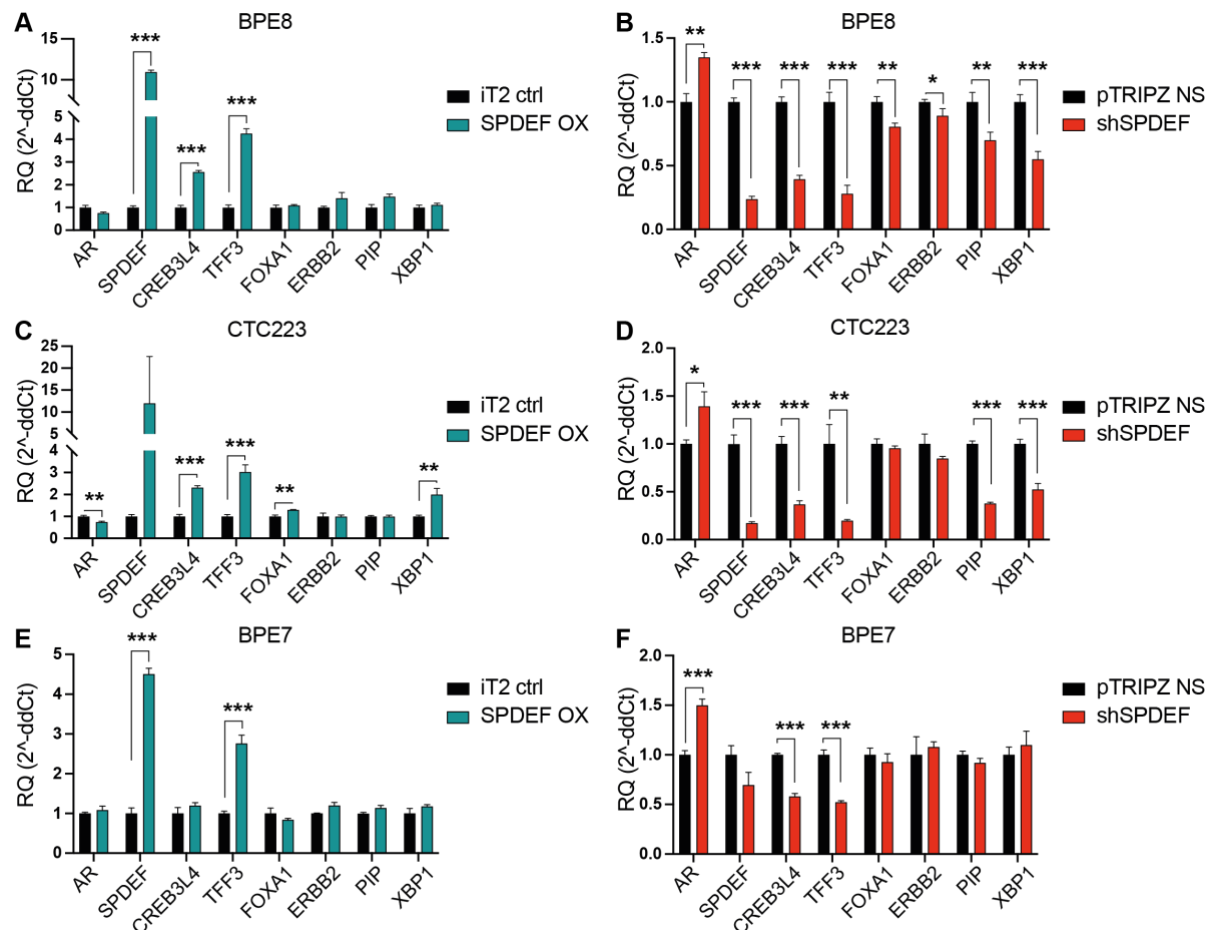


**Figure 33: AR target genes validation in BPE8, CTC223 and BPE7 SPDEF overexpression and knockdown cell models.** (A) Representative RT-qPCR analysis of AR target genes in BPE8 SPDEF-overexpressing (OX) and iT2 empty vector control (iT2) cells; (B) in BPE8 shSPDEF and pTRIPZ non-silencing (NS) control cells; (C) in CTC223 SPDEF OX and iT2 control cells; (D) in CTC223 shSPDEF and pTRIPZ NS control cells; (E) in BPE7 SPDEF OX and iT2 control cells; (F) in BPE7 shSPDEF and pTRIPZ NS control cells (n= 3 technical replicates/cell line). shSPDEF and pTRIPZ NS control cells were treated with doxycycline for one week before RNA was extracted. Values are given as two-fold change relative to control group; RQ, relative quantification. P-value was calculated using an unpaired two-tailed t-test; \* p < 0.05, \*\* p < 0.01, \*\*\* p < 0.001; not significant when no indication. cDNA synthesis and RT-qPCRs were performed by Ornella Kossi.

Upregulation of *AR* mRNA levels was also confirmed in BPE8 cells upon SPDEF depletion mediated by CRISPR/Cas9 gene editing (Figure 34). However, *SPDEF* gene expression was also increased in SPDEF KO#1 cells (Figure 34A). In agreement, AR-associated target genes were found to be increased as well. In contrast, SPDEF and AR-associated target genes' expression was unchanged in SPDEF KO#2 cells (Figure 34B). This again supports the hypotheses that SPDEF transcription factor negatively regulates *AR* transcription. In addition, *SPDEF* mRNA is thought to be upregulated upon KO as negative feedback loop.

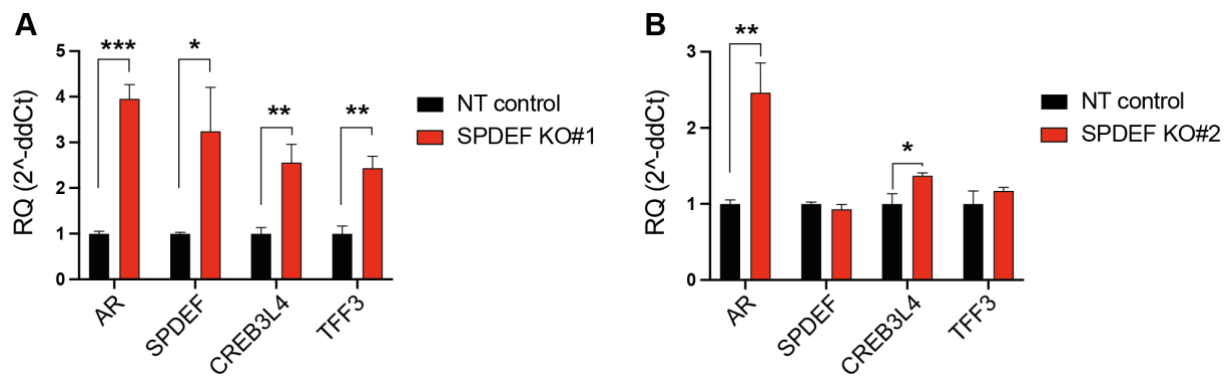


**Figure 34: AR and associated target genes are upregulated upon SPDEF knock-out.** (A) Representative RT-qPCR analysis of AR target genes in BPE8 non-targeting (NT) control and SPDEF knock-out (KO) #1 and (B) SPDEF KO#2 cells (n= 3 technical replicates/cell line). Values are given as two-fold change relative to control group; RQ, relative quantification. P-value was calculated using an unpaired two-tailed t-test; \* p < 0.05, \*\* p < 0.01, \*\*\* p < 0.001; not significant when no indication. RNA extraction, cDNA synthesis and RT-qPCRs were performed by Ornella Kossi.

### 3.6.2 Pharmacological activation of AR regulates AR and SPDEF gene expression in AR<sup>+</sup> breast cancer cells

To further elucidate the androgen-dependent transcriptional profile of AR/SPDEF<sup>+</sup> breast cancer cells, transcriptional consequences of pharmacological AR agonist activation or inhibition was assessed by RT-qPCR analysis. For this purpose, AR<sup>+</sup> MDA-MB-453 cells were treated with either synthetic testosterone R1881 or AR inhibitor enzalutamide (Enza) for 72h *in vitro* before RNA was harvested. AR<sup>+</sup> (LNCaP) and AR<sup>-</sup> (PC3) PCa cells were used as positive and negative control, respectively. In AR<sup>+</sup> LNCaP cells, *SPDEF* was upregulated upon treatment with R1881, and downregulated when AR was inhibited by Enza treatment (Figure 35A, left). In contrast, no major changes were observed in AR<sup>-</sup> PC3 cells as expected (Figure 35A, middle). Furthermore, *SPDEF* levels did not change upon treatment for 72h in MDA-MB-453 cells (Figure 35A, right). *AR* and its target genes' expression including *PIP*, *GATA3*, *ERBB2*, and *TFF3* were deregulated upon AR activation (Figure 35B). However, I found that *SPDEF* gene expression gradually increased over time when performing a long-term R1881 treatment assay over 12 days (Figure 35C). Observed increase in *SPDEF* expression was time-delayed in comparison to *AR* transcript levels, which gradually decreased suggesting that AR negatively regulates *SPDEF* gene expression (Figure 35D).



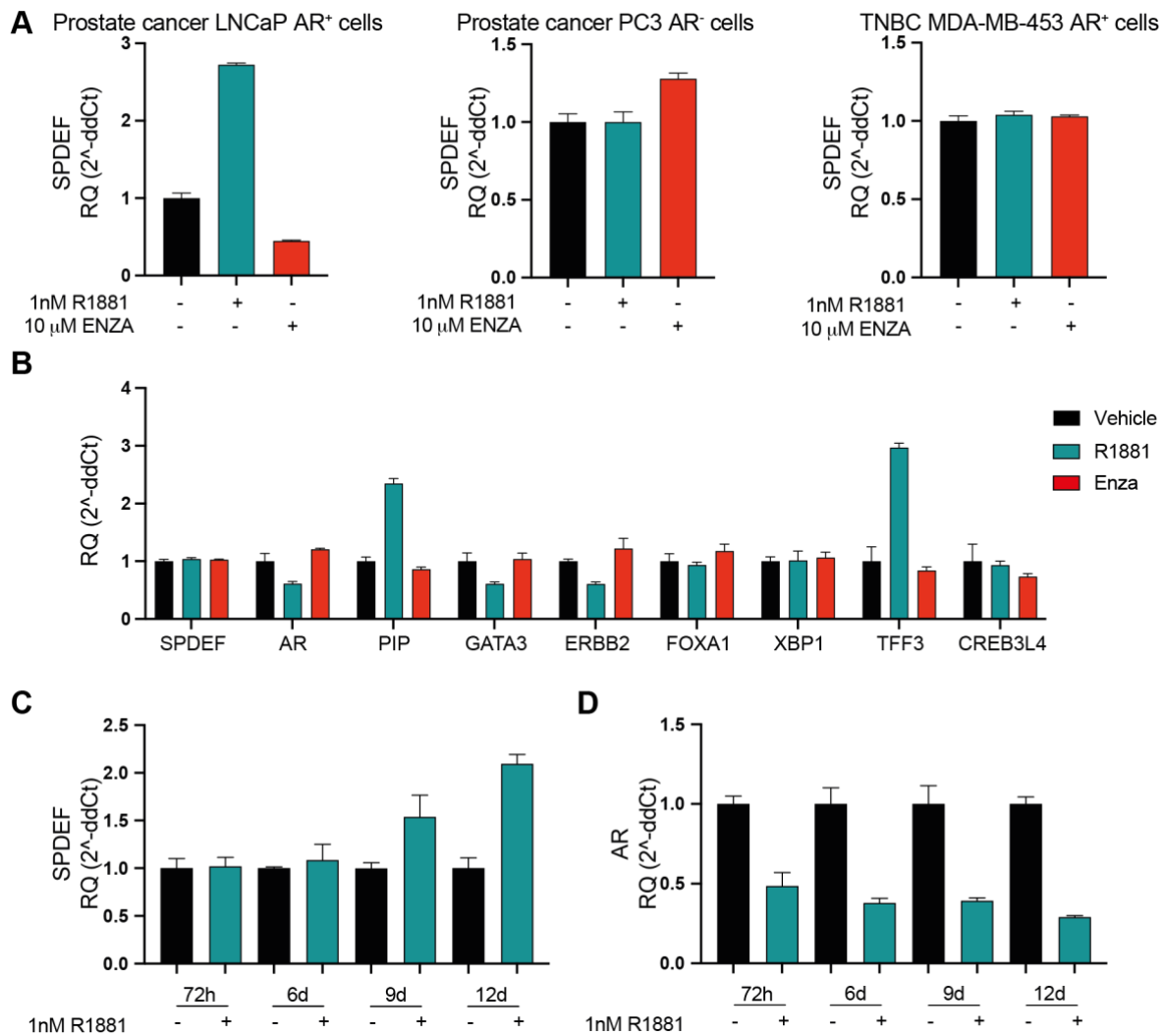


**Figure 35: AR agonist activation regulates AR gene and targets expression in AR<sup>+</sup> breast cancer cells.** MDA-MB-453 or control cells were treated with 1nM R1881, 10 μM enzalutamide (Enza) or vehicle control for 72h before RNA was extracted. (A) *SPDEF* expression in AR<sup>+</sup> LNCaP cells served as positive control (left), in AR<sup>-</sup> PC3 cells served as negative control (middle) and in MDA-MB-453 cells (right). (B) AR target genes' expression upon 72h treatment in MDA-MB-453 cells. (C, D) Time course experiment over 12 days in MDA-MB-453 cells treated with 1nM R1881. (C) *SPDEF* expression and (D) *AR* expression. cDNA synthesis and RT-qPCRs were performed by Ornella Kossi.

### 3.6.3 AR knock-out impairs *SPDEF* expression

To fully elucidate the requirement of AR expression in *SPDEF* signaling and function, I utilized CRISPR/Cas9 gene editing to disrupt AR expression in AR<sup>+</sup> TNBC BPE8 and MDA-MB-453 cell lines. To this end, I used two different guide RNAs (gRNAs) targeting AR, referred to as AR KO#1 and AR KO#2. In MDA-MB-453 cells, three different electroporation (EP) protocols were tested using the MaxCyte<sup>®</sup> EP technologies (Figure 36A). AR protein expression was

dramatically reduced in MDA-MB-453 and BPE8 AR KO#1 cells (Figure 36). Total AR knock-out efficiency was 94.4% in AR KO#1 cells (data not shown). AR knock-out (KO) resulted in decreased *AR* mRNA levels (Supplementary Figure 19E, F) in line with protein expression. Although AR protein was clearly detected in AR KO#2 cells, I validated total knock-out efficiency of 33.4% using the Tide web tool<sup>215</sup>. AR direct target gene *PIP* was downregulated in AR KO cells, however gene expression levels of other AR-associated target genes were not affected (Supplementary Figure 19E, F). In BPE8 AR KO cells, *SPDEF* gene expression was unchanged (Supplementary Figure 19E, F). In contrast, SPDEF protein expression was increased in MDA-MB-453 and BPE8 cells when AR was deleted (Figure 36A, C). This is in agreement with previous findings that *SPDEF* mRNA expression increased when AR expression gradually decreased. Vice versa, AR protein expression was significantly decreased upon SPDEF KO in BPE8 cells (Figure 36C), although *AR* mRNA levels were increased (Figure 34), suggesting a reciprocal regulatory mechanism.

In BPE8 cells, AR and SPDEF protein expression increased upon treatment with synthetic testosterone R1881 or dihydrotestosterone (DHT) for six days *in vitro* (Figure 36C). Although AR protein expression was decreased in SPDEF KO cells, R1881 or DHT treatment resulted in upregulation of AR expression compared to vehicle-treated SPDEF KO#2 cells.

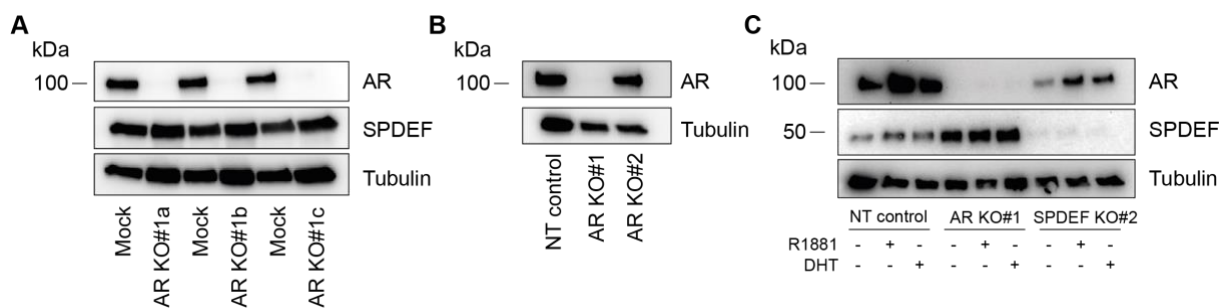


**Figure 36: CRISPR/Cas9-mediated AR knock-out in AR<sup>+</sup> breast cancer cells.** (A) Representative western blot analysis of AR and SPDEF protein expression in MDA-MB-453 control (Mock) and AR knock-out (KO) #1 and AR KO#2 cells. (B) AR protein expression in BPE8 non-targeting (NT) control, AR KO#1 and AR KO#2 cells. (C) AR and SPDEF protein expression in BPE8 NT control, AR KO#1 and SPDEF KO#2 cells treated with 1nM R1881, 1nM dihydrotestosterone (DHT) or vehicle control (-) for six days *in vitro* before protein lysates were harvested. Tubulin served as loading control. kDa, kilo dalton.

Taken together, these data show that there is a complex regulatory mechanism underlying AR and SPDEF expression. AR protein expression was decreased upon SPDEF downregulation or depletion whereas *AR* mRNA levels were upregulated suggesting a negative feedback loop. Vice versa, AR regulates SPDEF expression that was increased in AR-deficient cells though. AR agonist activation increased both, AR and SPDEF protein expression suggesting that both proteins regulate each other.

### 3.6.4 AR knock-out does not impair *in vivo* tumor growth

SPDEF knockdown and knock-out significantly inhibited tumor growth *in vivo* (3.3.1 and 3.3.2). Since AR protein expression was decreased in SPDEF KO cells, I hypothesized that SPDEF impairs tumor growth by interrupting AR signaling pathway. To investigate whether AR is required for tumor growth of BPE8 AR<sup>+</sup> breast cancer cells *in vivo*, either NT control or AR KO#1 cells were injected orthotopically into the mammary fat pad of immunocompromised mice. Tumor growth was followed by caliper measurements. Abolishing AR expression did not affect primary tumor growth compared to NT control in BPE8 cells (Figure 37A). The experiment was terminated after 22 weeks when the NT control group reached maximal tumor volume. No difference could be observed in final tumor weight measured *ex vivo* when endpoint was reached (Figure 37B). To conclude, AR KO did not impair tumor growth of the BPE8 AR<sup>+</sup> breast cancer model suggesting that either the *in vivo* phenotype observed upon SPDEF knockdown and knock-out was not mediated through downregulation of AR or that SPDEF upregulation through AR KO was sufficient to rescue *in vivo* tumorigenicity of cells. Further, AR might not be activated in BPE8 cells without ligand activation. Also, I cannot exclude that AR-expressing wild-type BPE8 cells grew out.

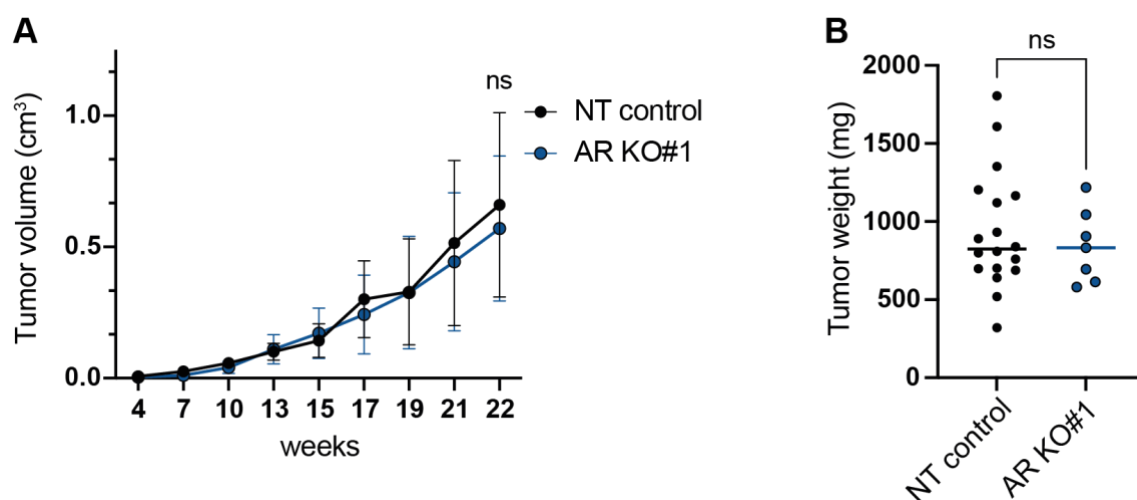


**Figure 37: AR knock-out does not impair *in vivo* tumor growth of BPE8 AR<sup>+</sup> cells.** (A) Growth followed over time of mammary fat pad (MFP) tumors generated from BPE8 non-targeting (NT) control and AR knock-out (KO) #1 cells in NSG mice (NT control, n= 20 mice/group; AR KO#1, n= 10 mice/group; 10,000 cells/mouse). Same NT control group was used as in the experiment illustrated in Figure 17 (3.3.2) in order to minimize animal numbers. Experiments were conducted at the same time point. Tumor volumes were measured by caliper. Error bars depict mean  $\pm$  SD. Mann-Whitney U-test was used to assess statistical significance (B) Tumor weight was measured *ex vivo* at endpoint; median is depicted. P-value was calculated for the last time point using an unpaired two-tailed t-test; \* p < 0.05, \*\* p < 0.01, \*\*\* p < 0.001; ns, not significant.

### 3.7 SPDEF regulates FBP1 expression in AR<sup>+</sup> breast cancer cells

#### 3.7.1 SPDEF regulates gene expression of the rate-limiting enzymes in gluconeogenesis *FBP1* and *PCK2* in AR<sup>+</sup> breast cancer cells

Gene expression analysis based on microarray data nominated genes encoding metabolic enzymes and proteins to be differentially expressed in SPDEF OX and shSPDEF cells relative to controls. Subsequent GSEA revealed that metabolic pathways including carbohydrate and glucose metabolism were enriched in SPDEF OX and shSPDEF cell lines, respectively. To further elucidate the metabolic profiles on transcriptional level, gene expression of metabolic enzymes involved in glycolysis and gluconeogenesis were validated by RT-qPCR analysis.

Glucose is converted to pyruvate producing ATP without the requirement of oxygen during glycolysis. This process takes place in the cytosol of the cells. In contrast, gluconeogenesis is the reverse pathway synthesizing glucose from non-carbohydrate carbon sources. These two reversed pathways share many common enzymes with exception of three enzymes. Of high interest, *FBP1* and *PCK2* encoding fructose-1,6-biphosphatase and mitochondrial phosphoenolpyruvate carboxykinase are the two rate-limiting enzymes of gluconeogenesis and both, found to be downregulated upon SPDEF knockdown in AR<sup>+</sup> BPE8, CTC223 and MDA-MB-453 cells (Figure 38B, D and Supplementary Figure 18C). Vice versa, both genes were upregulated in BPE8 SPDEF OX cells relative to the control (Figure 38A). Whereas *PCK2* expression did not change in CTC223 cells after overexpression of SPDEF, *FBP1* gene was also downregulated in SPDEF OX cells (Figure 38C). Strikingly, this was also observed for CTC288 cells (Supplementary Figure 20C). Both, CTC223 and CTC288 showed reduced *in vivo* tumor growth upon either SPDEF overexpression or knockdown. Overall, CTC223- and CTC288-SPDEF cell lines showed the greatest changes in the glycolytic gene panel compared to other cell lines (Figure 38C, D and Supplementary Figure 20C,D). In AR<sup>-</sup> BPE7 cells, only minor differences were observed in glycolytic genes expression (Figure 38E, F).

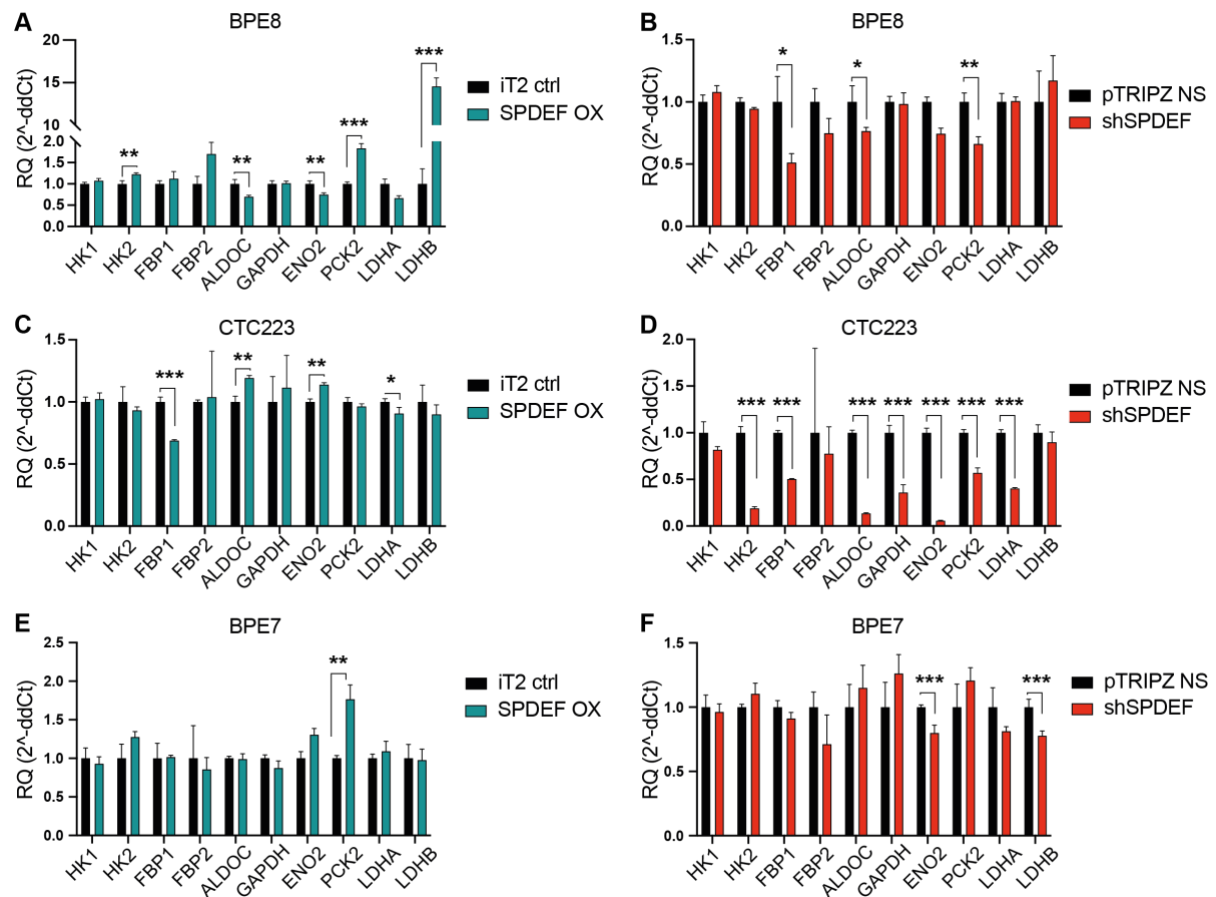


**Figure 38: Glycolytic target genes validation in BPE8, CTC223 and BPE7 SPDEF overexpression and knockdown cell models.** (A) Representative RT-qPCR analysis of target genes involved in glycolysis and gluconeogenesis in BPE8 SPDEF-overexpressing (OX) and iT2 empty vector control (iT2) cells; (B) in BPE8 shSPDEF and pTRIPZ non-silencing (NS) control cells; (C) in CTC223 SPDEF OX and iT2 control cells; (D) in CTC223 shSPDEF and pTRIPZ NS control cells; (E) in BPE7 SPDEF OX and iT2 control cells; (F) in BPE7 shSPDEF and pTRIPZ NS control cells (n= 3 technical replicates/cell line). shSPDEF and pTRIPZ NS control cells were treated with doxycycline for one week before RNA was extracted. Values are given as two-fold change relative to control group; RQ, relative quantification. P-value was calculated using an unpaired two-tailed t-test; \* p < 0.05, \*\* p < 0.01, \*\*\* p < 0.001; not significant when no indication. cDNA synthesis and RT-qPCR analysis were performed by Ornella Kossi.

Although only minor changes in glycolytic genes' expression was observed in BPE8 shSPDEF cells, genes involved in glycolysis and gluconeogenesis were significantly downregulated in BPE8 SPDEF KO cells. Especially gene expression of *HK1*, *FBP1*, *GAPDH* and *PCK2* were found to be more than 50% reduced when SPDEF was depleted (Figure 39).

Since changes in glycolytic enzymes' gene expression upon SPDEF downregulation or knock-out were mainly observed in AR<sup>+</sup> cell lines, I hypothesized that glycolytic genes might be co-regulated by SPDEF and AR transcription factor. To this end, glycolytic target mRNA levels were assessed in BPE8 AR KO cell lines (Supplementary Figure 19C, D). Indeed, gene expression of several candidates, namely *LDHA*, *HK1*, *FBP1*, *FBP2*, *ALDOC*, *ENO2* and *PCK2* was significantly reduced in AR KO#1 cells relative to NT control (Supplementary Figure 19C).

These data suggest that SPDEF and AR transcription factors regulate gene expression of glycolytic enzymes catalyzing glycolysis and gluconeogenesis especially in AR<sup>+</sup> breast cancer cells.

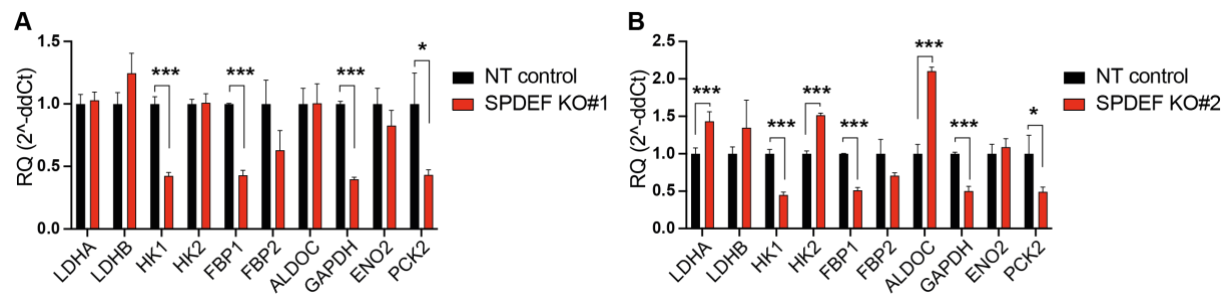


**Figure 39: Glycolysis/gluconeogenesis-associated genes are deregulated upon SPDEF knock-out.** (A) Representative RT-qPCR analysis of target genes involved in glycolysis and gluconeogenesis in BPE8 non-targeting (NT) and SPDEF knock-out (KO) #1 and (B) SPDEF KO#2 cells (n= 3 technical replicates/cell line). Values are given as two-fold change relative to control group; RQ, relative quantification. P-value was calculated using an unpaired two-tailed t-test; \* p < 0.05, \*\* p < 0.01, \*\*\* p < 0.001; not significant when no indication. RNA extraction, cDNA synthesis and RT-qPCRs were performed by Ornella Kossi.

### 3.7.2 Glycolysis genes are upregulated in AR<sup>-</sup> breast tumors upon SPDEF downregulation

Although glycolytic target genes were not significantly differentially expressed in BPE7 shSPDEF cells *in vitro*, GSEA revealed positive enrichment of pyruvate and glucose metabolic processes in shSPDEF tumors compared to controls (Figure 32). For this reason, I assessed glycolytic genes' expression in shSPDEF and pTRIPZ NS control tumors. *HK2*, *FBP2*, *ALDOA*, *ALDOC*, *ENO2*, and *LDHA* were significantly upregulated in shSPDEF tumors relative to controls (Figure 40). Strikingly, the same gene sets and panel expression were found to be downregulated in AR<sup>+</sup> breast cancer cells when SPDEF was downregulated or deleted (Figure 27, Figure 38, Figure 39). Therefore, high expression of pyruvate and glucose metabolic genes is associated with increased tumorigenicity *in vivo*. Moreover, these data indicate that SPDEF either enhances or represses transcription of glycolytic genes dependent on the co-expression with AR. AR<sup>+</sup> and AR<sup>-</sup> breast cancer cells may have distinct metabolic profiles and differently rely on glycolysis. Since glycolysis and gluconeogenesis are reverse pathways sharing many common enzymes, the regulation of these genes may be highly complex.

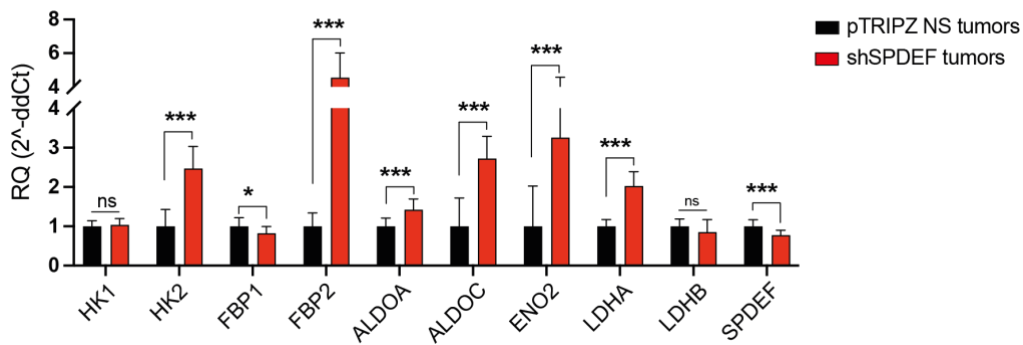


**Figure 40: Glycolytic genes are upregulated in AR<sup>+</sup> BPE7 shSPDEF tumors relative to controls.** Gene expression analysis of targets involved in glycolysis and gluconeogenesis in BPE7 shSPDEF and pTRIPZ non-silencing (NS) tumors (n= 4 biological replicates/group). Values are given as two-fold change relative to control group; RQ, relative quantification. P-value was calculated using an unpaired two-tailed t-test; \* p < 0.05, \*\* p < 0.01, \*\*\* p < 0.001; ns, not significant. cDNA synthesis and RT-qPCRs were performed by Ornella Kossi.

### 3.7.3 SPDEF and FBP1 are co-expressed in AR<sup>+</sup> breast cancer models

FBP1 is a rate-limiting enzyme in gluconeogenesis which catalyzes the conversion of fructose-1,6-bisphosphate into fructose-6-phosphate and inorganic phosphate. My previous findings suggested that SPDEF regulates *FBP1* gene expression in AR<sup>+</sup> breast cancer cells. For this reason, I assessed FBP1 protein expression in AR KO and SPDEF KO cell lines, respectively. In line with increased SPDEF expression, FBP1 protein was increased in MDA-MB-453 AR KO cells relative to mock control (Figure 41A). This observation was confirmed in BPE8 AR KO cells (Figure 41B). In BPE8 control cells, FBP1 expression increased upon AR agonist activation, by treatment with synthetic testosterone R1881 or DHT treatment (Figure 41B). This was in line with increasing AR and SPDEF protein levels. In contrast, FBP1 protein expression significantly increased in SPDEF KO cells relative to NT control (Figure 41B, right).

These data indicate that SPDEF and AR regulate FBP1 protein expression, however FBP1 protein was also increased upon SPDEF depletion suggesting a feedback regulatory mechanism.

Further, I confirmed endogenous co-expression of SPDEF and FBP1 proteins in PDX-derived breast cancer cell lines (Figure 41C). FBP1 was found to be highly expressed in CTC223 cells which showed high SPDEF expression levels (Figure 41C). In contrast, FBP1 protein was not detected in AR<sup>-</sup> low SPDEF-expressing BPE7 cells. This was validated in additional breast cancer cell lines. AR<sup>+</sup> MDA-MB-453 and SK-BR3 cells showed high co-expression of SPDEF

and FBP1 protein (Figure 41D). In contrast, TNBC MDA-MB-231 cells were negative for all three proteins of interest. AR<sup>+</sup> LNCaP and AR<sup>-</sup> PC3 PCa cells served as positive and negative control for AR and SPDEF expression, respectively. FBP1 protein expression was also observed in AR<sup>+</sup> PCa cells but not in AR<sup>-</sup> PCa cells.

Taken together, these data showed that SPDEF and FBP1 protein are co-expressed in AR<sup>+</sup> breast cancer cell models.

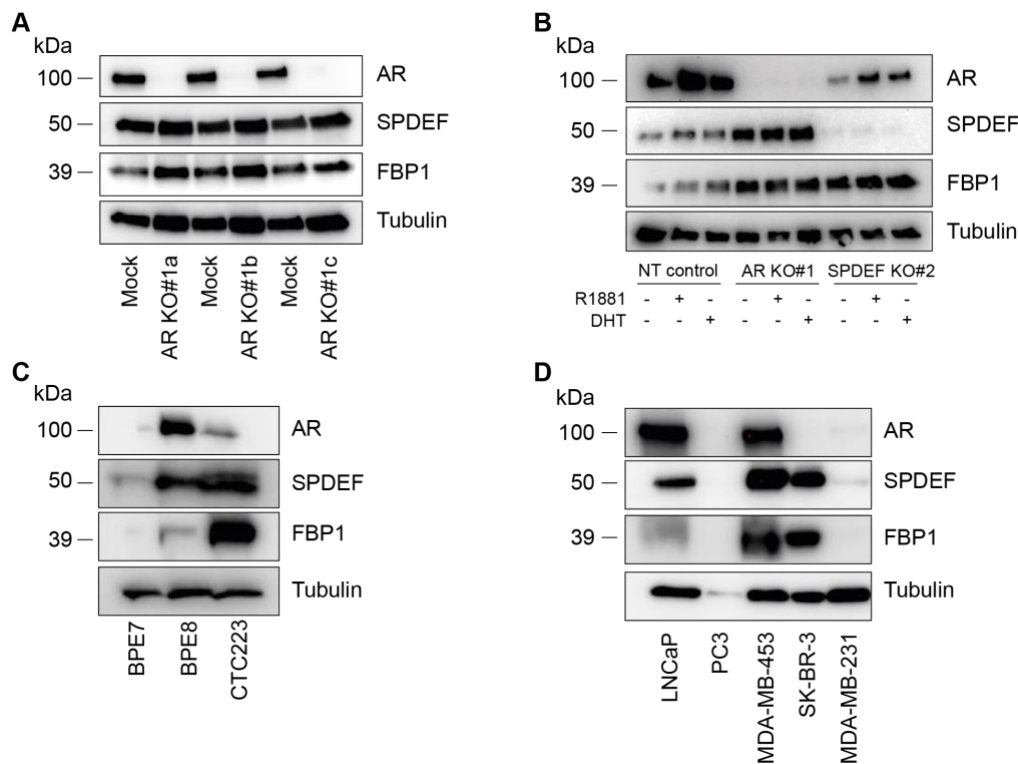


**Figure 41: SPDEF and FBP1 protein are co-expressed in AR<sup>+</sup> breast cancer cell models.** (A) Representative western blot analysis of FBP1 protein expression in MDA-MB-453 control (Mock) and AR knock-out (KO) #1 and AR KO#2 cells. Same blot as in Figure 36A. (B) FBP1 protein expression in BPE8 non-targeting (NT) control, AR KO#1 and SPDEF KO#2 cells treated with 1nM R1881, 1nM dihydrotestosterone (DHT) or vehicle control (-) for six days *in vitro* before protein lysates were harvested. Same blot as in Figure 36C. (C) FBP1 protein expression in patient derived xenograft (PDX) cell lines BPE7, BPE8 and CTC223. Same blot as in Figure 12C. (D) FBP protein expression in prostate cancer LNCaP and PC3, and in breast cancer MDA-MB-453, SK-BR-3 and MDA-MB-231 cells. Same plot as in Figure 12D. Tubulin served as loading control. kDa, kilo dalton.

### 3.7.4 FBP1 is a direct target gene of SPDEF

In order to assess whether FBP1 is a direct target gene of SPDEF, I made use of a previously published set of transcription networks and related data sets. Chromatin immunoprecipitation-sequencing (ChIP-seq) data for SPDEF in MCF7 cells is available within the R package *Fletcher2013b*. Re-analyzing the ChIP-seq data, I identified SPDEF binding sites within



promoter regions of direct target genes. *FBP1* was identified as one of many direct target genes of SPDEF in MCF7 cells. This showed that *FBP1* is directly regulated by SPDEF and might be a candidate involved in tumorigenic potential of SPDEF-expressing AR<sup>+</sup> breast cancer cells.

### 3.7.5 FBP1 knock-out impairs glycolytic genes' expression

To further investigate the function of FBP1 in AR<sup>+</sup> breast cancer cells, I utilized CRISPR/Cas9-based gene editing in order to generate FBP1-deleted BPE8 cells. To this end, I used two gRNAs targeting FBP1 sequence. Total KO efficiency of 96.5% in FBP1 KO#1 and 54.3% in FBP1 KO#2 cells was achieved as determined by using Tide web tool<sup>215</sup>. FBP1 protein expression was significantly decreased in BPE8 FBP1 KO#2 cells compared to NT control, and not detectable in FBP1 KO#1 cells by western blot analysis (Figure 42A). In line with protein expression, *FBP1* mRNA levels were significantly reduced in FBP1 KO cells relative to control (Figure 42B, C). Interestingly, *FBP2* gene expression was significantly increased in FBP1 KO#2 but not in FBP1 KO#1 cells relative to NT control (Figure 42C). Next to *FBP1*, other genes encoding enzymes involved in glycolysis and gluconeogenesis were significantly downregulated similar to what has been observed for SPDEF KO cells (Figure 42B, C). Only *LDHA* mRNA levels were significantly increased in both FBP1 KO cell lines compared to the control. To conclude, FBP1 depletion in BPE8 cells was highly efficient resulting in downregulation of genes involved in glycolysis and gluconeogenesis pathways.

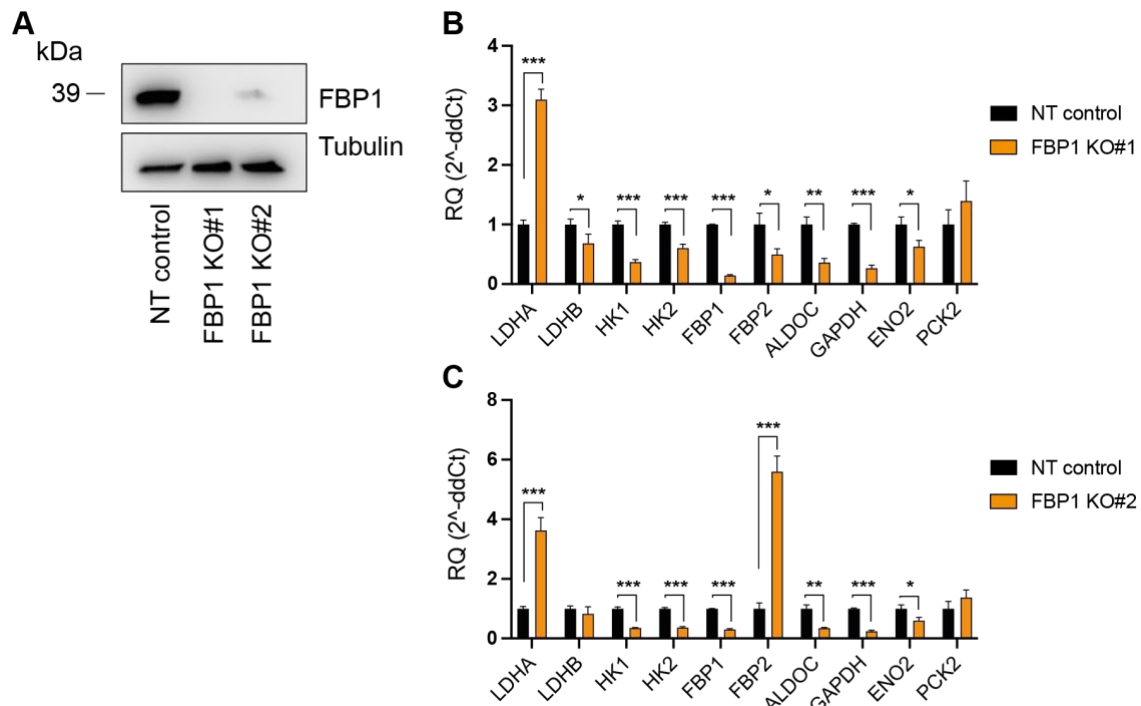


**Figure 42: Glycolysis/gluconeogenesis-associated genes are downregulated in FBP1 knock-out cells.** (A) FBP1 protein analysis in BPE8 non-targeting (NT) control and FBP1 knock-out (KO) #1 and FBP1 KO#2 cells by western blot analysis. Tubulin served as loading control. (B) Representative RT-qPCR analysis of target genes involved in glycolysis and gluconeogenesis in BPE8 NT control and FBP1 KO#1 and (C) FBP1 KO#2 cells (n= 3 technical replicates/cell line). Values are given as two-fold change relative to control group. kDa, kilo Dalton; RQ, relative quantification. P-value was calculated using an unpaired two-tailed t-test; \* p < 0.05, \*\* p < 0.01, \*\*\* p < 0.001; not significant when no indication.

### 3.7.6 FBP1 knock-out does not impair *in vivo* tumor growth

SPDEF knockdown and knock-out significantly inhibited tumor growth *in vivo* in AR<sup>+</sup> and ER<sup>+</sup> breast cancer cells (3.3.1 and 3.3.2). In order to identify the underlying mechanism how SPDEF impairs tumor growth, target genes of SPDEF transcription factor were investigated previously. I identified *FBP1* as a direct target gene of SPDEF and found it to be downregulated in shSPDEF and SPDEF KO cells of several AR<sup>+</sup> breast cancer models, respectively. I hypothesized that SPDEF might impair tumor growth by repressing FBP1 metabolic function. To investigate whether FBP1 is required for tumor growth of BPE8 AR<sup>+</sup> breast cancer cells *in vivo*, FBP1 KO#1 cells were injected orthotopically into the mammary fat pad of immunocompromised mice. Tumor growth was compared to NT control cells and followed by caliper measurements. Abolishing FBP1 expression did not affect primary tumor growth compared to NT control in BPE8 cells (Figure 43A). The experiment was terminated after 22

weeks when the NT control group reached maximal tumor volume. No difference could be observed in final tumor weight measured *ex vivo* when endpoint was reached (Figure 43B).

In conclusion, FBP1 KO did not impair tumor growth of the BPE8 AR<sup>+</sup> breast cancer model suggesting that the *in vivo* phenotype observed upon SPDEF knockdown and knock-out was not mediated through downregulation of FBP1 function. However, I can neither exclude that cells lost the KO construct nor that wild-type cells grew out *in vivo* by using this model.

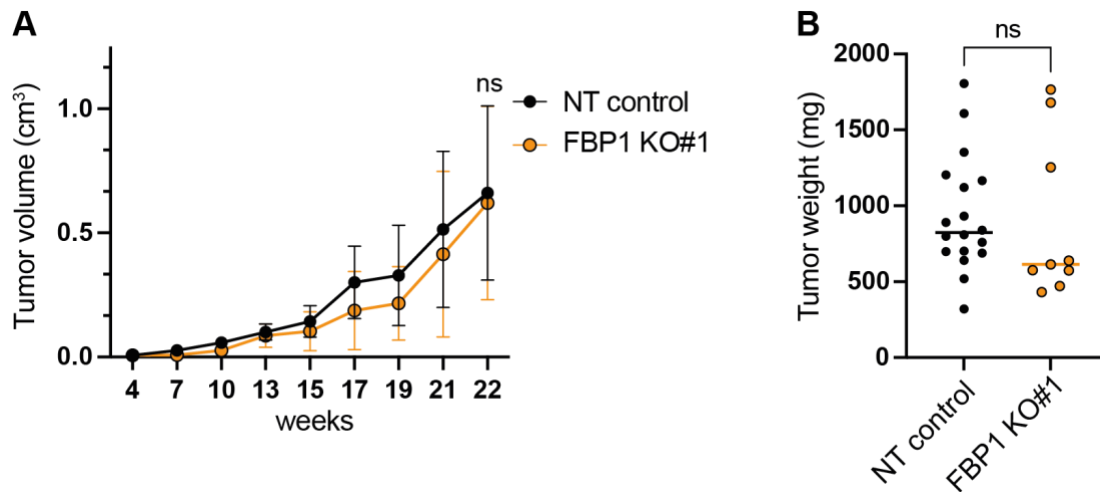


**Figure 43: FBP1 knock-out does not impair *in vivo* tumor growth of BPE8 AR<sup>+</sup> cells.** (A) Growth followed over time of mammary fat pad (MFP) tumors generated from BPE8 non-targeting (NT) control and FBP1 knock-out (KO) #1 cells in NSG mice (NT control, n= 20 mice/group; FBP1 KO#1, n= 10 mice/group; 10,000 cells/mouse). The same NT control group was used as in the experiment illustrated in Figure 17 (3.3.2) in order to minimize animal numbers. Experiments were conducted at the same time point. Tumor volumes were measured by caliper. Error bars depict mean  $\pm$  SD. (B) Tumor weight was measured *ex vivo* at endpoint; median is depicted. P-value was calculated for the endpoint using the Mann-Whitney U-test; \* p < 0.05, \*\* p < 0.01, \*\*\* p < 0.001; ns, not significant.

### 3.7.7 SPDEF and FBP1 are co-expressed in breast cancer patients

To nominate SPDEF target genes, I assessed breast cancer mRNA expression data using The Cancer Genome Atlas (TCGA) data set. Genes were rank-ordered based on Spearman's correlation score and identified *FBP1* gene to be among the top 40 targets associated with *SPDEF* expression (Spearman: 0.56; data not shown). *FBP1* and *SPDEF* correlation was confirmed by analyzing the METABRIC data set. Both genes were found to be highly co-expressed in ER<sup>-</sup> and ER<sup>+</sup> breast cancer patients to a similar degree (Figure 44A, B). Almost all ER<sup>+</sup> tumors showed positive expression levels for both genes, *FBP1* and *SPDEF*. In contrast, a subpopulation which was negative for both mRNAs existed within the ER<sup>-</sup> patients cohort similar to what has been observed previously for *SPDEF* and *AR* co-expression (Figure 10B).

To test whether high *SPDEF* and *FBP1* co-expression in ER<sup>-</sup> BC patients was associated with AR status, I analyzed the differentially expressed genes between AR<sup>high</sup> and AR<sup>low</sup> tumors and found that *FBP1* was among the top 1% variant genes associated with AR expression (data not shown).

*FBP1* gene expression stratified patients based on survival probability. However, in ER<sup>-</sup> BC patients, high *FBP1* expression was associated with a better outcome (Figure 44C). Vice versa, in ER<sup>+</sup> BC patients, high expression levels of *FBP1* mRNA predicted worse survival probabilities (Figure 44D).

To sum up, *SPDEF* and *FBP1* are highly co-expressed in breast cancer and predict different outcomes in dependence on the HR status.

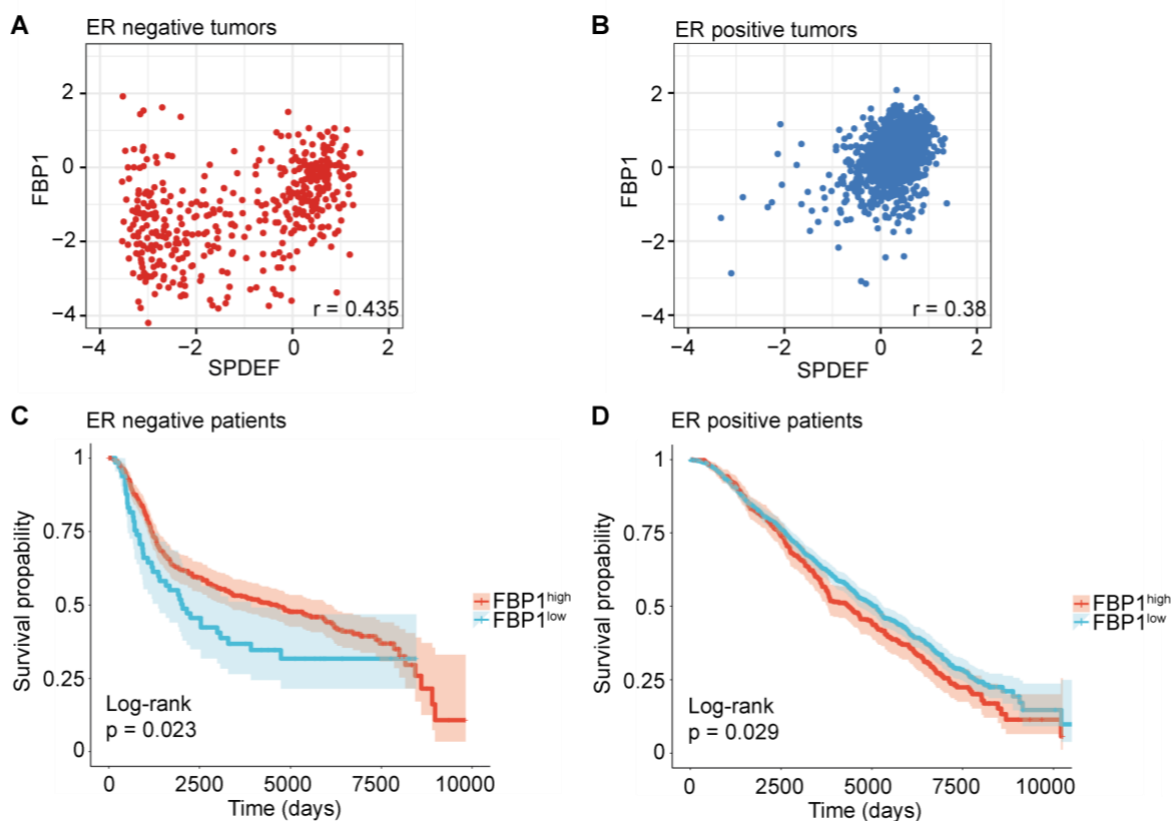


**Figure 44: *SPDEF* and *FBP1* are co-expressed in human breast cancers and *FBP1* expression predicts survival.** (A, B) Linear correlation of *SPDEF* and *FBP1* gene expression in (A) ER negative (red) and (B) ER positive (blue) breast cancer patients. Depicted is the Pearson correlation coefficient  $r$  calculated with R package ggpubr. (C, D) Kaplan-Meier estimator for survival probability of (C) ER<sup>-</sup> breast cancer and (D) ER<sup>+</sup> breast cancer patients stratified based *FBP1* gene expression. Data is extracted from METABRIC data set including 445 ER<sup>-</sup> breast cancer patients.

### 3.8 SPDEF regulates fatty acid metabolism in AR<sup>+</sup> breast cancer cells

#### 3.8.1 SPDEF regulates gene expression of the rate-limiting enzymes in *de novo* fatty acid biosynthesis in AR<sup>+</sup> breast cancer cells

Fatty acids play an essential role in a variety of biological processes including synthesis of membrane phospholipids, signal transduction pathways, and energy production and storage<sup>178</sup>. Lipid metabolism encompasses (1) uptake of lipids transported via the cell membrane into the cells, (2) storage of lipids in the form of triacylglycerols, (3) *de novo* biosynthesis of lipids in the cytosol, and (4) degradation via  $\beta$ -oxidation in the mitochondria of the cells<sup>179</sup>.

In the AR<sup>+</sup> TNBC BPE8 model, I found fatty acid metabolism signature to be positively enriched *in vitro* and *in vivo* in SPDEF-overexpressing tumors and cells. Increased expression of enzymes involved in *de novo* fatty acid biosynthesis, ATP citrate lyase (*ACLY*), acetyl-CoA carboxylase (*ACACA/B*, also known as *ACC*) and fatty acid synthase (*FASN*), was observed upon overexpression of SPDEF on the transcriptional level (Figure 45A). Vice versa, these genes were significantly downregulated in SPDEF knockdown cells (Figure 45B). Similar phenotypes were observed in CTC223 (Figure 45C, D) and ER<sup>+</sup> AR<sup>-</sup> CTC288 (Supplementary Figure 20A, B) cells. No major changes were noticed in the AR<sup>-</sup> TNBC BPE7 model except of *FASN* that was upregulated in shSPDEF cells (Figure 45E, F). Strikingly, the downregulation of *de novo* fatty acid biosynthesis on the transcriptional level was accompanied by a dramatic upregulation of the fatty acid transporter gene *CD36* in AR<sup>+</sup> cell lines BPE8, CTC223 and MDA-MB-453 (Figure 45B, D and Supplementary Figure 18B).

These data based on the transcriptional level suggest that AR<sup>+</sup> breast cancer cells have a distinct lipogenic, metabolic profile and rely on *de novo* fatty acid biosynthesis. Metabolic genes involved in this process seem to be regulated by SPDEF. Interestingly, *CD36* was significantly upregulated when fatty acid synthesis genes were reduced.

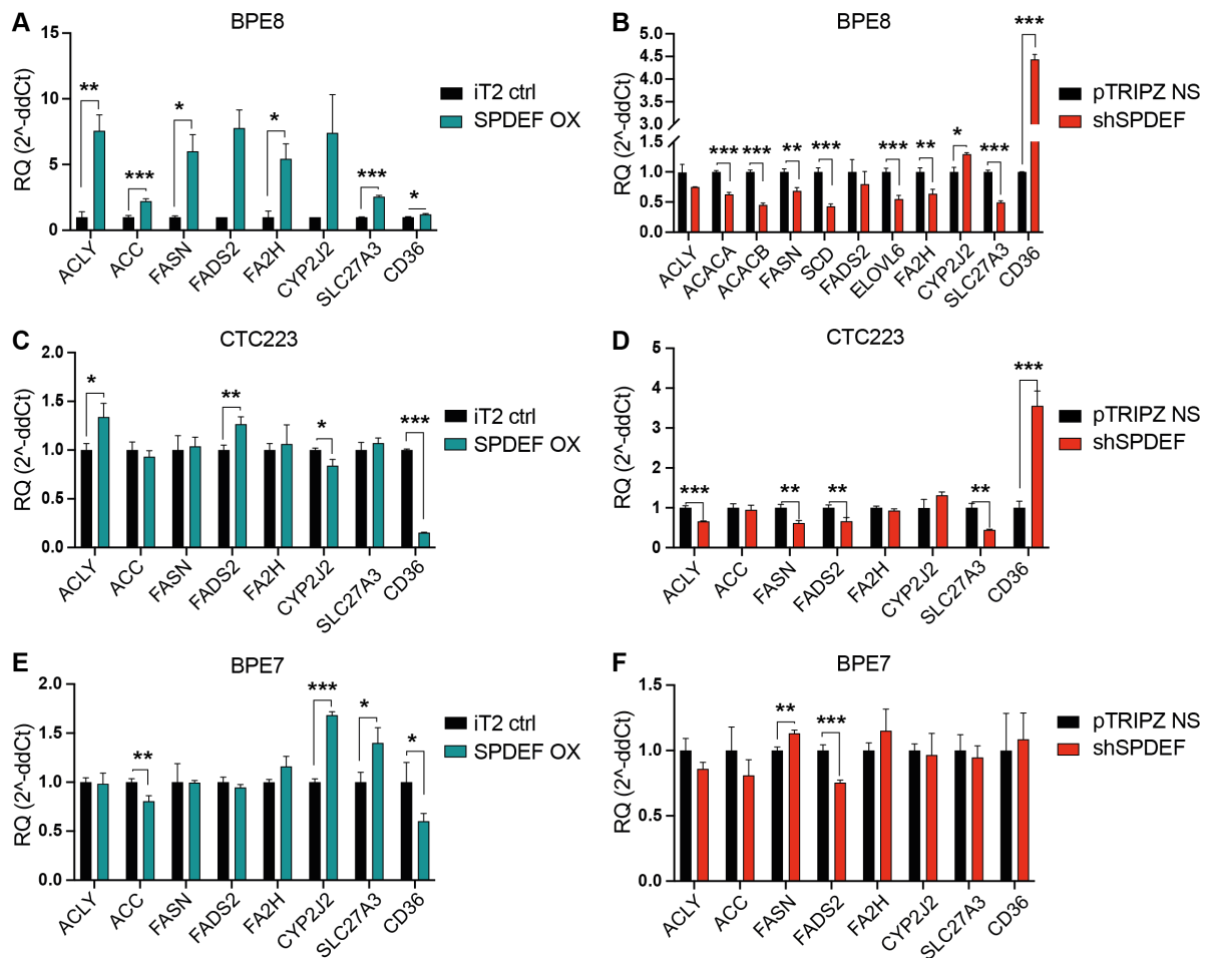


**Figure 45: Fatty acid metabolism target genes validation in BPE8, CTC223 and BPE7 SPDEF overexpression and knockdown cell models.** (A) Representative RT-qPCR analysis of target genes involved in fatty acid metabolism in BPE8 SPDEF-overexpressing (OX) and iT2 empty vector control (iT2) cells; (B) in BPE8 shSPDEF and pTRIPZ non-silencing (NS) control cells; (C) in CTC223 SPDEF OX and iT2 control cells; (D) in CTC223 shSPDEF and pTRIPZ NS control cells; (E) in BPE7 SPDEF OX and iT2 control cells; (F) in BPE7 shSPDEF and pTRIPZ NS control cells (n= 3 technical replicates/cell line). shSPDEF and pTRIPZ NS control cells were treated with doxycycline for one week before RNA was extracted. Values are given as two-fold change relative to control group; RQ, relative quantification. P-value was calculated using an unpaired two-tailed t-test; \* p < 0.05, \*\* p < 0.01, \*\*\* p < 0.001; not significant when no indication. cDNA synthesis and RT-qPCRs were performed by Ornella Kossi.

These findings were confirmed utilizing CRISPR/Cas9-mediated SPDEF KO cells (Figure 46). FA synthesis genes' expression was even more decreased in SPDEF-deficient cells relative to NT control, compared to shSPDEF cells (relative to pTRIPZ NS control). Especially, *ACLY*, *FASN*, *FADS2* and *FA2H* expression levels were more than 50% reduced in both SPDEF KO cell lines. These data suggest that SPDEF transcription factor regulates expression of genes involved in fatty acid biosynthesis and metabolism.

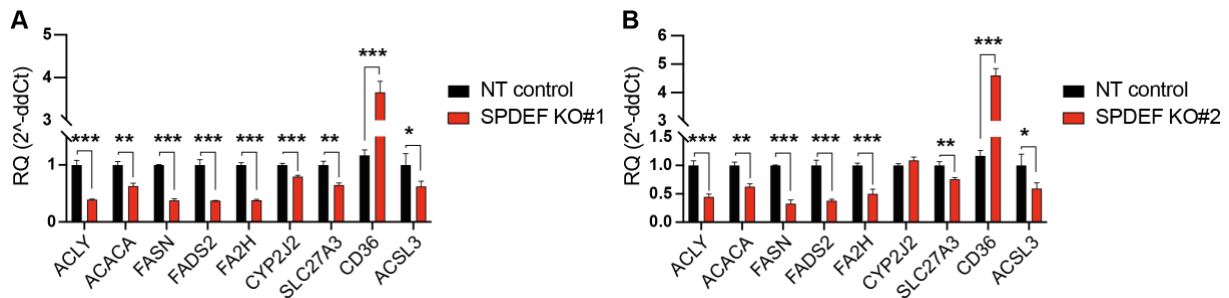


**Figure 46: Fatty acid metabolic genes are deregulated in BPE8 SPDEF knock-out cells.** (A) Representative RT-qPCR analysis of target genes involved in fatty acid biosynthesis and metabolism in BPE8 non-targeting (NT) and SPDEF knock-out (KO) #1 and (B) SPDEF KO#2 cells (n= 3 technical replicates/cell line). Values are given as two-fold change relative to control group; RQ, relative quantification. P-value was calculated using an unpaired two-tailed t-test; \* p < 0.05, \*\* p < 0.01, \*\*\* p < 0.001; not significant when no indication. RNA extraction, cDNA synthesis and RT-qPCRs were performed by Ornella Kossi.

AR-driven PCa has been shown to be more lipogenic and less glycolytic in comparison to other solid tumors. AR was suggested to regulate fatty acid metabolism in prostate carcinoma<sup>216</sup>. Having demonstrated that SPDEF regulates fatty acid metabolic genes in AR<sup>+</sup> breast cancer models, I wondered whether AR would be involved in this regulatory mechanism. To this end, I assessed fatty acid metabolic genes' expression levels in AR KO cells (Supplementary Figure 19). In line with increased SPDEF protein expression in AR KO#1 cells, genes involved in fatty acid biosynthesis were upregulated on transcriptional level relative to NT control (Supplementary Figure 19A). In addition, AR activation by testosterone treatment enhanced FA genes' expression in AR<sup>+</sup> MDA-MB-453 cells treated with testosterone (data not shown).

These findings suggest that AR regulating SPDEF is involved in the regulation of fatty acid metabolic genes' expression. However, FA genes were also differentially expressed in AR<sup>-</sup> ER<sup>+</sup> CTC288 cells suggesting that SPDEF expression is sufficient to regulate those.

### 3.8.2 Fatty acid synthesis genes are downregulated in AR<sup>+</sup> breast tumors upon SPDEF downregulation

Based on the findings *in vitro*, I hypothesized that differential gene expression of targets involved in fatty acid biosynthesis regulated by SPDEF is crucial for *in vivo* AR<sup>+</sup> breast tumor growth. For this reason, I assessed gene expression levels of enzymes catalyzing FA biosynthesis in BPE8 shSPDEF and pTRIPZ NS control cells. First, I validated downregulation of SPDEF in shSPDEF tumors relative to the controls. *ACLY*, *ACACA*, *ACAC*, *FASN* and *SCD* expression levels were significantly decreased in SPDEF knockdown tumors (Figure 47). This agrees with downregulation of the gene sets 'fatty acid metabolism' and 'fatty acid metabolic

process' in BPE8 shSPDEF tumors relative to pTRIPZ NS controls as revealed by GSEA (Figure 31). Taken together, these data suggest that fatty acid biosynthesis is transcriptionally regulated by SPDEF in AR<sup>+</sup> breast cancer.

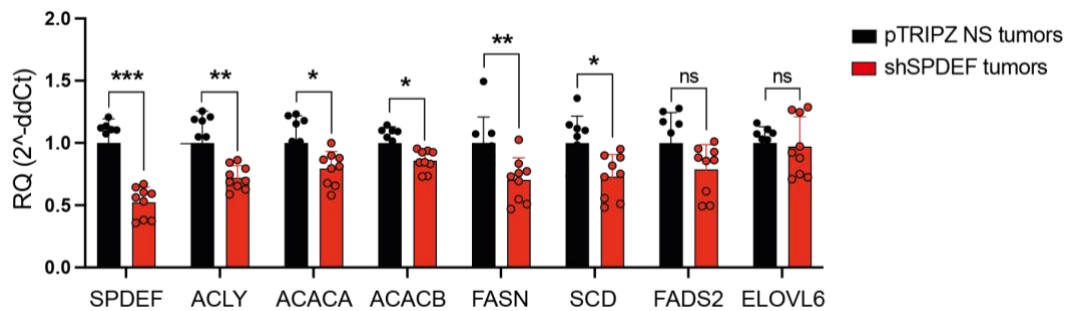


**Figure 47: Fatty acid synthesis genes are downregulated in AR<sup>+</sup> BPE8 shSPDEF tumors relative to the controls.** Gene expression analysis of enzymes involved in fatty acid biosynthesis in BPE8 shSPDEF and pTRIPZ non-silencing (NS) tumors (n= 3 biological replicates/group). Values are given as two-fold change relative to control group; RQ, relative quantification. P-value was calculated using an unpaired two-tailed t-test; \* p < 0.05, \*\* p < 0.01, \*\*\* p < 0.001; ns, not significant. cDNA synthesis and RT-qPCRs were performed by Ornella Kossi.

### 3.8.3 SPDEF regulates fatty acid biosynthesis enzymes and CD36 protein expression

Genes involved in *de novo* fatty acid biosynthesis were downregulated upon SPDEF knockdown and knock-out in AR<sup>+</sup> breast cancer cells, respectively. In contrast, *CD36* gene expression was significantly increased in shSPDEF and SPDEF KO cells relative to controls. Next, I analyzed protein expression of the rate-limiting enzymes involved in FA biosynthesis, ACLY, ACC, FASN and the main fatty acid transporter CD36 in BPE8 SPDEF OX, shSPDEF and SPDEF KO cell lines. Marked upregulation of CD36 protein levels was observed in shSPDEF cells relative to pTRIPZ NS control (Figure 48A). This was confirmed in SPDEF KO#1 and SPDEF KO#2 cells (Figure 48B). Vice versa, CD36 protein was barely detectable in SPDEF-overexpressing cells by western blot analysis (Figure 48A). ACLY protein expression increased in SPDEF OX cells relative to iT2 control, and decreased in shSPDEF cells (Figure 48A). ACLY protein levels significantly decreased in SPDEF KO cells (Figure 48C). FASN protein levels were decreased in shSPDEF and SPDEF KO cell lines compared to respective controls (Figure 48A, B). Increase in FASN levels upon SPDEF OX was not observed (Figure 48A). ACC protein levels were reduced in SPDEF-overexpressing and knockdown cell lines. Anti-ACC detects both protein isoforms ACC1 and ACC2. Downregulation of ACC protein was validated in SPDEF-deficient cells (Figure 48C).



Because CD36 is a fatty acid transporter localized at the cell surface, I confirmed enhanced plasma membrane localization of CD36 in BPE8 shSPDEF cells relative to control by flow cytometry analysis (Figure 48D). Vice versa, cell surface CD36 expression was reduced in SPDEF OX cells.

Based on these data, I conclude that enzymes catalyzing fatty acid biosynthesis are positively regulated by SPDEF and CD36 is upregulated upon downregulation of SPDEF. Therefore, I hypothesized that shSPDEF cells may decrease *de novo* fatty acid biosynthesis and subsequently upregulate CD36 expression and fatty acid uptake as a compensatory pathway.

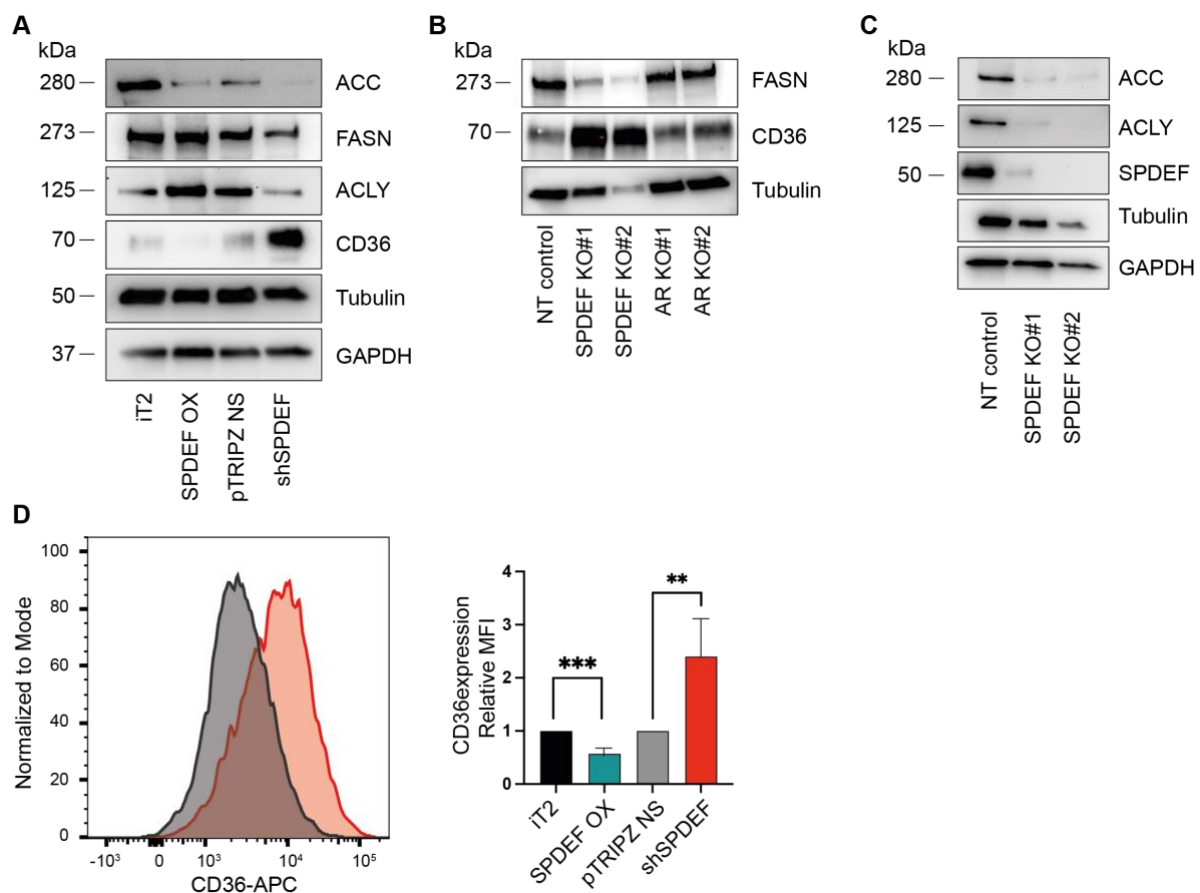


**Figure 48: SPDEF regulates ACLY, ACC, FASN and CD36 protein expression.** (A) Representative western blot analysis of ACLY, ACC, FASN and CD36 protein expression in BPE8 iT2 empty vector control (iT2), SPDEF overexpression (OX), pTRIPZ non-silencing (NS) control and shSPDEF cells. pTRIPZ NS and shSPDEF cells were pre-treated with doxycycline for one week *in vitro* before protein lysates were harvested. (B) Western blot analysis of FASN and CD36 in BPE8 non-targeting (NT) control, SPDEF knock-out (KO) #1, SPDEF KO#2, AR KO#1 and AR KO#2 cells. (C) Western blot analysis of ACC, ACLY and SPDEF in BPE8 NT control, SPDEF KO#1 and SPDEF KO#2 cells. Tubulin and GAPDH served as loading control. (D) Surface CD36 protein expression in BPE8 iT2 control, SPDEF OX, pTRIPZ NS control and shSPDEF cells was assessed by flow cytometry analysis. Representative FACS plot of pTRIPZ NS control (black) and shSPDEF (red) cells for CD36 expression assessed using anti-CD36 APC antibody (left). Results are shown for SPDEF OX, n= 5 individual experiments using two different antibodies, shSPDEF, n= 3 individual experiments using two different antibodies. Error bars show mean  $\pm$  SEM. P-value was calculated using an unpaired two-tailed t-test; \*  $p < 0.05$ , \*\*  $p < 0.01$ , \*\*\*  $p < 0.001$ ; not significant; kDa, kilo Dalton; MFI, mean fluorescence intensity.

### 3.8.4 SPDEF knockdown cells decrease *de novo* fatty acid synthesis but increase exogenous fatty acid uptake of specific fatty acids

Based on my previous findings, I hypothesized that SPDEF knockdown cells decrease *de novo* fatty acid biosynthesis and subsequently upregulate CD36 expression and exogenous fatty acid uptake as a compensatory pathway. To functionally assess the metabolic profile of AR<sup>+</sup> breast cancer cells upon SPDEF regulation, I traced the fate of carbohydrate sources used as substrates for *de novo* fatty acid biosynthesis (Figure 49). During glycolysis, glucose is processed to two-carbon acetyl-CoA which serves as a substrate for FASN. Acetate can serve as direct substrate for acetyl-CoA generation. In addition, glutamine is incorporated into the TCA cycle producing oxaloacetate and acetyl-CoA. Citrate is shuttled into the cytoplasm where it becomes cleaved into acetyl-CoA and oxaloacetate by ACLY<sup>182</sup>. Acetyl-CoA is carboxylated by ACC to produce malonyl-CoA which in turn is assembled into a 16-carbon long chain fatty acid palmitate (C16:0) by FASN<sup>183,184</sup>. Thus, the incorporation of <sup>13</sup>C-labeled two carbon units from <sup>13</sup>C-glucose, <sup>13</sup>C-glutamine and <sup>13</sup>C-acetate into palmitate and subsequent elongated and desaturated long chain fatty acids displays fatty acid biosynthesis activity. Isotope tracing experiments were performed in collaboration with Dr. Marteinn T. Snaebjörnsson, Schulze Lab, DKFZ Heidelberg.

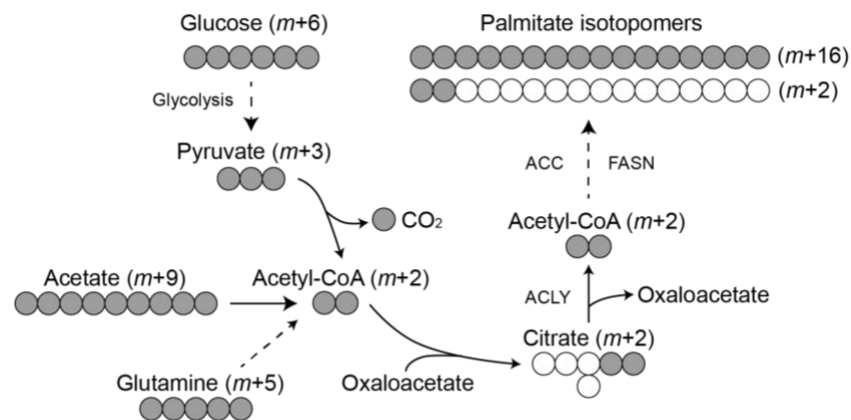


**Figure 49: Isotope tracing experiment scheme.** Schematic depicts how carbons from fully labeled <sup>13</sup>C-glucose, <sup>13</sup>C-glutamine and <sup>13</sup>C-acetate (indicated by grey circles) are incorporated into palmitate. (*m*+*x* illustrates number of labeled carbon atoms). Figure is recreated according to Ferraro *et al.*<sup>192</sup>.

We aimed to achieve metabolic steady-state and determined duration of labeling testing three different time points, 24h, 72h and 96h. BPE8 iT2 control, SPDEF OX, pTRIPZ NS and shSPDEF cells were cultured in CSC BC medium supplemented with <sup>13</sup>C-labeled glucose at the same concentrations as unlabeled glucose was usually added within the master mix (Table

1). Mass spectrometry analysis revealed that metabolic steady-state was reached after 72h. In comparison, isotopologue distribution did not change any further after 96h. Supplementary Figure 21A illustrates exemplary palmitate isotopomers observed in BPE8 iT2 control cells. However, isotopologue distribution was shifted to the left in all samples suggesting that glucose was not primarily used as carbon source for fatty acid synthesis. Due to low levels of total acetyl-CoA labeling, M+0 was composed of both, fatty acid synthesis and exogenous fatty acid uptake. To evaluate activity of fatty acid synthesis versus uptake upon overexpression or knockdown of SPDEF, we used three different tracers simultaneously,  $^{13}\text{C}$ -glucose,  $^{13}\text{C}$ -glutamine and  $^{13}\text{C}$ -acetate, to increase the total  $^{13}\text{C}$ -labeled two-carbon pool. However, the source from which the carbons found in palmitate and subsequently derived fatty acids are derived from cannot be distinguished. An appreciable fraction of palmitate was labeled in all samples. Palmitate isotopomer distribution in shSPDEF and control cells is shown in Figure 50A. No significant difference in total palmitate labeling was observed between shSPDEF and pTRIPZ NS control cells. Palmitate is elongated and desaturated to generate long chain fatty acids of various lengths and degrees of saturation<sup>185-187</sup>. Palmitate is desaturated by SCD enzyme to generate palmitoleate (C16:1), a monounsaturated fatty acid (Figure 50B). Palmitate is elongated by elongases to generate stearate (C18:0) (Figure 50C) that when desaturated produces oleate (C18:1) (Figure 50D). Isotopomer labeling trended to be higher in pTRIPZ NS control compared with shSPDEF cells.

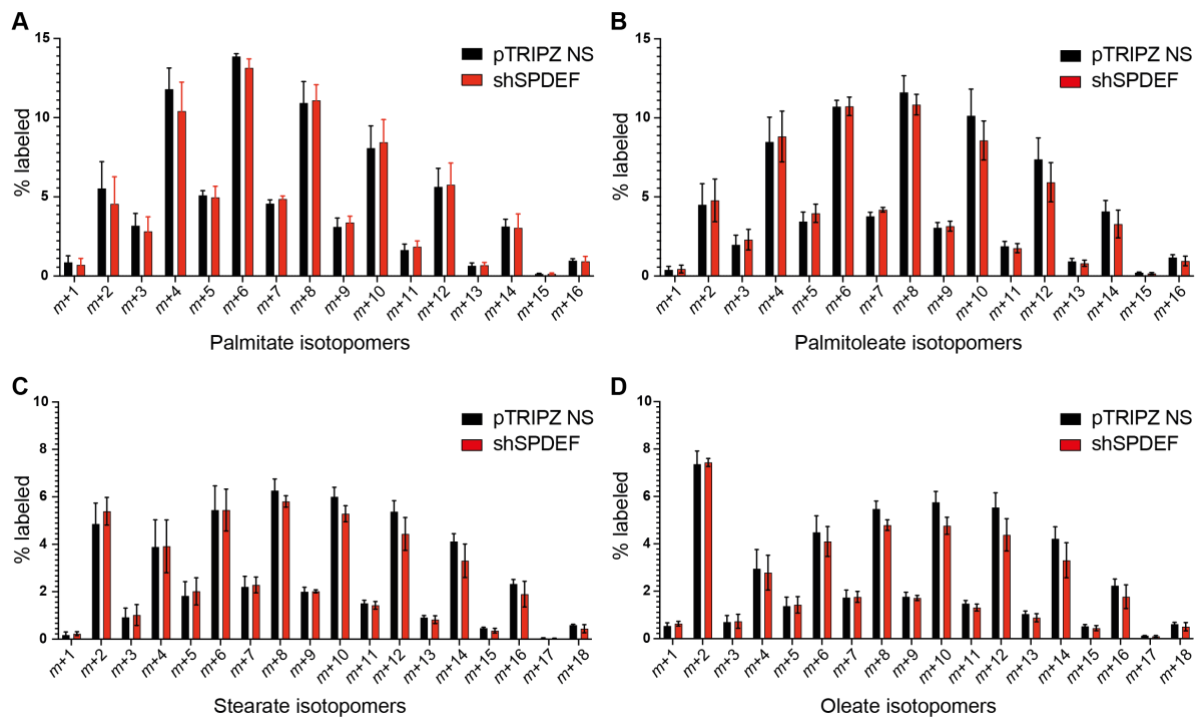


**Figure 50: Isotopologues distribution in BPE8 shSPDEF and pTRIPZ NS control cells.** The distribution of  $^{13}\text{C}$ -label in isotopologues of (A) palmitate (C16:0), (B) palmitoleate (C16:1), (C) stearate (C18:0) and (D) oleate (C18:1) from  $^{13}\text{C}$ -glucose,  $^{13}\text{C}$ -glutamine and  $^{13}\text{C}$ -acetate in BPE8 shSPDEF and pTRIPZ non-silencing (NS) cells ( $n = 3$  biological replicates/group). Error bars show mean  $\pm$  SEM. LC/MS analyses were performed by Dr. Marteinn T. Snaebjörnsson.

Sum of isotopologues is reflective of fatty acid synthesis from glucose, glutamine and acetate. The sum of labeled isotopologues showed a significant decreased  $^{13}\text{C}$ -incorporation from labeled carbon sources into stearate and palmitoleate in shSPDEF cells compared to pTRIPZ NS control (Figure 51C, D). In addition, oleate synthesis seemed to be reduced in shSPDEF cells. This is in agreement with my previous experiments tracing  $^{13}\text{C}$ -glucose incorporation into newly synthesized fatty acids. No significant difference was observed in total labeling for SPDEF OX cells relative to iT2 control (Supplementary Figure 21B-E).

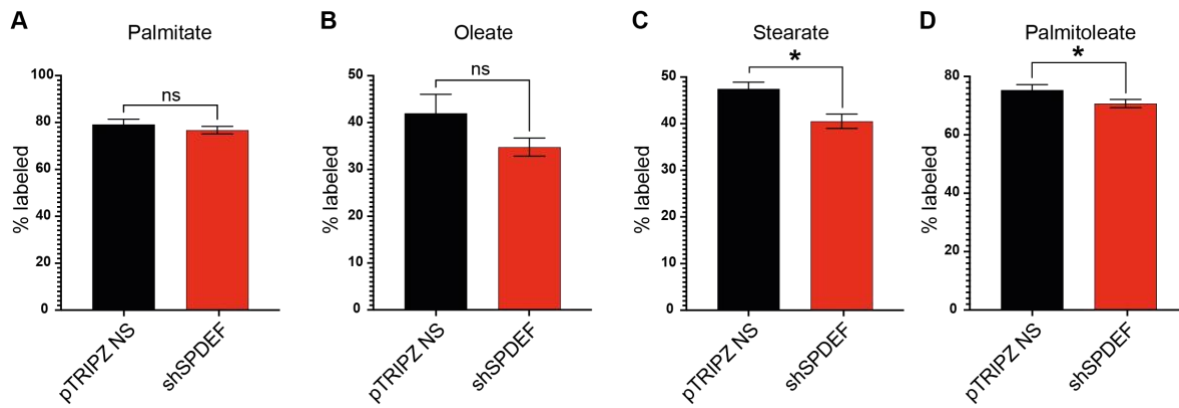


**Figure 51: Evidence for decreased fatty acid synthesis in BPE8 shSPDEF cells compared to control.** Sum of labeled isotopologues from  $^{13}\text{C}$ -glucose,  $^{13}\text{C}$ -glutamine and  $^{13}\text{C}$ -acetate in BPE8 pTRIPZ non-silencing (NS) and shSPDEF cells ( $n = 3$  biological replicates/shSPDEF;  $n = 2$  biological replicates/pTRIPZ NS). (A) Sum of palmitate isotopomers  $m+1$  to  $m+16$ . (B) Sum of oleate isotopomers  $m+3$  to  $m+18$ . (C) Sum of stearate isotopomers  $m+3$  to  $m+18$ . (D) Sum of palmitoleate isotopomers  $m+1$  to  $m+16$ . Error bars show mean  $\pm$  SEM. P-value was calculated using an unpaired two-tailed t-test; \*  $p < 0.05$ , \*\*  $p < 0.01$ , \*\*\*  $p < 0.001$ ; ns, not significant. LC/MS analyses were performed by Dr. Marteinn T. Snaebjörnsson.

In this experiment, the amount of fatty acid molecules derived from fatty acid synthesis completely unlabeled is negligible, therefore isotopomers  $m+0$  represent uptake of exogenous fatty acids. In line with decreased levels of newly synthesized oleate, stearate and palmitoleate, shSPDEF cells showed enhanced uptake of these fatty acids compared to pTRIPZ NS control cells. These data suggest that especially exogenous uptake of mono-unsaturated fatty acids (MUFAs) were enhanced upon downregulation of SPDEF. No differences were noted in fatty acid synthesis or uptake in SPDEF OX cells relative to iT2 control (data not shown).

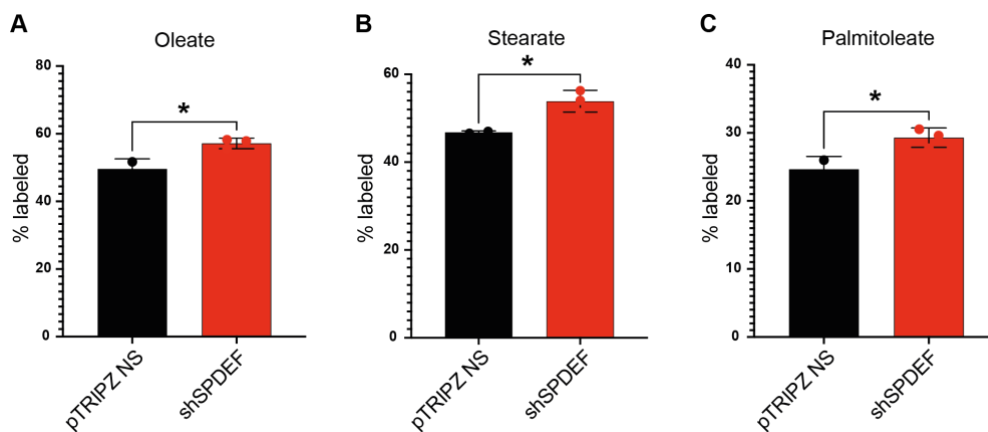


**Figure 52: Fatty acid uptake is increased in BPE8 shSPDEF cells compared to control.** (A) Oleate, (B) stearate and (C) palmitoleate isotopomers  $m+0$  are increased in BPE8 shSPDEF cells compared to pTRIPZ non-silencing (NS) control ( $n = 3$  biological replicates/shSPDEF;  $n = 2$  biological replicates/pTRIPZ NS). Error bars show mean  $\pm$  SEM. P-value was calculated using an unpaired two-tailed t-test; \*  $p < 0.05$ , \*\*  $p < 0.01$ , \*\*\*  $p < 0.001$ ; ns, not significant. LC/MS analyses were performed by Dr. Marteinn T. Snaebjörnsson.

Taken together, decreased  $^{13}\text{C}$  labeling of elongated and desaturated fatty acids upon downregulation of SPDEF coupled to decreased expression levels of fatty acid synthesis

enzymes suggest that SPDEF promotes fatty acid biosynthesis in AR<sup>+</sup> breast cancer cells. In addition, I showed that shSPDEF cells restore their cellular lipid pool by CD36 upregulation and enhanced exogenous fatty acid uptake with preference for MUFAs.

### **3.8.5 Abolishing CD36 expression in SPDEF knockdown cells impairs *in vitro* cell growth**

Previous experiments suggested that CD36 was upregulated upon SPDEF knockdown and knock-out in order to compensate for the decrease in fatty acid synthesis. If this hypothesis holds true, abolishing CD36 in shSPDEF cells would affect cell viability.

Thus, I investigated whether targeting CD36 would thus impair viability of shSPDEF cells. To address this question, I generated CD36 KO in shSPDEF or non-silencing control cells using three different gRNAs targeting CD36. Non-targeting gRNA (NT control) was used as control. CRSPR/Cas9-mediated CD36 depletion was highly efficient using either of the three gRNAs. CD36 protein expression was no longer detectable by western blot analysis in CD36 KO#1-3 cell lines (Supplementary Figure 22A). Flow cytometry analysis revealed that only 3-7% of cells still expressed CD36 on cell surface after CD36 disruption (Supplementary Figure 22B).

First, I confirmed that NT control gRNA had no effect on CD36 expression in shSPDEF and pTRIPZ NS cells (Figure 53A). As expected, CD36 expression was increased upon downregulation of SPDEF. After six days of Dox induction, CD36 expression was analyzed in shSPDEF CD36 KO and control cells by flow cytometry (Figure 53C). I found that CD36 expression was significantly increased in shSPDEF cells relative to control cells, even in CD36 KO sample suggesting that the small subpopulation of CD36<sup>+</sup> cells remaining in the KO pool have a growth advantage (Figure 53B, C). To validate this finding, either shSPDEF NT control and shSPDEF CD36 KO cells, or NS control NT control and NS control CD36 KO cells were mixed in a 1:1 ratio (Figure 54A). Subsequently, CD36 expression was analyzed at multiple time points (Figure 54B). After ten days, CD36<sup>+</sup> cells grew out significantly faster when SPDEF was downregulated relative to control, although the total number of CD36<sup>+</sup> cells increased in both cell lines (Figure 54B, C). These results strongly suggest that shSPDEF cells upregulated CD36 as compensatory pathway, while abolishing CD36 in shSPDEF cells significantly affected cell viability.

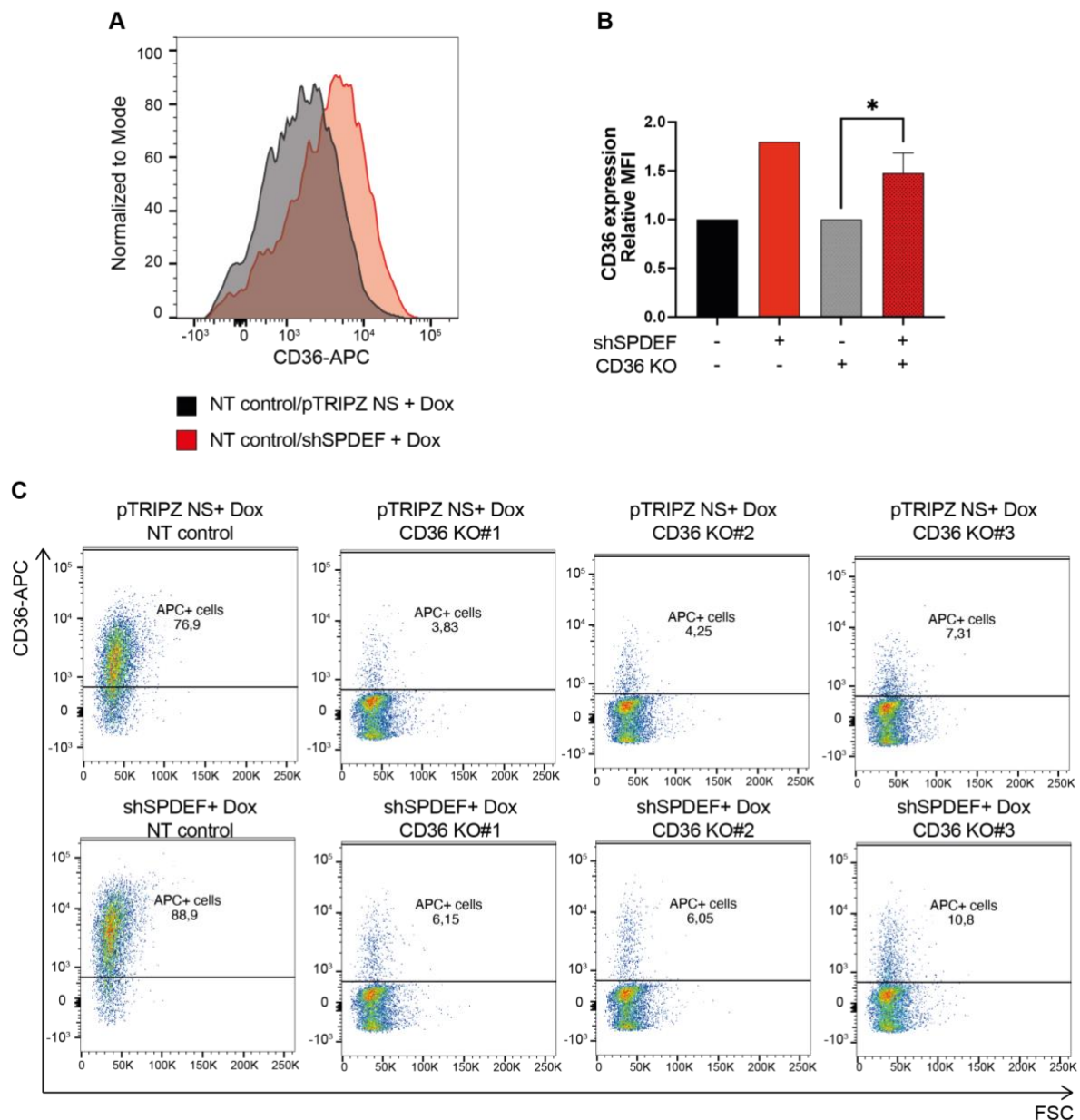


**Figure 53: CD36 expression confers growth advantage to SPDEF knockdown cells.** (A-C) BPE8 pTRIPZ NS NT control, pTRIPZ NS CD36 KO#1-3, shSPDEF NT control and shSPDEF CD36 KO#1-3 cells were analyzed for CD36 expression using anti-CD36 APC antibody by flow cytometry analysis six days after doxycycline (Dox) induction. (A) Histogram for CD36-APC expression in pTRIPZ NS NT control and shSPDEF NT control cells normalized to mode. (B) Mean fluorescence intensity (MFI) for CD36 expression was normalized on respective NT control cells (n= 3 biological replicates CD36 KO#1-3;  $\pm$ SD). P-value was calculated using an unpaired two-tailed t-test; \*  $p < 0.05$ , \*\*  $p < 0.01$ , \*\*\*  $p < 0.001$ ; ns, not significant. NT, non-targeting; NS, non-silencing; KO, knock-out; Dox, doxycycline; FC, fold change.

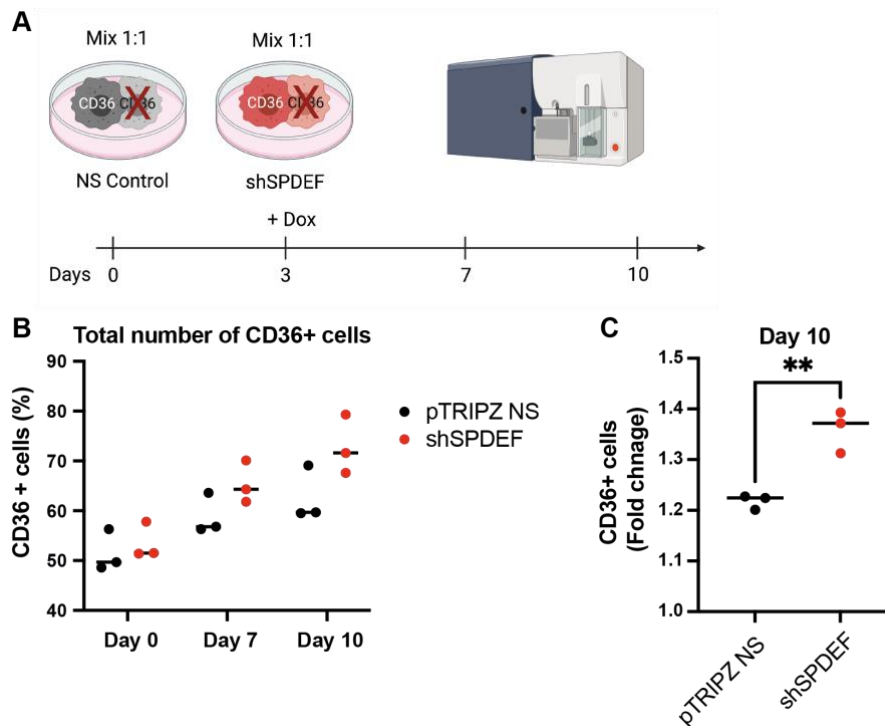


**Figure 54: CD36<sup>+</sup> cells grow out faster in BPE8 shSPDEF cells.** (A) Schematic depicts experimental layout. BPE8 pTRIPZ NS control NT control and CD36 KO cells were mixed in a 1:1 ratio. Similar, BPE8 shSPDEF NT control and CD36 KO cells were mixed in a 1:1 ratio. Cells were induced with doxycycline (Dox) on day 3, CD36 expression was assessed by flow cytometry on day 7 and day 10 (n = 3 biological replicates CD36 KO#1-3). (B) Total number of CD36 positive cells. (C) Fold change of CD36 positive cells on day 10 (from B) normalized on pTRIPZ NS control cells. P-value was calculated using an unpaired two-tailed t-test; \* p < 0.05, \*\* p < 0.01, \*\*\* p < 0.001; ns, not significant. NT, non-targeting; NS, non-silencing; KO, knock-out; Dox, doxycycline; FC, fold change.

Pharmacological inhibition of CD36 using sulfosuccinimidyl-oleate (SSO), a CD36 inhibitor<sup>217,218</sup>, resulted in similar reduction of cell growth in shSPDEF cells relative to pTRIPZ NS control as observed upon genetic disruption of CD36 expression (Figure 55A). No significant difference in total cell number was observed when pTRIPZ NS control cells were treated with SSO for six days, neither when cultured in CSC BC medium (Figure 55A), nor in human plasma-like medium (HPLM) (Figure 55B). SSO treatment significantly reduced total number of shSPDEF cells relative to treated pTRIPZ NS control cells in CSC BC medium (Figure 55A). Cells cultured in HPLM showed a significant growth disadvantage upon SPDEF downregulation relative to control (Figure 55C, D). In addition, SSO treatment significantly inhibited cell growth of shSPDEF cells (Figure 55C, D). This experiment was performed by Corinna Schumacher as part of her MD thesis (HI-STEM, unpublished).

Taken together, these findings show that shSPDEF cells highly rely on upregulation of CD36 expression upon SPDEF downregulation. This suggests that CD36 transporter expression is upregulated to enhance fatty acid uptake from the microenvironment and maintain lipid metabolism upon downregulation of fatty acid synthesis (based on FA transcriptomic profiles).



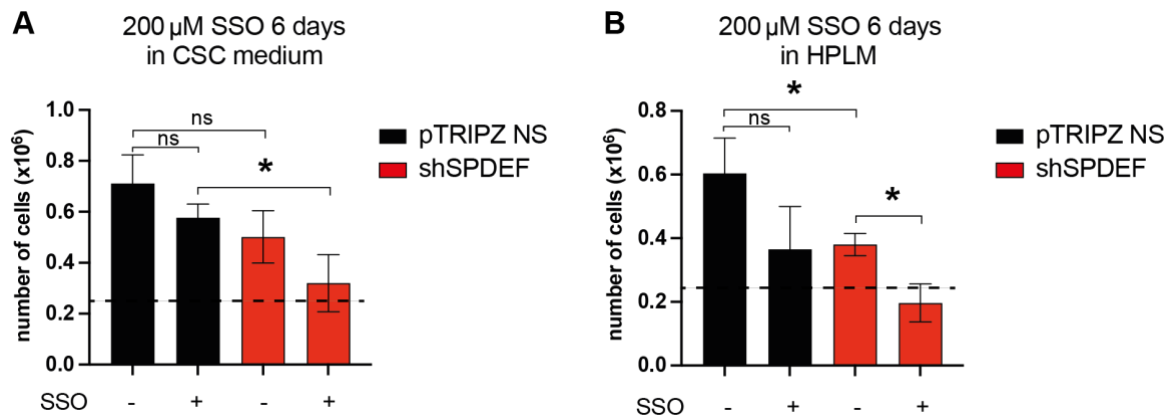


**Figure 55: Pharmacological CD36 inhibition in shSPDEF cells significantly inhibits cell growth.** BPE8 shSPDEF and pTRIPZ non-silencing (NS) control cells were treated with 200 $\mu$ M sulfosuccinimidyl-oleate (SSO) or vehicle control for six days cultured either in (A) breast cancer-specific cancer stem cell (CSC) medium or (B) human plasma-like medium (HPLM). Total number of cells after six days of treatment is depicted. Cells were pre-treated with doxycycline (Dox) for one week *in vitro* before cells were seeded for treatment assay. Cell number was counted after six days using Beckman ViCell Counter. Error bars depict mean  $\pm$  SD; n= 3 independent experiments. P-value was calculated using an unpaired two-tailed t-test between indicated groups; \* p < 0.05, \*\* p < 0.01, \*\*\* p < 0.001; ns, not significant. This experiment was conducted by Corinna Schumacher as part of her MD thesis (unpublished).

### 3.8.6 SPDEF knockdown cells have a growth disadvantage in lipid-depleted environment

Pharmacological inhibition of CD36 or CRISPR/Cas9-mediated CD36 disruption significantly decreased cell viability in shSPDEF cells relative to control. I hypothesized that abolishing CD36 would result in restriction of exogenous fatty acid uptake. If this holds true, culturing shSPDEF cells in lipid-depleted medium should affect cell viability in a similar way. Extracellular lipid availability and uptake are crucial for *de novo* fatty acid biosynthesis.

Usual cell culture media including our breast cancer-specific CSC medium, contain glucose, amino acids, and lipids among other metabolites at concentrations that mostly do not reflect those found in the patient. This is a major issue when studying the metabolic profiles of cancer cells. Here, BPE8 cells were originally derived from a pleural effusion sample of a mBC patient. For this reason, I utilized the human plasma-like medium (HPLM) ‘resembling the natural cellular environment found in the body, mimicking the metabolic profile of human plasma’<sup>219</sup>. In order to provide conditions that BPE8 cells survived and grew, HPLM was supplemented with breast-cancer specific growth factors and hormones, but not with lipid mix usually added to CSC medium (Table 1).

To investigate cell growth under physiological relevant conditions upon SPDEF overexpression or downregulation, BPE8 SPDEF OX, shSPDEF and respective control cells were cultured for eight days in HPLM (Figure 56A). Growth rate was significantly reduced upon downregulation of SPDEF compared to pTRIPZ NS control, or shSPDEF-not induced cells (Figure 56A, Figure 55C, C). No significant changes were observed upon overexpression of SPDEF. In general, growth rates were quite similar in SPDEF OX and control cell lines cultured in HPLM in comparison to cells cultured in fully-supplemented CSC BC medium (Figure 56). In contrast, no significant growth difference was observed in shSPDEF cells relative to control when cells were cultured in CSC BC medium (Figure 56B).

Together, these findings suggest that SPDEF regulates lipid metabolism in AR<sup>+</sup> BPE8 cells *in vitro*. However, this experiment shows that the metabolic phenotype was masked *in vitro* due to saturated, artificial medium conditions not reflecting the patient's metabolic environment. As an outlook, it would be interesting to see whether the observed phenotype could be rescued by adding certain lipids to HPLM and accomplish fatty acid metabolism.

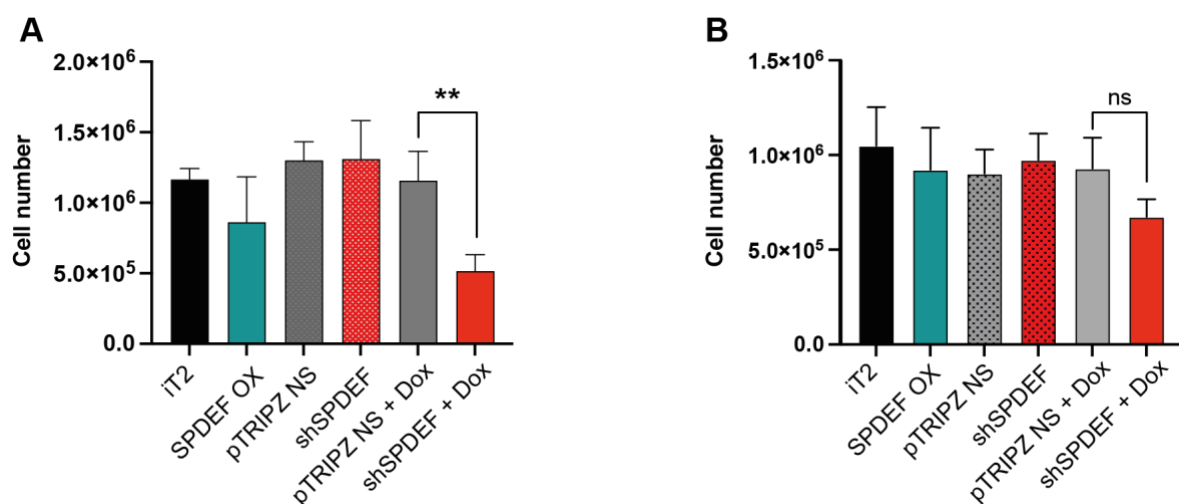


**Figure 56: shSPDEF cells exhibit a growth disadvantage when cultured in HPLM.** BPE8 iT2 empty vector control (iT2), SPDEF overexpressing (OX), pTRIPZ NS ( $\pm$  Dox) and shSPDEF ( $\pm$  Dox) cells were cultured in (A) human plasma-like medium (HPLM) supplemented with breast cancer-specific hormones and growth factors or (B) breast cancer-specific cancer stem cells (CSC) medium. pTRIPZ NS and shSPDEF cells + Dox were pre-treated with Dox for one week *in vitro* before cells were seeded. 250,000 cells were seeded on day 0, cells were counted on day 8 using ViCell Counter (in HPLM, n = 3 independent experiments; in CSC, n = 3 independent experiments). P-value was calculated using an unpaired two-tailed t-test; \* p < 0.05, \*\* p < 0.01, \*\*\* p < 0.001; ns, not significant. OX, overexpression; NS, non-silencing; Dox, doxycycline. Last biological replicate in HPLM was produced by Ornella Kossi.

To ensure that shSPDEF cells showed similar transcriptomic response to lipid deprivation as observed in full CSC BC medium, metabolic genes of interest were validated in SPDEF OX, shSPDEF and respective control cells cultured in HPLM (Figure 57 and Supplementary Figure 23). Similar results were observed upon SPDEF OX or downregulation, respectively, as when

cultured in CSC BC medium (Figure 45A, B). Interestingly, downregulation of genes involved in fatty acid synthesis was even stronger in shSPDEF cells cultured in HPLM when compared to transcriptional profiles of shSPDEF cells cultured in CSC BC medium (Figure 57B). This suggests that shSPDEF growth disadvantage in HPLM was in agreement with stronger transcriptional response to lipid deprivation as compared to saturated medium conditions.

Taken together, these data suggest that SPDEF regulates fatty acid metabolism in AR<sup>+</sup> breast cancer cells relying on *de novo* fatty acid biosynthesis. Whereas extracellular lipids are available in CSC BC medium, shSPDEF cells cannot compensate lipid uptake via enhanced upregulation of CD36 in lipid-depleted HPLM conditions.

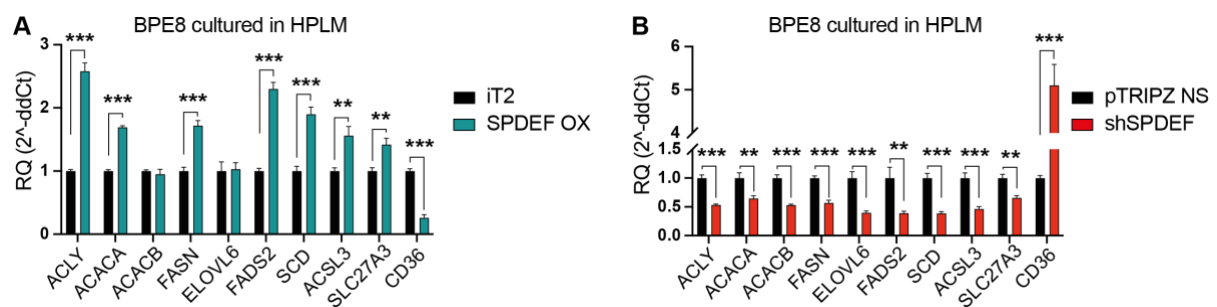


**Figure 57: Fatty acid metabolism target genes are deregulated in BPE8 SPDEF overexpression and knockdown cells cultured in HPLM.** (A) Representative RT-qPCR analysis of target genes involved in fatty acid metabolism in BPE8 SPDEF-overexpressing (OX) and iT2 empty vector control (iT2) cells; (B) in BPE8 shSPDEF and pTRIPZ non-silencing (NS) control cells cultured in human plasma-like medium (HPLM) supplemented with breast cancer-specific growth factors and hormones (n= 3 technical replicates/cell line). shSPDEF and pTRIPZ NS control cells were treated with doxycycline for one week before RNA was extracted. Values are given as two-fold change relative to control group; RQ, relative quantification. P-value was calculated using an unpaired two-tailed t-test; \* p < 0.05, \*\* p < 0.01, \*\*\* p < 0.001; not significant when no indication. RNA extraction, cDNA synthesis and RT-qPCR were performed by Ornella Kossi.

### 3.8.7 SPDEF and FASN are co-expressed in PDX-derived cell models and breast cancer patients

To explore whether increased expression of fatty acid synthase is associated with SPDEF expression in breast cancer patients, I re-analyzed the previously used published data set, METABRIC, for *FASN* and *CD36* mRNA levels. *SPDEF* and *FASN* mRNA expression strongly correlated in ER<sup>-</sup> BC patients (Figure 58A) and to a much lesser extent in luminal tumors (Figure 58B). In contrast, no appreciable correlation was observed for *SPDEF* and *CD36* mRNA (Supplementary Figure 24A, B). In agreement with high *SPDEF* expression, *FASN* mRNA levels significantly stratified ER<sup>-</sup> BC patients based on survival probability with high *FASN* levels being associated with worse prognosis (Figure 58C). In contrast, in ER<sup>+</sup> breast

cancers, high *FASN* levels were associated with better outcome (Figure 58D). Similar finding was noted for *CD36* expression. Low levels of *CD36* mRNA were associated with decreased survival probability in ER<sup>+</sup> BC patients, whereas no significant stratification based on *CD36* expression was observed for survival probability in ER<sup>-</sup> BC patients (Supplementary Figure 24C, D).

To test whether high *SPDEF* and *FASN* co-expression in ER<sup>-</sup> BC patients was associated with AR status, I analyzed the differentially expressed genes between AR<sup>high</sup> and AR<sup>low</sup> tumors and found that *FASN* was among the top 100 variant genes associated with AR expression (data not shown). GSEA revealed that fatty acid metabolism was enriched in AR<sup>+</sup> tumors (Figure 58E).

Endogenous co-expression of AR, SPDEF and FASN protein was confirmed in our PDX-derived cell models (Figure 58F). In addition, I found that CD36 protein showed higher expression levels in AR<sup>+</sup> BPE8 and CTC223 cells compared to the AR<sup>-</sup> BPE7 cell line.

Together, these results suggest that *FASN* expression is associated with *SPDEF* and AR expression in breast cancer patients, and that AR<sup>+</sup> breast cancer cells have a distinct lipogenic metabolic protein profile.

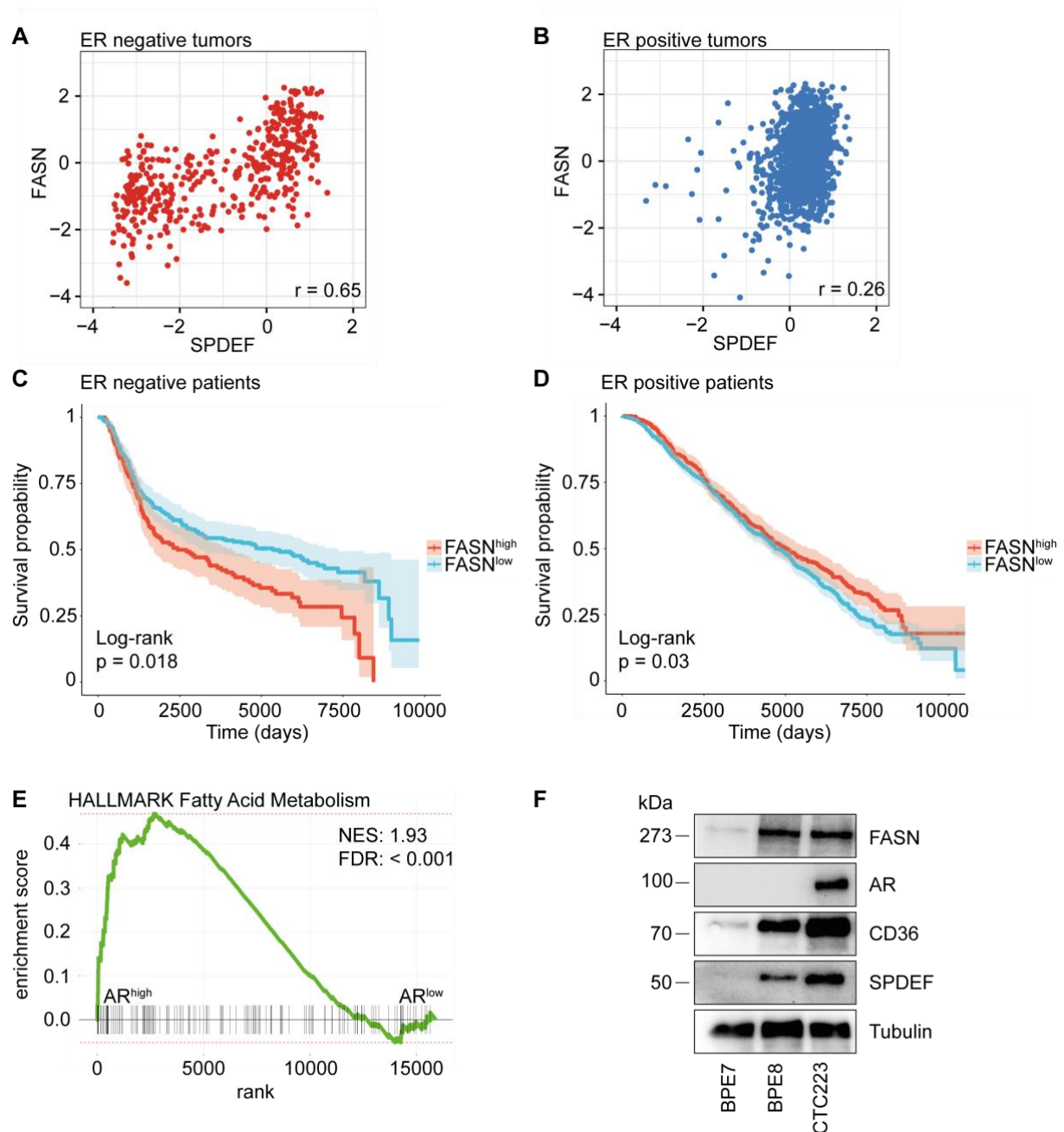


**Figure 58: Fatty acid synthase is enriched in AR<sup>+</sup> breast cancers.** (A, B) Linear correlation of *SPDEF* and *FASN* gene expression in (A) ER negative (red) and (B) ER positive (blue) breast cancer patients. Depicted is the Pearson correlation coefficient  $r$  calculated with R package *ggpubr*. (C, D) Kaplan-Meier estimator for survival probability of (C) ER<sup>-</sup> breast cancer and (D) ER<sup>+</sup> breast cancer patients stratified based on *FASN* gene expression. Data is extracted from METABRIC data set including 445 ER<sup>-</sup> breast cancer patients. (E) Gene set enrichment analysis applied on differentially expressed genes between AR<sup>high</sup> and AR<sup>low</sup> ER<sup>-</sup> breast cancer patients based on *AR* mRNA expression revealed that Hallmark Fatty Acid Metabolism is enriched in AR<sup>high</sup> tumors. (F) Representative western blot analysis of *FASN*, *AR*, *CD36* and *SPDEF* protein expression in BPE7, BPE8 and CTC223 cells. Tubulin served as loading control. ER, estrogen receptor; NES, normalized enrichment score; FDR, false discovery rate; kDa, kilo Dalton.

### 3.9 SPDEF regulates mitochondrial metabolism

#### 3.9.1 SPDEF regulates mitochondrial respiration activity in AR<sup>+</sup> breast cancer cell models

Previous findings suggested that SPDEF regulates cell metabolism in AR<sup>+</sup> breast cancer cells. I found that genes involved in gluconeogenesis and *de novo* fatty acid biosynthesis were downregulated in shSPDEF cells relative to control. Furthermore, GSEA revealed that energy production pathways including ATP and NADH metabolic processes were significantly enriched in SPDEF-expressing cells. To functionally investigate the metabolic profiles of the cells, I performed Mito Stress assays measuring mitochondrial respiration activity using Agilent Seahorse technologies. The assay allows simultaneous measurement of multiple parameters including basal and maximal respiration activity and ATP production using molecular oxygen. The spare respiratory capacity allows to evaluate the cells' ability to meet certain energetic challenges needed to engraft and survive in circulation or at distant organs (Agilent). The protocol involves three serial injections of inhibitors targeting different complexes of the mitochondrial electron transport chain: oligomycin, FCCP and rotenone/antimycin A. Some of the experiments were conducted in co-work with Dr. Mattia Falcone and Dr. Andrea Geist.

In AR<sup>+</sup> BPE8 control cells, basal oxygen consumption rate (OCR) was quite high suggesting that they are reliant on OxPhos for energy production (Figure 59). Upon overexpression of SPDEF, basal and maximal respiration was significantly increased (Figure 59A, C). The spare respiratory capacity was also 4-fold increased in SPDEF OX cells compared to control advocating that SPDEF-overexpressing cells are more robust and adjustable to energetic demands (Figure 59A). ATP production using molecular oxygen was significantly enhanced when SPDEF was overexpressed. Figure 59C displays a representative experiment and measurements upon acute serial injections. Vice versa, basal mitochondrial respiration activity was significantly decreased in shSPDEF cells relative to pTRIPZ NS control cells (Figure 59B, D). In addition, extracellular acidification rate (ECAR) was noticeably lower in SPDEF knockdown cells suggesting that not only OxPhos but also glycolytic rate was decreased (Figure 59F).

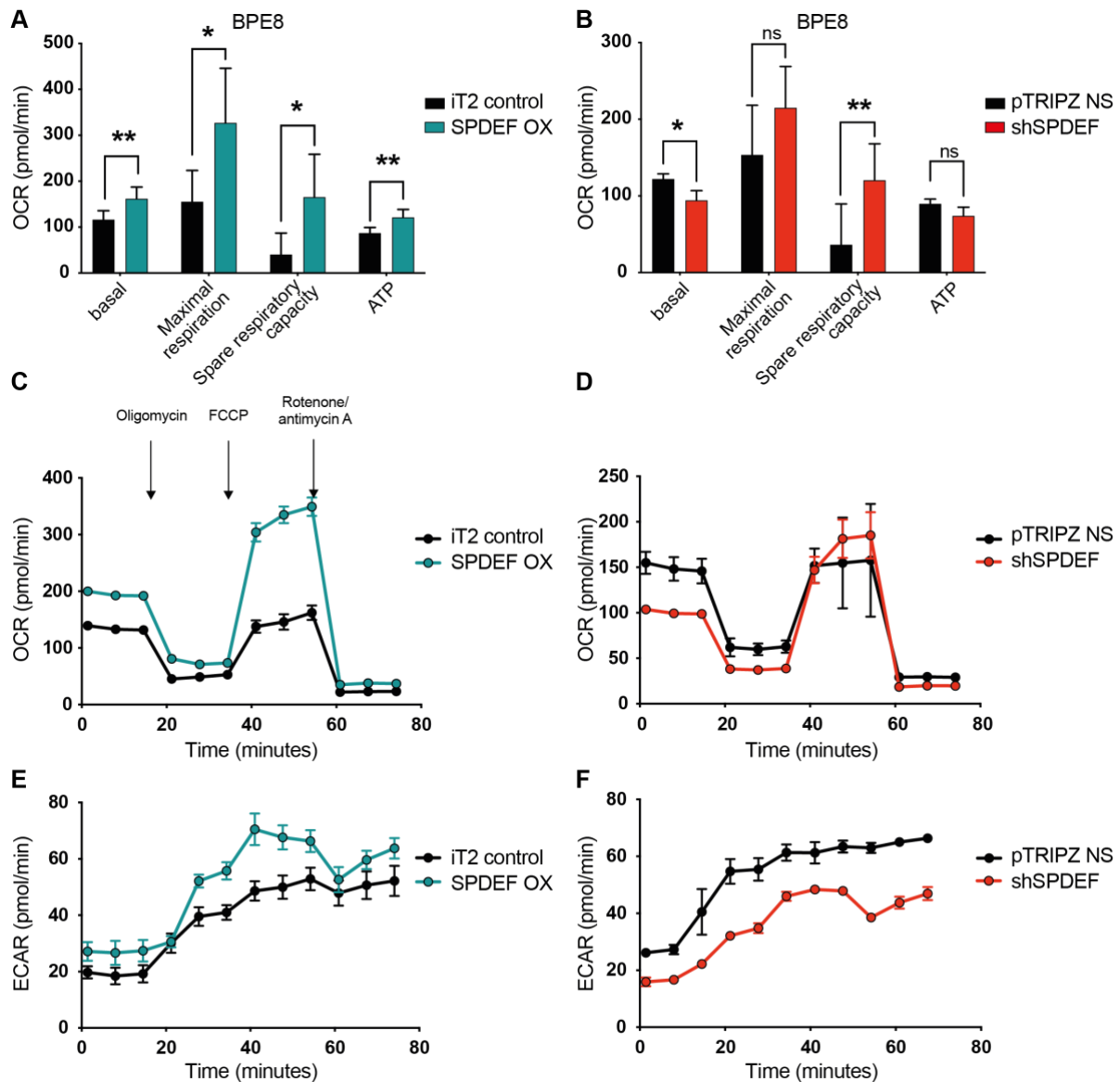


**Figure 59: SPDEF controls mitochondrial respiration activity in AR<sup>+</sup> BPE8 cells.** Mitochondrial respiration activity was measured in BPE8 SPDEF-overexpressing (OX) and iT2 empty vector control (iT2 control) (A), and shSPDEF and pTRIPZ non-silencing (NS) cells (B) using Agilent Seahorse Technologies. shSPDEF and pTRIPZ NS cells were pretreated with doxycycline for one week before assay was started. Basal and maximal respiration, spare respiratory capacity and ATP production were assessed (n= 3 independent experiments/6-8 technical replicates/group). Error bars depict mean  $\pm$  SD. P-value was calculated for three independent experiments using an unpaired two-tailed t-test; \* p < 0.05, \*\* p < 0.01, \*\*\* p < 0.001; ns, not significant. (C-F) Representative Mito Stress experiment in BPE8 SPDEF OX and iT2 control (C, E) and shSPDEF and pTRIPZ NS (D, F) cells (n= 6 technical replicates/group). Three inhibitors, oligomycin, FCCP and rotenone/antimycin A, were serially injected at indicated time points. Error bars depict mean  $\pm$  SEM. OCR, oxygen consumption rate; ECAR, extracellular acidification rate.

The phenotype observed for molecular apocrine BPE8 cells could be confirmed in AR<sup>+</sup> CTC223 cells. Basal respiration levels were slightly higher in SPDEF OX cells compared to iT2 control cells. Basal mitochondrial respiration activity was notably decreased in shSPDEF cells (Figure 60A-D). Figure 60D illustrates a representative experiment showing that shSPDEF cells' OCR was dramatically low. Maximal respiration activity and ATP production were

noticeably reduced when SPDEF was downregulated (Figure 60B). In line, spare respiratory capacity was highly decreased suggesting that shSPDEF cells were less robust in responding to energetic demands. In AR<sup>+</sup> MDA-MB-453 cells, basal oxygen consumption rates were similar in experimental and control cells (Supplementary Figure 25). However, maximal respiration activity was highly reduced in shSPDEF cells. SPDEF downregulation seemed to impair cells' ability to adapt to energetic challenges since the spare respiratory capacity was highly decreased (Supplementary Figure 25B). This suggest that SPDEF knockdown in MDA-MB-453 cells affects cell energy metabolism only under stressed conditions. Taken together, these data characterize SPDEF as a required metabolic transcription factor in AR<sup>+</sup> breast cancer cells regulating mitochondrial respiration activity.

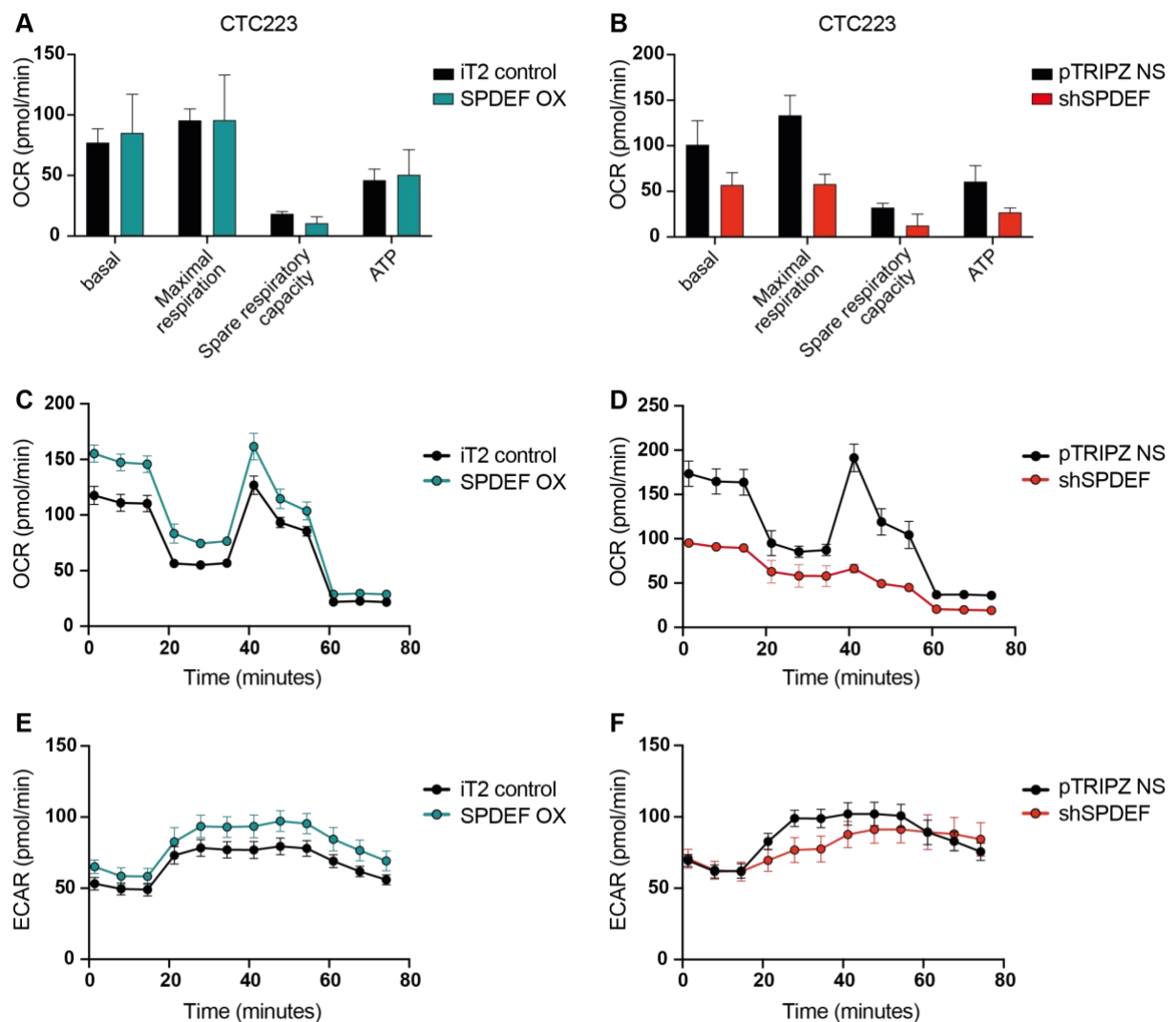


**Figure 60: SPDEF controls mitochondrial respiration activity in AR<sup>+</sup> CTC223 cells.** Mitochondrial respiration activity was measured in CTC223 SPDEF-overexpressing (OX) and iT2 empty vector control (iT2 control) (A), and shSPDEF and pTRIPZ non-silencing (NS) cells (B) using Agilent Seahorse Technologies. shSPDEF and pTRIPZ NS cells were pretreated with doxycycline for one week before assay was started. Basal and maximal respiration, spare respiratory capacity and ATP production were assessed (n= 2 independent experiments/6 technical replicates/group). (figure legend continues on the next page).



### 3.9.2 Pharmacological activation or inhibition of AR impairs mitochondrial respiration activity

AR regulates mitochondrial metabolism in PCa<sup>220</sup>. Further, I found that SPDEF regulates mitochondrial respiration activity in AR<sup>+</sup> breast cancer cells. I hypothesized that SPDEF might regulate mitochondrial respiration via AR signaling in breast cancer. To this end, I utilized AR<sup>+</sup> MDA-MB-453 cells and treated them with either AR agonists, R1881 or DHT, or antagonist enzalutamide for 72h *in vitro*. Synthetic testosterone treatment with R1881 and DHT treatment significantly increased basal and maximal oxygen consumption rates (OCR) of MDA-MB-453 cells (Figure 61A, C, D). In contrast, Enza-treated cells showed reduced levels of mitochondrial respiration activity (Figure 61B, C, D). In addition, Enza treatment could partly reverse the DHT-induced increase in OCR (Figure 61C, D). These results suggest that not only SPDEF, but also AR is involved in regulating mitochondrial energy metabolism in AR<sup>+</sup> breast cancer cells. To further elucidate this mechanism, I measured OCRs in BPE8 AR KO cells. Basal and maximal respiration was increased in AR KO cells relative to NT control (data not shown). However, this experiment was only performed once and needs to be repeated in order to evaluate this finding. Nonetheless, increased OCR upon AR KO was in line with increased SPDEF expression upon AR depletion.

---

(C-F) Representative Mito Stress experiment in CTC223 SPDEF OX and iT2 control (C, E) and shSPDEF and pTRIPZ NS (D, F) cells (n= 6 technical replicates/group). Three inhibitors, oligomycin, FCCP and rotenone/antimycin A, were serially injected. OCR, oxygen consumption rate; ECAR, extracellular acidification rate.

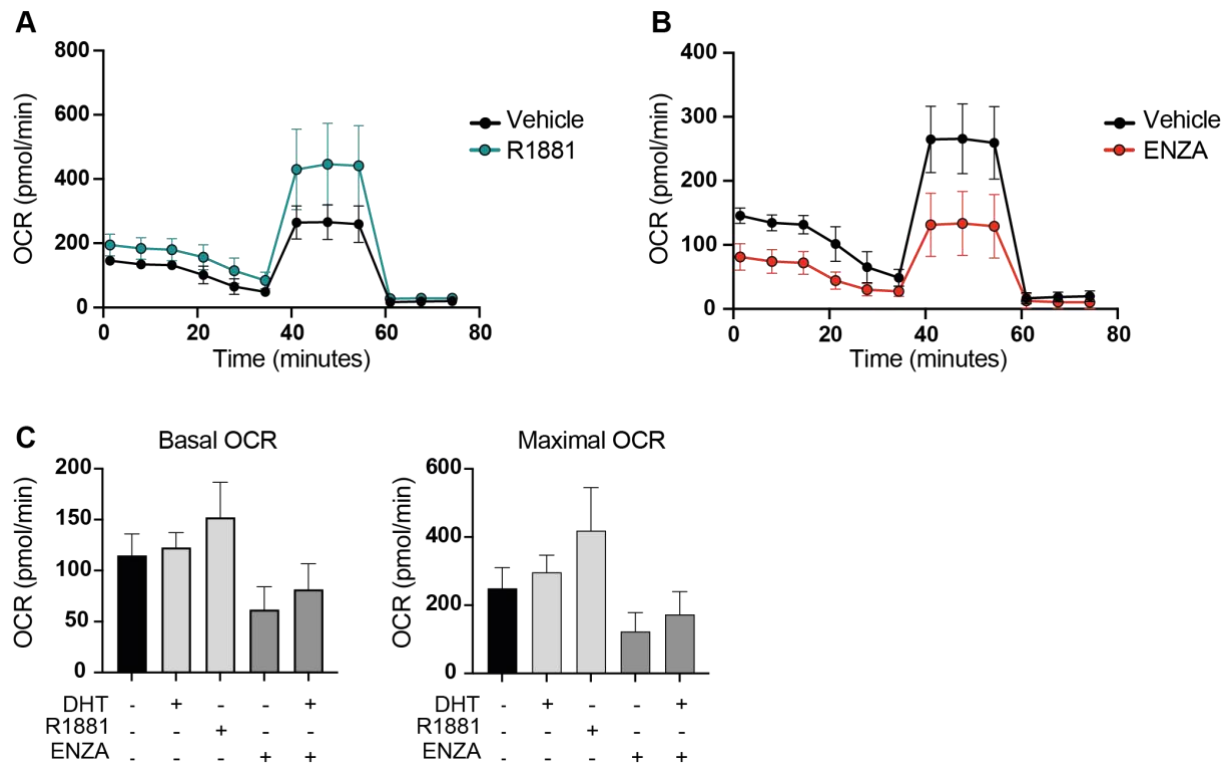


**Figure 61: Pharmacological regulation of AR controls mitochondrial respiration activity in AR<sup>+</sup> MDA-MB-453 cells.** Seahorse Mito Stress assay was measured in MDA-MB-453 cells. Cells were pretreated with either 1nM DHT, 1nM R1881, 10  $\mu$ M enzalutamide (ENZA) or vehicle control for 72h before assay was started. Basal and maximal oxygen consumption rate (OCR) were assessed (n= 6 technical replicates/group). (A, B) Representative Mito Stress experiment in MDA-MB-453 cells treated with (A) R1881 or (B) ENZA. (C) Basal OCR and (D) Maximal OCR (n= 6 technical replicates/group). Three inhibitors, oligomycin, FCCP and rotenone/antimycin A, were serially injected. OCR, oxygen consumption rate; DHT, dihydrotestosterone.

To test whether AR activation could also restore the decrease in mitochondrial respiration activity upon SPDEF downregulation, I treated CTC223 shSPDEF and pTRIPZ NS control cells with synthetic testosterone analogue R1881 for six days *in vitro* and measured OCRs (Figure 62). AR agonist activation resulted in enhanced basal and maximal respiration in CTC223 pTRIPZ control cells similar to what has been observed in MDA-MB-453 cells previously (Figure 62A, B). Testosterone treatment did not restore reduction in mitochondrial respiration activity when SPDEF was downregulated. Moreover, pharmacological AR inhibition decreased OCRs on basal and maximal level in CTC223 control cells (Figure 62). However, Enza treatment had no additional effect in SPDEF knockdown cells. Based on these findings, I conclude that AR regulates mitochondrial metabolism via SPDEF. Further, SPDEF is indispensable for regulation of mitochondrial respiration activity in AR<sup>+</sup> breast cancer cells.

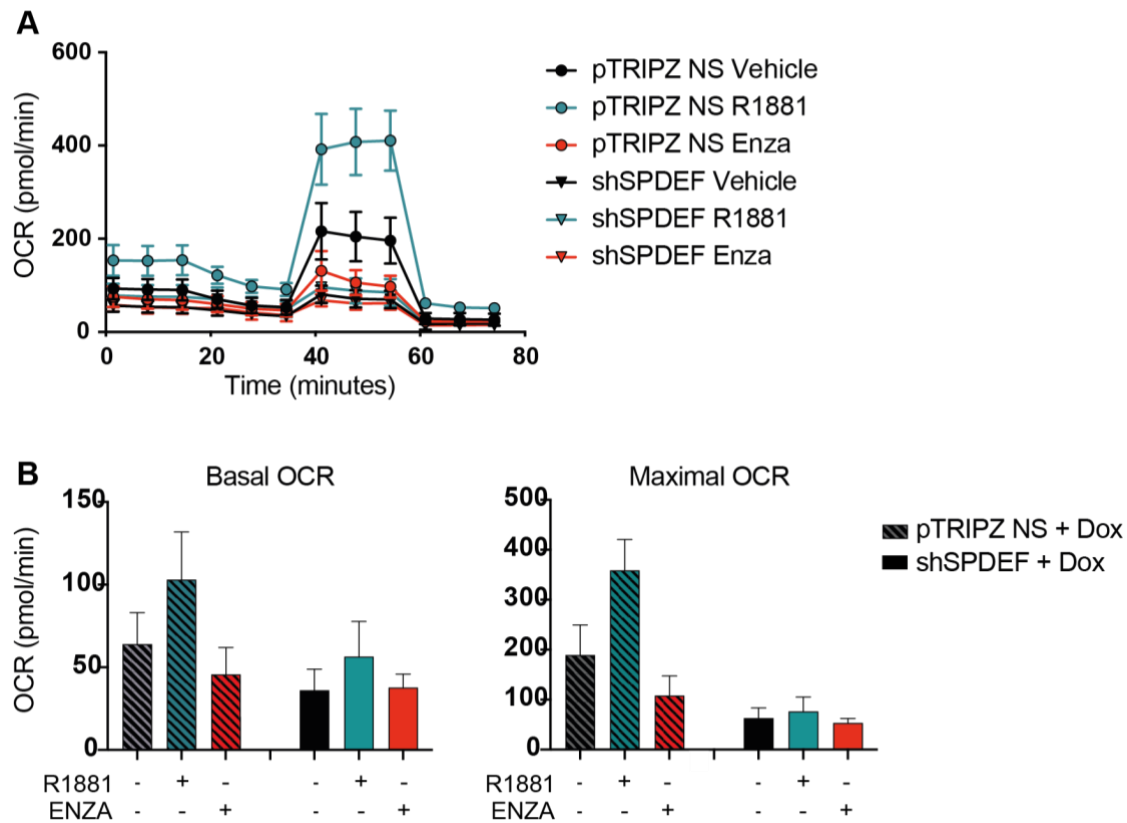


**Figure 62: Pharmacological activation of AR increases mitochondrial respiration activity in AR<sup>+</sup> CTC223 cells but does not restore the decrease in mitochondrial respiration in shSPDEF cells.** Seahorse Mito Stress assay was measured in CTC223 pTRIPZ non-silencing (NS) control and shSPDEF cells. Cells were pretreated with doxycycline (Dox) for one week before assay was started. Cells were treated with either 1nM R1881, 10  $\mu$ M enzalutamide (Enza) or vehicle control for six days before assay was started. Basal and maximal oxygen consumption rate (OCR) were assessed (n= 6 technical replicates/group). (A) Representative Mito Stress experiment in CTC223 pTRIPZ NS control and shSPDEF cells. (B) Bar chart depicts basal OCR (left) and maximal OCR (right). Three inhibitors, oligomycin, FCCP and rotenone/antimycin A, were serially injected.

### 3.9.3 SPDEF regulates mitochondrial proteins

Previous experiments suggested that mitochondrial metabolism is regulated by AR and SPDEF transcription factor. Finding that oxidative phosphorylation was decreased upon SPDEF downregulation, mitochondrial marker proteins were evaluated in SPDEF KO and AR KO cells. Using a variety of antibodies directed against mitochondrial markers for western blot analysis, several proteins were found to be decreased upon SPDEF depletion. Cytochrome c is localized to the mitochondrial inner membrane space and part of the electron transport chain (Figure 63A). Interestingly, cytochrome c was not detected in SPDEF KO#2 cells by western blot analysis (Figure 63B). Cytochrome c oxidase (COX) is a heterooligomeric enzyme consisting of 13 subunits and localized to the inner mitochondrial membrane (Figure 63A). COX IV

protein expression was quite similar in SPDEF KO cells when normalized to tubulin loading control (Figure 63B). However, COX IV expression seemed to be increased in AR KO cells. Since SPDEF protein levels were previously observed to be upregulated in AR KO cells, this is in agreement with COX IV expression in SPDEF KO cells. Voltage-dependent anion channel (VDAC) is located in the mitochondrial outer membrane and serves as metabolite transporter in and out of mitochondria (Figure 63A). Whereas VDAC protein expression was increased in AR KO cells relative to NT control, SPDEF KO cells showed decreased VDAC protein levels (Figure 63B). Pyruvate dehydrogenase (PDH) is the E1 subunit of a multi-enzyme complex which converts pyruvate into acetyl-CoA by pyruvate decarboxylation. Thus, this enzyme is essential for using carbohydrates such as glucose for energy production. Strikingly, PDH protein expression was barely detectable in SPDEF KO#2 cells by western blot analysis whereas it was increased in AR KO cells relative to NT control (Figure 63B). Further, HSP60 is a chaperone responsible for correct folding of protein imported into mitochondria. Mitochondrial HSP60 protein was found to be highly decreased in SPDEF KO cells relative to NT control. Lastly, mitochondrial electron transport chain complex II protein expression was assessed finding that succinate dehydrogenase (SDHA) was decreased in SPDEF KO cells relative to the NT control. In agreement with these findings, gene ontology analysis revealed gene sets including 'Inner mitochondrial membrane protein complex' to be positively enriched in SPDEF-overexpressing cells, and vice versa, 'Mitochondrial respiratory chain complex I biogenesis' to be decreased in shSPDEF cells. However, mitochondrial protein expression was not assessed in shSPDEF and SPDEF-overexpressing cells.

Western blot analysis of mitochondrial proteins suggested that essential proteins involved in mitochondrial energy production were decreased in SPDEF KO cells. Due to lethality, mitochondrial respiration activity could not be assessed in SPDEF KO cells. However, this might be an explanation why basal OCRs were reduced upon SPDEF downregulation. In addition, these data suggest that total mitochondrial content might be reduced in SPDEF-depleted cells. Nicely, AR KO cells displayed upregulation of mitochondrial proteins, most likely constituted via upregulation of SPDEF.

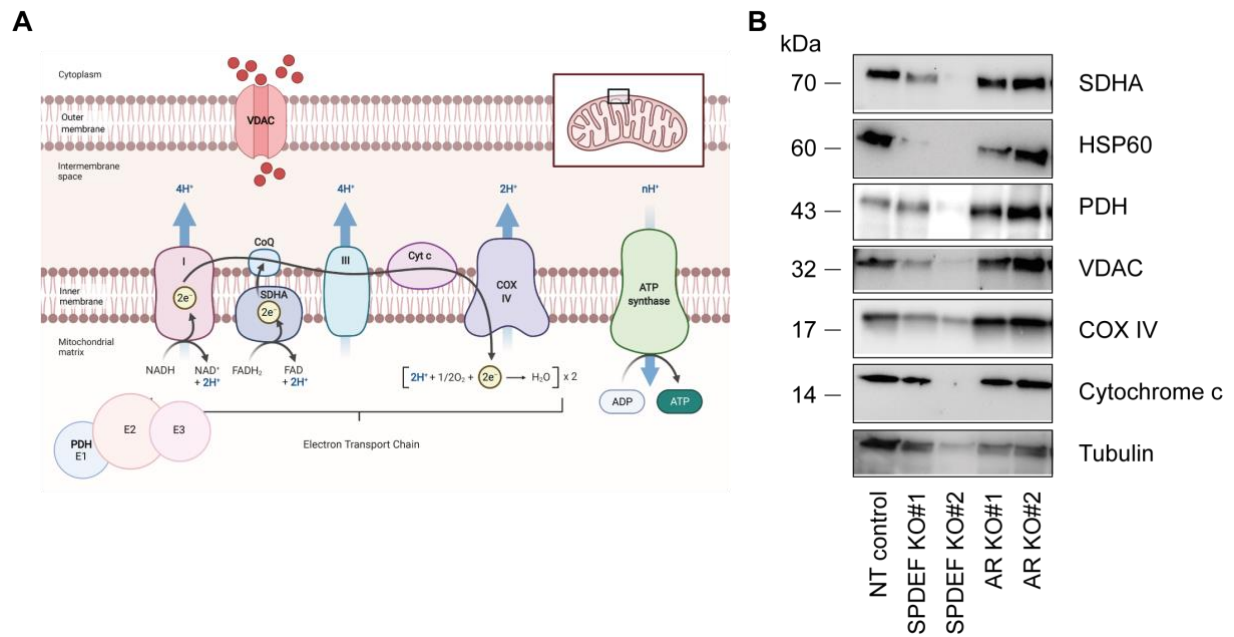


**Figure 63: Mitochondrial marker expression in SPDEF KO cells.** (A) Schematic illustrates mitochondrial electron transport chain including mitochondrial proteins and enzymes. (B) Western blot analysis of mitochondrial markers in BPE8 non-targeting (NT) control, SPDEF knock-out (KO) #1, SPDEF KO#2, AR KO#1, AR KO#2 cells. Tubulin served as loading control. kDa, kilo Dalton.

## 4 Discussion

### 4.1 SPDEF regulates AR signaling in breast cancer

SPDEF was first described as co-regulatory protein of AR and activator of prostate-specific antigen in prostate carcinoma<sup>127</sup>. In this study, I identified the co-expression of SPDEF and AR in ER<sup>-</sup> breast cancer. *SPDEF* was the most differentially expressed gene associated with high *AR* mRNA expression in ER<sup>-</sup> BC patients. Several studies have identified the expression of AR in breast cancer<sup>89-91</sup>. In agreement, differential gene expression analysis between QNBC and AR<sup>+</sup> TNBC tumors revealed *SPDEF* to be associated with AR expression<sup>89,90</sup>. Curated gene sets (C2) based on these studies, namely ‘Farmer Breast Cancer Cluster’ and ‘Doane Breast Cancer Classes up’, were enriched in my SPDEF-overexpressing cells relative to control, and decreased when SPDEF was downregulated. Based on RNA-sequencing analysis of tumor biopsies pre- and post-enzalutamide treatment, Lehmann and colleagues generated a gene expression signature which could be applied to identify patients who benefit from anti-androgen treatment<sup>91,113</sup>. Among these, cell cycle genes, AR target genes and cofactors including *SPDEF* were decreased upon AR inhibition<sup>113</sup>, suggesting that AR regulates *SPDEF* expression<sup>113,137,221</sup>. In agreement with Lehmann *et al.*, AR<sup>+</sup> SPDEF<sup>high</sup>-expressing cell lines showed response towards enzalutamide treatment. In my studies, SPDEF mRNA and protein expression increased upon AR agonist activation in AR<sup>+</sup> MDA-MB-453 and BPE8 cell lines. Whereas *AR* mRNA expression decreased in a time-dependent manner in AR<sup>+</sup> BC cells treated with DHT or synthetic testosterone analogue R1881, AR protein levels significantly increased upon AR activation. This suggests that AR mRNA and protein levels do not necessarily correlate with each other as described previously<sup>222</sup>. However, SPDEF protein expression significantly increased upon AR depletion. Vice versa, AR protein expression decreased in SPDEF-deficient cells relative to control while *AR* mRNA levels were upregulated upon SPDEF knockdown or knock-out in all cell lines. This finding supports that AR mRNA and protein levels do not correlate with each other and suggests a negative reciprocal loop. In addition, I could show that SPDEF regulates *AR* expression. This finding was supported by the observation that AR-associated target genes were downregulated in SPDEF knockdown and knock-out cells relative to controls. Lehmann and colleagues have suggested that AR protein detection by IHC is not sufficient to predict the molecular apocrine phenotype and anti-

androgen response in breast cancer patients<sup>113</sup>. In agreement, my data demonstrates that the expression levels of AR mRNA and protein are highly dynamic and that assessing the expression of AR target genes including *SPDEF* might be more informative.

The role of *SPDEF* and AR in breast cancer tumorigenesis is controversial. Recent studies have suggested that the function of AR in driving tumorigenesis in breast cancer may differ in the presence or absence of ER. Similar findings were observed for *SPDEF* in breast cancer. Buchwalter *et al.* found that *SPDEF* is highly co-expressed with ER and essential for cell survival of luminal breast cancers<sup>128</sup>. The authors performed Kaplan-Meier survival analysis and demonstrated that high *SPDEF* expression is associated with worse overall survival of ER<sup>+</sup> BC patients. Further, *SPDEF* has been identified as predictor of survival within a Cox regression model<sup>128,129</sup>. In agreement, I found that survival probability was significantly reduced in *SPDEF*<sup>high</sup>-expressing breast cancer patients - irrespective of ER status. However, differences in survival probabilities based on *SPDEF* expression were much stronger in the ER<sup>-</sup> patients cohort compared to luminal patients. I made similar findings for AR expression. This is in agreement with previous studies demonstrating that *SPDEF* is significantly overexpressed in AR<sup>+</sup> tumors predicting worse overall survival in ER<sup>-</sup> BC patients<sup>221</sup>.

Buchwalter and colleagues demonstrated that downregulation of *SPDEF* by shRNA reduced *in vivo* tumor growth of ER<sup>+</sup> MCF-7 cells. In contrast, overexpression of *SPDEF* resulted in decreased final tumor weight of TNBC SUM-159 cells relative to control. Based on these findings, the authors suggested that *SPDEF* acts pro-tumorigenic in ER<sup>+</sup> tumors and functions as tumor suppressor in TNBC models<sup>128</sup>. In agreement with reduced tumor growth of ER<sup>+</sup> breast cancer cells upon *SPDEF* downregulation<sup>128</sup>, I found that *SPDEF* knockdown significantly reduced *in vivo* tumor growth of CTC288 and CTC223 cells. Further, I found that *SPDEF* also acts pro-tumorigenic in AR<sup>+</sup> ER<sup>-</sup> breast cancer cells. In contrast, tumor growth was significantly enhanced upon *SPDEF* knockdown in QNBC BPE7 cells. Vice versa, overexpression of *SPDEF* in BPE7 cells repressed *in vivo* tumor growth. Although Buchwalter *et al.* suggested that *SPDEF* acts tumor-suppressive in TNBC<sup>128</sup>, I show that this holds true only, when cells are negative for all hormone receptors including AR. Thus, I suggest that *SPDEF* functions as tumor suppressor in QNBC rather than TNBC models. The TNBC SUM-159 cell model used within their study is low for AR expression and not sensitive towards anti-androgen treatment based on literature research<sup>223-225</sup>, similar to BPE7 cells. Therefore, my findings are in agreement with their results, although I suggest that *SPDEF* function is rather dependent on AR than ER expression. In line, endogenous *SPDEF* expression is high in AR<sup>+</sup> breast cancer cell lines whereas *SPDEF* expression is low in BPE7 cells. Cao and colleagues stated similar results

finding that SPDEF drives tumor growth in MDA-MB-453 and SK-BR3 TNBC cell lines in the presence of AR protein<sup>137</sup>.

However, overexpression of SPDEF in ER<sup>+</sup> CTC288 and CTC223 cells significantly reduced tumor growth similar to what has been observed for downregulation of SPDEF. Endogenous SPDEF expression is high in both cell lines. Further upregulation of SPDEF may result in a reciprocal feedback loop repressing genes and pathways that are actually positively regulated by SPDEF. These data indicate that SPDEF tumorigenic function is highly dependent on its expression level. Similar findings have been observed for AR expression in ER<sup>+</sup> breast cancer. Moreover, SPDEF and AR function might be different in the presence of ER, as mentioned previously<sup>214</sup>. A recent study has demonstrated that AR activation appears to have an anti-proliferative effect and AR expression predicts a beneficial clinical outcome in ER<sup>+</sup> breast cancer patients. A possible explanation is the altered genomic distribution of ER and essential co-activators upon AR activation. This results in repression of ER-regulated cell cycle genes and upregulation of AR targets including known tumor suppressor genes<sup>75</sup>. Although the authors did not directly address SPDEF in this study, it is a well-known co-factor of both hormone receptors, ER<sup>128</sup> and AR<sup>127,137,226</sup>, and may therefore be a crucial factor in this process.

Based on the close relationship of SPDEF and AR, I hypothesized that SPDEF drives tumorigenesis by regulating AR expression. However, AR silencing in BPE8 cells did not affect *in vivo* tumor growth compared to control cells. Several explanations might be possible: (1) although AR knock-out efficiency was 94.4%, I cannot rule out that AR<sup>+</sup> cells selectively grew out resulting in tumor formation, (2) AR signaling might not be activated *in vivo* in female NSG mice implanted with 17 $\beta$ -estradiol pellet and (3) SPDEF protein levels were significantly upregulated upon AR depletion which may be sufficient to rescue *in vivo* tumor growth. SPDEF upregulation may represent an explanation why anti-androgen treatment fail to inhibit molecular apocrine breast cancer growth. To further investigate this, SPDEF and AR should be blocked simultaneously. Moreover, activation of AR *in vivo* by DHT treatment may provide further information about AR signaling and the role of SPDEF in breast cancer. The overall limited expression of SPDEF in normal human tissues may be an advantage to specifically tackle cancer cells with minimal toxicity against normal cells<sup>226</sup>.



## 4.2 SPDEF regulates FBP1 and glucose metabolism in AR<sup>+</sup> breast cancer

Cancer cells are known to highly rely on glycolysis even in the presence of oxygen, a phenomenon called aerobic glycolysis<sup>146,148</sup>. Glucose metabolism is reciprocally controlled by gluconeogenesis and oxidative phosphorylation. However, gluconeogenesis is less well investigated in tumor growth<sup>227</sup>. FBP1 and PCK are two rate-limiting enzymes in gluconeogenesis. FBP1 catalyzes the hydrolysis of F-1,6-BP to fructose-6-phosphate and inorganic phosphate. PCK2 is localized in the mitochondria and catalyzes the conversion of oxaloacetate to phosphoenolpyruvate, a glycolytic intermediate found in gluconeogenesis and glycolysis. In the present study, I identified *FBP1* as a direct target gene of SPDEF in breast cancer. *FBP1* mRNA expression was significantly downregulated in SPDEF knockdown and knock-out AR<sup>+</sup> breast cancer cells. Further, *FBP1* mRNA levels decreased in ER<sup>+</sup> breast tumors upon overexpression and downregulation of SPDEF, respectively. Hence, a decrease in *FBP1* mRNA levels in luminal or molecular apocrine breast cancer cells was accompanied by reduced tumor growth *in vivo*. Although *FBP1* mRNA levels in BPE7 cells did not show significant changes *in vitro*, *FBP1* expression was significantly reduced in shSPDEF tumors which showed a dramatically increased proliferation rate compared to the controls. These results suggest that FBP1 regulated by SPDEF acts pro-tumorigenic in luminal and molecular apocrine breast cancer cells, and tumor suppressive in QNBC tumors – similar to what I observed for SPDEF. Further, I found that endogenous FBP1 expression was low in QNBC cells whereas high expression levels were observed in AR<sup>+</sup> SPDEF<sup>high</sup>-expressing cell lines. In agreement, FBP1 is higher expressed in luminal compared to basal-like tumors and cell lines<sup>153,228</sup>. Additionally, FBP1 has been identified as a marker to distinguish ER<sup>+</sup> and ER<sup>-</sup> tumors<sup>229</sup>. Loss of FBP1 has been associated with tumor progression in lung, ovarian and basal-like breast cancers and low FBP1 expression predicts poor prognosis<sup>153,154,230–232</sup>. Further, FBP1 has been identified as negative regulator of tumor invasiveness<sup>156,231</sup>. Overexpression of FBP1 suppressed *in vitro* tumor cell proliferation<sup>153,154,232</sup> and *in vivo* tumor growth of ovarian, lung and basal-like cancer cells<sup>153,156,231</sup>. Hence, previous studies agree with the tumor suppressive role of FBP1 observed in BPE7 cells whereas the pro-tumorigenic function of FBP1 suggested in luminal and molecular apocrine breast cancers is new.

F-1,6-BP, the substrate of FBP1, is an allosteric activator of pyruvate kinase isozyme type M2 (PKM2) which catalyzes the last step in glycolysis converting phosphoenolpyruvate to pyruvate<sup>233</sup>. Reduced levels of FBP1 substrate may inhibit glycolysis in tumor cells. In this

context, genes encoding enzymes involved in glycolysis were significantly downregulated in ER<sup>+</sup> shSPDEF cells *in vitro* relative to the controls. In line with *FBP1* expression, hexokinase 2 (*HK2*) gene expression was downregulated in CTC288 shSPDEF and SPDEF OX tumors, respectively. In ER<sup>-</sup> AR<sup>+</sup> BPE8 cells, no major changes in glycolytic genes were observed upon downregulation of SPDEF but in SPDEF-deficient cells. Strikingly, the opposite phenotype was observed for QNBC BPE7 shSPDEF tumors which showed significant upregulation of various genes involved in glucose oxidation. GSEA revealed that glycolysis was positively enriched in BPE7 shSPDEF tumors relative to the controls. In agreement, FBP1 overexpression has previously been demonstrated to result in decreased protein expression levels of glucose transporter GLUT1, HK2 and lactate dehydrogenase A<sup>154</sup>. Further, glucose uptake and lactate production are reduced in FBP1-overexpressing cells *in vitro*<sup>153,154,231,232</sup> and *in vivo*<sup>154</sup>. In ovarian cancer cells, one study shows that FBP1 overexpression leads to reduced glycolytic activity and oxygen consumption rates<sup>154</sup>. In contrast, FBP1 induced a metabolic switch from glycolysis to OxPhos in lung cancer. Zhang *et al*, showed that glucose uptake was inhibited resulting in reduced lactate production whereas basal and maximal mitochondrial respiration increased upon FBP1 restoration<sup>231</sup>. This work has been supported by a study in basal-like breast cancer cells, finding that loss of FBP1 induces glycolysis but inhibits oxygen consumption by suppressing mitochondrial complex I activity<sup>153</sup>. In my work, FBP1 depletion mediated by CRISPR-Cas9 decreased gene expression of glycolytic enzymes and pre-liminary data suggest that FBP1 KO promotes oxidative phosphorylation in AR<sup>+</sup> breast cancer cells (data not shown). However, these results were in contrast to findings for SPDEF controlling mitochondrial respiration discussed below. In addition, I observed that FBP1 protein expression was increased in SPDEF-deficient cells. This might be an explanation why FBP1 KO increased OxPhos while at the same time not showing any effects on *in vivo* tumor growth of BPE8 cells. However, I cannot rule out that FBP1-expressing cells selectively promoted *in vivo* tumor growth due to technical limitations of the approach. In order to make a final statement about the pro-tumorigenic function of FBP1 in breast cancer, I suggest to assess *in vivo* tumor growth upon inducible downregulation or overexpression of FBP1 instead of complete deletion of the protein.

In addition, previous studies have shown that *FBP1* expression is regulated by methylation of its promoter<sup>153,154,231</sup>. Li and colleagues have stated that c-Myc binds at the promoter region of *FBP1* and thereby represses *FBP1* expression. The authors further observed a negative association of endogenous FBP1 and c-Myc protein levels in ovarian cancer cell lines. Downregulation of c-Myc resulted in upregulation of FBP1 expression<sup>154</sup>. Interestingly, I found

c-Myc protein expression to be dramatically increased in BPE8 shSPDEF and SPDEF KO cells. In addition, Myc targets were negatively enriched upon overexpression of SPDEF. Zhang *et al.* have shown that Zeb-1 enhances *FBP1* promotor methylation resulting in repressed *FBP1* expression in lung cancer. Similarly, Snail and vimentin have been demonstrated to inversely correlate with *FBP1* expression in basal-like breast cancer cells. Endogenous Snail binds at the *FBP1* promotor in basal-like but not luminal breast cancer cells and inhibits *FBP1* expression<sup>153</sup>. Both, Zeb-1 and Snail, are known inducer of epithelial-to-mesenchymal transition (EMT) and have been shown to suppress luminal markers such as E-cadherin<sup>153,231,234,235</sup>. In contrast, SPDEF has been stated to promote luminal differentiation in breast cancer cells<sup>128</sup>. In agreement, I found that SPDEF positively regulates EpCAM expression (data not shown). Further, EMT markers and SPDEF have been observed to inversely correlate in breast cancer<sup>208</sup>. Taken together, my findings are in agreement with previously published results. *FBP1* regulated by SPDEF acts tumor-suppressive in QNBC BPE7 cells and based on the transcriptional profile, BPE7 cells upregulate glycolysis driving tumor growth upon SPDEF downregulation. To further elucidate this finding, functional glycolytic measurements by Seahorse analysis may provide further knowledge.

### 4.3 SPDEF regulates fatty acid metabolism in AR<sup>+</sup> breast cancer

Cancer cells generate more than 90% of their cellular fatty acid pool *de novo*<sup>180,181</sup>. Several studies have demonstrated the importance of fatty acid biosynthesis for cancer cell survival and growth<sup>178,179,236</sup>. Increased FA biosynthesis could be either a response to high metabolic demands of rapidly dividing cancer cells, or an adaptation to the tumor microenvironment with reduced lipid availability<sup>178</sup>. In the present study, I show that SPDEF regulates genes encoding enzymes involved in *de novo* fatty acid biosynthesis specifically in molecular apocrine breast cancer models. Previous studies have characterized molecular apocrine breast tumors by specific expression patterns including expression of AR target genes and *FASN* among others<sup>89-91</sup>. Gene ontology analysis of molecular apocrine tumors revealed numerous metabolic pathways to be enriched in AR<sup>+</sup> tumors compared to QNBCs<sup>91</sup>. Among them, ‘fatty acid metabolism’ and ‘lipid metabolism’ encompassing many genes for FA biosynthesis were positively associated with *AR* and *SPDEF* co-expression<sup>90,91</sup>. In the presented study, patient data analysis based on AR expression revealed fatty acid metabolism to be enriched when *AR* and *SPDEF* mRNA expression was high.

Furthermore, I found that the three major enzymes of FA biosynthesis, ACLY, ACC and FASN are upregulated upon overexpression of SPDEF and decreased in shSPDEF and SPDEF-deficient BPE8 cells. Downregulation of FA synthesis genes was also observed in shSPDEF tumors relative to the controls. Numerous studies have investigated the functional role of fatty acid biosynthesis in cancer cells and the consequence upon depletion or inhibition of this pathway<sup>178,236</sup>. ACLY connects glucose and fatty acid metabolism by converting cytosolic citrate to oxaloacetate and acetyl-CoA. Acetyl-CoA is an essential metabolite in various metabolic processes and serves as precursor for FA synthesis. Downregulation of ACLY mediated by shRNA has been demonstrated to inhibit xenograft tumor formation of human cancer cells. ACLY knockdown led to decrease in glucose-dependent fatty acid synthesis and reduced proliferation rate. The authors observed similar results after pharmacological inhibition of ACLY by SB-204990 treatment<sup>237</sup>. Another study has shown that shRNA targeting *ACLY* impaired AKT-mediated tumorigenesis in murine tumor models<sup>188</sup>. In my work, ACLY protein expression was significantly decreased in BPE8 shSPDEF cells and increased in BPE8 SPDEF OX cells. In line with published data, ACLY reduction was associated with decreased *in vivo* tumor growth of BPE8 cells. Further, inhibition of acetyl-CoA generation may result in changes in histone acetylation and gene expression. Wellen *et al.* have shown that ACLY is required for increased histone acetylation during differentiation upon growth factor stimulation<sup>238</sup>. Thus, it would be interesting to analyze the acetylation profile in AR<sup>+</sup> breast cancer cells upon deregulation of SPDEF. ACC carboxylates acetyl-CoA to generate malonyl-CoA, and is the most highly regulated enzyme in the FA biosynthesis pathway. Downregulation of ACC1 by siRNA has been stated to induce apoptosis in prostate and breast cancer cells<sup>239,240</sup>. Chajès and colleagues have demonstrated that silencing of either ACC or FASN in breast cancer cells results in a significant decrease in FA biosynthesis and thereby induce programmed cell death. Supplementation of exogenous palmitate completely restored cell viability upon ACC or FASN knockdown<sup>240</sup>. In the present study, ACC expression was reduced by SPDEF downregulation and associated with decreased *in vivo* tumor growth, in line with previous studies. Contra vise, silencing of ACC1 or ACC2 enhanced tumor growth of lung cancer cells through AMPK-mediated NADPH maintenance<sup>241</sup>. FASN catalyzes the last step in FA biosynthesis which is the condensation of acetyl-CoA and malonyl-CoA to generate 16-carbon palmitate. FASN is the most studied metabolic enzyme regarding cancer disease. In line with my results, overexpression of FASN and increased FASN activity have been observed in various cancer types and strongly correlate with poor prognosis<sup>181</sup>. Extremely high levels of *FASN* expression has been observed in epithelial cancers including breast, prostate and ovary among others<sup>181</sup>. In

contrast, high *FASN* expression was associated with better outcome in ER<sup>+</sup> breast cancer patients in my analysis, although the stratification based on *FASN* expression was quite weak. In the ER<sup>-</sup> patients cohort, high *FASN* expression correlated with decreased survival probabilities similar to findings for *AR* and *SPDEF*, and in agreement with previous studies. Functional studies of *FASN*-deficient AR<sup>+</sup> and AR<sup>-</sup> breast cancer cells may provide further information about the lipogenic profile of molecular apocrine and hormone-dependent breast cancer cells. In normal conditions, *FASN* is highly expressed in hormone-responsive tissues (similar to *SPDEF*) and is regulated by estradiol and progesterone<sup>242</sup>. During the menstrual cycle, expression of *FASN* is dynamically regulated and linked to Ki67 proliferation marker as well as ER and PR expression in human endometrium. This suggests a functional connection between *FASN* and hormone signaling in the control of normal endometrial cell proliferation<sup>243</sup>. Furthermore, *FASN* is known to be an androgen-responsive target gene regulated by AR and involved in prostate tumorigenesis<sup>216</sup>. Doane *et al.* have stated that *FASN* was upregulated in AR<sup>+</sup> breast cancer cells (MDA-MB-453) upon synthetic androgen treatment<sup>89</sup>. In agreement, my data shows that AR regulates *SPDEF* expression that in turn regulates *FASN* expression. *FASN* protein expression was decreased in BPE8 sh*SPDEF* and *SPDEF* KO cells. In contrast, *FASN* protein levels did not change in AR-deficient cells. However, I show that *SPDEF* is upregulated in AR-deficient cells that may restore *FASN* expression. shRNA-mediated downregulation of *FASN* in AR<sup>+</sup> prostate cancer cells has been shown to decrease synthesis of triglycerides and phospholipids and induce morphological changes including loss of cell-cell contacts<sup>244</sup>. Interestingly, I observed similar morphological changes as BPE8 *SPDEF*-overexpressing cells did not form cell-cell contacts to neighboring cells (data not shown). Moreover, De Schrijver and colleagues have found that LNCaP cell growth was inhibited while apoptosis was induced upon *FASN* silencing<sup>244</sup>. In agreement, numerous studies have demonstrated that *FASN* inhibition induces cell cycle arrest resulting in decreased cancer cell proliferation and ultimately programmed cell death<sup>245-250</sup>.

Moreover, genes encoding enzymes involved in fatty acid modification including desaturation and elongation were significantly downregulated in sh*SPDEF* and *SPDEF*-deficient AR<sup>+</sup> breast cancer cells. Stearoyl-CoA desaturase (SCD) and fatty acid desaturase 2 (FADS2) catalyze the formation of double bonds to generate mono- and polyunsaturated FAs<sup>251</sup>. SCD expression has been shown to be upregulated in some types of cancers that were highly sensitive to SCD inhibition<sup>186,187</sup>. Some studies have demonstrated that inhibition of SCD caused cancer cell death and reduced *in vivo* tumor growth, most likely due to the accumulation of saturated fatty acids being toxic at high concentrations<sup>252,253</sup>. A recent study has described that FADS2

expression is increased in cells resistant to SCD inhibition and illustrates an alternative pathway for fatty acid desaturation. Inhibition of both enzymes, SCD and FADS2 caused a moderate reduction in tumor growth<sup>187</sup>. Changes in gene expression levels of SCD and FADS2 suggest that the abundance of unsaturated fatty acids might have decreased upon downregulation of SPDEF. Isotope tracing experiments suggest that *de novo* synthesis of MUFAs, oleate and palmitoleate, is decreased upon downregulation of SPDEF. However, shSPDEF cells showed increased uptake of these MUFAs. Intracellular measurements of total unsaturated fatty acids may provide further information about the lipid content in SPDEF knockdown cell lines.

In order to address fatty acid biosynthesis and the lipogenic profile of cancer cells, the majority of *in vitro* experiments published have been performed in lipid-depleted conditions. In agreement, I did not observe major changes in cell proliferation or apoptosis upon deregulation of SPDEF when cells were cultured in fully saturated CSC BC medium. However, the growth rate was significantly reduced upon downregulation of SPDEF when cells were exposed to HPLM conditions.

Downregulation of fatty acid biosynthesis genes by SPDEF resulted in upregulation of the fatty acid transporter CD36. Increased functional localization of CD36 at the plasma membrane was accompanied by increased exogenous fatty acid uptake of oleate, stearate and palmitoleate from the microenvironment. This suggests that fatty acid uptake via CD36 is upregulated as a compensatory pathway for the decrease in newly synthesized fatty acids regulated by SPDEF. To proof whether increased FA uptake is constituted via CD36, isotope tracing experiments in CD36-deficient cells may provide this information. In agreement, several studies have suggested that cancer cells take up exogenous fatty acids from the microenvironment when substrates for FA biosynthesis are limited. Addition of palmitate or oleate has been observed to fully restore cancer cell viability after inhibition of FASN<sup>254</sup>. Lipid uptake as a compensatory pathway is thus likely to lead to resistance to FASN depletion or pharmacological inhibition of fatty acid biosynthesis<sup>178</sup>. Hence, it may be required to target several routes of fatty acid metabolism simultaneously in order to limit metabolic flexibility. Targeting CD36 by either genetic depletion or pharmacological inhibition in shSPDEF cells resulted in significant reduced cell growth. Pharmacological inhibition of CD36 by SSO treatment induced a cytostatic effect in shSPDEF cells cultured in HPLM conditions suggesting that shSPDEF cells highly rely on CD36 function.

Endogenous CD36 expression was high in AR<sup>+</sup> BPE8 and CTC223 cells compared to AR<sup>-</sup> BPE7 cells suggesting that AR<sup>+</sup> breast cancer cells exhibit a lipogenic profile including high

expression of genes involved in fatty acid synthesis and uptake. Moreover, SPDEF, FASN, AR and CD36 expression were found to be co-expressed in metastatic breast cancer cell lines. Pascual *et al.* have shown that metastasis-initiating cells are highly positive for CD36 expression and additional genes involved in distinct fatty acid metabolic processes. Supplementation of palmitic acid or high-fat diet enhanced the metastatic potential of CD36-expressing cells. Genetic or pharmacological inhibition of CD36 prevented metastases formation. Interestingly, CD36-expressing cells showed overall lower expression of EMT-associated genes relative to CD36<sup>-</sup> cells<sup>255</sup>. MCF-7 breast cancer cells that have been noted to express AR and SPDEF were utilized within their study<sup>108,256</sup>. This is in line with my findings that CD36 is highly co-expressed with SPDEF in epithelial breast cancer cells. However, no increase in metastatic potential was observed for shSPDEF cells upregulating CD36 expression. Lung metastases formation was similar in shSPDEF and control groups whereas downregulation of SPDEF prevented brain metastatic lesions, as discussed below. Pascual *et al.* have suggested that high CD36 expression is associated with worse overall survival in lung, bladder and luminal A breast cancer patients<sup>255</sup>. No CD36 expression was observed in TNBC models (S. Benitah, personal communication). In the present work, patient data analysis has suggested that high *CD36* expression is associated with better outcome in luminal breast cancers. In addition, *SPDEF* and *CD36* expression did not correlate in neither ER<sup>+</sup> nor ER<sup>-</sup> breast cancer patients. Considering patient data set included patients of early cancer stage, PDX models may better reflect the metastatic disease that is also in line with findings from the Benitah lab. However, I suggest that CD36 is also expressed in TNBC but molecular apocrine tumors.

Downregulation of SPDEF did not only alter primary tumor growth but also inhibited brain metastasis formation of AR<sup>+</sup> breast cancer cells. The blood-brain barrier limits access to nutrients from circulation that creates a hypoxic and nutrient-depleted microenvironment in the brain<sup>257,258</sup>. In general, the brain is a lipid-rich tissue, however it contains specialized lipids that differ from those found at other sites<sup>259</sup>. Ferraro and colleagues have shown that low levels of lipids are found in the brain compared to mammary fat pad and studied the differential metabolic dependencies of primary and metastatic breast cancer cells. They demonstrate that fatty acid biosynthesis is required for breast cancer cells growing in the brain. Genetic or pharmacological inhibition of FASN prevents breast cancer brain metastases<sup>192</sup>. In agreement, *FASN* was significantly downregulated in BPE8 shSPDEF tumors and SPDEF knockdown cells could not form brain metastases compared to control cells. In addition, Ferraro *et al.* noted that *FASN* expression is higher in breast cancer brain metastases compared to other metastatic sites

including liver, lungs and bones. Compatibly, the frequency of metastatic lesions in the lungs was not impaired by downregulation of SPDEF expression in my studies. Although Ferraro *et al.* show that silencing of *FASN* disrupts fatty acid biosynthesis and proliferation *in vitro*, primary tumor growth in the mammary fat pad derived from sgFASN cells was only slightly impaired<sup>192</sup>. Contra vise, I observed significant reduced tumor growth upon SPDEF downregulation. Regarding the results found in their study, either SPDEF diminished tumor growth independent of reduced *FASN* expression, or reduced clonogenicity and proliferation due to decreased *FASN* expression could be better analyzed using our cell culture models. The great advantage of using the heterogeneous PDX cell lines is that they better reflect the metastatic disease found in the patient<sup>208</sup> compared to clonal BT474 cells derived from primary breast tumors. Interestingly, both cell lines used for their study, BT474 and MDA-MB-361, are positive for AR expression<sup>224</sup>.

Many drugs directly targeting *FASN* have been developed and investigated [listed in Röhrig and Schulze, 2016]<sup>178</sup>. Since *de novo* fatty acid biosynthesis activation is specific to cancer cells except of lipogenic tissues, chemical inhibitors of *FASN* preferentially target cancer cells. However, dose-limiting toxicity may arise in adipose tissues or the liver<sup>178</sup>. In addition, severe weight loss has been observed in animals upon *FASN* inhibition<sup>260</sup>. Therefore, it is indispensable to better understand the dynamic metabolic dependencies and plasticity of cancer cells in order to develop new treatment options. In addition to directly block FA enzymes, their metabolic activities may be reduced by decreasing transcription of their encoded genes. In the present study, I found that SPDEF regulates transcription of FA synthesis genes and therefore inhibiting SPDEF in cancer cells possibly prevents tumor growth. SPDEF is an attractive target since it is specifically expressed in hormone-responsive tissues and not found ubiquitously throughout the body. However, targeting ligand-independent transcription factors may be difficult. Initial data suggested that SPDEF downregulation can be mimicked by pharmacological inhibition of AR. Therefore, targeting AR and CD36 simultaneously might be a promising treatment strategy for AR<sup>+</sup> breast cancer patients.

Fatty acids have numerous functions in cancer cells encompassing the synthesis of membrane phospholipids, signaling molecules, energy storage and production<sup>178</sup>. Reduction of fatty acid biosynthesis can result in overall changes of saturation levels of membrane lipids by decreasing the number of saturated FAs, while MUFAs and polyunsaturated FAs (PUFAs) are preferentially derived from dietary lipids. The degree of saturated lipids determines protection of cancer cells against ROS as saturated membrane lipids are less susceptible to peroxidation<sup>205</sup>. However, preliminary data suggest that lipid peroxidation is increased upon overexpression and



downregulation of SPDEF (data not shown). SPDEF overexpression enhanced mitochondrial respiration activity, as discussed below. ROS production might thus be increased in SPDEF-overexpressing cells relative to the control. shSPDEF cells showed increased uptake of MUFAs that may change the overall saturation levels of the cellular lipid pool in these cells. This could be an explanation why lipid peroxidation was increased in both settings. Moreover, preliminary data suggest that excess fatty acids are stored as lipid droplets upon overexpression of SPDEF (data not shown). Excess FAs stored in lipid droplets may be utilized for energy production via  $\beta$ -oxidation at later time points<sup>206</sup>. Altered FA biosynthesis can also impair mitochondrial membrane composition. Cardiolipins are structurally distinct phospholipids localized to the inner mitochondrial membrane where they control the activity of the electron transport chain complexes and apoptosis induction. Cardiolipin length and saturation degree control the activity of the inner mitochondrial membrane. In particular, the mobilization of cytochrome c transferring electrons from complex III to complex IV, is tightly regulated by cardiolipins<sup>261</sup>. Therefore, changes in FA biosynthesis or uptake can directly affect cellular bioenergetics by modulating OxPhos. Abnormalities in mitochondrial cardiolipin profiles have been found in mouse brain tumors in comparison to normal tissues. Alterations in cardiolipins correlated with impaired mitochondrial respiration activity<sup>262</sup>. Peck and colleagues have demonstrated that inhibition of fatty acid desaturation by targeting SCD induced changes in the abundance of specific cardiolipin species. Consequently, mitochondrial respiration activity was reduced and apoptosis was triggered by the release of cytochrome c from the inner mitochondrial membrane<sup>263</sup>.

In order to analyze the fate of newly synthesized or exogenous fatty acids, [ $^{13}\text{C}$ ]-palmitate tracing experiments may provide further knowledge about the importance and functional role of fatty acids in AR<sup>+</sup> breast cancer cells.

#### **4.4 SPDEF regulates mitochondrial metabolism in AR<sup>+</sup> breast cancer**

Tumor cells undergo metabolic reprogramming to meet bioenergetic and -synthetic demands in order to survive and maintain rapid proliferation. Increased biosynthesis of macromolecules requires ATP and reducing equivalents, supported by active mitochondrial metabolism. Several studies have indicated that mitochondrial metabolism is essential for tumor growth whereas defects in respiratory function prevent malignant transformation<sup>172,264–267</sup>. Recent work suggests that metabolic reprogramming is a dynamic process and cancer cells constantly need

to adjust to changes in the microenvironment with limited nutrient supply and oxygen availability during tumor progression<sup>176,268</sup>. Circulating tumor cells (CTCs) that are able to survive in the circulatory system and initiate metastasis at secondary sites may adjust their metabolic strategy. LeBleu and colleagues have demonstrated that oxidative phosphorylation was enriched in CTCs relative to primary tumor cells. Differential gene expression analysis revealed genes involved in mitochondrial biogenesis and respiration to be upregulated in CTCs. Human breast cancer xenograft-derived CTCs showed increased amounts of mitochondrial DNA, enhanced basal oxygen consumption rates and ATP production compared with matched primary tumor cells. Further, the authors have shown that OxPhos and mitochondrial biogenesis were controlled by the transcription coactivator peroxisome proliferator-activated receptor gamma, coactivator 1 alpha (PCG-1 $\alpha$ ) on transcriptional level. Silencing of PCG-1 $\alpha$  in tumor cells interrupted mitochondrial biogenesis and respiration, reduced their invasive potential and resulted in attenuated metastasis without affecting cell proliferation<sup>161</sup>. A recent study has identified a distinct transcriptional program that is specifically upregulated in micro-metastatic breast cancer cells. Single-cell RNA sequencing of matched primary tumor and micro-metastatic cells revealed upregulation of mitochondrial respiration on the molecular level accompanied by increased mitochondrial membrane potential and distinct metabolic profiles. Interestingly, EpCAM was among the top 20 differentially expressed genes and significantly predictive of breast cancer relapse. Pharmacological inhibition of mitochondrial complexes specifically in cancer cells attenuated metastatic seeding in the lungs without affecting cell viability and proliferation *in vitro*<sup>175</sup>. In the present study, I found that mitochondrial respiration activity increased in SPDEF-overexpressing AR<sup>+</sup> breast cancer cells, resulting in enhanced ATP production compared to control cells. In contrast, oxygen consumption rates were significantly decreased when SPDEF was downregulated. Preliminary data suggest that mitochondrial respiration activity was decreased due to reduced glucose oxidation in AR<sup>+</sup> CTC223 shSPDEF cells (data not shown). In agreement with previous studies, basal oxygen consumption rates were high in AR<sup>+</sup> PDX cell lines originally derived from CTCs or BPEs. I further observed that reduced mitochondrial respiration activity was associated with reduced *in vivo* tumor growth without affecting cell viability and proliferation *in vitro*. However, shSPDEF cells displaying decreased OxPhos activity had a significant growth disadvantage in nutrient-depleted environment. In addition, downregulation of SPDEF prevented brain metastasis formation. In contrast to the findings of Davis *et al.*, downregulation of SPDEF and consequent decrease in mitochondrial respiration did not affect lung metastatic lesions. The aforementioned studies suggest that mitochondrial biogenesis and respiration is regulated on the transcriptional

level<sup>161,175</sup>. In agreement, SPDEF may regulate the expression of genes involved in these processes, observing that expression of several enzymes of mitochondrial electron transport chain were decreased on protein level in SPDEF-deficient cells. Based on the transcriptional level, AR<sup>+</sup> breast cancer cells may be highly lipogenic, less glycolytic and rely on OxPhos for energy production whereas AR<sup>-</sup> BPE7 cells showed upregulation of glycolytic enzymes associated with enhanced tumor growth. In line with this hypothesis, a recent study has demonstrated that inhibition of mitochondrial pyruvate carrier (MPC) results in disruption of mitochondrial metabolism, OxPhos and lipogenesis specifically in AR-driven prostate cancer cells. Pharmacological treatment targeting MPC significantly decreased cell proliferation and tumor growth in androgen-responsive but not in AR<sup>-</sup> prostate cancer cells<sup>220</sup>. These results suggest fundamental differences in the metabolic profiles of AR<sup>+</sup> and AR<sup>-</sup> prostate cancer cells. My data suggest that AR may regulate mitochondrial metabolism in breast cancer in similar ways. Additional studies have shown that prostate cancers are highly lipogenic, less glycolytic and promote mitochondrial respiration as compared to other solid tumors<sup>269,270</sup>. Cancer cells may harbor metabolic features being characteristic of their tissue of origin<sup>162</sup>. In agreement, some cancer types have been observed to be more glycolytic whereas others are dependent on functional mitochondrial metabolism<sup>162,163</sup>. Breast cancers of triple negative subtype have been associated with high expression of glycolytic markers and glucose uptake highly correlates with proliferation index in these tumors<sup>271–274</sup>. Activation of OxPhos by specifically enhancing mitochondrial complex I activity in TNBC cell lines inhibited tumor growth and metastasis by regulating NAD<sup>+</sup>/NADH redox balance<sup>275</sup>. In contrast, luminal breast cancers have been shown to express lower levels of glycolytic markers and rely on OxPhos<sup>272</sup>. Although these studies did not consider AR expression, more than 90% of luminal tumors are found to be AR positive<sup>59</sup>. Hence, OxPhos regulation might be constituted by AR expression in breast cancer. In my studies, AR agonist activation significantly increased basal and maximal oxygen consumption rates in AR<sup>+</sup> breast cancer cells, and restored mitochondrial respiration upon pharmacological inhibition of AR by enzalutamide. However, AR activation could not rescue the decrease in mitochondrial respiration activity when SPDEF was downregulated. This suggests that SPDEF is downstream of AR and involved in controlling mitochondrial metabolism. Depletion of AR did not affect *in vivo* tumor growth, most likely because SPDEF was overexpressed upon AR knock-out. In line, preliminary data suggest that AR KO cells showed enhanced basal and maximal OCRs similar to SPDEF-overexpressing cells (data not shown). Therefore, my findings show that SPDEF regulates mitochondrial respiration activity in AR<sup>+</sup> breast cancer. In order to determine whether SPDEF overexpression inhibits BPE7 tumor growth by regulating

OxPhos activity, functional experiments are needed to further analyze the metabolic profile of QNBC cells *in vivo*. Furthermore, overexpression and knockdown of SPDEF in ER<sup>+</sup> breast cancer cells resulting in decreased tumor growth indicate that SPDEF expression levels must be adjusted in order to balance bioenergetic and -consuming processes to optimally fuel tumor growth.

## 5 Material and Methods

### 5.1 Cell lines and cell culture

Patient-derived xenograft cell lines were cultured in Corning® Primaria™ T75 or T25 (#353810, Corning) cell culture flasks in specified cancer stem cell (CSC) breast cancer (BC) medium previously established in our lab (Table 1, Table 2). In order to passage PDX cell lines, suspension cells were transferred into a 15 mL falcon tube and centrifuged at 300 x g for 3 min at room temperature (RT). Meanwhile 1.5 -3 mL Accutase (#A11105, Life Technologies) was added to adherent cells on flask. After centrifugation, supernatant was removed and cell pellet was resuspended in 0.5 mL Accutase, and transferred back to cells in flask. Cells in Accutase were incubated at 37°C and 5% CO<sub>2</sub> for roughly 10-15 min until they were completely dissociated and detached. Subsequently, 5-7 mL CO<sub>2</sub>-independent medium (#18045070, Life Technologies) supplemented with 1% BSA (#11020-039, Thermo Fisher) and 2mM glutamine (#25030024, Life Technologies) was added to collect cells in a total volume of 7-10 mL for centrifugation at 300 x g for 5 min at RT. Supernatant was removed and cell pellet was resuspended in 1mL CSC BC medium.

**Table 1: Cancer stem cell breast cancer medium.**

Component	Product number, company	Final concentration and volume
<b>Advanced DMEM F-12</b>	12634028, Life Technologies Thermo Fisher	500 mL
Animal-free recombinant human epidermal growth factor	AF-100-15-1000, Peprotech	20 ng/mL (250 µL)
Fibroblast growth factor	100-18B-1000, Peprotech	50 ng/ mL (200 µL)
LONG R3 Insulin growth factor-1 human	I1271-1MG, Sigma	20 ng/mL (5 µL)
Recombinant human hepatocyte growth factor	100-39H-500, Peprotech	20 ng/mL (125 µL)
Insulin, human Recombinant, Zinc Solution 5ml	12585014, Life Technologies	625 µL
17-beta estradiol	E8875-1G, Sigma Merck	0.5 ng/ mL (12.5 µL pre-diluted in BSA)
Hydrocortisone	H0888, Sigma	100 ng/ mL (20 µL)
N2 supplement	17502048, Life Technologies Thermo Fisher	1X

B27 supplement without vitamin A	12587010, Thermo Fisher	1X
L-glutamine	25030024, Life Technologies	2 mM (5 mL)
O-phosphoryl-ethanolamine (OPE)	P0503, Sigma	0.1 mM (250 $\mu$ L)
Glutathione (GSH)	G6013-5G, Sigma	1 $\mu$ g/ mL (250 $\mu$ L)
L-ascorbic acid 2-phosphate magnesium	A8960-5g, Sigma	6.4 $\mu$ g/ mL (500 $\mu$ L)
<b>CSC Mastermix</b>		8.45 mL

**Table 2: Cancer stem cell mastermix.**

<b>Component</b>	<b>Product number, company</b>	<b>Final concentration and volume</b>
D-glucose 45%	G8769, Sigma	17 mL
Trace A	25-021-CL, VWR	2.5 mL
Trace B	MDTC25-022-CI, VWR	5 mL
Trace C	MDTC25-023-CI, VWR	5 mL
Gibco™ AlbuMAX™ I Lipid-Rich BSA 20% in PBS	11020-039, Thermo Fisher	15 mL
Heparine	H3149-10KU, Sigma	5 mL
HEPES	h0887-100, Sigma	25 mL
Chemically defined lipid mixture 1	L0288, Sigma	10 mL

Prostate cancer cell lines LNCaP and PC3 were purchased from DMZK. Breast cancer cell lines MDA-MB-453, MDA-MB-231, MDA-MB-436, MDA-MB-468, SUM-159 and SK-BR-3 were already present in our lab. Cells were cultured in T75 cell culture flasks in ATCC-recommended medium (Table 3). In order to passage FCS-supplemented cell lines, cell culture medium of adherent cells was aspirated, cells were washed once with PBS and 3 mL Trypsin (#T3924, Sigma Aldrich) was added to cells on flask. Suspension cells were transferred into a 15 mL falcon tube and centrifuged at 300 x g for 3 min at room temperature (RT). Meanwhile 2.5 mL Trypsin was added to adherent cells on flask. After centrifugation, supernatant was removed and cell pellet was resuspended in 0.5 mL Trypsin, and transferred back to cells in flask. Cells in Trypsin were incubated at 37°C and 5% CO<sub>2</sub> for roughly 5-10 min until they were completely dissociated and detached. Subsequently, 7 mL appropriate FCS-containing medium was added to collect cells in a total volume of 10 mL in order to stop trypsinization. Next, cells were centrifuged at 300 x g for 5 min at RT. Supernatant was removed and cell pellet was resuspended in 1mL appropriate cell culture medium (Table 3).

**Table 3: Cell culture conditions.** Medium was purchased from Gibco, Life Technologies.

Cell line	Cancer subtype	Cell culture medium
MDA-MB-468	QNBC	DMEM + 10% FCS
MDA-MB-231	QNBC	DMEM + 10% FCS
BT20	QNBC	EMEM + 10% FCS
SUM159	TNBC AR+	DMEM:Ham's F12 (1:1), 5% FCS, 5 ug/mL insulin zinc salt, 1ug/mL HC
MDA-MB-453	TNBC/HER2 enriched AR+	DMEM + 10% FCS
LNCaP	Prostate cancer AR+	RPMI 1640 + 10% FCS
PC3	Prostate cancer AR-	F12K + 10% FCS
SKBR3	HER2 enriched AR+	McCoy's 5a Medium Modified + 10% FCS
MDA-MB-436	TNBC AR+	DMEM:Ham's F12 (1:1) GlutaMAX + 10% FCS

For cell counting, the Beckman automated cell counter ViCell was used. 50  $\mu$ L of cell suspension was diluted in (1:10 ratio) in 450  $\mu$ L PBS supplemented with 0.1% Pluronic™ F-68 Non-ionic Surfactant (#24040032, Thermo Fisher) in ViCell tubes.

For cryopreservation, cells were dissociated as previously described and cell pellet was resuspended in 1mL CryoStor® CS10 cell freezing medium from Sigma-Aldrich (#C2874) per one cryovial used. Cryovials were transferred to a Mr. Frosty™ freezing container from Thermo Scientific to achieve a cooling rate close to -1°C/minute, and stored at -80°C overnight. For long-term storage, cryovials were stored in liquid nitrogen.

For thawing frozen cells, appropriate cell culture medium was equilibrated in cell culture flasks at 37°C and 5% CO<sub>2</sub>. 15 mL falcon tubes were prepared containing 7 mL CO<sub>2</sub>-independent medium supplemented with 1% BSA (bovine serum albumin) and 2mM glutamine. Frozen cell vials were rapidly thawed in a 37°C water bath and subsequently transferred to the prepared falcon tube containing CO<sub>2</sub>-independent medium. Cells were centrifuged at 300 x g for 5 min at RT. Supernatant was removed and cell pellet was gently resuspended in appropriate cell culture medium and vessels. In case of PDX cell lines, 10  $\mu$ M Y-27632, ROCK-inhibitor (#LKT-Y1000.25, Biomol) was added to CSC BC medium to increase portion of cells that survive the thawing procedure.

## 5.2 Cell growth assay

Cells were dissociated and counted as previously described. Cells were transferred into a 1.5 mL Eppendorf tube and centrifuged at 300 x g for 5 min at RT. Supernatant was aspirated completely and cells were resuspended in 2 mL CSC BC medium or human plasma-like medium (HPLM) prepared as illustrated in Table 4. For growth assays,  $2.5 \times 10^5$  cells/well were seeded in a Corning® Primaria™ 6-well plate. 2 mL fresh medium was added every 72 h. After eight days, cells were harvested as previously described. Cell pellet was resuspended in 0.5 mL PBS supplemented with 0.1% Pluronic™ F-68 Non-ionic Surfactant and transferred to a ViCell tube. Cells were counted using the Beckman ViCell Counter and analyzed using GraphPad prism. Statistical differences between two groups were detected using an unpaired two-tailed Student's t-test.

**Table 4: Human plasma-like medium recipe.**

Component	Product number, company	Final concentration and volume
<b>Human plasma-like medium</b>	A4899101, Thermo Fisher	500 mL
Animal-free recombinant human epidermal growth factor	AF-100-15-1000, Peprotech	20 ng/mL (250 µL)
Fibroblast growth factor	100-18B-1000, Peprotech	50 ng/ mL (200 µL)
LONG R3 Insulin growth factor-1 human	I1271-1MG, Sigma	20 ng/mL (5 µL)
Recombinant human hepatocyte growth factor	100-39H-500, Peprotech	20 ng/mL (125 µL)
Insulin, human Recombinant, Zinc Solution 5ml	12585014, Life Technologies	625 µL
17-beta estradiol	E8875-1G, Sigma Merck	0.5 ng/ mL (12.5 µL pre-diluted in BSA)
Hydrocortisone	H0888, Sigma	100 ng/ mL (20 µL)
N2 supplement	17502048, Life Technologies	1X
O-phosphoryl-ethanolamine (OPE)	P0503, Sigma	0.1 mM (250 µL)
Glutathione (GSH)	G6013-5G, Sigma	1 µg/ mL (250 µL)
L-ascorbic acid 2-phosphate magnesium	A8960-5g, Sigma	6.4 µg/ mL (500 µL)
Trace A	25-021-CL, VWR	250 µL
Trace B	MDTC25-022-CI, VWR	500 µL
Trace C	MDTC25-023-CI, VWR	500 µL
Gibco™ AlbuMAX™ I Lipid-Rich BSA	11020-039, Thermo Fisher	3 mL 20% BSA in PBS



Heparine	H3149-10KU, Sigma	2 mg/mL (0.5 mL)
----------	-------------------	------------------

### 5.3 Immunohistochemistry

Hematoxylin and eosin (H&E) and immunohistochemistry (IHC) staining were performed by Vanessa Vogel and Ornella Kossi (HI-STEM gGmbH). Tumor specimen were fixed in 10% formalin purchased from Sigma for at least 48h. Subsequently, samples were dehydrated with increasing concentrations of ethanol, followed by xylene and finally embedded in paraffin.

H&E staining was conducted using an automatic tissue stainer. Briefly, slides were incubated in hematoxylin according to Mayer (Sigma), rinsed in water and stained with Eosine Y (Sigma). Staining was fixed with acetic acid, followed by increasing concentrations of ethanol. Afterwards, slides were covered with a xylene-based mounting medium and a cover slip.

For IHC staining, paraffin-embedded tumor blocks were cut into serial sections, and slices were deparaffinized with xylol and ethanol. This was followed by heat-induced epitope retrieval using damp heat in a steam pot with citrate buffer (pH 6.0) (#S2368, Dako 1:10). Primary antibodies were incubated 30 min at RT or overnight at 4°C. Slides were washed three times with PBS/Tween buffer and peroxidase blocking solution (#S2023, Dako) was added for 5 min at RT. Afterwards, EnVision+ Dual Link System-HRP (#K4061, Dako) was applied and incubated for 20-30 min at RT. Slides were washed again three times with PBS/Tween buffer and liquid DAB+ Substrate Chromogen System #K3468, Dako) was applied to visualize staining. Slides were covered with aqueous based mounting medium (Sigma) and a cover slip.

### 5.4 Western blot analysis

Cells harvested for protein lysis were cultured in Corning® Primaria™ (#353846, Corning) or non-coated 6-well plates or 100 mm dishes (#353803, Corning) as usual unless stated otherwise. Protein lysis buffer was prepared using the following reagents:

10X RIPA buffer (CSC)	100µl
100X AEBSF	10µl
100X EDTA	10µl

100X Protease and Inhibitor Cocktail	10 $\mu$ l
H <sub>2</sub> O	870 $\mu$ l
<b>Total</b>	<b>1000<math>\mu</math>l</b>

Cells in suspension were transferred to a 15 mL falcon tube and centrifuged at 300 x g for 5 min at 4°C. Meanwhile, adherent cells were washed once with ice-cold PBS on ice and 150  $\mu$ l protein lysis buffer was added. After centrifugation, cell pellet was washed once with ice-cold PBS. Cells were centrifuged at 300 x g for 5 min at 4°C and cell pellet was resuspended in 150  $\mu$ l protein lysis buffer and transferred to cells on dish. Cells were incubated for 5 min on ice and scraped using a cell scraper, followed by another incubation time of 15 min on ice. Cell suspension was transferred into a pre-cooled Eppendorf tube and centrifuged at 17,000 x g for 15 min at 4°C. Subsequently, the supernatant was transferred into a new pre-cooled Eppendorf tube and either used for immediate protein quantification or stored at -80°C.

Protein concentration was quantified using the Pierce™ BCA Protein Assay (#23255, Thermo Fisher Scientific) or Qubit™ Protein Assay (#Q33211, Thermo Fisher Scientific). For either assay, protein quantification was determined according manufacturer's instructions. Usually protein was diluted in a 1:10 ratio.

For protein denaturation, 2X protein buffer was prepared as followed:

10X Reducing agent (TCEP)	200 $\mu$ l
4X NUPage LDS sample buffer	500 $\mu$ l
H <sub>2</sub> O	300
<b>Total</b>	<b>1000<math>\mu</math>l</b>

500  $\mu$ g protein lysate was mixed with 250  $\mu$ l H<sub>2</sub>O and 250  $\mu$ l 2X protein buffer to obtain a protein concentration of 1  $\mu$ g/ $\mu$ L, and incubated at 75°C for 10 min. Afterwards, samples were immediately put back on ice and stored at -20°C.

For western blot analysis, the BioRad Laboratories System was used. 4–20% Criterion™ TGX Stain-Free™ protein gels (#5678094, BioRad) were rinsed with VE water and put into chamber filled with 1 L running buffer (100 mL 10X Tris/glycine/SDS (TGS)/NUPage + 900 mL MilliPore water). 20  $\mu$ g protein lysate was loaded onto gel and 8  $\mu$ L Spectra™ Multicolor Broad Range Protein Ladder (#26634, Thermo Fisher) was used as molecular weight standard. Gel was run at 100 V for 10 min, then voltage was increased up to 140V for another 90 min roughly. After run was finished, gel was removed from the cassette, placed on imaging tray and stain-

free dye was activated with an exposure time of 45 seconds. In brief, gel and PVDF membrane (Trans-Blot® Turbo™ Midi PVDF Transfer Packs, #1704157, BioRad) were assembled inside the Trans-Blot Turbo transfer system cassette. For this purpose, membrane was activated in 100% methanol for 1 min until the membrane was translucent and washed in Turbo-Blot transfer buffer (100 mL 5X Turbo-Blot transfer buffer + 100 mL 100% ethanol + 300 mL H<sub>2</sub>O). Transfer stacks were soaked in transfer buffer and put into the blotting cassette. The transfer sandwich was assembled as follows: bottom (+) cassette, bottom ion reservoir stack, blotting membrane, protein gel, top ion reservoir stack, top (-) cassette electrode (from bottom to top). Transfer was run applying the program ‘Mixed (or High) Molecular Weight’ for 7-10 min. Membranes were blocked in 5% BSA-Tris-buffered saline (TBS) with 0.05% Tween 20 (TBST-T) or 5% skim-milk TBS-T blocking buffer for 2h at RT or overnight at 4°C shaking. Primary antibodies were diluted in appropriate blocking buffer and incubated on membranes overnight at 4°C shaking. Primary antibodies (Table 5) in working solution were supplemented with 0.01% final concentration of sodium acetate and stored at 4°C. Membranes were washed thrice with 1X TBS-T and secondary HRP-coupled antibodies diluted 1:10,000 in blocking buffer were added, followed by an incubation time of 1h at RT on a rocker. Secondary antibodies were discarded and membranes were washed three times with 1X TBS-T again. 2 mL Clarity (Max)™ Western ECL substrate was prepared by mixing 1 mL of each part in the kit (#170506 0/2, BioRad) and applied to the membrane. ChemiDoc™ imaging system was used to acquire colorimetric and chemiluminescent images of blots. For image acquisition and analysis, Image Lab software (v. 6.0) was used.

**Table 5: Primary antibodies used for western blot analysis.**

Primary antibodies	IgG	Dilution	kDa	Product number	Company
PDEF	mouse IgG1	1:500	50	sc-166846	Santa Cruz
Androgen Receptor (D6F11) XP® Rabbit mAb	rabbit	1:2000	110	#5153	Cell Signaling Technologies
α-Tubulin (DM1A) Mouse mAb	mouse IgG1	1:1000	50	#3873	Cell Signaling Technologies
GAPDH (14C10) Rabbit mAb	rabbit	1:5000	37	#2118S	Cell Signaling Technologies
FBP1/FBPase 1 (D1B6A) Rabbit mAb	rabbit	1:1000	39	#72736	Cell Signaling Technologies
FASN Antibody (C20G5) Rabbit mAb	rabbit	1:1000	273	#3180	Cell Signaling Technologies
CD36 (D8L9T) Rabbit mAb	rabbit	1:1000	70-110	#14347	Cell Signaling Technologies

c-Myc (D84C12) Rabbit mAb	rabbit	1:1000	57-65	#5605	Cell Signaling Technologies
PI3 Kinase p110 $\alpha$ (C73F8) Rabbit mAb	rabbit	1:1000	110	#4249	Cell Signaling Technologies
Akt (pan) (C67E7) Rabbit mAb	rabbit	1:1000	60	#4691	Cell Signaling Technologies
Phospho-Akt (Ser473) (D9E) XP <sup>®</sup> Rabbit mAb	rabbit	1:1000	60	#4060	Cell Signaling Technologies
Acetyl-CoA 120enes et120se (C83B19) Rabbit mAB	rabbit	1:1000	280	#3676	Cell Signaling Technologies
ATP-Citrate Lyase (D1X6P)	rabbit	1:1000	125	#13390	Cell Signaling Technologies
<b>Mitochondrial Marker Antibody Sampler Kit #8674</b>					Cell Signaling Technologies
VDAC	rabbit	1:1000	32		
SOD1	mouse IgG1	1:1000	18		
SDHA	rabbit	1:1000	70		
PDH	rabbit	1:1000	43		
Prohibitin 1	rabbit	1:1000	32		
HSP60	rabbit	1:1000	60		
Cytochrome c	rabbit	1:1000	14		
COX IV	rabbit	1:1000	17		

Secondary antibodies	IgG	Dilution	Product number	Company
Anti-rabbit IgG, HRP-linked Antibody	rabbit	1:10000	#7074	Cell Signaling Technologies
Goat Anti-Mouse IgG1-HRP	mouse	1:10000	#1071-05	Biozol

## 5.5 Quantitative real-time PCR analysis

Cells harvested for RNA isolation were cultured in Corning 6-well plates as usual unless stated otherwise. Suspension cells were transferred into a 15 mL falcon tube and centrifuged at 300 x g for 5 min at 4°C. Meanwhile, 500  $\mu$ L QIAzol<sup>®</sup> lysis reagent was added to cells attached to wells. After centrifugation, supernatant was discarded and cell pellet was resuspended in 200  $\mu$ L QIAzol<sup>®</sup> lysis reagent. Cells in lysis reagent were reunited obtaining a final volume of 700  $\mu$ L, transferred into a 1.5 mL Eppendorf tube and snap-frozen in liquid nitrogen. Samples were stored at -80°C until RNA isolation. Total RNA was extracted using the miRNeasy Mini kit (#217004, Qiagen) following the manufacturer's protocol. In most cases, optional Dnase digest

was performed according to instructions in Appendix D of the handbook. RNA concentration and quality were determined using Nanodrop or Qubit 3.0 fluorometer (Thermo Scientific) according to manufacturer's instructions. RNA was reverse-transcribed using the high capacity cDNA reverse-transcription kit (#4374966, Applied Biosystems) according to the manufacturer's instructions. 60 ng of synthesized cDNA in triplicates served as template for quantitative real-time polymerase chain reaction (RT-qPCR) analysis which were largely performed by Ornella Kossi (HI-STEM gGmbH). TaqMan™ gene expression assays using the Fast Advance Master Mix and according dual-labeled TaqMan™ probes (Table 6) were used in order to acquire gene expression data with the VIIA7 Real-Time PCR or QuantStudio 5 Real-Time PCR Systems (Thermo Scientific). The  $\Delta\Delta C_t$ -method was applied to calculate the relative fold gene expression of samples. Acquired  $C_t$ -values for genes of interest were normalized to the geometric mean of up to three housekeeping genes (*RPL13A*, *POLR2A* and *PPIA*). In order to obtain the relative fold gene expression of each target,  $\Delta C_t$ -values were normalized to the respective  $\Delta C_t$ -value of the control sample. The QuantStudio™ Design and Analysis software (v. 1.4.3) was used for data acquisition and Microsoft Excel for data analysis. Data were further analyzed using GraphPad Prism9 (Version 9.3.1). Statistical differences between two groups were detected using an unpaired two-tailed Student's t-test.

**Table 6: TaqMan gene expression assays used for RT-qPCR analysis.**

<b>TaqMan™ Gene Expression Assay</b>
TaqMan Gene Expression Assay AR Hs00171172_m1
TaqMan Gene Expression Assay SPDEF Hs00171942_m1
TaqMan Gene Expression Assay CREB3L4 Hs00370116_m1
TaqMan Gene Expression Assay TFF3 Hs00902278_m1
TaqMan Gene Expression Assay FOXA1 Hs04187555_m1
TaqMan Gene Expression Assay ERBB2 Hs01001580_m1
TaqMan Gene Expression Assay PIP Hs00160082_m1
TaqMan Gene Expression Assay XBP1 Hs00231936_m1
TaqMan Gene Expression Assay HK1 Hs00175976_m1
TaqMan Gene Expression Assay HK2 Hs00606086_m1
TaqMan Gene Expression Assay FBP1 Hs00983323_m1
TaqMan Gene Expression Assay FBP2 Hs00427791_m1
TaqMan Gene Expression Assay ALDOC Hs00902799_g1
TaqMan Gene Expression Assay ALDOA Hs00605108_g1
TaqMan Gene Expression Assay GAPDH Hs02786624_g1
TaqMan Gene Expression Assay ENO2 Hs00157360_m1
TaqMan Gene Expression Assay PCK2 Hs01091129_g1
TaqMan Gene Expression Assay LDHA Hs01378790_g1

TaqMan Gene Expression Assay LDHB Hs00929956_m1
TaqMan Gene Expression Assay ACLY Hs00982738_m1
TaqMan Gene Expression Assay ACACA Hs01046047_m1
TaqMan Gene Expression Assay ACACB Hs01565914_m1
TaqMan Gene Expression Assay FASN Hs01005622_m1
TaqMan Gene Expression Assay FADS2 Hs00927433_m1
TaqMan Gene Expression Assay FA2H Hs00757813_m1
TaqMan Gene Expression Assay CYP2J2 Hs00356035_m1
TaqMan Gene Expression Assay SLC27A3 Hs00225680_m1
TaqMan Gene Expression Assay CD36 Hs00354519_m1
TaqMan Gene Expression Assay SCD Hs01682761_m1
TaqMan Gene Expression Assay ACSL3 Hs00244853_m1
TaqMan Gene Expression Assay ESR1 Hs01046816_m1
TaqMan Gene Expression Assay ALDH6A1 Hs00194421_m1
TaqMan Gene Expression Assay CYP1B1 Hs00164383_m1
TaqMan Gene Expression Assay HSD11B2 Hs00388669_m1
TaqMan Gene Expression Assay FGFR4 Hs01106910_g1
TaqMan Gene Expression Assay ELOVL6 Hs00907564_m1

## 5.6 Transcriptional profiling by microarray analysis

Total RNA was isolated from iT2 empty vector control, SPDEF overexpression, pTRIPZ non-silencing (NS)  $\pm$  doxycycline (Dox) and shSPDEF  $\pm$  Dox cells of the PDX cell lines CTC288, CTC223, BPE8 and BPE7, respectively, from three cell passages each. pTRIPZ NS and shSPDEF cells were pre-treated with 1  $\mu$ g/mL Dox for at least one week before RNA was extracted. Total RNA was isolated as described previously (5.5). Gene expression analysis was performed for three RNA samples/group using the Affymetrix GeneChip® Human Genome U133 Plus 2.0 Array at the Genomics and Proteomics Core Facility of the DKFZ Heidelberg. Gene expression data and data quality was analyzed using R Studio (3.5.1) and Bioconductor (v 2.7). R-script used in the end was a combination of several packages set up with the help of Dr. Felix Geist and Dr. Manuel Reitberger. The Bioconductor ‘affy’ (v.1.60.0), ‘affyPLM’ (v.1.58.0) and ‘simpleaffy’ (v.2.58.0) packages were used for exploratory oligonucleotide array analysis. In order to assess the quality of the set of arrays in an AffyBatch object ‘affyQCReport’ (v. 1.60.0) was applied. Probes were annotated using the Affymetrix Human Genome U133 Plus 2.0 Array annotation dataset, hgu133plus2.db-R package (v.3.2.3). The quality of normalized array data was determined using the ‘arrayQualityMetrics’ package

(v.3.44.0). Kolmogorov-Smirnov statistic test was applied to compare the array's distribution  $K_a$  and the distribution of the pooled data (illustrated as box plots). Hoeffding's  $D$ -statistic similar to distance correlation was applied to test whether samples are independent from each other (MA plots). Based on distance between arrays, boxplots and MA plots, outliers could be identified and removed from the analysis, if classified as outlier in at least two metrics. Probes with little variation across samples or missing annotation potentially interfere with downstream data analysis and thus were excluded from data analysis using 'genefilter' (v.1.68.0). Probe with maximal intensity for each gene was considered for gene expression analysis whereas duplicate probes were removed. Final probe set was plotted using ggplot2 (v.3.2.1) and pheatmap (v.1.0.12).

Principal component analysis (PCA) was conducted on top 500 variant genes between experimental and control groups unless stated otherwise. PMA package was used to perform sparse PCA.

To perform differential gene expression (DGE) analysis between contrast groups, the 'limma pipeline' was applied. Gene (or transcript) was identified as differentially expressed in a contrast group, if  $\log_2$  fold-change (L2FC) of expression  $\geq q$  a cut-off and with adjusted p-value  $<$  a cut-off. L2FCs were calculated based on count per million reads (CPMs). An unpaired, two-tailed  $t$ -test was applied to determine statistical significance (p-value  $<$  0.05) followed by Benjamini-Hochberg correction in order to identify DEG with an adjusted p-value (false discovery rate, FDR)  $<$  0.05.

Gene Set Enrichment Analysis (GSEA) was performed using the 'GSEABase' and 'fgSEA' packages. The latter implements an algorithm for fast GSEA allowing 'to make more permutations and get more fine-grained p-values, which allows to use accurate standard approaches to multiple hypothesis correction'. The pre-ranked gene list was based on DEGs identified previously including all genes with  $L2FC > 0$  and rank-ordered according to t-values considering  $\log_{FC}$  and FDR. All annotated gene sets used were provided by the Molecular Signature Database (MsigDB, release v. 7.0, UC San Diego and Broad Institute).

## 5.7 *In vitro* drug treatment assays

CellTiter-Blue® (CTB) cell viability assay (#G8021, Promega) was used to assess drug response towards enzalutamide (Enza, MDV3100 #S1250, Selleckchem) treatment in PDX cell

lines. For this purpose, 10,000 cells/well of a Corning® Primaria™ 96-well plate (#353872, Corning) were seeded in 100 µL CSC BC medium in quadruplicates for BPE8, CTC223 and BPE7 cell lines. Cells were incubated for 2h at 37°C and 5% CO<sub>2</sub>. Subsequently, Enza treatment was added to wells starting at a concentration of 100 µM in a 1:3 serial dilution. After 72h, 100 µL fresh CSC BC medium supplemented with Enza was added on top of cells. After six days of treatment, cell viability was assessed by adding 20 µL CTB reagent to each well and incubated for 4h. Conversion of the redox dye resazurin to resorufin by metabolically active cells was measured by fluorescence intensity (560<sub>Ex</sub>/590<sub>Em</sub>) using the SpectraMax iD3 microplate reader (Molecular Devices). Staurosporine (STS, #S1421, Selleckchem/Hölzel) treatment was used as positive control and fluorescent background. Each drug concentration was screened in quadruplicates and relative cell viability was calculated by normalizing to DMSO vehicle control.

For AR agonist activation, 2.5 x 10<sup>5</sup> cells/well were seeded in an appropriate 6-well plate and treated with 1 nM dihydrotestosterone (DHT, S4757, Selleckchem), 1 nM R1881 (R0908, Sigma) or DMSO vehicle control for three or six days *in vitro* as indicated.

## 5.8 siRNA transfection of HEK293T cells

HEK293T cells were cultured in T175 cell culture flasks in IMDM supplemented with 10% FCS. In order to passage cells, cell culture medium was aspirated, cells were washed once with PBS and 3 mL Trypsin (#T3924, Sigma Aldrich) was added to cells on flask. Cells in Trypsin were incubated at 37°C and 5% CO<sub>2</sub> for roughly 5-10 min until they were completely dissociated and detached. Subsequently, 7 mL IMDM was added to collect cells in a total volume of 10 mL in order to stop trypsinization. Next, cells were centrifuged at 300 x g for 5 min at RT. Supernatant was removed and cell pellet was resuspended in 1mL IMDM. Cells were seeded in a 6-well plate. On the next day, medium was changed. (1) 2 µg in 20 µL of SPDEF human untagged clone pCMV6-XL5 DNA (#sc115408, Origene) was diluted in 250 µL Opti-MEM I Reduced Serum Medium and mixed gently (#31985062, Thermo Fisher). (2) 5 µL of Lipofectamine 2000™ RNAi MAX transfection reagent (13778030, Thermo Fisher) was diluted in 250 µL Opti-MEM. Both, (1) and (2) reactions were incubated for 5 min at RT. Subsequently, (1) and (2) were combined, mixed gently and incubated for 20 min at RT. Next,



transfection mix was added dropwise onto cells. Cells were incubated at 37°C, 5% CO<sub>2</sub> for few hours. After 48 h, cells were harvested for protein lysis.

## 5.9 SPDEF overexpression and knockdown vector constructs

SPDEF overexpression construct was cloned by Dr. Franziska Maria Zickgraf as described within her dissertation<sup>213</sup>. The LeGO iT2 vector (#27343, Addgene) was utilized as backbone for SPDEF overexpression construct (Figure 64).



**Figure 64: LeGO iT2 plasmid map.** Figure illustrates LeGO iT2 vector showing digestion enzyme sites, antibiotic resistance, promoter regions, reporter genes and insert site.

In brief, the vector was cut using *Bam*HI and *Not*I within the multiple cloning site according to manufacturer's instructions. SPDEF coding sequence (NM\_012391.2) was amplified using 10 μM each of SPDEF\_FW and SPDEF\_Rev primer pair, and Q5<sup>®</sup> Hot Start High-Fidelity master mix (#M04094S, New England Biolabs) according to the manufacturer's protocol. The following PCR settings were used:

98°C	30 s	
98°C	10 s	} 30 cycles
68°C	30 s	
72°C	30 s	
72°C	2 min	

PCR fragments were purified using the QIAquick PCR purification kit (#28106, Qiagen) according to manufacturer's instructions. LeGO iT2 backbone was dephosphorylated using the Antarctic Phosphatase Kit (M0289S, New England Biolabs) according to manufacturer's instructions. Kit components were incubated with 5 µg LeGO iT2 DNA for 15 min at 37°C, followed by heat-inactivation for 5 min at 70°C. Digested and purified SPDEF insert and dephosphorylated LeGO iT2 vector were ligated. To this end, DNA was incubated with T4 DNA ligase and respective ligase buffer for 1 h at RT, followed by heat-inactivation at 65°C for 15 min. Insert and vector DNA were mixed in a ratio of 3:1.

For transformation, chemo competent STBL3 bacteria were used. Bacteria were thawed on ice, ligated vector was added to bacteria and incubated for 1 h on ice. Subsequently, cells were put into water bath at 42°C for 45 s and afterwards put back on ice for 2 min. 250 µL SOC medium was added to bacteria and shaken for 1 h at 37°C at 225 rpm. Afterwards, the mixture was transferred on a pre-warmed LB agar plate supplemented with 100 µg/mL carbenicillin and incubated at 37°C overnight.

A colony-PCR was performed to verify correct amplification of plasmid of interest as previously described by Dr. Franziska Maria Zickgraf<sup>213</sup>. For plasmid purification, a single colony from LB agar plate was picked and transferred into a bacterial flask filled with LB medium supplemented 100 µg/mL carbenicillin. Mini cultures were shaken at 37°C for 8 h at 225 rpm. Mini cultured were used to inoculate maxi cultures prepared in 250 mL LB medium supplemented 100 µg/mL carbenicillin. Maxi cultured were shaken at 37°C overnight. Purification of plasmids was performed using the QIAGEN Plasmid Maxi Kit (#12163, Qiagen) according to manufacturer's instructions. Plasmid DNA quality and quantity was assessed using the NanoDrop Spectrophotometer (Thermo Scientific). The obtained plasmid DNA was further cleaned-up by ethanol precipitation. To this end, 1 mL of plasmid DNA was mixed with 100 µL 3M sodium acetate, pH 5.2 (1:10) and distributed to two Eppendorf tubes. Two volumes of ice-cold ethanol were added to each tube, gently mixed and incubated at -20°C for 5 min. Subsequently, samples were centrifuged at 15,000 rpm for 15 min at 4°C. Supernatant was discarded and two volumes of ice-cold 70% ethanol was added to each tube. Samples were centrifuged at 15,000 rpm for 15 min at 4°C again, supernatant was discarded. DNA was air-dried and resuspended in 300 µL sterile TE buffer.

For shSPDEF construct, inducible Dharmacon™ pTRIPZ™ lentiviral shRNA targeting SPDEF was ordered from Dharmacon and manufacturer's instructions were followed for plasmid amplification and purification (Figure 65). The following shRNA sequence was utilized:

pTRIPZ shSPDEF V3THS\_376889

ACAGCATGTCAAAGTAGGA

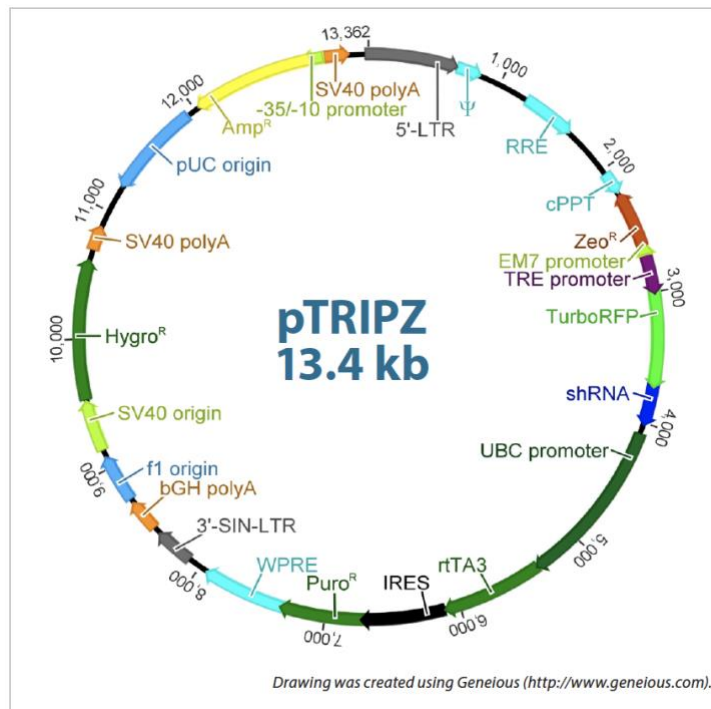


**Figure 65: pTRIPZ plasmid map.** Figure illustrates pTRIPZ lentiviral vector obtained from Dharmacon.

## 5.10 Virus production

On the day before transfection, HEK293T cells were seeded in T150 cell culture flasks in IMDM supplemented with 10% FCS and incubated at 37°C, 5% CO<sub>2</sub> overnight. On the day of transfection, optimal confluency of cells was roughly 70%. Medium was aspirated and replaced by IMDM supplemented with 10% heat-inactivated FCS and 25 µM chloroquine. For this purpose, FCS was incubated at 52°C for 1h before added to the medium. Calcium-phosphate co-precipitation method was applied to transfect HEK293T cells. Respective reagents were thawed on ice and transfection mix was prepared in a 50 mL falcon tube as follows:

- 50 µg lentiviral plasmid of interest
- 37.5 µg pSPAX2 (Gag/pol) packaging 1 mg/mL
- 5 µg pMD2.G envelope plasmid 1 mg/mL
- 72 µL 2.5 mM CaCl<sub>2</sub>
- filled up to a total volume of 750 µL with sterile ddH<sub>2</sub>O

Equal amount of 2X HBS (750  $\mu\text{L}$ ) was added to the transfection mix and vigorously shaken, followed by an incubation time of 15 min at RT. Previously prepared IMDM supplemented with 25  $\mu\text{M}$  chloroquine was added with transfection mix and given on HEK293T cells. Cells were incubated at 37°C, 5%  $\text{CO}_2$  in a S2-incubator. On the next morning (8-12 h after transfection), medium was carefully aspirated and replaced by freshly prepared collection medium: IMDM supplemented with 10% heat-inactivated FCS, 4 mM caffeine and 1 mM sodium butyrate. 48h post-transfection, collection medium was harvested and filtered using a Millipore™ Stericup™ Quick Release-HV Vacuum Filtration System 0.45  $\mu\text{m}$  (#S2HVU02RE). Filtered collection medium was transferred to autoclaved, sterile Beckman tubes (#326823, Beckman Coulter) and centrifuged at 21000 rpm for 2h at 4°C in the ultracentrifuge. Afterwards, supernatant was aspirated and remaining liquid was carefully removed with clean wipes. Pellet was resuspended in 500x concentrated volume of PBS or Advanced DMEM F12. Virus was aliquoted at 10-15  $\mu\text{L}$  and stored at -80°C.

In order to determine virus titer, 50,000 HEK293T or BPE8 cells were seeded in a 6-well plate/well. On the next day, medium was aspirated and fresh IMDM supplemented with 10% heat-inactivated FCS and 10  $\mu\text{g}/\text{mL}$  polybrene (#TR-1003, Sigma) was added to cells. 10  $\mu\text{L}$  virus in a 1:10 dilution series was added to the cells in duplicates. Medium was changed 14 h after transduction. 72h post-transduction, cells were harvested as usual and analyzed by flow cytometry. Transfection efficiency and virus titer was calculated according to the following formula:

$$\text{Titer} \left( \frac{\text{transducing units}}{\text{mL}} \right) = \text{number of seeded cells (count at day 1)} \times \frac{\% \text{ of fluorescent cells}/100}{\text{volume of virus in mL}}$$

### 5.11 Transduction of cell lines

For virus transduction, required volume of virus was calculated according to the following formula:  $\text{virus particles} = \text{MOI} \times \text{cell number seeded}$

$$\text{volume of virus (mL)} = \text{virus/titer} \left[ \frac{\text{transducing units}}{\text{mL}} \right]$$

$1 \times 10^6$  cells were seeded in a 100 mm Corning® Primaria™ dish (#353803) in CSC BC medium supplemented with 10  $\mu\text{g}/\text{mL}$  polybrene. Three to four hours after seeding, PDX cell lines were transduced with x  $\mu\text{L}$  virus as calculated previously in order to achieve a transduction efficiency of roughly 30%. 14 h post-transduction, medium was changed as usual. Subsequently, cells

were cultured as usual and sorted by fluorescent activated cell sorting (FACS) for fluorescent marker.

### **5.12 Flow cytometry**

For FACS and flow cytometry analysis, cells were harvested as usual and cell pellet was resuspended in sterile PBS supplemented with 1% BSA. Cells were filtered to achieve a single-cell suspension and transferred to appropriate FACS tubes. FACS sorting experiments were performed at the Beckman Coulter Aria I, II or Aria Fusion at the DKFZ Flow Cytometry Core Facility. For flow cytometry analysis, Beckman Coulter Fortessa or LSR II were used. For CD36 protein analysis, cells were resuspended in 100  $\mu$ L PBS supplemented with 1% BSA and 5  $\mu$ L anti-CD36 antibody (anti-CD36 APC antibody #336207, Biolegend) was added. Cells were incubated in the dark for 15 min on ice and washed once with PBS supplemented with 1% BSA. Cell pellet was resuspended in 150-100  $\mu$ L PBS supplemented with 1% BSA according to cell number and analyzed by flow cytometry. Data analysis was performed using the FlowJo software. Data were further analyzed using GraphPad Prism9 (Version 9.3.1). Statistical differences between two groups were detected using an unpaired two-tailed Student's t-test.

### **5.13 Microscope image acquisition**

Brightfield microscope images were acquired using the Zeiss Axio Scan.Z1 slidescanner at the DKFZ Light Microscopy Facility. The following settings were used:

Coarse: 1-4

Focus: 'run auto focus' after navigating on tumor region

Navigator range: 400  $\mu$ m, 3800 – 4200

Fine: 70  $\mu$ m

Lossy compression: 85%

## 5.14 CRISPR/Cas9-mediated knock-out

Breast cancer cell lines were dissociated as previously described and counted using ViCell Counter.  $0.5 \times 10^6$  cells were used for each electroporation reaction (EP). CRISPR-RNAs (crRNA) targeting SPDEF, AR, FBP1 and CD36 were ordered from IDT (Table 7). Alt-R CRISPR-Cas9 negative control crRNA#1 (#1079138, IDT) was utilized as control. Electroporation was performed using either the MaxCyte instrument or NEON (Thermo Scientific) according to manufacturer's instructions. In brief, gene targeting Alt-R guide RNA (gRNA) was prepared by mixing the Alt-R CRISPR-Cas9 crRNA XT (200  $\mu$ M, IDT) and Alt-R CRISPR-Cas9 tracrRNA (200  $\mu$ M, #1072533, IDT) dissolved in IDT buffer in equimolar concentrations. Mixture was heated for 5 min at 95°C and subsequently cooled down to RT. For each reaction, Alt-R S.p. Cas9 Nuclease V3 enzyme (62  $\mu$ M, #1081058, IDT) was diluted to 36  $\mu$ M. 0.5  $\mu$ L Cas9 protein and 0.5  $\mu$ L Alt-R gRNA were mixed and incubated for 10 min at RT. For each EP, cells were resuspended in 8  $\mu$ L buffer R (Neon Transfection System 10  $\mu$ L Kit #MPK1025, Thermo Scientific). 2  $\mu$ L Alt-R Cas9 Electroporation Enhancer (10.8  $\mu$ M, #1075916, IDT) and Alt-R RNP complex were added to cells. 10  $\mu$ L EP reaction mix was taken using the NEON tip and inserted into the pipette station. Electroporation was performed with 1300 V for 20 ms and 2 pulses. 10  $\mu$ L EP cells were transferred into 500  $\mu$ L pre-equilibrated appropriate cell culture medium in a 24-well plate. Cells were incubated at 37°C, 5% CO<sub>2</sub> as usual. Validation of knock-out was performed by flow cytometry analysis in case of a membrane-localized protein, protein detection by western blot analysis and sanger sequencing (EurofinsGenomics) of target region.

**Table 7: CRISPR-Cas9 guideRNAs used for knock-out experiments.**

<b>Predesigned Alt-R CRISPR-Cas9 gRNAs</b>	
Hs.Cas9.AR.1.AA	CTGGGACGCAACCTCTCTCG
Hs.Cas9.AR.1.AB	TTGCATGTACGCCCCACTTT
Hs.Cas9.SPDEF.1.AA	GGGGATACGCTGCTCAGACC
Hs.Cas9.SPDEF.1.AB	CCAATACCGGCTGCCCCCA
Hs.Cas9.FBP1.1.AA	GTGTTGACGTCCGTGTCGAA
Hs.Cas9.FBP1.1.AB	CCTTAACGAGGGCTACGCA
Hs.Cas9.CD36.1.AA	TTCGAACCTTCACTATCAGT
Hs.Cas9.CD36.1.AB	ACCTTTATATGTGTCGATTA
Hs.Cas9.CD36.1.AC	TGGGCTGTGACCGGAAGTGT

## 5.15 Sanger sequencing

Genomic DNA was extracted from cells using the Dneasy Blood and Tissue Kit (#69506, Qiagen) according to manufacturer's instructions. DNA quality and quantity were determined using the NanoDrop Spectrophotometer (Thermo Scientific). In order to determine knock-efficiency of CRISPR-Cas9 KO cells, the DNA region surrounding the target region of the gene of interest was amplified by PCR using the Q5<sup>®</sup> Hot Start High-Fidelity master mix (#M04094S, New England Biolabs) according to the manufacturer's protocol. PCR and sanger sequencing primer are illustrated in Table 8. PCR purification and sanger sequencing were performed at EurofinsGenomics. TIDE webtool was utilized to assess knock-out efficiencies by comparing DNA sequences of non-targeting control and knock-out samples.

**Table 8: Primer used for DNA amplification and sanger sequencing.**

Primer	Sequence
human_AR_AB_Fwd	CCCCACTTTCCCCGGCTTAAGC
human_AR_AB_Rev	TCTTCAGTGCTCTTGCCTGCGC
human_SPDEF_AA_Fwd	CAATGACCCGGAAGCCCCAAC
human_SPDEF_AA_Rev	CCCAGCTGCTGTCCTCAGGGTA
human_SPDEF_AB_Fwd	GGCCTGTCTGGGGCTGACCTAT
human_SPDEF_AB_Rev	AGCATCCTGTCCCTGGCTTGGA
human_FBP1_AA_Fwd	CGGCAGTCGGTCTGTCAGTCCT
human_FBP1_AA_Rev	TCCCCAGGCAGACAGACAGGAC
human_FBP1_AB_Fwd	TCTCGGGGCCCAAGATGAGTG
human_FBP1_AB_Rev	CCAAGGCCCTCGATCCCAAGGA
human_AR_AA_Fwd	CGCGAAGTGATCCAGAACCCGG
human_AR_AA_Rev	AAGGAGTTGCATGGTGCTGGCC

## 5.16 Animal experiments

Animal experiments were approved by the national authorities (Regierungspräsidium Karlsruhe). Studies were conducted according to authorization number (Tierversuchsantrag) G-290/19. Mice were housed and bred at the DKFZ Animal Facility under specific pathogen free (SPF) conditions and maintained in individually ventilated cages (IVCs). For xenograft experiments, female NOD.Cg-Prkdc<sup>scid</sup> Il2rg<sup>tm1Wjl/SzJ</sup> (NSG) immunocompromised mice were used. Breast cancer cells were injected into the mammary fat pad (mfp). For doxycycline-

constructs, mice were pre-treated with doxycycline (2 mg/mL, #D9891, Sigma) in drinking water up to one week before cells were implanted. Doxycycline in drinking water was given throughout the whole experiments. In detail, mice were anaesthetized with 3% isoflurane and 1.5% O<sub>2</sub>. Isoflurane was decreased to 1.7% once mice were asleep. Before surgery, mice were weighted and weight was noted for every mouse. Approx. 100-150  $\mu$ L carprofen (5 mg/kg) were injected subcutaneously. The right hind legs of mice were shaved and disinfected using iodine solution. A straight cut was performed at the abdominal wall with scarp scissors and widened. 90 day-release 0.18 mg 17 $\beta$ -estradiol pellets (#NE-121, Innovative America) were implanted using straight tweezers and 100  $\mu$ L cells in 132enes et/PBS were injected into the mammary fat pad. The incision was clamped using 3-4 wound clamps which were removed ten days after surgery. Carprofen was given every 9-12 h for three days after surgery. To generate mfp tumors for growth curve analysis, 10,000 cells were injected. Tumor growth was followed by caliper measurements. To this end, mice were anaesthetized as previously described. To assess metastatic burden, 100,000 cells were injected into the mfp. Tumors were resected once primary tumors reached a volume of 0.1-0.5 cm<sup>3</sup>. For this purpose, mice were intraperitoneally injected with xylazine hydrochloride (14.5 mg/kg) and ketamine (90 mg/kg) in 10  $\mu$ L/g sodium chloride (NaCl). Eyes were covered with Bepanthen® eye and nose ointment. The right hind legs of mice were shaved and disinfected using iodine solution. A straight cut was performed at the abdominal wall with scarp scissors and widened. Tumor was resected and wound was clamped using 3-4 wound clamps which were removed ten days after surgery. Carprofen was given every 9-12 h for three days after surgery. To assess metastatic lesions, PDX cells were transduced *in vitro* with a luciferase transgene as previously described and monitored using the IVIS 200 bioluminescence imaging system. For bioluminescence imaging, mice were intraperitoneally injected with D-Luciferine Firefly Potassium salt (150 mg/kg in 100  $\mu$ L PBS, #L8220, Biosynth Carbosynth). Six minutes after injection, mice were anaesthetized with 3% isoflurane and 1.5% O<sub>2</sub>. Isoflurane was decreased to 1.7% once mice were asleep. Bioluminescent signal was measured and data was analyzed using the Living Image software. Data were further analyzed using GraphPad Prism9 (Version 9.3.1). Normal (Gaussian) distribution was tested applying the Shapiro-Wilk normality test and considered normally distributed, if significance level ( $\alpha$ ) > 0.05. Statistical differences between two groups were detected using an unpaired two-tailed Student's t-test. In the case of non-parametric data distribution, the Mann-Whitney U-test was applied. Statistical significances were illustrated as \*  $p < 0.05$ , \*\*  $p < 0.01$ , \*\*\*  $p < 0.001$ ; ns, not significant.



## 5.17 Seahorse assays

Agilent Seahorse Mito Stress assay (#103015, Agilent) was utilized for measuring mitochondrial respiration activity. Oxygen consumption rate (OCR) and extracellular acidification rate (ECAR) are measured upon three serial injections of inhibitors targeting different complexes of the mitochondrial electron transport chain: oligomycin, carbonylcyanide-4 (trifluoromethoxy) phenylhydrazone (FCCP), and rotenone/antimycin A (Figure 66A). This allows simultaneous measurements of multiple parameters including basal and maximal respiration activity, spare respiratory capacity, ATP production and non-mitochondrial respiration (Figure 66B).

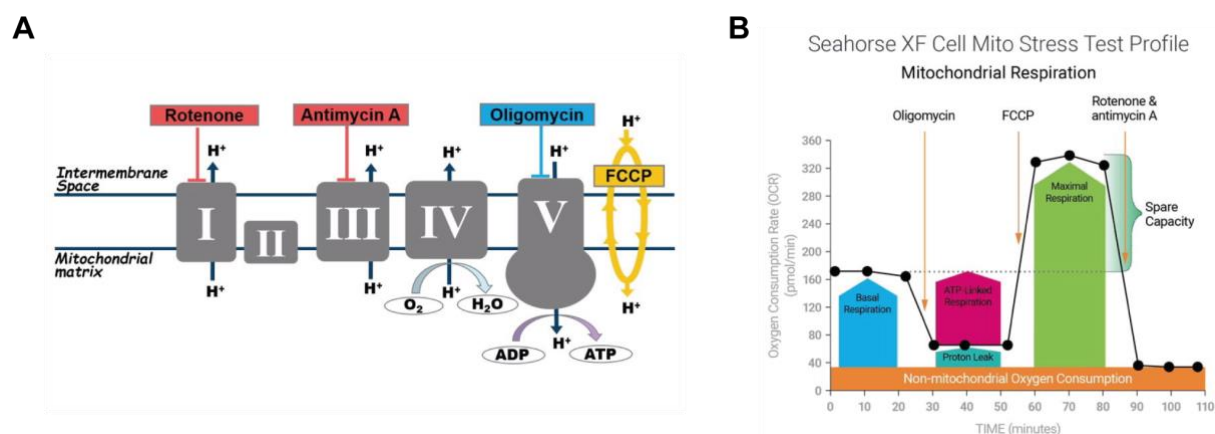


**Figure 66: Overview of Seahorse XF Mito Stress Assay.** (A) Schematic illustrates inhibitors, rotenone, antimycin A, oligomycin and FCCP targeting different complexes of the mitochondrial electron transport chain. (B) Figure illustrates profile of Seahorse XF Cell Mito Stress Test measuring oxygen consumption rate (OCR). After three measurements of basal OCR, oligomycin is injected onto cells which inhibits ATP synthase, complex V of the electron transport chain, resulting in reduction of OCR. After each injection, three measurements are performed. Second, uncoupling agent carbonylcyanide-4 (trifluoromethoxy) phenylhydrazone (FCCP) is injected disrupting the mitochondrial membrane potential. Third, mixture of rotenone and antimycin A targeting complex I and III, respectively are injected shutting down mitochondrial respiration. Based on these measurements, parameters including basal respiration, ATP-linked respiration, proton leak, maximal respiration, spare capacity and non-mitochondrial oxygen consumption are calculated.

For detailed protocol, manufacturer's instructions were followed. On the day prior to assay, sensor cartridge hydrated in sterile water (200  $\mu$ L/well) and Seahorse XF calibrant solution were incubated at 37°C in a non-CO<sub>2</sub> incubator overnight. In order to measure suspension cells, either Agilent Seahorse Xfe96 cell culture microplates coated with Cell-Tak Cell and Tissue Adhesive (#354240, Corning) or Seahorse Xfe PDL cell culture plates (#103730-100, Agilent) were used. The latter were pre-incubated at 37°C in a non-CO<sub>2</sub> incubator overnight on day before the assay. On the day of the assay, water from sensor cartridge was discarded and filled with pre-warmed Seahorse XF calibrant solution (200  $\mu$ L/well). Assembled sensor cartridge and utility plate were placed at 37°C in a non-CO<sub>2</sub> incubator for 45-60 min prior to loading the

injection ports of the sensor cartridge. Next, Seahorse XF Cell Mito Stress Assay medium was prepared as follows:

Seahorse XF DMEM 100 mL

1 mM pyruvate 1 mL

2 mM glutamine 1 mL

10 mM glucose 400  $\mu$ L

Seahorse XF assay medium was pre-warmed at 37°C in water bath and pH was adjusted to 7.4 using 0.1 NaOH solution. Medium was sterile filtered and kept at 37°C until needed for the assay. If needed, Seahorse XF cell culture microplate was coated with Cell-Tak Cell and Tissue Adhesive as follows:

NaHCO<sub>3</sub> 2.4 mL

Cell-Tak 23  $\mu$ L

1N NaOH 11.5  $\mu$ L

25  $\mu$ L/well were added to each well and incubated for 20 min at RT. Subsequently, plate was washed thrice with sterile water. Cells were dissociated as previously described and washed with pre-warmed Seahorse XF assay medium. 50,000 cells/well were seeded in 50  $\mu$ L/well and centrifuged at 200 x g for 1 min at RT. Corner wells filled with medium only were used as background reference. Wells were filled up to a final volume of 180  $\mu$ L/well with assay medium. Subsequently, cells were incubated at 37°C in a non-CO<sub>2</sub> incubator for 20 min. Meanwhile, stock compounds were prepared by resuspension in pre-warmed assay medium as follows:

Oligomycin in 630  $\mu$ L

FCCP in 720  $\mu$ L

ROT/AA in 540  $\mu$ L

Three 15 mL tubes containing 2.7 mL pre-warmed assay medium were prepared and 300  $\mu$ L of each compound was added to one vial each. 20  $\mu$ L/well oligomycin (final concentration: 1.5  $\mu$ M) was pipetted to port A, 22  $\mu$ L/well FCCP (final concentration: 1  $\mu$ M) was added to port B, and 25  $\mu$ L/well ROT/AA (final concentration: 0.5  $\mu$ M) was pipetted to port C using a multichannel-pipet. Sensor cartridge was placed at 37°C in a non-CO<sub>2</sub> incubator until run was started. Mito Stress assay was measured using the Seahorse Xfe 96 Extracellular Flux Analyzer (Agilent) and the WAVE software. Data analysis was automatically performed by WAVE. Data were analyzed using GraphPad Prism9 (Version 9.3.1). Normal (Gaussian) distribution was

tested applying the Shapiro-Wilk normality test and considered normally distributed, if significance level ( $\alpha$ ) > 0.05. Statistical differences between two groups were detected using an unpaired two-tailed Student's t-test. In the case of non-parametric data distribution, the Mann-Whitney U-test was applied. Statistical significances were illustrated as \*  $p < 0.05$ , \*\*  $p < 0.01$ , \*\*\*  $p < 0.001$ ; ns, not significant.

## 5.18 Isotope tracing experiments

For [ $^{13}\text{C}$ ]-glucose isotope tracing experiments, CSC BC medium was prepared as previously described except of adding glucose to CSC master mix. Glucose was replaced by [ $^{13}\text{C}$ ]-glucose (#CLM1396, Cambridge Isotope Laboratories) at same concentrations usually applied. For [ $^{13}\text{C}$ ]-glucose, [ $^{13}\text{C}$ ]-glutamine and [ $^{13}\text{C}$ ]-acetate isotope tracing experiments, CSC BC medium was prepared as previously described expect of adding glucose and glutamine to medium. Glucose and glutamine were replaced by [ $^{13}\text{C}$ ]-glucose and [ $^{13}\text{C}$ ]-glutamine (#605166, Eurisotop) at same concentrations usually applied. [ $^{13}\text{C}$ ]-sodium acetate (#282014, Sigma) was added to medium to achieve a final concentration of 400  $\mu\text{M}$ . Media were sterile filtered as previously described. BPE8 cell lines were dissociated and counted using the ViCell Counter as previously described.  $1 \times 10^6$  cells/well were seeded in 2 mL isotope tracing medium in Corning® Primaria™ 6-well plates. To determine metabolic steady-state and duration of labeling, cells were harvested after 24, 72, and 96 h. For [ $^{13}\text{C}$ ]-glucose, [ $^{13}\text{C}$ ]-glutamine and [ $^{13}\text{C}$ ]-acetate isotope tracing experiments, cells were harvested after 72 h. In brief, cells were transferred to a 15 mL falcon tube on ice and centrifuged at  $350 \times g$  for 5 min at  $4^\circ\text{C}$ . 1 mL of ice-cold 154 mM ammonium acetate was added to adherent cells on wells kept on ice. Cells were scraped using a cell scraper as previously described. After centrifugation, supernatant was aspirated and cells were washed using 0.5 mL of ice-cold 154 mM ammonium acetate. Cells from well and 15 mL tube were combined in a pre-cooled 1.5 mL safe-lock Eppendorf tube and centrifuged at  $350 \times g$  for 5 min at  $4^\circ\text{C}$ . Supernatant was completely aspirated and samples were snap-frozen in liquid nitrogen. Subsequently, samples were transferred and stored at  $-80^\circ\text{C}$  until liquid chromatography (LC) mass spectrometry (MS) analysis. LC/MS analysis was performed by Dr. Marteinn T. Snaebjörnsson, Schulze Lab, DKFZ Heidelberg as described in Ruiz-Pérez *et al.*, 2021<sup>276</sup>. For [ $^{13}\text{C}$ ]-glucose, [ $^{13}\text{C}$ ]-glutamine and [ $^{13}\text{C}$ ]-acetate isotope tracing experiments, three independent experiments were performed. LC/MS analysis was performed simultaneously for the three replicates. BPE8 pTRIPZ NS showed one significant outlier which

was removed from the analysis calculating total sum of isotopologues labeling and  $m+0$ . In the first experiment, cells were induced with doxycycline for one week before isotope tracing experiment was started. Doxycycline was not supplemented to shSPDEF and pTRIPZ NS cells cultured in tracing medium for 72h. For this reason, BPE8 pTRIPZ NS outlier could be removed. BPE8 shSPDEF samples did not exhibit any variance such that the first sample could not be identified and no values were excluded from the analysis. Normal (Gaussian) distribution was tested applying the Shapiro-Wilk normality test and considered normally distributed, if significance level ( $\alpha$ ) > 0.05. Statistical differences between two groups were detected using an unpaired two-tailed Student's t-test.

### 5.19 Patient data analysis

For patient data analysis, the breast cancer METABRIC data set including 1904 breast cancer patients was applied. RNA-sequencing results and patient data were obtained from cBioportal. Survival probabilities were analyzed by estimate a survival function on patient survival data. Patients were assigned to groups based on mRNA expression of gene of interest or according to hormone receptor status. Kaplan Meier estimators were calculated and log rank test was applied to test for significant differences of Kaplan Meier estimators based on gene or hormone receptor status<sup>277</sup>. R packages 'survival' and 'survminer' were used for analysis and visualization of survival data<sup>278,279</sup>.

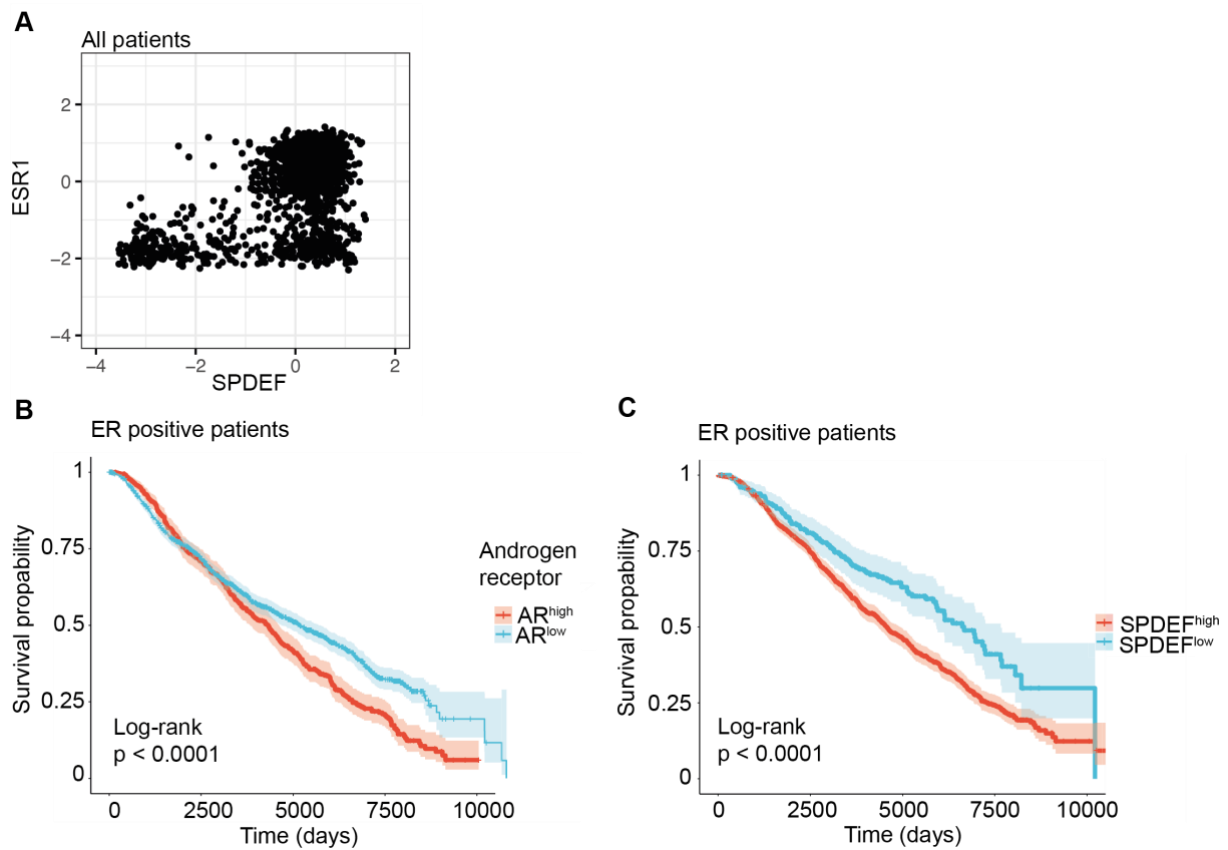
### 5.20 Graphics software

GraphPad Prism, R-Studio, Adobe Illustrator and BioRender were used to design figures.

## 6 Supplements

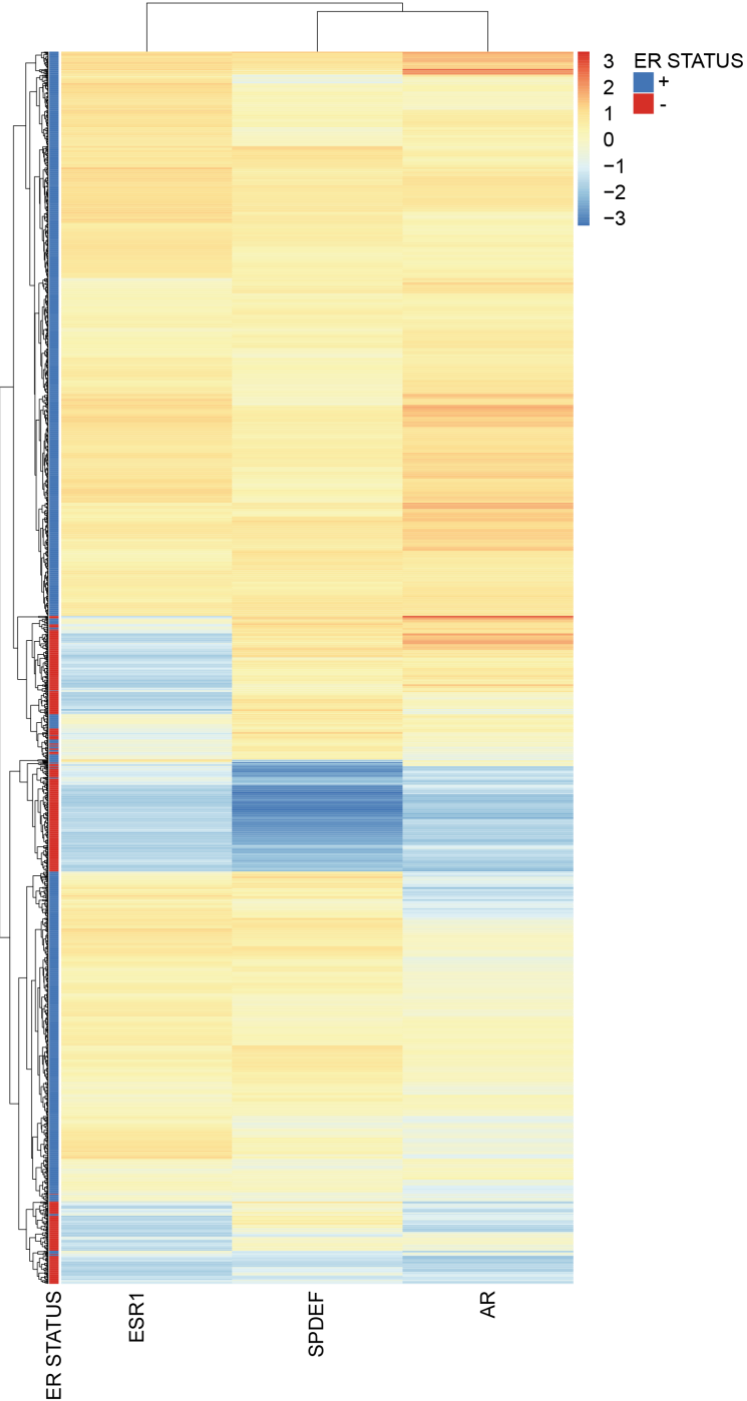
**Supplementary Table 1: Correlation Scores in ER positive (ER+) and negative (ER-) breast cancer patients.**

<b>ER- patients</b>	<b>445</b>		
<b>SPDEF</b>		<b>Pearson</b>	<b>Spearman</b>
	<b>AR</b>	0.7705874	0.7668253
	<b>FASN</b>	0.6521966	0.657707
	<b>CD36</b>	0.1008589	0.1035789
	<b>FBP1</b>	0.435547	0.4626275
	<b>ERBB2</b>	0.7145301	0.7068991
	<b>ESR1</b>	0.2669145	0.2518156
	<b>AKT1</b>	0.6618543	0.6757781
<b>ER+ patients</b>	<b>1459</b>		
<b>SPDEF</b>		<b>Pearson</b>	<b>Spearman</b>
	<b>AR</b>	0.34416	0.3337294
	<b>FASN</b>	0.2576266	0.2231418
	<b>CD36</b>	-0.1779137	-0.1956683
	<b>FBP1</b>	0.3827826	0.3369663
	<b>ERBB2</b>	0.2988261	0.3223993
	<b>ESR1</b>	0.2321178	0.166449
	<b>AKT1</b>	0.4251537	0.4520164

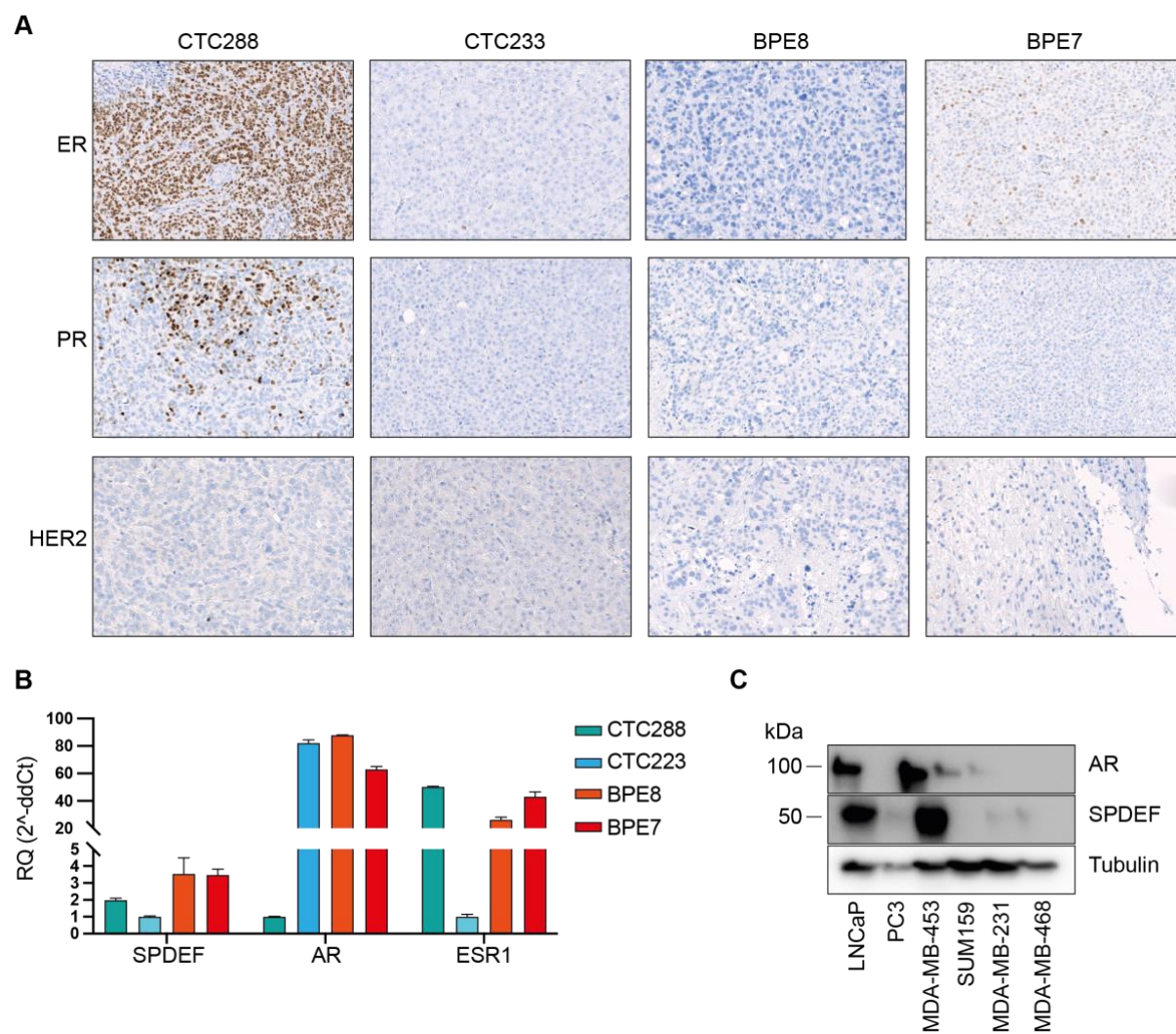


**Supplementary Figure 1: *SPDEF* and *ER* association in breast cancer patients.** (A) Linear correlation of *SPDEF* and *ESR1* gene expression in all breast cancer patients included in METABRIC data set ( $n = 1904$ ). (B, C) Kaplan-Meier estimator for survival probability of ER positive breast cancer patients stratified based on AR (C) and *SPDEF* (D) gene expression. Patients' data is extracted from METABRIC data set including ER<sup>+</sup> patients ( $n = 1459$  patients).

A



**Supplementary Figure 2: Heatmap of breast cancer patients for *ESR1*, *SPDEF* and *AR* gene expression.** Heatmap illustrates *ESR1*, *SPDEF* and *AR* gene expression in ER<sup>+</sup> (ER status blue) and ER<sup>-</sup> (ER status red) breast cancer patients from METABTIC data set (n= 1904).

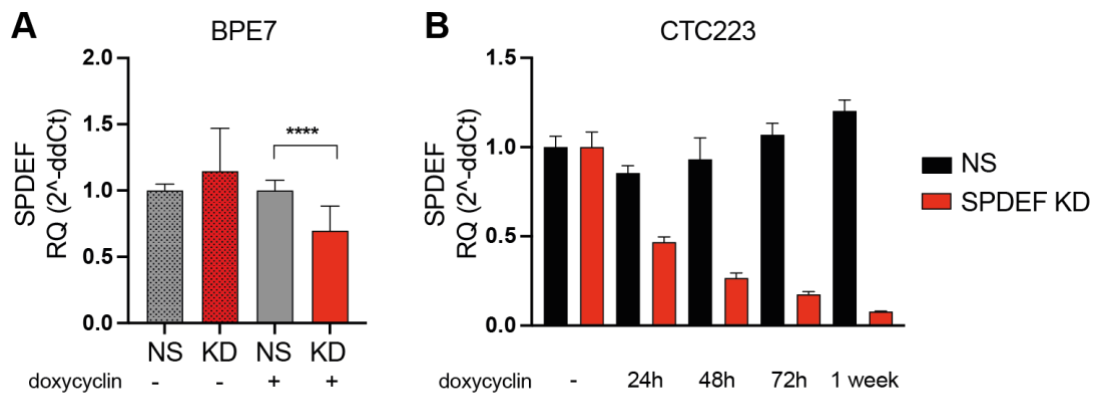


**Supplementary Figure 3: Characterization of PDX tumors and cell lines.** (A) Immunohistochemistry staining (IHC) for estrogen receptor (ER), progesterone receptor (PR) and HER2 receptor in patient-derived xenograft (PDX) tumors. IHC staining was performed by Vanessa Vogel. (B) RT-qPCR analysis of *SPDEF*, *AR* and *ESR1* gene expression in PDX cell lines. (C) Representative western blot analysis of AR and SPDEF protein expression in commercially available cell lines. AR<sup>+</sup> and AR<sup>-</sup> prostate cancer cell lines were used as controls. Tubulin as loading control; kDa kilo Dalton.

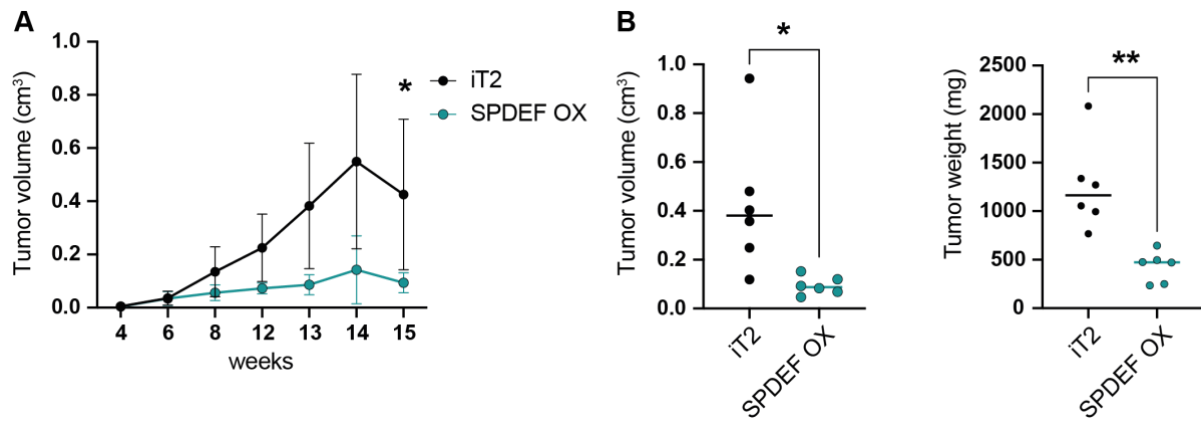
**Supplementary Table 2: Hormone receptor status in PDX breast cancer patients.**

Patient ID	ER	PR	HER2
CTC288	+	+	-
CTC223	+	+	-
BPE8	-	-	-
BPE7	-	-	-

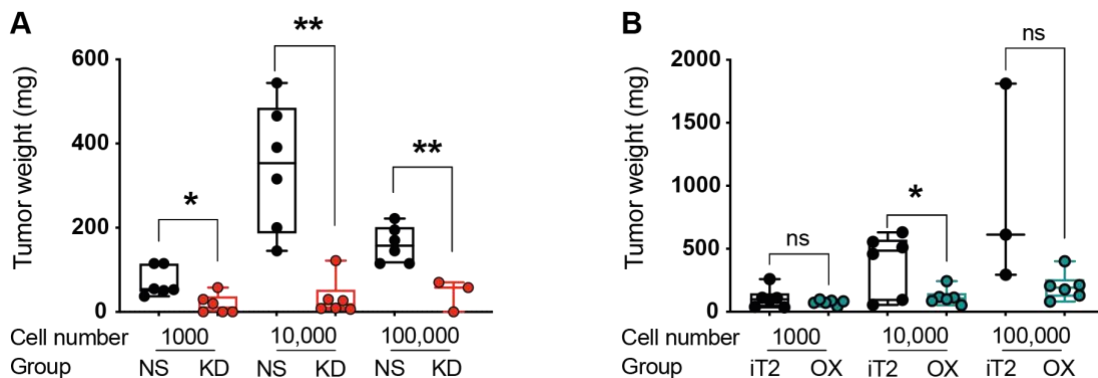




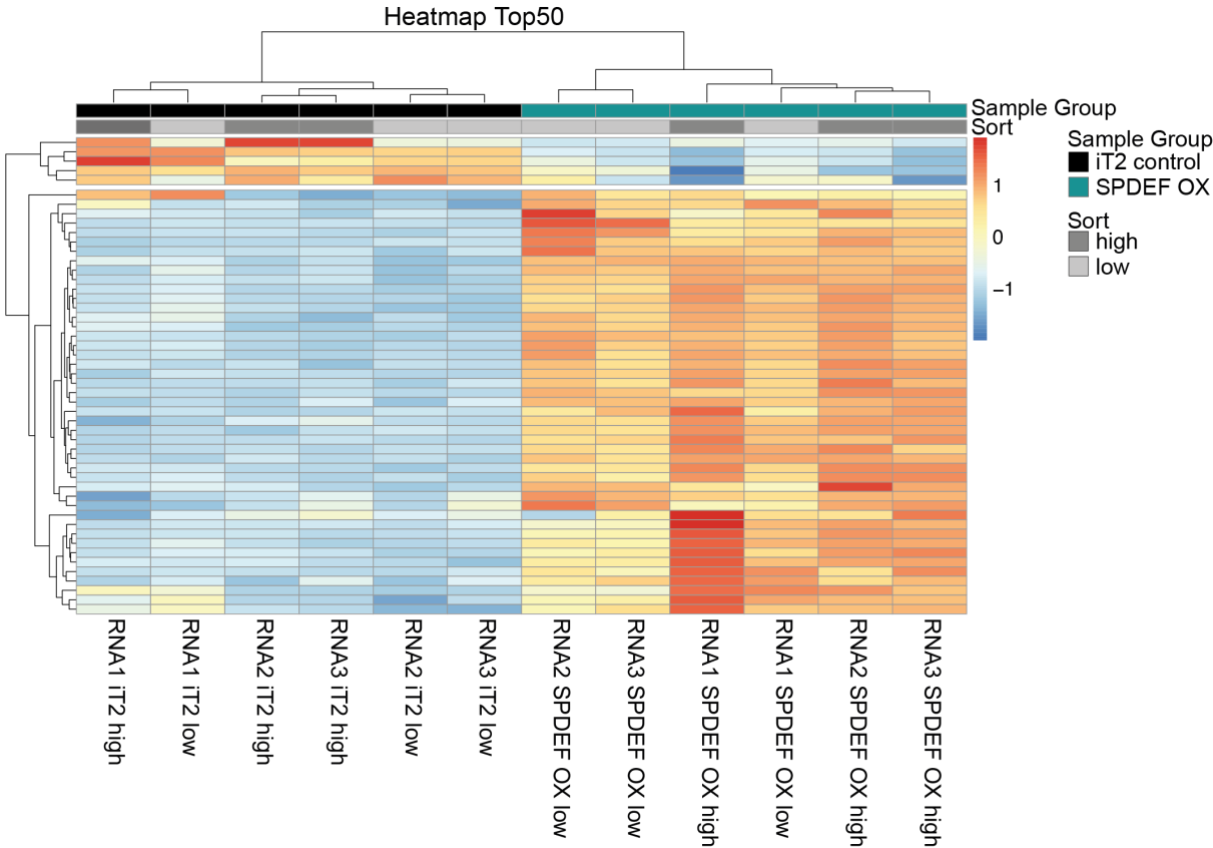
**Supplementary Figure 4: Validation of *SPDEF* gene expression by RT-qPCR analysis.** (A) *SPDEF* gene expression in BPE7 pTRIPZ non-silencing (NS) control and *SPDEF* knockdown (KD) cells. Cells were treated with doxycycline for one week before RNA was extracted (+ doxycycline) (n=5). Error bars depict standard deviation (SD) of five biological replicates à three technical replicates). (B) *SPDEF* gene expression was analyzed in a time-course experiment after 24h, 48h, 72h and one week upon doxycycline treatment in CTC223 NS and *SPDEF* KD cells. Error bars depict SD of three technical replicates. P-value was calculated using an unpaired two-tailed t-test; \* p < 0.05, \*\* p < 0.01, \*\*\* p < 0.001. RNA extraction, cDNA synthesis and RT-qPCR analysis were performed by Ornella Kossi.



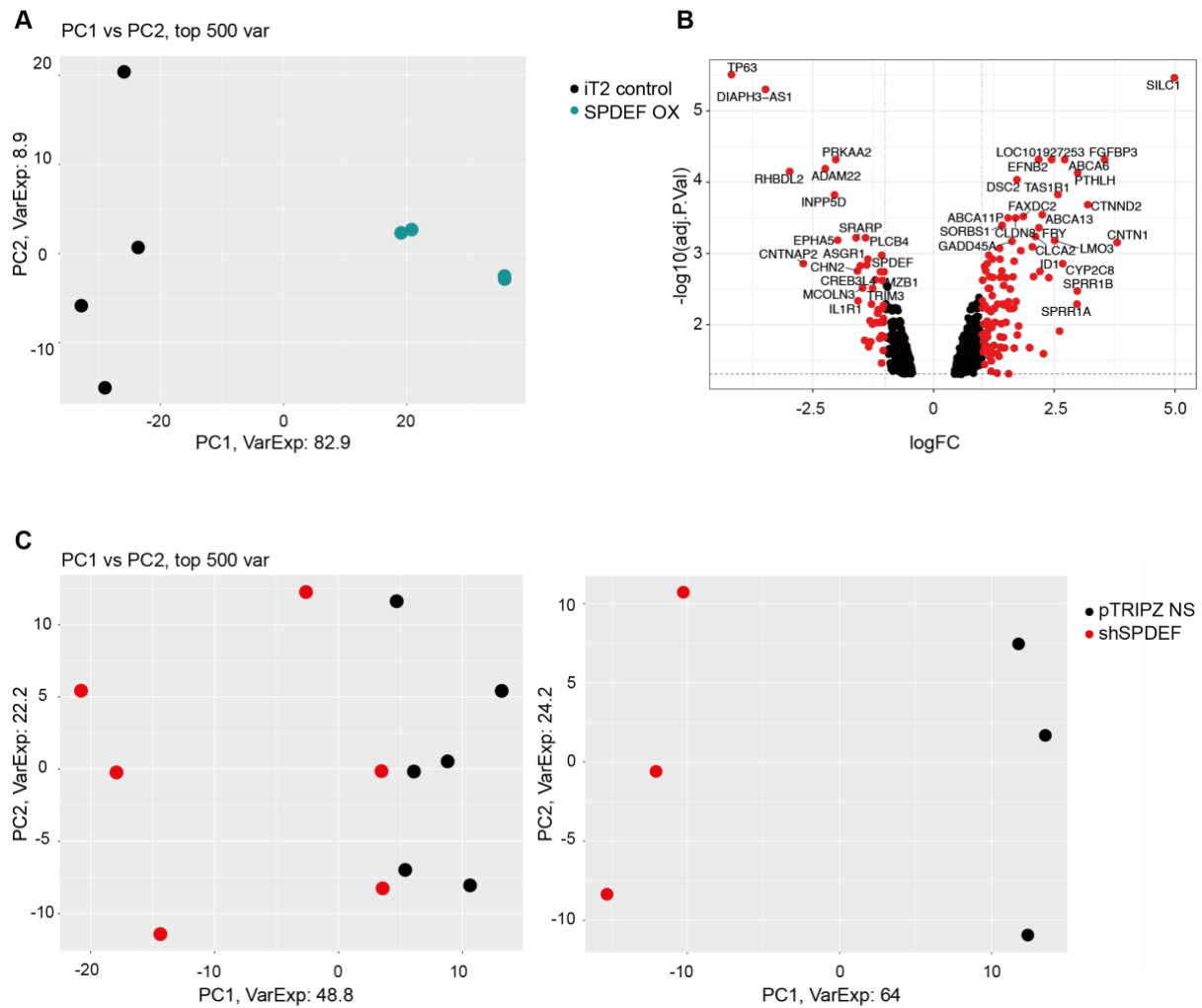
**Supplementary Figure 5: SPDEF overexpression reduces *in vivo* tumor growth of AR<sup>+</sup> ER<sup>+</sup> CTC223 cells.** (A) Growth followed over time of mammary fat pad (mfp) tumors generated from SPDEF-overexpressing (OX) CTC223 and iT2 empty vector control (iT2) CTC223 cells in NSG mice (n= 10 mice/group; 10,000 cells/mouse). Tumor volumes were measured by caliper. Error bars depict mean  $\pm$  SD. (B) Bar chart depicts median of tumor volume at last time point of (A) (left). Tumor weight was measured *ex vivo* at endpoint; median is depicted (right). P-value was calculated for the last time point using an unpaired two-tailed t-test; \* p < 0.05, \*\* p < 0.01, \*\*\* p < 0.001; ns, not significant.



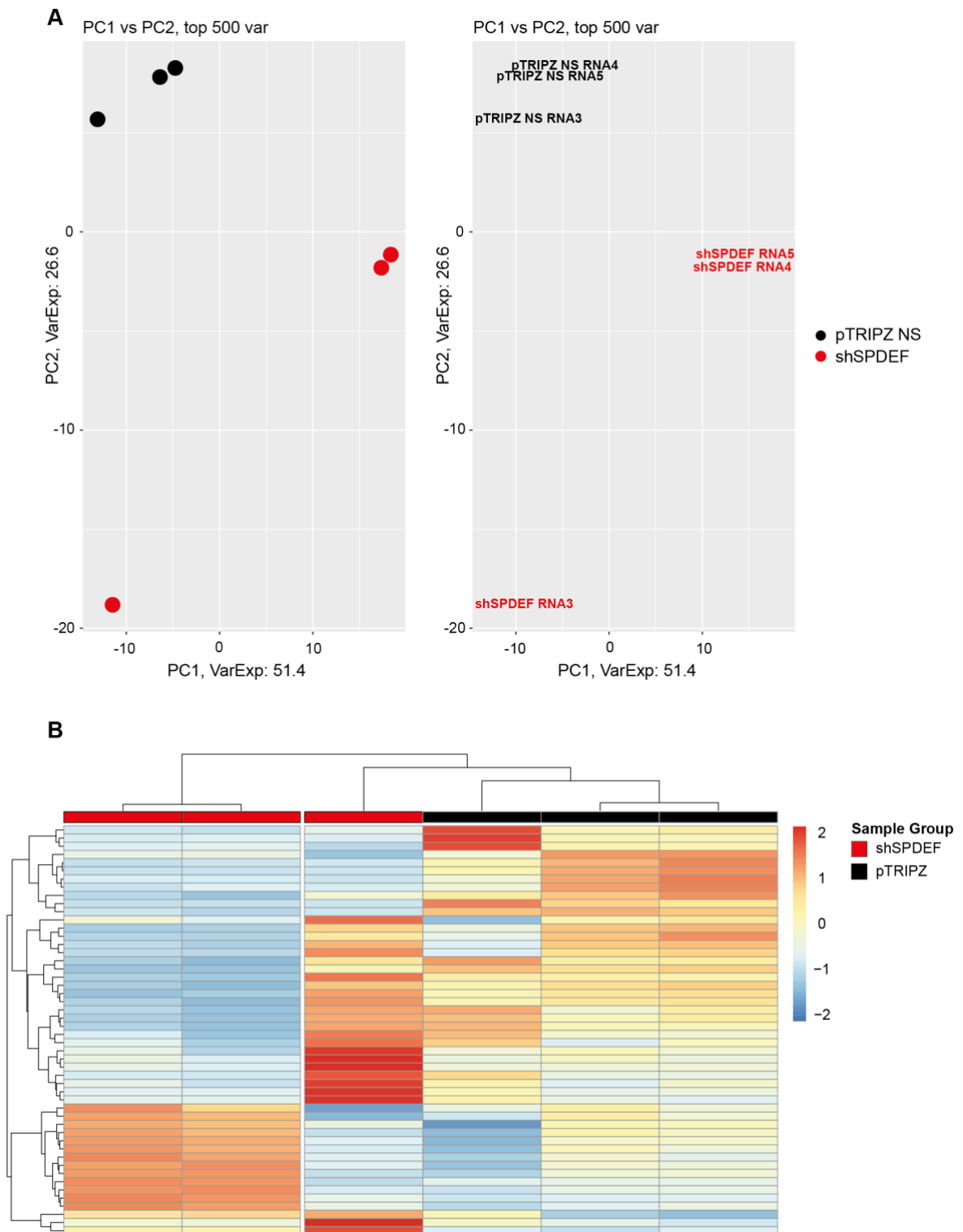
**Supplementary Figure 6: SPDEF up- and downregulation reduces *in vivo* tumor-initiating capacity in AR<sup>+</sup> ER<sup>+</sup> CTC288 cells.** (A) Mice injected with doxycycline-inducible pTRIPZ non-silencing (NS) or shSPDEF (SPDEF knockdown, KD) were pretreated with doxycycline in drinking water up to one week before cells were injected. pTRIPZ NS and shSPDEF cells were pretreated with Dox *in vitro* one week before the experiment was started. Tumor weight was measured *ex vivo* when endpoint was reached. Either 1000, 10,000 or 100,000 cells of pTRIPZ NS or KD cells (A), or iT2 empty vector or SPDEF-overexpressing (OX) cells (B), were injected into mfp of mice (n= 6 mice/group). Whisker plots show all individual mice through their quartiles. P-value was calculated using an unpaired, two-tailed t-test. (A, 1000 and 10000 cells) Mann-Whitney U-test was applied as appropriate; \* p < 0.05, \*\* p < 0.01, \*\*\* p < 0.001; ns, not significant. Orthotopic injections into mfp of NSG mice were performed by Corinna Klein.



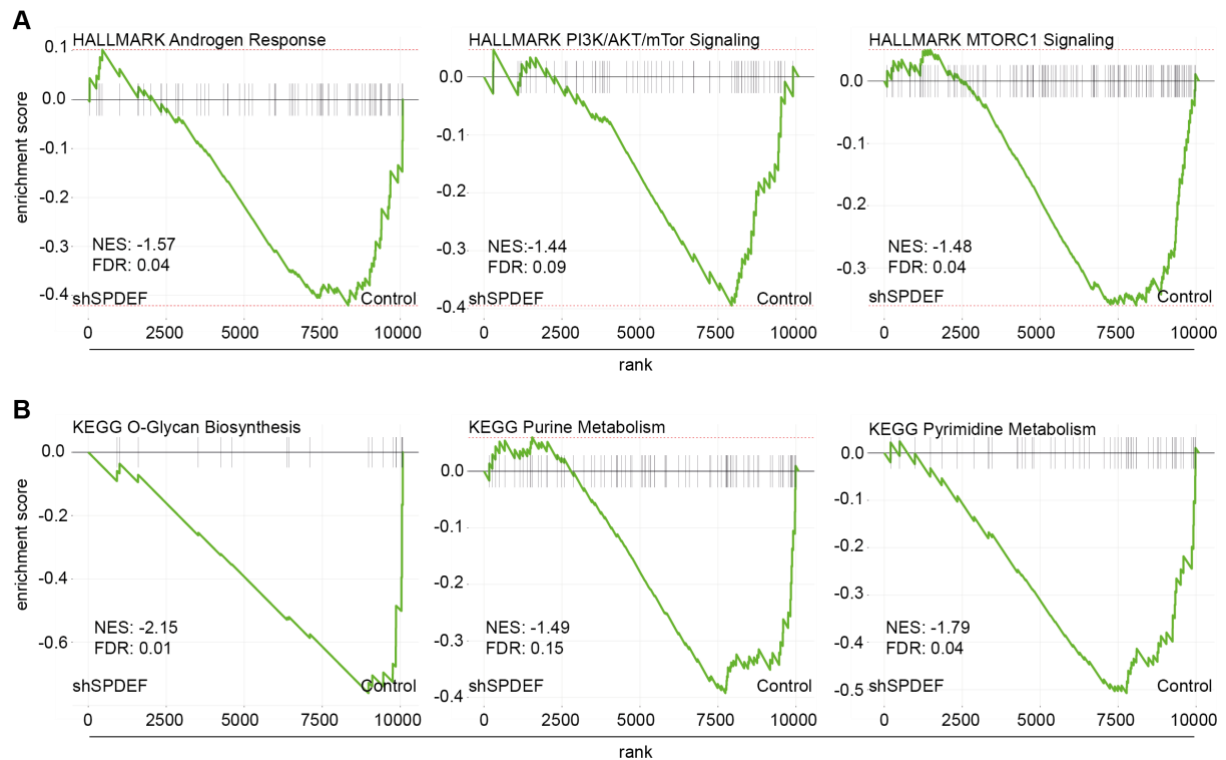
**Supplementary Figure 7: Gene expression-based stratification of BPE8 SPDEF-overexpressing and iT2 control samples.** Heatmap illustrates top 100 variant genes between BPE8 SPDEF-overexpressing (OX) and iT2 empty vector (iT2) control samples (n=6 samples/group). Hierarchical clustering separated groups based SPDEF expression.



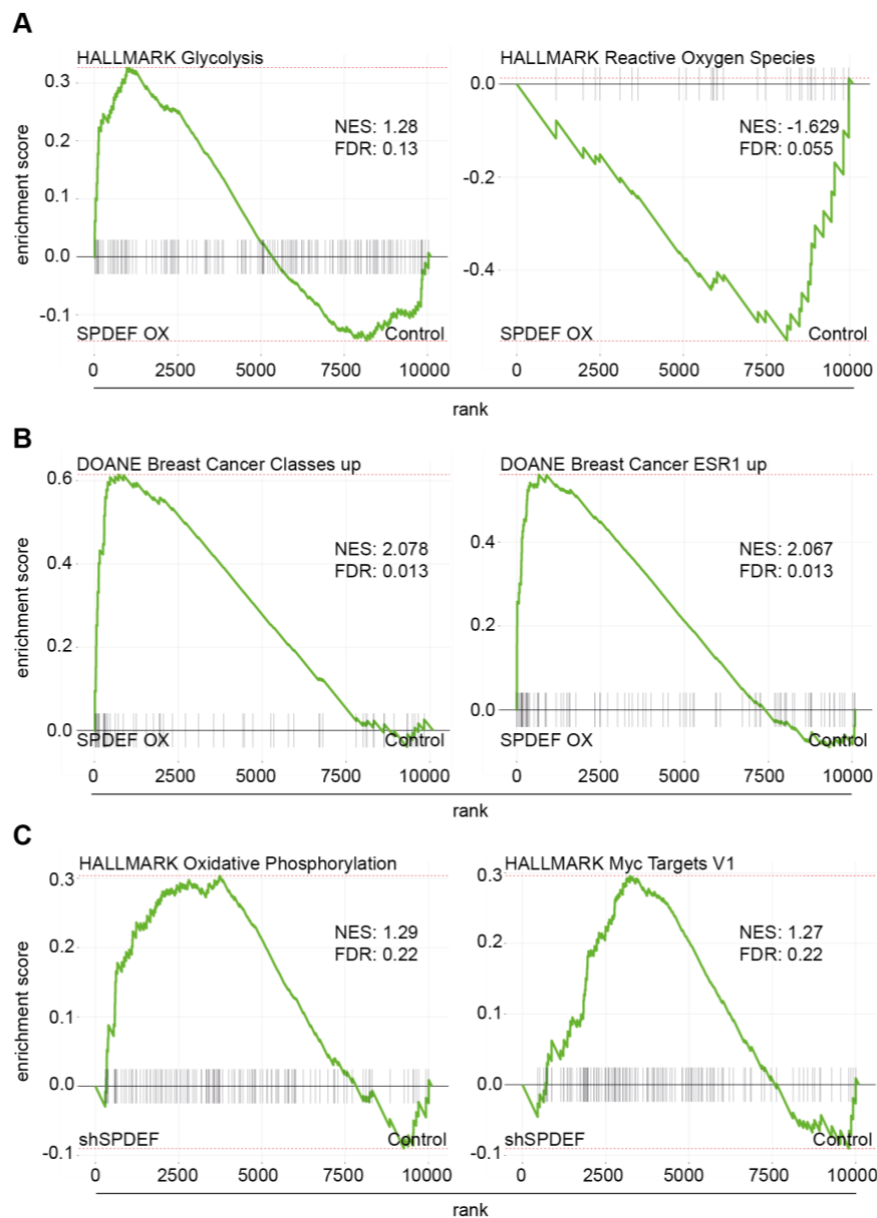
**Supplementary Figure 8: Gene expression-based stratification of CTC288 SPDEF cell lines.** (A) Principal component (PC) analysis of CTC288 iT2 empty vector (iT2) control and SPDEF-overexpressing (OX) cells (n=4 samples/group). Percentage indicates proportion of variance explained by each component. (B) Volcano plot represents all significant differentially expressed genes between CTC288 pTRIPZ non-silencing (NS) and shSPDEF cells. Highlighted in red are all genes with an adjusted p-value < 0.05 and log-fold change (FC) > 1. Annotated are all genes with an adjusted p-value < 0.005. (C) PCA of CTC288 pTRIPZ non-silencing (NS) control and shSPDEF cells (n=6 samples/group). Cells were treated with doxycycline for at least one week before RNA was harvested. RNA samples of shSPDEF ‘low-intensity’ sorted cells clustered with pTRIPZ NS control samples. (D) Same PCA analysis as in (C) including only ‘high-intensity’ sorted cells-derived RNA samples.



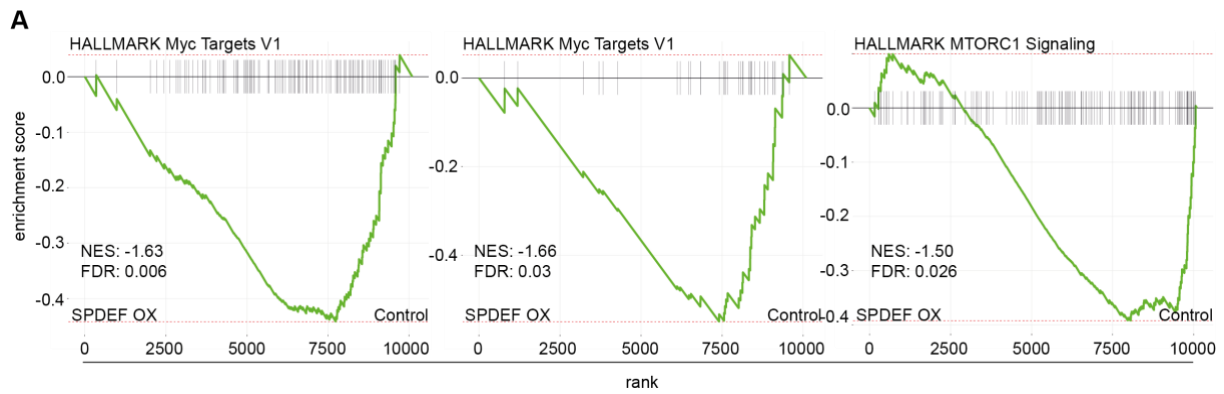
**Supplementary Figure 9: Top variant gene stratification in BPE7 shSPDEF cells.** (A) Principal component (PC) analysis of BPE7 pTRIPZ non-silencing (NS) control and shSPDEF cells (n=3 samples/group). Percentage indicates proportion of variance explained by each component. Left: samples displayed as dots; right: samples displayed with RNA passage indicated. (B) Heatmap of top 50 variant gene expression in BPE7 shSPDEF and pTRIPZ NS samples.



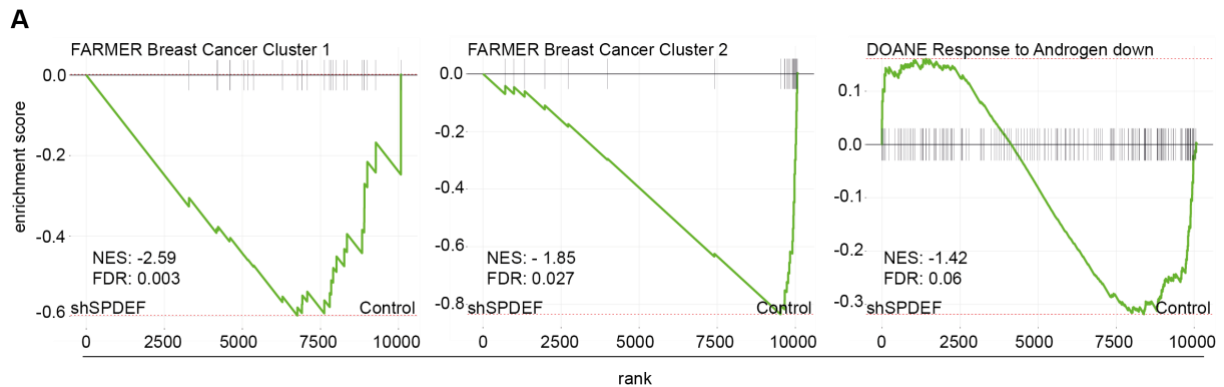
**Supplementary Figure 10: Gene Enrichment Analysis of BPE8 shSPDEF cells compared to respective control.** (A, B) Gene Set Enrichment Analysis (GSEA) of BPE8 shSPDEF and pTRIPZ non-silencing control (Control) samples (n= 3/group). Statistical significance was assessed using 10,000 permutations on the phenotype. All differentially expressed genes were pre-ranked based on t-value. NES, normalized enrichment score; FDR, false discovery rate.



**Supplementary Figure 11: Gene Set Enrichment Analysis of CTC223 SPDEF-overexpressing and shSPDEF cells compared to respective controls. (A, B) Gene Set Enrichment Analysis (GSEA) between CTC223 SPDEF-overexpressing (OX) and iT2 empty vector control (Control) cells (n= 3/group). (C) GSEA between CTC223 shSPDEF and pTRIPZ non-silencing control (Control) cells (n=3/group). Statistical significance was assessed using 10,000 permutations on the phenotype. All differentially expressed genes were pre-ranked based on t-value. NES, normalized enrichment score; FDR, false discovery rate.**

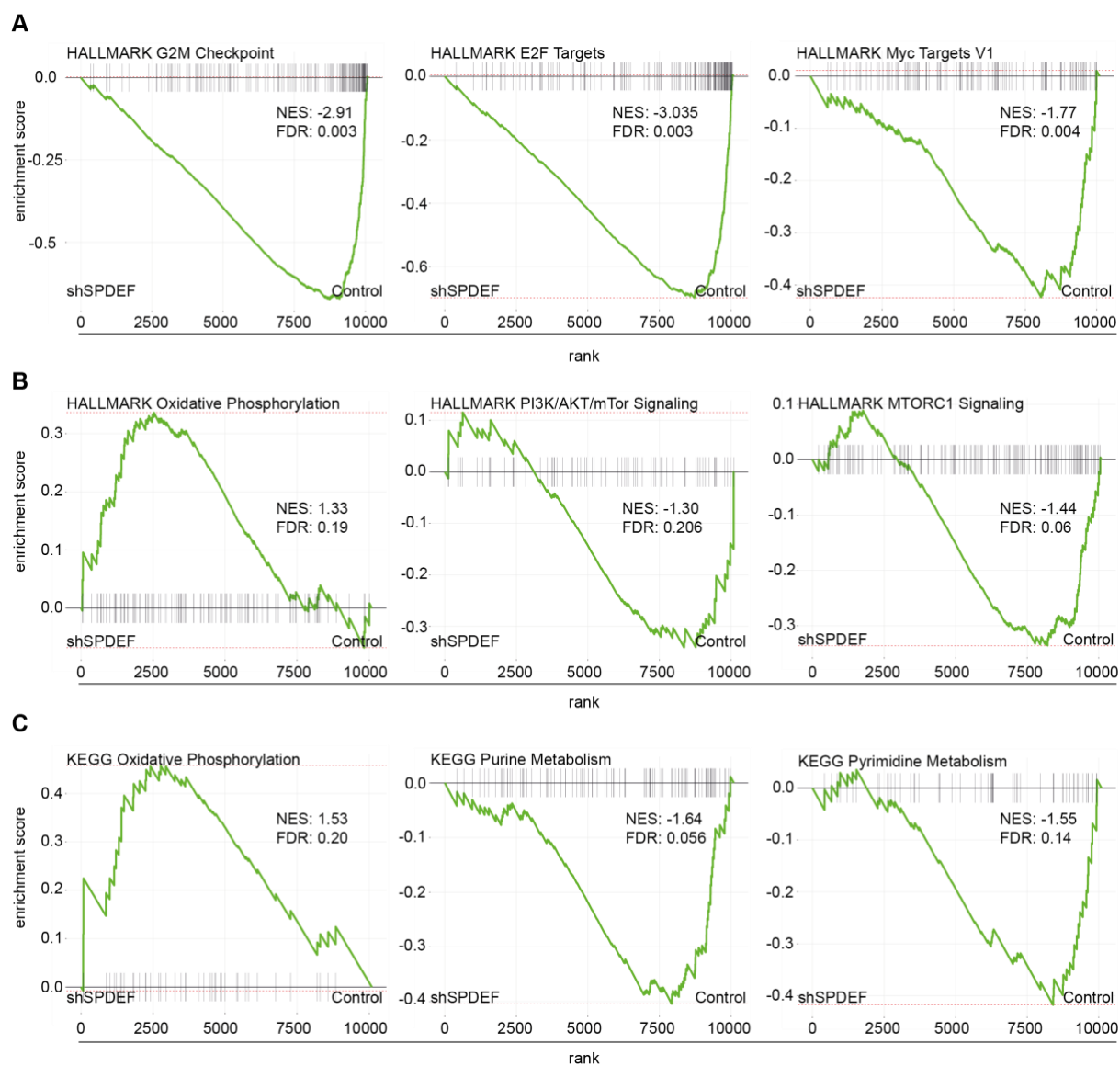


**Supplementary Figure 12: Gene Set Enrichment Analysis for Hallmark gene sets of CTC288 SPDEF-overexpressing and iT2 control cells.** (A) Gene Set Enrichment Analysis for HALLMARK gene sets between CTC288 SPDEF-overexpressing (OX) and iT2 empty vector control (Control) cells (n= 3/group). Statistical significance was assessed using 10,000 permutations on the phenotype. All differentially expressed genes were pre-ranked based on t-value. NES, normalized enrichment score; FDR, false discovery rate.

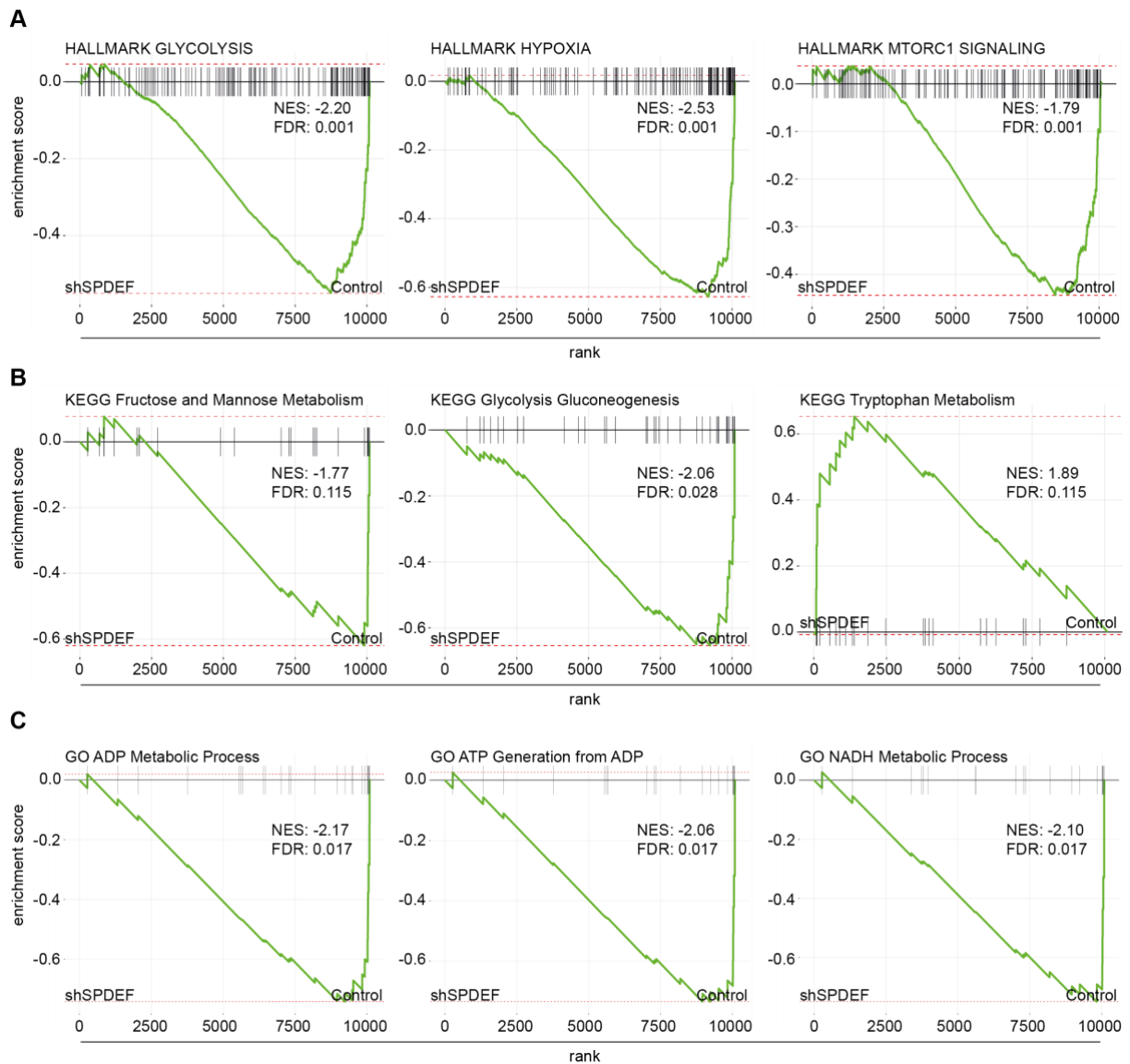


**Supplementary Figure 13: Gene Set Enrichment Analysis for C2 curated gene sets of CTC288 shSPDEF and pTRIPZ non-silencing control cells.** (A) Gene Set Enrichment Analysis for C2 curated gene sets between CTC288 shSPDEF and pTRIPZ non-silencing control (Control) cells (n=3/group). Statistical significance was assessed using 10,000 permutations on the phenotype. All differentially expressed genes were pre-ranked based on t-value. NES, normalized enrichment score; FDR, false discovery rate.

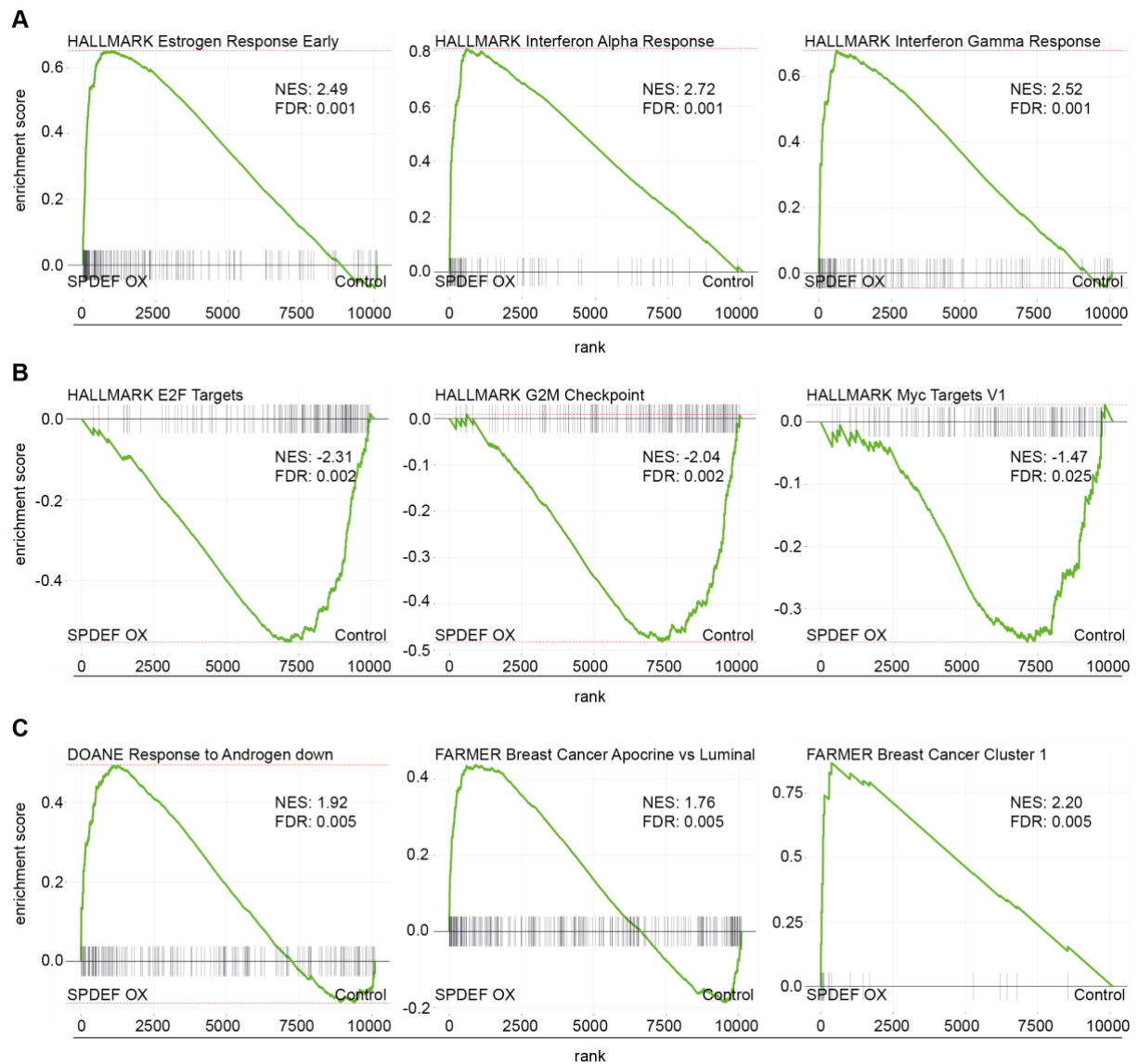




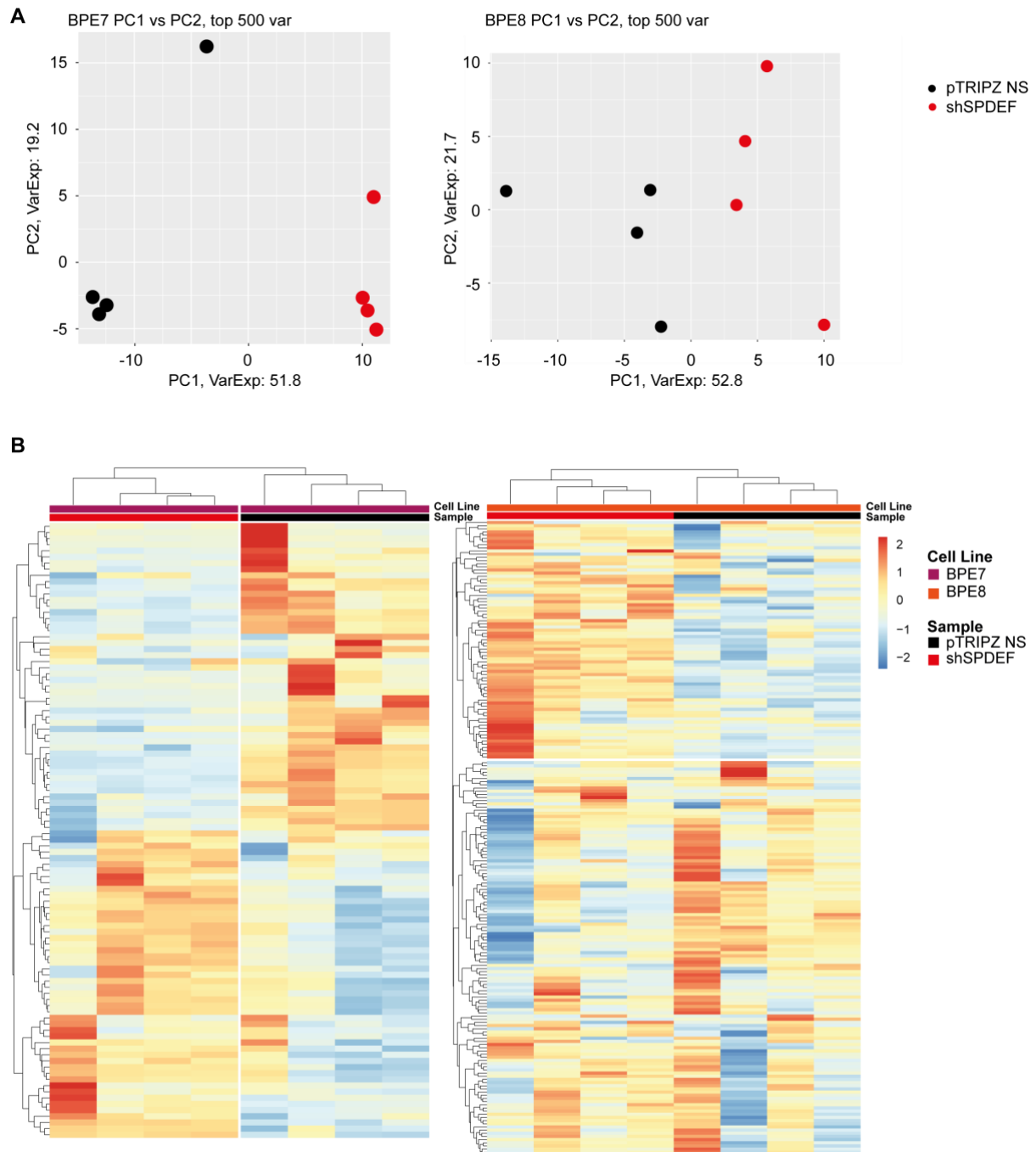
**Supplementary Figure 14: Gene Set Enrichment Analysis of CTC288 shSPDEF and pTRIPZ non-silencing control cells.** Gene Set Enrichment Analysis (GSEA) between CTC223 shSPDEF and pTRIPZ non-silencing control (Control) cells (n=3/group). (A, B) HALLMARK gene sets. (C) KEGG pathways gene sets. Statistical significance was assessed using 10,000 permutations on the phenotype. All differentially expressed genes were pre-ranked based on t-value. NES, normalized enrichment score; FDR, false discovery rate.



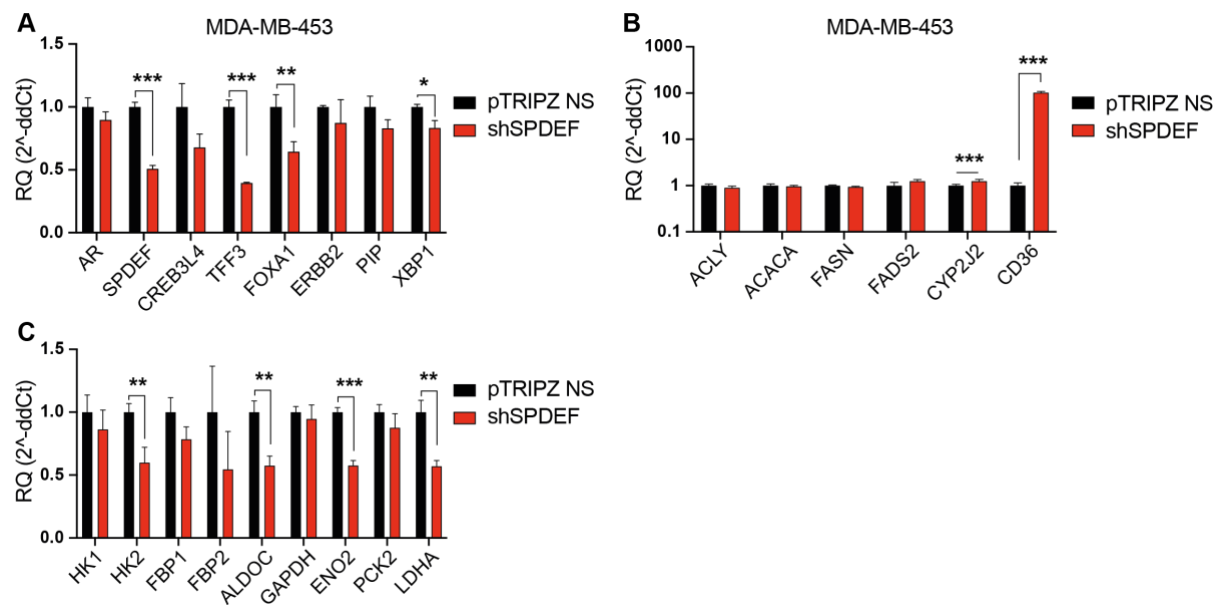
**Supplementary Figure 15: Gene Set Enrichment Analysis of shSPDEF cells of BPE8, CTC223 and CTC288 lines relative to respective controls.** Gene Set Enrichment Analysis (GSEA) between shSPDEF and pTRIPZ non-silencing control (Control) samples of the cell lines BPE8, CTC223 and CTC288 (n=3/group/cell line). Statistical significance was assessed using 10,000 permutations on the phenotype. All differentially expressed genes were pre-ranked based on t-value. (A) HALLMARK gene sets. (B) KEGG pathways gene sets. (C) Gene Ontology (GO) term gene sets. NES, normalized enrichment score; FDR, false discovery rate.



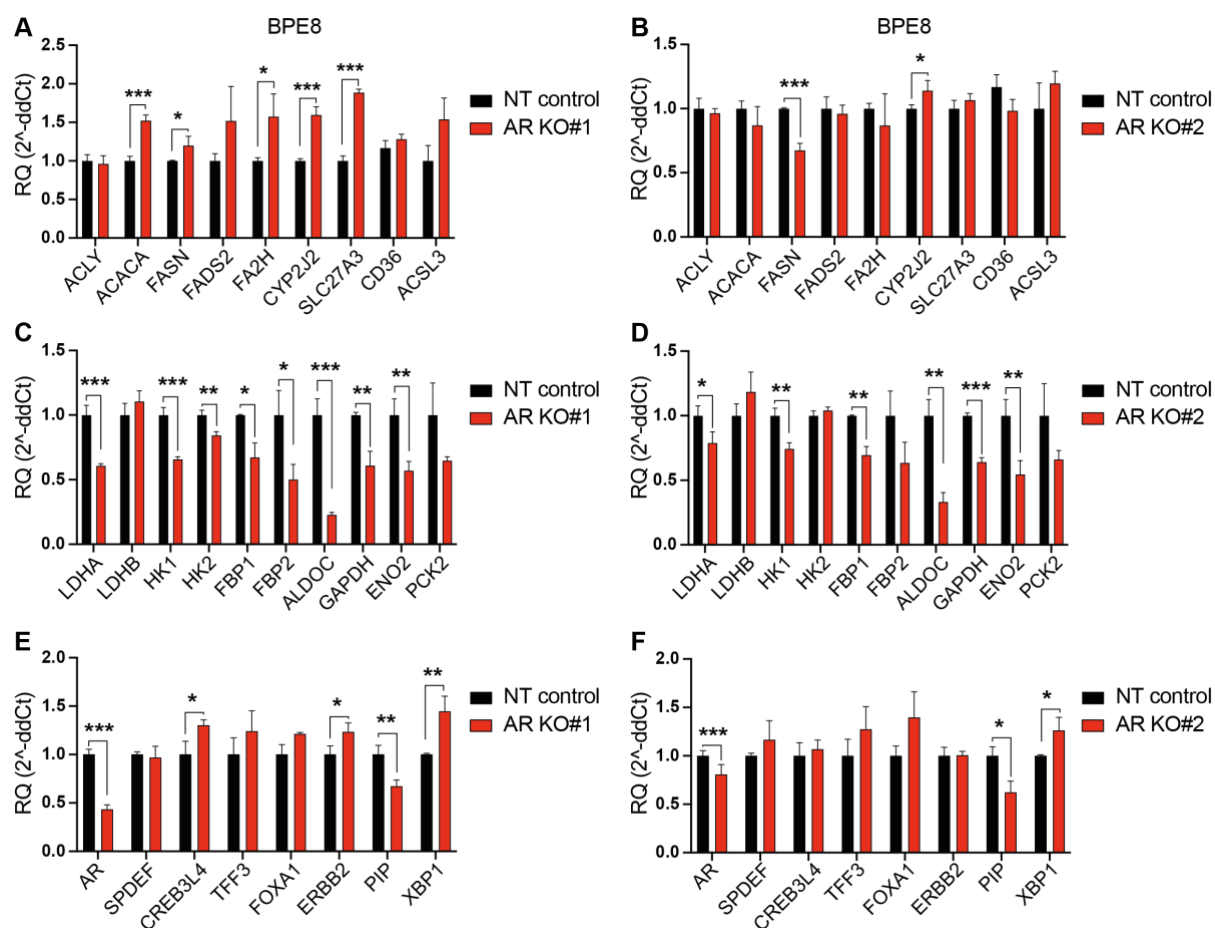
**Supplementary Figure 16: Gene Set Enrichment Analysis of BPE7 SPDEF-overexpressing compared to iT2 control cells.** Gene Set Enrichment Analysis (GSEA) between BPE7 SPDEF-overexpressing (OX) and iT2 empty vector control (Control) cells (n=3/group). Statistical significance was assessed using 10,000 permutations on the phenotype. All differentially expressed genes were pre-ranked based on t-value. (A, B) HALLMARK gene sets. (C) Gene Ontology (GO) term gene sets. NES, normalized enrichment score; FDR, false discovery rate.



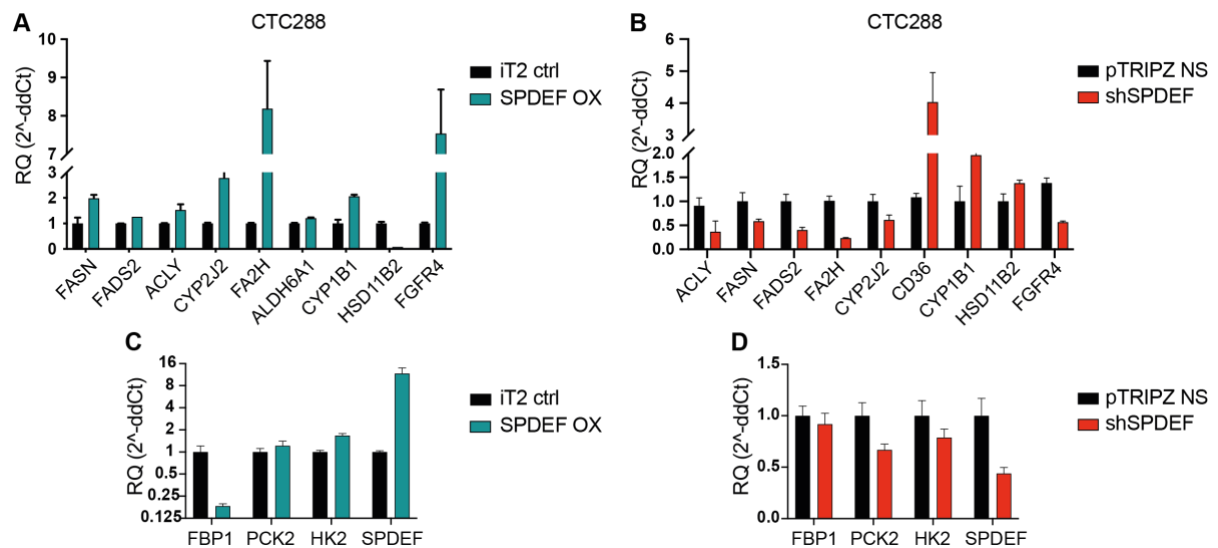
**Supplementary Figure 17: Top variant gene stratification in AR<sup>+</sup> and AR<sup>-</sup> shSPDEF tumors relative to controls.** (A) Principal component (PC) analysis of BPE7 (left) and BPE8 (right) pTRIPZ non-silencing (NS) control and shSPDEF tumors (n=4 samples/group). Percentage indicates proportion of variance explained by each component. (B) Heatmap of top 100 variant genes in BPE7 (left) and BPE8 (right) shSPDEF and pTRIPZ NS samples.



**Supplementary Figure 18: Target genes validation in MDA-MB-453 shSPDEF cells.** Representative RT-qPCR analysis in MDA-MB-453 shSPDEF and pTRIPZ non-silencing (NS) control cells of (A) AR target genes, (B) fatty acid metabolism target genes and (C) glycolytic target genes; (n= 3 technical replicates/cell line). shSPDEF and pTRIPZ NS control cells were treated with doxycycline for one week before RNA was extracted. Values are given as two-fold change relative to control group; RQ, relative quantification. P-value was calculated using an unpaired two-tailed t-test; \*  $p < 0.05$ , \*\*  $p < 0.01$ , \*\*\*  $p < 0.001$ ; not significant when no indication. RNA extraction, cDNA synthesis and RT-qPCR analysis were performed by Ornella Kossi.

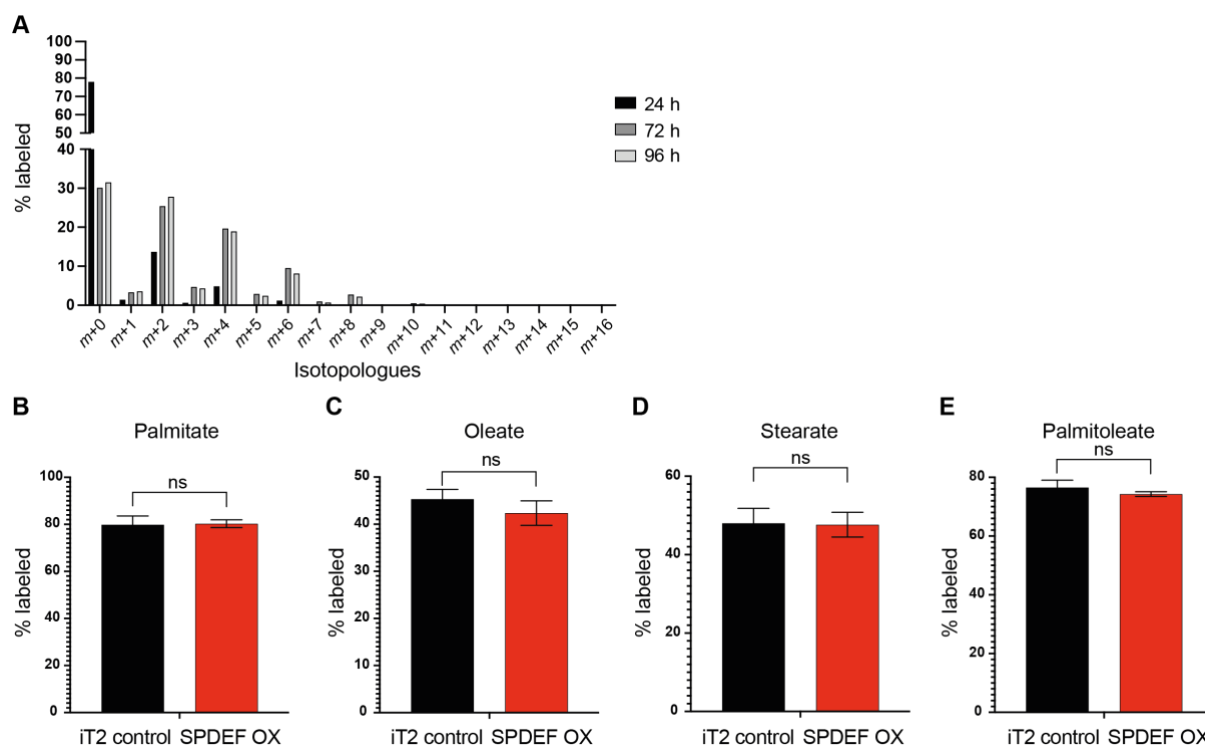


**Supplementary Figure 19: Target genes validation in BPE8 AR KO cells.** (A, B) RT-qPCR analysis of fatty acid metabolism target genes in BPE8 non-targeting (NT) control, AR knock-out (KO)#1 and AR KO#2 cells. (C, D) RT-qPCR analysis of glycolytic target genes in BPE8 NT control, AR KO#1 and AR KO#2 cells (n= 3 technical replicates/cell line). Values are given as two-fold change relative to control group; RQ, relative quantification. P-value was calculated using an unpaired two-tailed t-test; \* p < 0.05, \*\* p < 0.01, \*\*\* p < 0.001; not significant when no indication. RNA extraction, cDNA synthesis and RT-qPCR analysis were performed by Ornella Kossi.



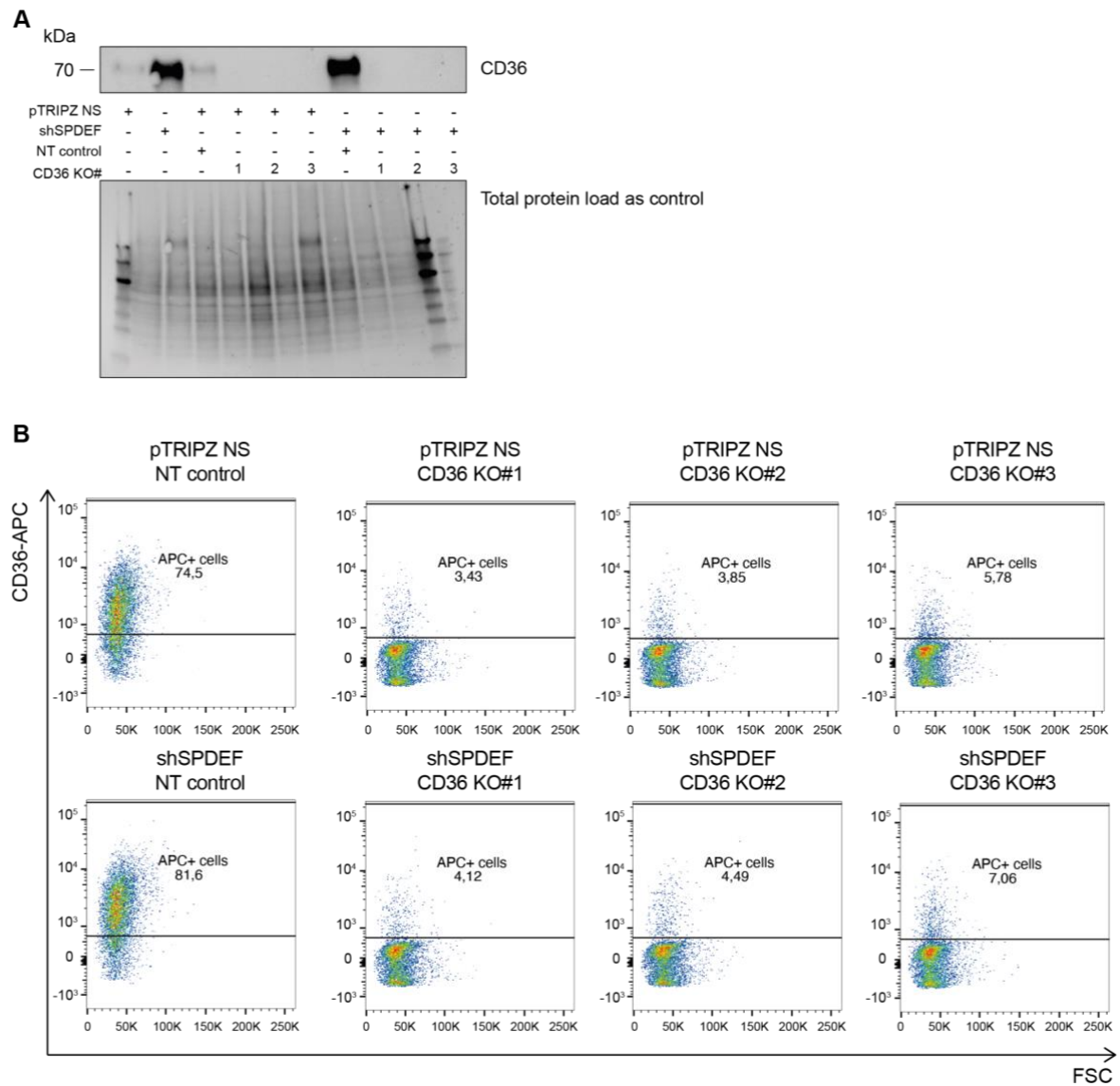
**Supplementary Figure 20: Target genes validation in CTC288 SPDEF-overexpressing and shSPDEF cells.**

(A) RT-qPCR analysis of fatty acid metabolism target genes in CTC288 SPDEF overexpression (OX) and iT2 empty vector control (iT2 ctrl) cells. (B) RT-qPCR analysis of fatty acid metabolism target genes in CTC288 shSPDEF and pTRIPZ non-silencing (NS) control cells. (C) RT-qPCR analysis of glycolytic target genes in CTC288 SPDEF overexpression (OX) and iT2 empty vector control (iT2 ctrl) cells. (D) RT-qPCR analysis of glycolytic target genes in CTC288 shSPDEF and pTRIPZ non-silencing (NS) control cells. (n= 3 technical replicates/cell line). shSPDEF and pTRIPZ NS control cells were treated with doxycycline for one week before RNA was extracted. Values are given as two-fold change relative to control group; RQ, relative quantification. cDNA synthesis and RT-qPCR analysis were performed by Ornella Kossi.

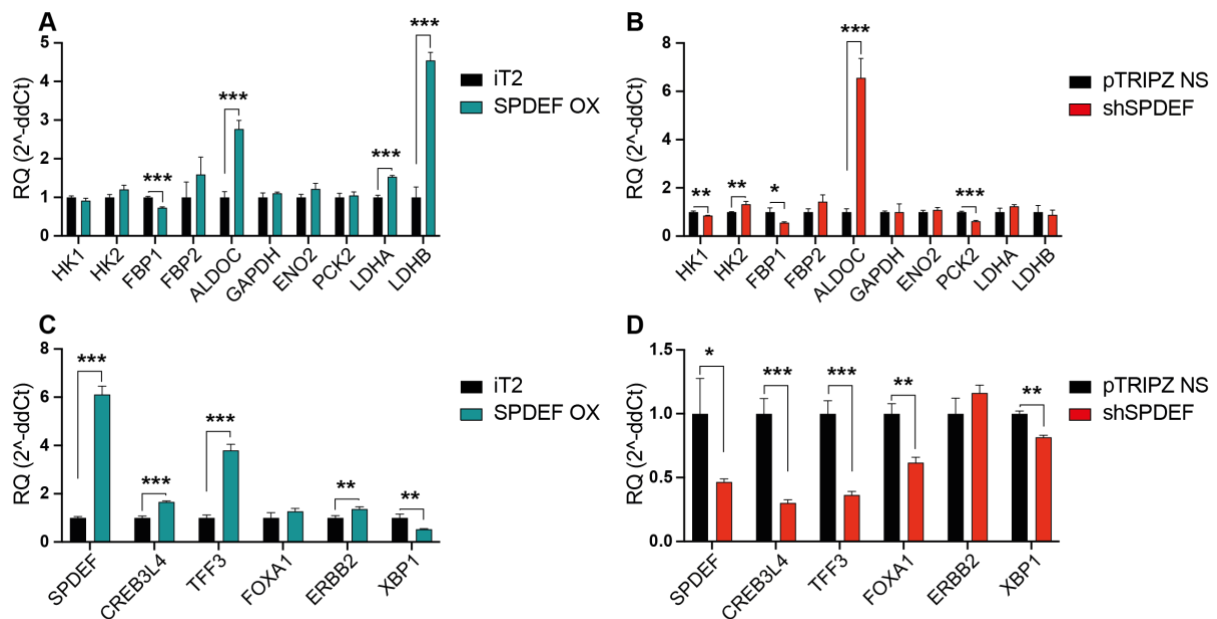


**Supplementary Figure 21: Isotope tracing experiments.** (A) The distribution of  $^{13}\text{C}$ -labeled isotopologues of palmitate from  $^{13}\text{C}$ -glucose in BPE8 iT2 control cells after 24 h (black), 72 h (grey) and 96 h (light grey) of labeling. (B-E) Sum of labeled isotopologues from  $^{13}\text{C}$ -glucose,  $^{13}\text{C}$ -glutamine and  $^{13}\text{C}$ -acetate in BPE8 iT2 control and SPDEF overexpression (OX) cells ( $n = 3$  biological replicates/sample). (B) Sum of palmitate isotopomers  $m+1$  to  $m+16$ . (C) Sum of oleate isotopomers  $m+3$  to  $m+18$ . (D) Sum of stearate isotopomers  $m+3$  to  $m+18$ . (E) Sum of palmitoleate isotopomers  $m+1$  to  $m+16$ . ( $n = 2-3$  biological replicates/sample). P-value was calculated using an unpaired, two-tailed t-test; ns, not significant. LS/MS analysis were performed by Dr. Marteinn T. Snaebjörnsson.

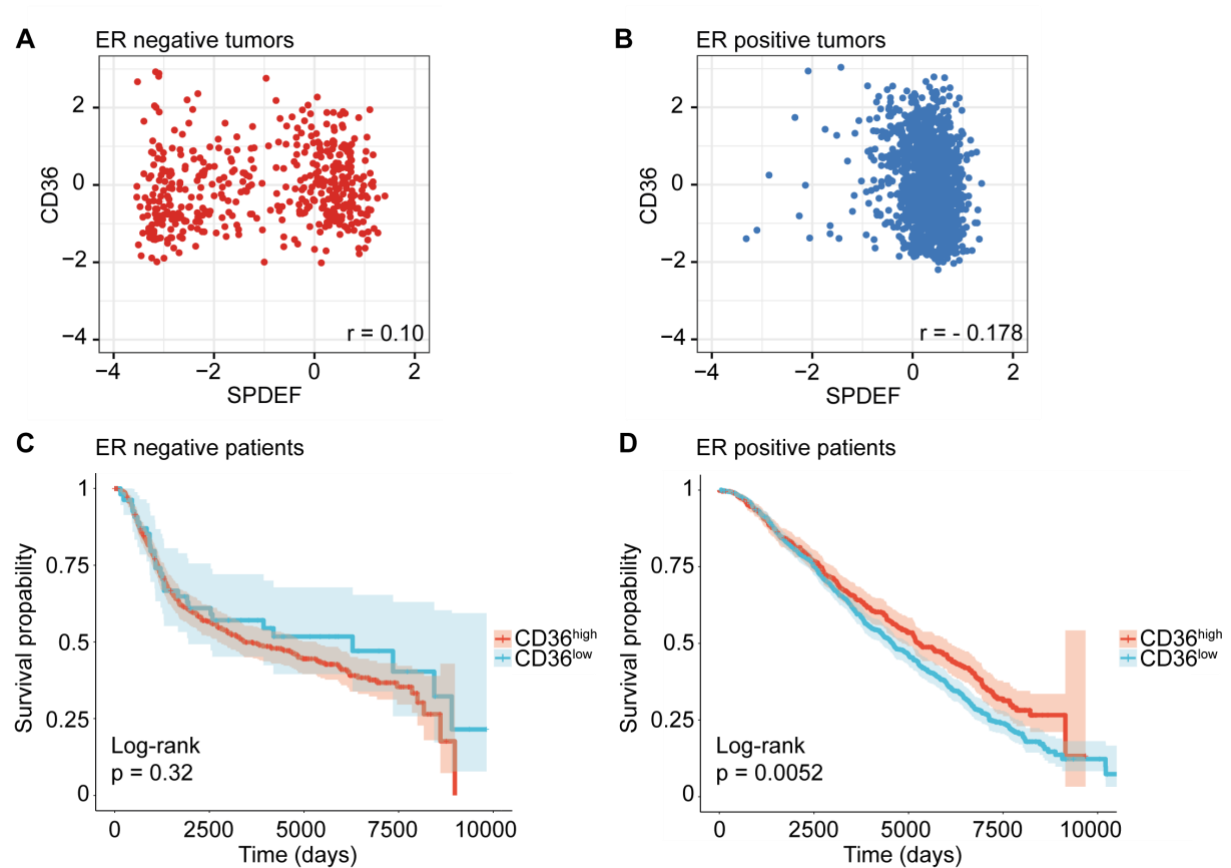




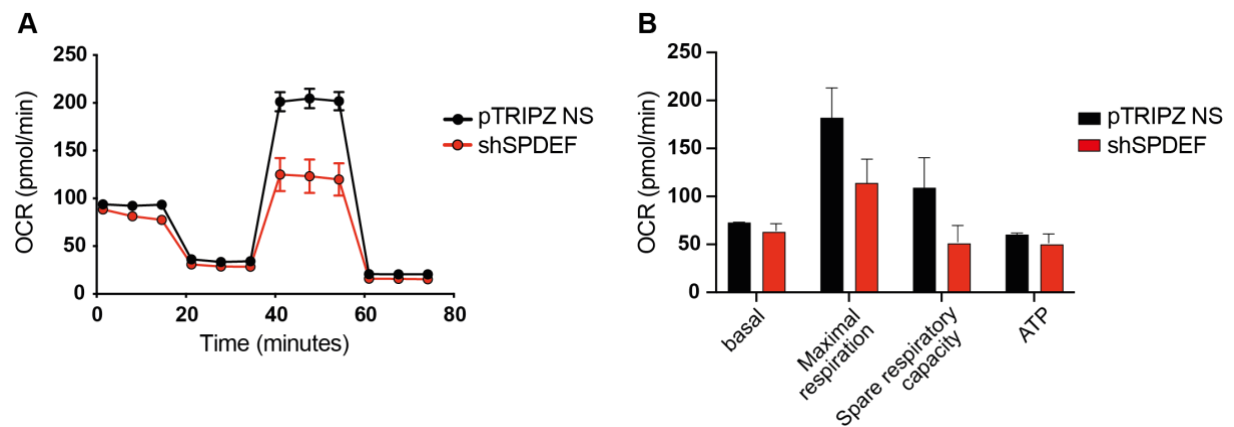
**Supplementary Figure 22: CRISPR/Cas9-mediated CD36 disruption in BPE8 shSPDEF and control cells.** (A) Validation of CD36 protein expression by western blot (A) and flow cytometry (B) analysis in BPE8 pTRIPZ NS NT control, pTRIPZ NS CD36 KO#1-3, shSPDEF NT control and shSPDEF CD36 KO#1-3 cell lines. Total protein amount serves as loading control. kDa, kilo Dalton; NT, non-targeting; NS, non-silencing; KO, knock-out; #1-3 refers to three different gRNAs targeting CD36.



**Supplementary Figure 23: Glycolytic and AR-associated target genes are deregulated in BPE8 SPDEF overexpression and knockdown cells cultured in HPLM.** (A) Representative RT-qPCR analysis of target genes involved in glucose metabolism in BPE8 SPDEF-overexpressing (OX) and iT2 empty vector control (iT2) cells; (B) in BPE8 shSPDEF and pTRIPZ non-silencing (NS) control cells cultured in human plasma-like medium (HPLM) supplemented with breast cancer-specific growth factors and hormones. (C) RT-qPCR analysis of AR-associated target genes in BPE8 SPDEF OX and iT2 control cells; (D) in BPE8 shSPDEF and pTRIPZ NS control cells cultured in HPLM supplemented with breast cancer-specific growth factors and hormones. (n= 3 technical replicates/cell line). shSPDEF and pTRIPZ NS control cells were treated with doxycycline for one week before RNA was extracted. Values are given as two-fold change relative to control group; RQ, relative quantification. P-value was calculated using an unpaired two-tailed t-test; \* p < 0.05, \*\* p < 0.01, \*\*\* p < 0.001; not significant when no indication. RNA extraction, cDNA syntheses and RT-qPCRs were performed by Ornella Kossi.



**Supplementary Figure 24: *CD36* expression is not associated with *SPDEF* expression in human breast cancers.** (A, B) Linear correlation of *SPDEF* and *CD36* gene expression in (A) ER negative (red) and (B) ER positive (blue) breast cancer patients. Depicted is the Pearson correlation coefficient  $r$  calculated with R package `ggpubr`. (C, D) Kaplan-Meier estimator for survival probability of (C) ER<sup>-</sup> breast cancer and (D) ER<sup>+</sup> breast cancer patients stratified based *CD36* gene expression. Data is extracted from METABRIC data set including 445 ER<sup>-</sup> breast cancer patients.



**Supplementary Figure 25: SPDEF controls mitochondrial respiration activity in AR<sup>+</sup> MDA-MB-453 cells.** (A, B) Mitochondrial respiration activity was measured in MDA-MB-453 shSPDEF and pTRIPZ non-silencing (NS) cells using Agilent Seahorse Technologies. shSPDEF and pTRIPZ NS cells were pretreated with doxycycline for one week before assay was started. Basal and maximal respiration, spare respiratory capacity and ATP production were assessed (n= 2 independent experiments/6 technical replicates/group). Three inhibitors, oligomycin, FCCP and rotenone/antimycin A, were serially injected. OCR, oxygen consumption rate; ECAR, extracellular acidification rate.

## 7 References

1. Siegel, R. L., Miller, K. D., Fuchs, H. E. & Jemal, A. Cancer statistics, 2022. *CA. Cancer J. Clin.* (2022).
2. Loibl, S., Poortmans, P., Morrow, M., Denkert, C. & Curigliano, G. Breast cancer. *Lancet* **397**, (2021).
3. Surveillance, Epidemiology, and End Results (SEER) Research Program. SEER\*Explorer: an interactive website for SEER cancer statistics. Accessed in Feb 25th, 2022. Available at: <https://seer.cancer.gov/statfacts/html/breast-subtypes.html>.
4. Harbeck, N. *et al.* Breast cancer. *Nat. Rev. Dis. Prim.* **5**, (2019).
5. Bray, F. *et al.* Cancer Incidence in Five Continents: Inclusion criteria, highlights from Volume X and the global status of cancer registration. *Int. J. Cancer* **137**, (2015).
6. Frank, G. A., Danilova, N. V., Andreeva, Y. Y. & Nefedova, N. A. WHO Classification of tumors of the breast, 2012. *Arkh. Patol.* **75**, (2013).
7. Lebeau, A. & Denkert, C. Updated WHO classification of tumors of the breast: the most important changes. *Pathologie* **42**, (2021).
8. Buonomo, O. C. *et al.* New insights into the metastatic behavior after breast cancer surgery, according to well-established clinicopathological variables and molecular subtypes. *PLoS One* **12**, (2017).
9. Perou, C. M. *et al.* Molecular portraits of human breast tumours. *Nature* **406**, (2000).
10. Wolff, A. C. *et al.* Human epidermal growth factor receptor 2 testing in breast cancer: American Society of Clinical Oncology/College of American Pathologists Clinical Practice Guideline Focused Update. *Archives of Pathology and Laboratory Medicine* **142**, (2018).
11. Hammond, M. E. H. *et al.* American society of clinical oncology/college of american pathologists guideline recommendations for immunohistochemical testing of estrogen and progesterone receptors in breast cancer. *Journal of Clinical Oncology* **28**, (2010).
12. Dowsett, M. *et al.* Assessment of Ki67 in Breast Cancer: Recommendations from the international Ki67 in breast cancer working Group. *Journal of the National Cancer Institute* **103**, (2011).

13. Cortazar, P. *et al.* Pathological complete response and long-term clinical benefit in breast cancer: The CTNeoBC pooled analysis. *Lancet* **384**, (2014).
14. Cardoso, F. *et al.* 4th ESO-ESMO international consensus guidelines for advanced breast cancer (ABC 4). *Ann. Oncol.* **29**, (2018).
15. Schmid, P. *et al.* Atezolizumab plus nab-paclitaxel as first-line treatment for unresectable, locally advanced or metastatic triple-negative breast cancer (IMpassion130): updated efficacy results from a randomised, double-blind, placebo-controlled, phase 3 trial. *Lancet Oncol.* **21**, (2020).
16. Schmid, P. *et al.* Atezolizumab and Nab-Paclitaxel in Advanced Triple-Negative Breast Cancer. *N. Engl. J. Med.* **379**, (2018).
17. Miles, D. *et al.* Primary results from IMpassion131, a double-blind, placebo-controlled, randomised phase III trial of first-line paclitaxel with or without atezolizumab for unresectable locally advanced/metastatic triple-negative breast cancer. *Ann. Oncol.* **32**, (2021).
18. Solinas, C. *et al.* Targeting immune checkpoints in breast cancer: An update of early results. *ESMO Open* **2**, (2017).
19. Robson, M. E. *et al.* OlympiAD final overall survival and tolerability results: Olaparib versus chemotherapy treatment of physician's choice in patients with a germline BRCA mutation and HER2-negative metastatic breast cancer. *Ann. Oncol.* **30**, (2019).
20. Litton, J. K. *et al.* Talazoparib in Patients with Advanced Breast Cancer and a Germline BRCA Mutation . *N. Engl. J. Med.* **379**, (2018).
21. Diéras, V. C. *et al.* Phase III study of veliparib with carboplatin and paclitaxel in HER2-negative advanced/metastatic gBRCA-associated breast cancer. *Ann. Oncol.* **30**, (2019).
22. Greene, G. L. *et al.* Sequence and expression of human estrogen receptor complementary DNA. *Science (80-. )*. **231**, (1986).
23. Walter, P. *et al.* Cloning of the human estrogen receptor cDNA. *Proc. Natl. Acad. Sci. U. S. A.* **82**, (1985).
24. Pawlak, M., Lefebvre, P. & Staels, B. General Molecular Biology and Architecture of Nuclear Receptors. *Curr. Top. Med. Chem.* **12**, (2012).
25. Auwerx, J. *et al.* A unified nomenclature system for the nuclear receptor superfamily. *Cell* **97**, (1999).

26. Patel, H. K. & Bihani, T. Selective estrogen receptor modulators (SERMs) and selective estrogen receptor degraders (SERDs) in cancer treatment. *Pharmacology and Therapeutics* **186**, (2018).
27. Kumar, V. & Chambon, P. The estrogen receptor binds tightly to its responsive element as a ligand-induced homodimer. *Cell* **55**, (1988).
28. Hall, J. M. & McDonnell, D. P. Coregulators in nuclear estrogen receptor action: From concept to therapeutic targeting. *Molecular Interventions* **5**, (2005).
29. Carroll, J. S. *et al.* Genome-wide analysis of estrogen receptor binding sites. *Nat. Genet.* **38**, (2006).
30. Ikeda, K., Horie-Inoue, K. & Inoue, S. Identification of estrogen-responsive genes based on the DNA binding properties of estrogen receptors using high-throughput sequencing technology. *Acta Pharmacologica Sinica* **36**, (2015).
31. Lacassagne, A. The Relation Between Hormones and Cancer. *Can. Med. Assoc. J.* **37**, (1937).
32. Lacassagne, A. Hormonal pathogenesis of adenocarcinoma of the breast. *Am. J. Cancer* **27**, (1936).
33. Carter, A. C. *et al.* Diethylstilbestrol: Recommended Dosages for Different Categories of Breast Cancer Patients: Report of the Cooperative Breast Cancer Group. *JAMA J. Am. Med. Assoc.* **237**, (1977).
34. Wittes, J. T., Kaufman, R. J. & Wittes, R. E. Diethylstilbestrol in Breast Cancer: Dose-Response Analysis. *JAMA: The Journal of the American Medical Association* **238**, (1977).
35. Cole, M. P., Jones, C. T. A. & Todd, I. D. H. A new anti-oestrogenic agent in late breast cancer an early clinical appraisal of ICI46474. *Br. J. Cancer* **25**, (1971).
36. Ward, H. W. C. Anti-oestrogen Therapy for Breast Cancer: A Trial of Tamoxifen at Two Dose Levels. *Br. Med. J.* **1**, (1973).
37. Wiseman, H. & Lewis, D. F. V. The metabolism of tamoxifen by human cytochromes P450 is rationalized by molecular modelling of the enzyme-substrate interactions: Potential importance to its proposed anti-carcinogenic/carcinogenic actions. *Carcinogenesis* **17**, (1996).
38. Pike, A. C. W. *et al.* Structural insights into the mode of action of a pure antiestrogen.

- Structure* **9**, (2001).
39. Brzozowski, A. M. *et al.* Molecular basis of agonism and antagonism in the oestrogen receptor. *Nature* **389**, (1997).
  40. Shiau, A. K. *et al.* The structural basis of estrogen receptor/coactivator recognition and the antagonism of this interaction by tamoxifen. *Cell* **95**, (1998).
  41. Klinge, C. M., Jernigan, S. C., Mattingly, K. A., Risinger, K. E. & Zhang, J. Estrogen response element-dependent regulation of transcriptional activation of estrogen receptors  $\alpha$  and  $\beta$  by coactivators and corepressors. *J. Mol. Endocrinol.* **33**, (2004).
  42. Jordan, V. C. The secrets of selective estrogen receptor modulation: Cell-specific coregulation. *Cancer Cell* **1**, (2002).
  43. Shang, Y. & Brown, M. Molecular determinants for the tissue specificity of SERMs. *Science (80-. )*. **295**, (2002).
  44. Wakeling, A. E. & Bowler, J. Novel antioestrogens without partial agonist activity. *J. Steroid Biochem.* **31**, (1988).
  45. Wakeling, A. E. & Bowler, J. Biology and mode of action of pure antioestrogens. *Drugs under Experimental and Clinical Research* **14**, (1988).
  46. Wakeling, A. E. & Bowler, J. Steroidal pure antioestrogens. *J. Endocrinol.* **112**, (1987).
  47. McDonnell, D. P., Wardell, S. E. & Norris, J. D. Oral Selective Estrogen Receptor Downregulators (SERDs), a Breakthrough Endocrine Therapy for Breast Cancer. *Journal of Medicinal Chemistry* **58**, (2015).
  48. Simpson, E. R. & Davis, S. R. Minireview: Aromatase and the regulation of estrogen biosynthesis - Some new perspectives. *Endocrinology* **142**, (2001).
  49. Dowsett, M. & Howell, A. Breast cancer: Aromatase inhibitors take on tamoxifen. *Nature Medicine* **8**, (2002).
  50. Dowsett, M. *et al.* Meta-analysis of breast cancer outcomes in adjuvant trials of aromatase inhibitors versus tamoxifen. *J. Clin. Oncol.* **28**, (2010).
  51. Rugo, H. S. *et al.* Endocrine therapy for hormone receptor-positive metastatic breast cancer: American society of clinical oncology guideline. *J. Clin. Oncol.* **34**, (2016).
  52. Jeselsohn, R., Buchwalter, G., De Angelis, C., Brown, M. & Schiff, R. ESR1 mutations- a mechanism for acquired endocrine resistance in breast cancer. *Nature Reviews Clinical*



- Oncology* **12**, (2015).
53. De Amicis, F. *et al.* Androgen receptor overexpression induces tamoxifen resistance in human breast cancer cells. *Breast Cancer Res. Treat.* **121**, (2010).
  54. Lea, O. A., Kvinnsland, S. & Thorsen, T. Improved Measurement of Androgen Receptors in Human Breast Cancer. *Cancer Res.* **49**, 7162–7167 (1989).
  55. Kuenen-Boumeester, V. *et al.* Immunohistochemical determination of androgen receptors in relation to oestrogen and progesterone receptors in female breast cancer. *Int. J. Cancer* **52**, (1992).
  56. Isola, J. J. Immunohistochemical demonstration of androgen receptor in breast cancer and its relationship to other prognostic factors. *J. Pathol.* **170**, (1993).
  57. Hall, R. E. *et al.* Expression of the androgen receptor and an androgen-responsive protein, apolipoprotein D, in human breast cancer. *Br. J. Cancer* **74**, (1996).
  58. Grogg, A. *et al.* Androgen receptor status is highly conserved during tumor progression of breast cancer. *BMC Cancer* **15**, (2015).
  59. Vera-Badillo, F. E. *et al.* Androgen receptor expression and outcomes in early breast cancer: A systematic review and meta-analysis. *J. Natl. Cancer Inst.* **106**, (2014).
  60. Gao, W., Bohl, C. E. & Dalton, J. T. Chemistry and structural biology of androgen receptor. *Chemical Reviews* **105**, (2005).
  61. Wilson, E. M. & French, F. S. Binding properties of androgen receptors. Evidence for identical receptors in rat testis, epididymis, and prostate. *J. Biol. Chem.* **251**, (1976).
  62. Askew, E. B., Gampe, R. T., Stanley, T. B., Faggart, J. L. & Wilson, E. M. Modulation of androgen receptor activation function 2 by testosterone and dihydrotestosterone. *J. Biol. Chem.* **282**, (2007).
  63. Migliaccio, A. *et al.* Inhibition of the SH3 domain-mediated binding of Src to the androgen receptor and its effect on tumor growth. *Oncogene* **26**, (2007).
  64. Migliaccio, A. Steroid-induced androgen receptor-oestradiol receptor beta-Src complex triggers prostate cancer cell proliferation. *EMBO J.* **19**, (2000).
  65. Zarif, J. C., Lamb, L. E., Schulz, V. V., Nollet, E. A. & Miranti, C. K. Androgen receptor non-nuclear regulation of prostate cancer cell invasion mediated by Src and matriptase. *Oncotarget* **6**, (2015).

66. Sarker, D., Reid, A. H. M., Yap, T. A. & De Bono, J. S. Targeting the PI3K/AKT pathway for the treatment of prostate cancer. *Clinical Cancer Research* **15**, (2009).
67. Baron, S. *et al.* Androgen Receptor Mediates Non-genomic Activation of Phosphatidylinositol 3-OH Kinase in Androgen-sensitive Epithelial Cells. *J. Biol. Chem.* **279**, (2004).
68. Yang, L. *et al.* Induction of androgen receptor expression by phosphatidylinositol 3-kinase/Akt downstream substrate, FOXO3a, and their roles in apoptosis of LNCaP prostate cancer cells. *J. Biol. Chem.* **280**, (2005).
69. Lin, H. K., Yeh, S., Kang, H. Y. & Chang, C. Akt suppresses androgen-induced apoptosis by phosphorylating and inhibiting androgen receptor. *Proc. Natl. Acad. Sci. U. S. A.* **98**, (2001).
70. Ueda, T., Mawji, N. R., Bruchovsky, N. & Sadar, M. D. Ligand-independent activation of the androgen receptor by interleukin-6 and the role of steroid receptor coactivator-1 in prostate cancer cells. *J. Biol. Chem.* **277**, (2002).
71. Ueda, T., Bruchovsky, N. & Sadar, M. D. Activation of the androgen receptor N-terminal domain by interleukin-6 via MAPK and STAT3 signal transduction pathways. *J. Biol. Chem.* **277**, (2002).
72. Roberts, P. J. & Der, C. J. Targeting the Raf-MEK-ERK mitogen-activated protein kinase cascade for the treatment of cancer. *Oncogene* **26**, (2007).
73. Fioretti, F. M., Sita-Lumsden, A., Bevan, C. L. & Brooke, G. N. Revising the role of the androgen receptor in breast cancer. *Journal of Molecular Endocrinology* **52**, (2014).
74. Wilson, S., Qi, J. & Filipp, F. V. Refinement of the androgen response element based on ChIP-Seq in androgen-insensitive and androgen-responsive prostate cancer cell lines. *Sci. Rep.* **6**, (2016).
75. Hickey, T. E. *et al.* The androgen receptor is a tumor suppressor in estrogen receptor-positive breast cancer. *Nat. Med.* **27**, 310–320 (2021).
76. Panet-Raymond, V., Gottlieb, B., Beitel, L. K., Pinsky, L. & Trifiro, M. A. Interactions between androgen and estrogen receptors and the effects on their transactivational properties. *Mol. Cell. Endocrinol.* **167**, (2000).
77. D'Amato, N. C. *et al.* Cooperative dynamics of AR and ER activity in breast cancer. *Mol. Cancer Res.* **14**, (2016).

78. Van Londen, G. J. *et al.* The impact of an aromatase inhibitor on body composition and gonadal hormone levels in women with breast cancer. *Breast Cancer Res. Treat.* **125**, (2011).
79. Bombardieri, E. *et al.* Biological activity of anastrozole in postmenopausal patients with advanced breast cancer: Effects on estrogens and bone metabolism. *Ann. Oncol.* **13**, (2002).
80. Dimitrakakis, C. & Bondy, C. Androgens and the breast. *Breast Cancer Research* **11**, (2009).
81. Rangel, N. *et al.* The role of the AR/ER ratio in ER-positive breast cancer patients. *Endocr. Relat. Cancer* **25**, (2018).
82. Chia, K. M. *et al.* Non-canonical AR activity facilitates endocrine resistance in breast cancer. *Endocr. Relat. Cancer* **26**, (2019).
83. Park, S. *et al.* Androgen receptor expression is significantly associated with better outcomes in estrogen receptor-positive breast cancers. *Ann. Oncol.* **22**, (2011).
84. Castellano, I. *et al.* A simple and reproducible prognostic index in luminal ER-positive breast cancers. *Ann. Oncol.* **24**, (2013).
85. Kim, Y., Jae, E. & Yoon, M. Influence of androgen receptor expression on the survival outcomes in breast cancer: A meta-analysis. *J. Breast Cancer* **18**, (2015).
86. Bozovic-Spasojevic, I. *et al.* The prognostic role of androgen receptor in patients with early-stage breast cancer: A metaanalysis of clinical and gene expression data. *Clin. Cancer Res.* **23**, (2017).
87. Peters, A. A. *et al.* Androgen receptor inhibits estrogen receptor- $\alpha$  activity and is prognostic in breast cancer. *Cancer Res.* **69**, (2009).
88. Ricciardelli, C. *et al.* The magnitude of androgen receptor positivity in breast cancer is critical for reliable prediction of disease outcome. *Clin. Cancer Res.* **24**, (2018).
89. Doane, A. S. *et al.* An estrogen receptor-negative breast cancer subset characterized by a hormonally regulated transcriptional program and response to androgen. *Oncogene* **25**, 3994–4008 (2006).
90. Farmer, P. *et al.* Identification of molecular apocrine breast tumours by microarray analysis. *Oncogene* **24**, 4660–4671 (2005).
91. Lehmann, B. D. *et al.* Identification of human triple-negative breast cancer subtypes and

- preclinical models for selection of targeted therapies. *J. Clin. Invest.* **121**, (2011).
92. Ni, M. *et al.* Targeting Androgen Receptor in Estrogen Receptor-Negative Breast Cancer. *Cancer Cell* **20**, (2011).
  93. Sadi, M. V., Walsh, P. C. & Barrack, E. R. Immunohistochemical study of androgen receptors in metastatic prostate cancer. Comparison of receptor content and response to hormonal therapy. *Cancer* **67**, (1991).
  94. Hu, J., Wang, G. & Sun, T. Dissecting the roles of the androgen receptor in prostate cancer from molecular perspectives. *Tumor Biology* **39**, (2017).
  95. Fujita, K. & Nonomura, N. Role of androgen receptor in prostate cancer: A review. *World Journal of Men's Health* **37**, (2019).
  96. Cannata, D. H., Kirschenbaum, A. & Levine, A. C. Androgen deprivation therapy as primary treatment for prostate cancer. *J. Clin. Endocrinol. Metab.* **97**, (2012).
  97. Perlmutter, M. A. & Lepor, H. Androgen deprivation therapy in the treatment of advanced prostate cancer. *Rev. Urol.* **9 Suppl 1**, (2007).
  98. Andriole, G. L. *et al.* Effect of the dual 5 $\alpha$ -reductase inhibitor dutasteride on markers of tumor regression in prostate cancer. *J. Urol.* **172**, (2004).
  99. Clark, R. V. *et al.* Marked Suppression of Dihydrotestosterone in Men with Benign Prostatic Hyperplasia by Dutasteride, a Dual 5 $\alpha$ -Reductase Inhibitor. *J. Clin. Endocrinol. Metab.* **89**, (2004).
  100. McConnell, J. D. Finasteride, an inhibitor of 5 alpha-reductase, suppresses prostatic dihydrotestosterone in men with benign prostatic hyperplasia. *J. Clin. Endocrinol. Metab.* **74**, (1992).
  101. Gao, W., Kim, J. & Dalton, J. T. Pharmacokinetics and pharmacodynamics of nonsteroidal androgen receptor ligands. *Pharmaceutical Research* **23**, (2006).
  102. Gucalp, A. *et al.* Phase II trial of bicalutamide in patients with androgen receptor-positive, estrogen receptor-negative metastatic breast cancer. *Clin. Cancer Res.* **19**, (2013).
  103. Lu, Q. *et al.* Bicalutamide plus Aromatase Inhibitor in Patients with Estrogen Receptor-Positive/Androgen Receptor-Positive Advanced Breast Cancer. *Oncologist* **25**, (2020).
  104. Schalken, J. & Fitzpatrick, J. M. Enzalutamide: Targeting the androgen signalling pathway in metastatic castration-resistant prostate cancer. *BJU Int.* **117**, 215–225 (2016).

105. Davis, I. D. *et al.* Enzalutamide with Standard First-Line Therapy in Metastatic Prostate Cancer. *N. Engl. J. Med.* **381**, (2019).
106. Armstrong, A. J. *et al.* Five-year Survival Prediction and Safety Outcomes with Enzalutamide in Men with Chemotherapy-naïve Metastatic Castration-resistant Prostate Cancer from the PREVAIL Trial. *Eur. Urol.* **78**, (2020).
107. Gucalp, A. & Traina, T. A. Targeting the androgen receptor in triple-negative breast cancer. *Current Problems in Cancer* **40**, (2016).
108. Cochrane, D. R. *et al.* Role of the androgen receptor in breast cancer and preclinical analysis of enzalutamide. *Breast Cancer Res.* **16**, 1–19 (2014).
109. Birrell, S. N. *et al.* Androgens induce divergent proliferative responses in human breast cancer cell lines. *J. Steroid Biochem. Mol. Biol.* **52**, 459–467 (1995).
110. Pfizer. Efficacy and Safety Study of Enzalutamide in Combination With Paclitaxel Chemotherapy or as Monotherapy Versus Placebo With Paclitaxel in Patients With Advanced, Diagnostic-Positive, Triple-Negative Breast Cancer (ENDEAR) NCT02929576. (2018).
111. Traina, T. A. *et al.* Adjuvant enzalutamide for the treatment of early-stage androgen receptor-positive (AR+) TNBC. *J. Clin. Oncol.* **37**, (2019).
112. Traina, T. A. *et al.* Abstract P5-12-09: Patient-reported outcomes (PROs) during one year of adjuvant enzalutamide for the treatment of early stage androgen receptor positive (AR+) triple negative breast cancer. in (2020). doi:10.1158/1538-7445.sabcs19-p5-12-09
113. Lehmann, B. D. *et al.* TBCRC 032 IB/II Multicenter Study: Molecular Insights to AR Antagonist and PI3K Inhibitor Efficacy in Patients with AR+ Metastatic Triple-Negative Breast Cancer. *Clin. Cancer Res.* **26**, (2020).
114. Findlay, V. J., LaRue, A. C., Turner, D. P., Watson, P. M. & Watson, D. K. Understanding the role of ETS-mediated gene regulation in complex biological processes. in *Advances in Cancer Research* **119**, (2013).
115. Karim, F. D. *et al.* The ETS-domain: a new DNA-binding motif that recognizes a purine-rich core DNA sequence. *Genes and Development* **4**, (1990).
116. Wei, G. H. *et al.* Genome-wide analysis of ETS-family DNA-binding in vitro and in vivo. *EMBO J.* **29**, (2010).

117. Klambt, C. The *Drosophila* gene pointed encodes two ETS-like proteins which are involved in the development of the midline glial cells. *Development* **117**, (1993).
118. Lacronique, V. *et al.* A TEL-JAK2 fusion protein with constitutive kinase activity in human leukemia. *Science (80-. )*. **278**, (1997).
119. Kim, C. A. *et al.* Polymerization of the SAM domain of TEL in leukemogenesis and transcriptional repression. *EMBO J.* **20**, (2001).
120. Baker, D. A., Mille-Baker, B., Wainwright, S. M., Ish-Horowicz, D. & Dibb, N. J. Mae mediates MAP kinase phosphorylation of Ets transcription factors in *Drosophila*. *Nature* **411**, (2001).
121. Charlot, C., Dubois-Pot, H., Serchov, T., Tourrette, Y. & Wasylyk, B. A review of post-translational modifications and subcellular localization of ets transcription factors: Possible connection with cancer and involvement in the hypoxic response. *Methods in Molecular Biology* **647**, (2010).
122. Hollenhorst, P. C., McIntosh, L. P. & Graves, B. J. Genomic and biochemical insights into the specificity of ETS transcription factors. *Annu. Rev. Biochem.* **80**, (2011).
123. Horn, S. *et al.* TERT promoter mutations in familial and sporadic melanoma. *Science (80-. )*. **339**, (2013).
124. Huang, F. W. *et al.* Highly recurrent TERT promoter mutations in human melanoma. *Science (80-. )*. **339**, (2013).
125. Vinagre, J. *et al.* Frequency of TERT promoter mutations in human cancers. *Nat. Commun.* **4**, (2013).
126. Chi, P. *et al.* ETV1 is a lineage survival factor that cooperates with KIT in gastrointestinal stromal tumours. *Nature* **467**, (2010).
127. Oettgen, P. *et al.* PDEF , a Novel Prostate Epithelium-specific Ets Transcription Factor , Interacts with the Androgen Receptor and Activates Prostate-specific Antigen Gene Expression PDEF , a Novel Prostate Epithe. **275**, 1216–1225 (2000).
128. Buchwalter, G. *et al.* PDEF Promotes Luminal Differentiation and Acts as a Survival Factor for ER-Positive Breast Cancer Cells. *Cancer Cell* **23**, 753–767 (2013).
129. Sood, A. K. *et al.* Sam-pointed domain containing Ets transcription factor in luminal breast cancer pathogenesis. *Cancer Epidemiol. Biomarkers Prev.* **18**, (2009).
130. Mukhopadhyay, A., Khoury, T., Stein, L., Shrikant, P. & Sood, A. K. Prostate derived

- Ets transcription factor and carcinoembryonic antigen related cell adhesion molecule 6 constitute a highly active oncogenic axis in breast cancer. *Oncotarget* **4**, (2013).
131. Sood, A. K. *et al.* Expression characteristics of prostate-derived Ets factor support a role in breast and prostate cancer progression. *Hum. Pathol.* **38**, 1628–1638 (2007).
132. Ghadersohi, A. & Sood, A. K. Prostate epithelium-derived Ets transcription factor mRNA is overexpressed in human breast tumors and is a candidate breast tumor marker and a breast tumor antigen. *Clin. Cancer Res.* **7**, (2001).
133. Turcotte, S., Forget, M. A., Beauseigle, D., Nassif, E. & Lapointe, R. Prostate-derived Ets transcription factor overexpression is associated with nodal metastasis and hormone receptor positivity in invasive breast cancer. *Neoplasia* **9**, (2007).
134. He, J. *et al.* Profile of Ets gene expression in human breast carcinoma. *Cancer Biol. Ther.* **6**, (2007).
135. Feldman, R. J., Sementchenko, V. I., Gayed, M., Fraig, M. M. & Watson, D. K. Pdef expression in human breast cancer is correlated with invasive potential and altered gene expression. *Cancer Res.* **63**, 4626–4631 (2003).
136. Ye, T., Feng, J., Wan, X., Xie, D. & Liu, J. Double agent: SPDEF gene with both oncogenic and tumor-suppressor functions in breast cancer. *Cancer Manag. Res.* **12**, (2020).
137. Cao, L. *et al.* AR–PDEF pathway promotes tumour proliferation and upregulates MYC-mediated gene transcription by promoting MAD1 degradation in ER-negative breast cancer. *Mol. Cancer* **17**, (2018).
138. Thompson, H. G. R., Harris, J. W., Wold, B. J., Lin, F. & Brody, J. P. p62 overexpression in breast tumors and regulation by prostate-derived Ets factor in breast cancer cells. *Oncogene* **22**, (2003).
139. Gunawardane, R. N. *et al.* Novel role for PDEF in epithelial cell migration and invasion. *Cancer Res.* **65**, (2005).
140. Ghadersohi, A. *et al.* Prostate-derived Ets transcription factor (PDEF) downregulates survivin expression and inhibits breast cancer cell growth in vitro and xenograft tumor formation in vivo. *Breast Cancer Res. Treat.* **102**, 19–30 (2007).
141. Schaefer, J. S. *et al.* Transcriptional regulation of p21/CIP1 cell cycle inhibitor by PDEF controls cell proliferation and mammary tumor progression. *J. Biol. Chem.* **285**, (2010).

142. Turner, D. P., Findlay, V. J., Kirven, A. D., Moussa, O. & Watson, D. K. Global gene expression analysis identifies PDEF transcriptional networks regulating cell migration during cancer progression. *Mol. Biol. Cell* **19**, (2008).
143. Findlay, V. J. *et al.* Prostate-derived ETS factor regulates epithelial-to-mesenchymal transition through both SLUG-dependent and independent mechanisms. *Genes and Cancer* **2**, (2011).
144. Hanahan, D. & Weinberg, R. A. Hallmarks of cancer: The next generation. *Cell* **144**, 646–674 (2011).
145. Hanahan, D. Hallmarks of Cancer: New Dimensions. *Cancer Discov.* **12**, 31–46 (2022).
146. Warburg, O. On the origin of cancer cells. *Science (80-. )*. **123**, 309–314 (1956).
147. Weinhouse, S., Warburg, O., Burk, D. & Schade, A. L. On respiratory impairment in cancer cells. *Science (80-. )*. **124**, (1956).
148. Warburg, O. The Metabolism of Tumours: Investigations from the Kaiser Wilhelm Institute for Biology, Berlin-Dahlem. *JAMA J. Am. Med. Assoc.* **96**, (1931).
149. POTTER, V. R. The biochemical approach to the cancer problem. *Fed. Proc.* **17**, (1958).
150. Heiden, M. G. V., Cantley, L. C. & Thompson, C. B. Understanding the warburg effect: The metabolic requirements of cell proliferation. *Science* **324**, (2009).
151. Lunt, S. Y. & Vander Heiden, M. G. Aerobic glycolysis: Meeting the metabolic requirements of cell proliferation. *Annu. Rev. Cell Dev. Biol.* **27**, (2011).
152. Pavlova, N. N. & Thompson, C. B. The Emerging Hallmarks of Cancer Metabolism. *Cell Metabolism* **23**, 27–47 (2016).
153. Dong, C. *et al.* Loss of FBP1 by snail-mediated repression provides metabolic advantages in basal-like breast cancer. *Cancer Cell* **23**, 316–331 (2013).
154. Li, H. *et al.* FBP1 regulates proliferation, metastasis, and chemoresistance by participating in C-MYC/STAT3 signaling axis in ovarian cancer. *Oncogene* **40**, (2021).
155. Li, F. *et al.* FBP1 loss disrupts liver metabolism and promotes tumorigenesis through a hepatic stellate cell senescence secretome. *Nat. Cell Biol.* **22**, (2020).
156. He, Y. *et al.* Loss of FBP1 promotes proliferation, migration, and invasion by regulating fatty acid metabolism in esophageal squamous cell carcinoma. *Aging (Albany. NY)*. **13**, (2021).



157. Kovacevic, Z. & McGivan, J. D. Mitochondrial metabolism of glutamine and glutamate and its physiological significance. *Physiological Reviews* **63**, (1983).
158. EAGLE, H., OYAMA, V. I., LEVY, M., HORTON, C. L. & FLEISCHMAN, R. The growth response of mammalian cells in tissue culture to L-glutamine and L-glutamic acid. *J. Biol. Chem.* **218**, (1956).
159. Heiden, M. G. Vander. Understanding the Warburg Effect. *Science (80-. )*. **1029**, 1029–1033 (2009).
160. Viale, A. *et al.* Oncogene ablation-resistant pancreatic cancer cells depend on mitochondrial function. *Nature* **514**, (2014).
161. Lebleu, V. S. *et al.* PGC-1 $\alpha$  mediates mitochondrial biogenesis and oxidative phosphorylation in cancer cells to promote metastasis. *Nat. Cell Biol.* **16**, 992–1003 (2014).
162. Elia, I., Schmieder, R., Christen, S. & Fendt, S. M. Organ-specific cancer metabolism and its potential for therapy. in *Handbook of Experimental Pharmacology* **233**, (2016).
163. Obre, E. & Rossignol, R. Emerging concepts in bioenergetics and cancer research: Metabolic flexibility, coupling, symbiosis, switch, oxidative tumors, metabolic remodeling, signaling and bioenergetic therapy. *International Journal of Biochemistry and Cell Biology* **59**, (2015).
164. Guppy, M., Leedman, P., Zu, X. L. & Russell, V. Contribution by different fuels and metabolic pathways to the total ATP turnover of proliferating MCF-7 breast cancer cells. *Biochem. J.* **364**, (2002).
165. Martínez-Reyes, I. *et al.* TCA Cycle and Mitochondrial Membrane Potential Are Necessary for Diverse Biological Functions. *Mol. Cell* **61**, (2016).
166. Weinberg, S. E. & Chandel, N. S. Targeting mitochondria metabolism for cancer therapy. *Nature Chemical Biology* **11**, (2015).
167. Camirand, A., Zakikhani, M., Young, F. & Pollak, M. Inhibition of insulin-like growth factor-1 receptor signaling enhances growth-inhibitory and proapoptotic effects of gefitinib (Iressa) in human breast cancer cells. *Breast Cancer Res.* **7**, (2005).
168. Sahra, I. Ben *et al.* The antidiabetic drug metformin exerts an antitumoral effect in vitro and in vivo through a decrease of cyclin D1 level. *Oncogene* **27**, (2008).
169. Buzzai, M. *et al.* Systemic treatment with the antidiabetic drug metformin selectively

- impairs p53-deficient tumor cell growth. *Cancer Res.* **67**, (2007).
170. Griss, T. *et al.* Metformin Antagonizes Cancer Cell Proliferation by Suppressing Mitochondrial-Dependent Biosynthesis. *PLoS Biol.* **13**, (2015).
171. Andrzejewski, S., Gravel, S.-P., Pollak, M. & St-Pierre, J. Metformin directly acts on mitochondria to alter cellular bioenergetics. *Cancer Metab.* **2**, (2014).
172. Wheaton, W. W. *et al.* Metformin inhibits mitochondrial complex I of cancer cells to reduce tumorigenesis. *Elife* **2014**, (2014).
173. Birsoy, K. *et al.* Metabolic determinants of cancer cell sensitivity to glucose limitation and biguanides. *Nature* **508**, (2014).
174. Lu, X., Bennet, B., Mu, E., Rabinowitz, J. & Kang, Y. Metabolomic changes accompanying transformation and acquisition of metastatic potential in a syngeneic mouse mammary tumor model. *J. Biol. Chem.* **285**, (2010).
175. Davis, R. T. *et al.* Transcriptional diversity and bioenergetic shift in human breast cancer metastasis revealed by single-cell RNA sequencing. *Nat. Cell Biol.* **22**, (2020).
176. Dupuy, F. *et al.* PDK1-dependent metabolic reprogramming dictates metastatic potential in breast cancer. *Cell Metab.* **22**, (2015).
177. Havas, K. M. *et al.* Metabolic shifts in residual breast cancer drive tumor recurrence. *J. Clin. Invest.* **127**, (2017).
178. Röhrig, F. & Schulze, A. The multifaceted roles of fatty acid synthesis in cancer. *Nature Reviews Cancer* **16**, 732–749 (2016).
179. Snaebjornsson, M. T., Janaki-Raman, S. & Schulze, A. Greasing the Wheels of the Cancer Machine: The Role of Lipid Metabolism in Cancer. *Cell Metabolism* **31**, 62–76 (2020).
180. Ookhtens, M., Kannan, R., Lyon, I. & Baker, N. Liver and adipose tissue contributions to newly formed fatty acids in an ascites tumor. *Am. J. Physiol. - Regul. Integr. Comp. Physiol.* **16**, (1984).
181. Menendez, J. A. & Lupu, R. Fatty acid synthase and the lipogenic phenotype in cancer pathogenesis. *Nature Reviews Cancer* **7**, (2007).
182. Zaidi, N., Swinnen, J. V. & Smans, K. ATP-citrate lyase: A key player in cancer metabolism. *Cancer Research* **72**, (2012).

183. Brownsey, R. W., Boone, A. N., Elliott, J. E., Kulpa, J. E. & Lee, W. M. Regulation of acetyl-CoA carboxylase. *Biochem. Soc. Trans.* **34**, (2006).
184. Maier, T., Leibundgut, M. & Ban, N. The crystal structure of a mammalian fatty acid synthase. *Science (80-. )*. **321**, (2008).
185. Jakobsson, A., Westerberg, R. & Jacobsson, A. Fatty acid elongases in mammals: Their regulation and roles in metabolism. *Progress in Lipid Research* **45**, (2006).
186. Igal, R. A. Stearoyl-coa desaturase-1: A novel key player in the mechanisms of cell proliferation, programmed cell death and transformation to cancer. *Carcinogenesis* **31**, (2010).
187. Vriens, K. *et al.* Evidence for an alternative fatty acid desaturation pathway increasing cancer plasticity. *Nature* **566**, (2019).
188. Bauer, D. E., Hatzivassiliou, G., Zhao, F., Andreadis, C. & Thompson, C. B. ATP citrate lyase is an important component of cell growth and transformation. *Oncogene* **24**, 6314–6322 (2005).
189. Wang, D., Yin, L., Wei, J., Yang, Z. & Jiang, G. ATP citrate lyase is increased in human breast cancer, depletion of which promotes apoptosis. *Tumor Biol.* **39**, (2017).
190. Migita, T. *et al.* ATP citrate lyase: Activation and therapeutic implications in non-small cell lung cancer. *Cancer Res.* **68**, (2008).
191. Milgraum, L. Z., Witters, L. A., Pasternack, G. R. & Kuhajda, F. P. Enzymes of the fatty acid synthesis pathway are highly expressed in in situ breast carcinoma. *Clin. Cancer Res.* **3**, (1997).
192. Ferraro, G. B. *et al.* Fatty acid synthesis is required for breast cancer brain metastasis. *Nat. Cancer* **2**, (2021).
193. Flavin, R., Peluso, S., Nguyen, P. L. & Loda, M. Fatty acid synthase as a potential therapeutic target in cancer. *Future Oncology* **6**, (2010).
194. Agostini, M. *et al.* Fatty acid synthase is required for the proliferation of human oral squamous carcinoma cells. *Oral Oncol.* **40**, (2004).
195. Cerqueira, N. M. F. S. A. *et al.* Cholesterol Biosynthesis: A Mechanistic Overview. *Biochemistry* **55**, (2016).
196. Ehmsen, S. *et al.* Increased Cholesterol Biosynthesis Is a Key Characteristic of Breast Cancer Stem Cells Influencing Patient Outcome. *Cell Rep.* **27**, (2019).

197. Papandreou, I., Cairns, R. A., Fontana, L., Lim, A. L. & Denko, N. C. HIF-1 mediates adaptation to hypoxia by actively downregulating mitochondrial oxygen consumption. *Cell Metab.* **3**, (2006).
198. Kamphorst, J. J. *et al.* Hypoxic and Ras-transformed cells support growth by scavenging unsaturated fatty acids from lysophospholipids. *Proc. Natl. Acad. Sci. U. S. A.* **110**, (2013).
199. Bensaad, K. *et al.* Fatty acid uptake and lipid storage induced by HIF-1 $\alpha$  contribute to cell growth and survival after hypoxia-reoxygenation. *Cell Rep.* **9**, (2014).
200. Michiels, C., Tellier, C. & Feron, O. Cycling hypoxia: A key feature of the tumor microenvironment. *Biochimica et Biophysica Acta - Reviews on Cancer* **1866**, (2016).
201. Yasui, H. *et al.* Low-field magnetic resonance imaging to visualize chronic and cycling hypoxia in tumor-bearing mice. *Cancer Res.* **70**, (2010).
202. Griner, E. M. & Kazanietz, M. G. Protein kinase C and other diacylglycerol effectors in cancer. *Nature Reviews Cancer* **7**, (2007).
203. Vanhaesebroeck, B., Stephens, L. & Hawkins, P. PI3K signalling: The path to discovery and understanding. *Nature Reviews Molecular Cell Biology* **13**, (2012).
204. Hilvo, M. *et al.* Novel theranostic opportunities offered by characterization of altered membrane lipid metabolism in breast cancer progression. *Cancer Res.* **71**, (2011).
205. Rysman, E. *et al.* De novo lipogenesis protects cancer cells from free radicals and chemotherapeutics by promoting membrane lipid saturation. *Cancer Res.* **70**, (2010).
206. Krahmer, N., Guo, Y., Farese, R. V. & Walther, T. C. SnapShot: Lipid Droplets. *Cell* **139**, (2009).
207. Carracedo, A., Cantley, L. C. & Pandolfi, P. P. Cancer metabolism: Fatty acid oxidation in the limelight. *Nat. Rev. Cancer* **13**, (2013).
208. Saini, M. Characterization of Metastasis-initiating Cells from Liquid Biopsies of Breast Cancer Patients. (2017).
209. Schrijver, W. A. M. E. *et al.* Receptor conversion in distant breast cancer metastases: A Systematic Review and Meta-analysis. *Journal of the National Cancer Institute* **110**, (2018).
210. He, L. *et al.* Targeting Androgen Receptor in Treating HER2 Positive Breast Cancer. *Sci. Rep.* **7**, (2017).

211. Chu, T. M., Murphy, G. P., Kawinski, E. & Mirand, E. A. Lncap model of human prostatic carcinoma. *Cancer Res.* **43**, (1983).
212. Tai, S. *et al.* PC3 is a cell line characteristic of prostatic small cell carcinoma. *Prostate* **71**, (2011).
213. Zickgraf, F. SPDEF is a mediator of tumorigenicity in SSEA1<sup>-</sup> tumor-initiating cells in high-grade serous ovarian cancer. (2018).
214. Michmerhuizen, A. R., Spratt, D. E., Pierce, L. J. & Speers, C. W. ARE we there yet? Understanding androgen receptor signaling in breast cancer. *npj Breast Cancer* **6**, (2020).
215. TIDE: Tracking of Indels by Decomposition. (2022). Available at: <https://tide.nki.nl>.
216. Swinnen, J. V., Esquenet, M., Goossens, K., Heyns, W. & Verhoeven, G. Androgens stimulate fatty acid synthase in the human prostate cancer cell line LNCaP. *Cancer Res.* **57**, (1997).
217. Coort, S. L. M. *et al.* Sulfo-N-succinimidyl esters of long chain fatty acids specifically inhibit fatty acid translocase (FAT/CD36)-mediated cellular fatty acid uptake. *Mol. Cell. Biochem.* **239**, (2002).
218. Kuda, O. *et al.* Sulfo-N-succinimidyl oleate (SSO) inhibits fatty acid uptake and signaling for intracellular calcium via binding CD36 lysine 164: SSO also inhibits oxidized low density lipoprotein uptake by macrophages. *J. Biol. Chem.* **288**, (2013).
219. Cantor, J. R. *et al.* Physiologic Medium Rewires Cellular Metabolism and Reveals Uric Acid as an Endogenous Inhibitor of UMP Synthase. *Cell* **169**, (2017).
220. Bader, D. A. *et al.* Mitochondrial pyruvate import is a metabolic vulnerability in androgen receptor-driven prostate cancer. *Nat. Metab.* **1**, 70–85 (2019).
221. Cao, L. *et al.* Clinical significance of PDEF factor expression and its relation to androgen receptor in ER – breast cancer. *Histopathology* **73**, (2018).
222. Govindan, S. *et al.* Androgen Receptor mRNA levels determine the prognosis in triple-negative breast cancer patients. *BMC Cancer* **20**, (2020).
223. Caiazza, F. *et al.* Preclinical evaluation of the AR inhibitor enzalutamide in triple-negative breast cancer cells. *Endocr. Relat. Cancer* **23**, (2016).
224. Cuenca-López, M. D. *et al.* Phospho-kinase profile of triple negative breast cancer and androgen receptor signaling. *BMC Cancer* **14**, (2014).

225. Michmerhuizen, A. R. *et al.* Seviteronel, a Novel CYP17 Lyase Inhibitor and Androgen Receptor Antagonist, Radiosensitizes AR-Positive Triple Negative Breast Cancer Cells. *Front. Endocrinol. (Lausanne)*. **11**, (2020).
226. Sood, A. K., Geradts, J. & Young, J. Prostate-Derived Ets factor, an oncogenic driver in breast cancer. *Tumor Biology* **39**, (2017).
227. Koppenol, W. H., Bounds, P. L. & Dang, C. V. Otto Warburg's contributions to current concepts of cancer metabolism. *Nature Reviews Cancer* **11**, (2011).
228. Liu, Y. *et al.* Invalidation of mitophagy by FBP1-mediated repression promotes apoptosis in breast cancer. *Tumor Biol.* **39**, (2017).
229. Van't Veer, L. J. *et al.* Gene expression profiling predicts clinical outcome of breast cancer. *Nature* **415**, (2002).
230. Sheng, H. *et al.* Down expression of FBP1 Is a negative prognostic factor for non-small-cell lung cancer. *Cancer Invest.* **33**, (2015).
231. Zhang, J. *et al.* Down-regulation of FBP1 by ZEB1-mediated repression confers to growth and invasion in lung cancer cells. *Mol. Cell. Biochem.* **411**, (2016).
232. Shi, L., He, C., Li, Z., Wang, Z. & Zhang, Q. FBP1 modulates cell metabolism of breast cancer cells by inhibiting the expression of HIF-1 $\alpha$ . *Neoplasma* **64**, (2017).
233. Jurica, M. S. *et al.* The allosteric regulation of pyruvate kinase by fructose-1,6-bisphosphate. *Structure* **6**, (1998).
234. Goossens, S., Vandamme, N., Van Vlierberghe, P. & Berx, G. EMT transcription factors in cancer development re-evaluated: Beyond EMT and MET. *Biochimica et Biophysica Acta - Reviews on Cancer* **1868**, (2017).
235. Lamouille, S., Xu, J. & Derynck, R. Molecular mechanisms of epithelial-mesenchymal transition. *Nature Reviews Molecular Cell Biology* **15**, (2014).
236. Currie, E., Schulze, A. & Zechner, R. Cellular Fatty Acid Metabolism and Cancer. *Cell Metab.* (2013).
237. Hatzivassiliou, G. *et al.* ATP citrate lyase inhibition can suppress tumor cell growth. *Cancer Cell* **8**, (2005).
238. Wellen, K. E. *et al.* ATP-citrate lyase links cellular metabolism to histone acetylation. *Science (80-. )*. **324**, (2009).

239. Brusselmans, K., De Schrijver, E., Verhoeven, G. & Swinnen, J. V. RNA interference-mediated silencing of the acetyl-Coa-carboxylase- $\alpha$  gene induces growth inhibition and apoptosis of prostate cancer cells. *Cancer Res.* **65**, (2005).
240. Chajès, V., Cambot, M., Moreau, K., Lenoir, G. M. & Joulin, V. Acetyl-CoA carboxylase  $\alpha$  is essential to breast cancer cell survival. *Cancer Res.* **66**, (2006).
241. Jeon, S. M., Chandel, N. S. & Hay, N. AMPK regulates NADPH homeostasis to promote tumour cell survival during energy stress. *Nature* **485**, (2012).
242. Kusakabe, T. *et al.* Fatty acid synthase is expressed mainly in adult hormone-sensitive cells or cells with high lipid metabolism and in proliferating fetal cells. *J. Histochem. Cytochem.* **48**, (2000).
243. Pizer, E. S., Kurman, R. J., Pasternack, G. R. & Kuhajda, F. P. Expression of fatty acid synthase is closely linked to proliferation and stromal decidualization in cycling endometrium. *Int. J. Gynecol. Pathol.* **16**, (1997).
244. De Schrijver, E., Brusselmans, K., Heyns, W., Verhoeven, G. & Swinnen, J. V. RNA interference-mediated silencing of the fatty acid synthase gene attenuates growth and induces morphological changes and apoptosis of LNCaP prostate cancer cells. *Cancer Res.* **63**, (2003).
245. Pizer, E. S. *et al.* Malonyl-coenzyme-A is a potential mediator of cytotoxicity induced by fatty-acid synthase inhibition in human breast cancer cells and xenografts. *Cancer Res.* **60**, (2000).
246. Pizer, E. S., Chrest, F. J., DiGiuseppe, J. A. & Han, W. F. Pharmacological inhibitors of mammalian fatty acid synthase suppress DNA replication and induce apoptosis in tumor cell lines. *Cancer Res.* **58**, (1998).
247. Pizer, E. S. *et al.* Inhibition of fatty acid synthesis induces programmed cell death in human breast cancer cells. *Cancer Res.* **56**, (1996).
248. Pizer, E. S. *et al.* Inhibition of fatty acid synthesis delays disease progression in a xenograft model of ovarian cancer. *Cancer Res.* **56**, (1996).
249. Zhou, W. *et al.* Fatty Acid Synthase Inhibition Triggers Apoptosis during S Phase in Human Cancer Cells. in *Cancer Research* **63**, (2003).
250. Bandyopadhyay, S. *et al.* Mechanism of apoptosis induced by the inhibition of fatty acid synthase in breast cancer cells. *Cancer Res.* **66**, (2006).

251. Paton, C. M. & Ntambi, J. M. Biochemical and physiological function of stearoyl-CoA desaturase. *American Journal of Physiology - Endocrinology and Metabolism* **297**, (2009).
252. Ariyama, H., Kono, N., Matsuda, S., Inoue, T. & Arai, H. Decrease in membrane phospholipid unsaturation induces unfolded protein response. *J. Biol. Chem.* **285**, (2010).
253. Fritz, V. *et al.* Abrogation of De novo lipogenesis by stearoyl-CoA desaturase 1 inhibition interferes with oncogenic signaling and blocks prostate cancer progression in mice. *Mol. Cancer Ther.* **9**, (2010).
254. Kuhajda, F. P. *et al.* Fatty acid synthesis: A potential selective target for antineoplastic therapy. *Proc. Natl. Acad. Sci. U. S. A.* **91**, (1994).
255. Pascual, G. *et al.* Targeting metastasis-initiating cells through the fatty acid receptor CD36. *Nature* **541**, (2017).
256. Ye, T. *et al.* The subtype-specific molecular function of SPDEF in breast cancer and insights into prognostic significance. *J. Cell. Mol. Med.* **25**, (2021).
257. Haddad-Tóvolli, R., Dragano, N. R. V., Ramalho, A. F. S. & Velloso, L. A. Development and function of the blood-brain barrier in the context of metabolic control. *Frontiers in Neuroscience* **11**, (2017).
258. McGale, E. H. F., Pye, I. F., Stonier, C., Hutchinson, E. C. & Aber, G. M. STUDIES OF THE INTER-RELATIONSHIP BETWEEN CEREBROSPINAL FLUID AND PLASMA AMINO ACID CONCENTRATIONS IN NORMAL INDIVIDUALS. *J. Neurochem.* **29**, (1977).
259. O'Brien, J. S. & Sampson, E. L. Lipid composition of the normal human brain: gray matter, white matter, and myelin. *J. Lipid Res.* **6**, (1965).
260. Loftus, T. M. *et al.* Reduced food intake and body weight in mice treated with fatty acid synthase inhibitors. *Science (80-. )*. **288**, (2000).
261. Schug, Z. T. & Gottlieb, E. Cardiolipin acts as a mitochondrial signalling platform to launch apoptosis. *Biochimica et Biophysica Acta - Biomembranes* **1788**, (2009).
262. Kiebish, M. A., Han, X., Cheng, H., Chuang, J. H. & Seyfried, T. N. Cardiolipin and electron transport chain abnormalities in mouse brain tumor mitochondria: Lipidomic evidence supporting the Warburg theory of cancer. *J. Lipid Res.* **49**, (2008).
263. Peck, B. *et al.* Inhibition of fatty acid desaturation is detrimental to cancer cell survival



- in metabolically compromised environments. *Cancer Metab.* **4**, (2016).
264. Ju, Y. S. *et al.* Origins and functional consequences of somatic mitochondrial DNA mutations in human cancer. *Elife* **3**, (2014).
265. Guo, J. Y. *et al.* Activated Ras requires autophagy to maintain oxidative metabolism and tumorigenesis. *Genes Dev.* **25**, (2011).
266. Weinberg, F. *et al.* Mitochondrial metabolism and ROS generation are essential for Kras-mediated tumorigenicity. *Proc. Natl. Acad. Sci. U. S. A.* **107**, (2010).
267. Joshi, S. *et al.* The Genomic Landscape of Renal Oncocytoma Identifies a Metabolic Barrier to Tumorigenesis. *Cell Rep.* **13**, (2015).
268. Faubert, B., Solmonson, A. & DeBerardinis, R. J. Metabolic reprogramming and cancer progression. *Science* **368**, (2020).
269. Costello, L. C. & Franklin, R. B. The clinical relevance of the metabolism of prostate cancer; zinc and tumor suppression: Connecting the dots. *Molecular Cancer* **5**, (2006).
270. Zadra, G., Photopoulos, C. & Loda, M. The fat side of prostate cancer. *Biochimica et Biophysica Acta - Molecular and Cell Biology of Lipids* **1831**, 1518–1532 (2013).
271. Doyen, J. *et al.* Expression of the hypoxia-inducible monocarboxylate transporter MCT4 is increased in triple negative breast cancer and correlates independently with clinical outcome. *Biochem. Biophys. Res. Commun.* **451**, (2014).
272. Choi, J., Kim, D. H., Jung, W. H. & Koo, J. S. Metabolic interaction between cancer cells and stromal cells according to breast cancer molecular subtype. *Breast Cancer Res.* **15**, (2013).
273. Tchou, J. *et al.* Degree of tumor FDG uptake correlates with proliferation index in triple negative breast cancer. *Mol. Imaging Biol.* **12**, (2010).
274. Hussien, R. & Brooks, G. A. Mitochondrial and plasma membrane lactate transporter and lactate dehydrogenase isoform expression in breast cancer cell lines. *Physiol. Genomics* **43**, (2011).
275. Santidrian, A. F. *et al.* Mitochondrial complex I activity and NAD<sup>+</sup>/NADH balance regulate breast cancer progression. *J. Clin. Invest.* **123**, (2013).
276. Ruiz-Pérez, M. V. *et al.* Inhibition of fatty acid synthesis induces differentiation and reduces tumor burden in childhood neuroblastoma. *iScience* **24**, (2021).

- 
277. Kaplan, E. L. & Meier, P. Nonparametric Estimation from Incomplete Observations. *J. Am. Stat. Assoc.* **53**, (1958).
278. Kassambara, A., Kosinski, M., Biecek, P. & Scheipl, F. survminer: drawing survival curves using ‘ggplot2’. (2021).
279. Harrington, D. P. & Fleming, T. R. A class of rank test procedures for censored survival data. *Biometrika* **69**, (1982).

## 8 List of Abbreviations

%	percent
°C	celsius
α-KG	alpha-ketogluterate
ACC	alpha-carboxylase
Acetyl-CoA	acetyl-coenzyme A
ACLY	ATP-citrate lyase
ACSL3	acyl-CoA synthetase long chain family member 3
ADT	androgen-deprivation therapy
AF	activation function
AI	aromatase inhibitor
AKT	AKT serine threonine kinase 1
ALDOC	aldolase isozyme C
AR	androgen receptor
ARE	androgen response element
ATP	adenosine triphosphate
BC	breast cancer
BPE	breast pleural effusion
BRCA	breast cancer <i>gene</i>
BSA	bovine serum albumin
CaCl <sub>2</sub>	calcium chloride
CBR	clinical benefit rate
CDK	cycline dependent kinase
cDNA	complementary deoxyribonucleic acid

---

cm	centimeter
CO <sub>2</sub>	carbon dioxide
COX	cyclooxygenase
CPM	counts per million
CREB3L4	CAMP responsive element binding protein 3 like 4
Crispr	clustered regularly interspaced short palindromic repeat
crRNA	CRISPR RNA
CSC	cancer stem cell
CTB	Cell Titer Blue
CTC	circulating tumor cells
CYP	cytochrome P450
DAG	diacylglycerol
DBD	DNA-binding domain
DCIS	ductal carcinoma in situ
ddH <sub>2</sub> O	sterile, nuclease-free water
Delta CT	Delta crossing threshold
DFS	disease-free survival
DGE	differential gene expression
DHT	dihydrotestosterone
DMSO	dimethylsulfoxide
DNA	deoxyribonucleic acid
Dox	doxycycline
E2	estradiol
ECAR	extracellular acidification rate
EGF	epidermal growth factor

---

ELOVL	elongase
ENO2	enolase 2
ENZA	enzalutamide
EP	electroporation
Epcam	epithelial cell adhesion molecule
ER	estrogen receptor
ERBB2/HER2	human epidermal growth factor receptor 2
ERE	estrogen response elements
ETS	E26 transformation specific
F-1,6-BP	fructose-1,6-bisphosphate
FA2H	fatty acid 2 hydroxylase
FACS	fluorescent activated cell sorting
FADH2	flavin adenine dinucleotide hydroquinone
FADS2	fatty acid desaturase 2
Fas	fatty acids
FASN	fatty acid synthetase
FBP1	fructose-1,6-bisphosphatase
FC	fold change
FCCP	carbonyl cyanide-p-trifluoromethoxyphenylhydrazone
FCS	fetal calf serum
FDR	false discovery rate
FGF	fibroblast growth factor
FOXA1	forkhead box A1
FW	forward
g	gram

---

GAPDH	glyceraldehyde-3-phosphate dehydrogenase
GlcNAc	acetylglucosamine
GLUT	glucose transporter
gRNA	guide RNA
GSEA	186enes et enrichment analysis
GSH	glutathione
GTP	guanine triphosphate
H&E	hematoxylin and eosine
HBS	HEPES buffered saline
HER2	human epidermal growth factor receptor 2
HK	hexokinase
h	hour
HPLM	human plasma-like medium
HR	hormone receptor
HRP	horseradish peroxidase
HSP	heat-shock protein
IgG	immunoglobulin G
IHC	immunohistochemistry
IVCs	individually ventilated cage
KD	knockdown
kDa	kilo Dalton
kg	kilo gram
KO	knock-out
L2FC	log <sub>2</sub> fold change
LAPP	L-ascorbate-2-phosphate

---

LB	lysogeny broth
LBD	ligand-binding domain
LC/MS	liquid chromatography/mass spectrometry
LDHA/B	lactate dehydrogenase A/B
mBC	metastatic breast cancer
MFI	mean fluorescence intensity
MFP	mammary fat pad
μg	microgram
μM	micromolar
mg	milligram
min	minutes
mL	milliliter
mM	millimolar
mPC	metastatic prostate cancer
mRNA	messenger ribonucleic acid
ms	milliseconds
MsigDB	Molecular signature data base
mTOR	mechanistic target of rapamycin
MUFAs	monounsaturated fatty acids
MW	molecular weight
NaCl	sodium chloride
NADH	nicotinamide dinucleotide hydrogen
NADPH	nicotinamide dinucleotide phosphate hydrogen
NR	nuclear hormone receptor
NS	non-silencing

---

NSG	NOD scid gamma
NT	non-targeting
O <sub>2</sub>	oxygen
OAA	oxalacetate
OCR	oxygen consumption rate
OS	overall survival
OX	overexpression
OxPhos	oxidative phosphorylation
P	phosphate
PBS	phosphate buffered saline
Pca	prostate carcinoma
PCA	principal component analysis
PCG-1 $\alpha$	peroxisome proliferator-activated receptor gamma, coactivator 1 alpha
PCK2	phosphoenolpyruvate carboxykinase 2
pCR	pathological complete response
PCR	polymerase chain reaction
PDH	pyruvate dehydrogenase
PDX	patient derived xenograft
pH	potential of hydrogen
PIP3	Phosphatidylinositol-3,4,5-trisphosphat
PK	pyruvate kinase
pmol	picomol
PNT	pointed domain
PR	partial response
PSA	prostate specific antigen



---

PUFAs	polyunsaturated fatty acids
QNBC	quadruple negative breast cancer
Rev	reverse
RFP	red fluorescent protein
RNA	ribonucleic acid
RNP	ribonucleic protein
ROS	reactive oxygen species
rpm	rounds per minute
RQ	relative quantification
RT	room temperature
RT-qPCR	reverse transcriptase-quantitative polymerase chain reaction
SCD	stearoyl-CoA desaturase
SDHA	succinate dehydrogenase
s	second
SEM	standard error of the mean
SERD	selective estrogen receptor degrader
SERM	selective estrogen receptor modulator
shRNA	short hairpin RNA
siRNA	small interfering RNA
SLC27A3	solute carrier family 27 member 3
SPDEF	SAM pointed domain-containing ETS transcription factor
SPF	special pathogen free
SSO	sulfo-N-succinimidyl oleate
STS	staurosporine
SucCoA	succinyl-CoA

---

TAG	triacylglyceride
TBS	tris buffered saline
TBST	tris buffered saline tween
TCA	tricarboxylic acid cycle
TCGA	The Cancer Genome Atlas
TFF3	trefoil factor 3
TNBC	triple negative breast cancer
tracrRNA	tracer RNA
V	voltage
VarExp	variance expression
VDAC	voltage-dependent anion channel
WT	wild-type
x g	relative centrifugal force
XBP1	X-box binding protein 1

## 9 List of Figures

Figure 1: Breast cancer.....	1
Figure 2: Breast cancer subtypes and statistics..	4
Figure 3: Structure and domains of nuclear hormone receptors..	5
Figure 4: Activation and pharmacological inhibition of estrogen receptor in breast cancer..	7
Figure 5: Activation and pharmacological inhibition of androgen receptor.	11
Figure 6: SPDEF protein structure.	14
Figure 7: Glucose metabolism in cancer cells.....	17
Figure 8: Fatty acid synthesis and uptake.	20
Figure 9: <i>SPDEF</i> and <i>AR</i> mRNA expression in different breast cancer subtypes.....	22
Figure 10: <i>SPDEF</i> and <i>AR</i> are co-expressed in breast cancer patients.	23
Figure 11: High <i>AR</i> and <i>SPDEF</i> expression are associated with worse prognosis for ER <sup>-</sup> breast cancer patients.	25
Figure 12: <i>SPDEF</i> and <i>AR</i> expression in PDX cell models.....	27
Figure 13: Generation of <i>SPDEF</i> overexpression and knockdown cell models.	28
Figure 14: Generation and validation of <i>SPDEF</i> overexpression and knockdown cell models. .....	30
Figure 15: <i>SPDEF</i> downregulation reduces <i>in vivo</i> tumor-initiating capacity of AR <sup>+</sup> breast cancer cells.	32
Figure 16: <i>SPDEF</i> downregulation inhibits <i>in vivo</i> tumor growth in AR <sup>+</sup> breast cancer models. .....	33
Figure 17: <i>SPDEF</i> knock-out inhibits <i>in vivo</i> tumor growth in AR <sup>+</sup> breast cancer model.	35
Figure 18: <i>SPDEF</i> downregulation inhibits <i>in vivo</i> brain metastasis formation in AR <sup>+</sup> breast cancer model.....	36
Figure 19: <i>SPDEF</i> acts tumor-suppressive in AR <sup>-</sup> triple negative breast cancer BPE7 cells.	38
Figure 20: Gene expression-based stratification of BPE8 <i>SPDEF</i> cell lines..	40

---

Figure 21: Gene Set Enrichment Analysis of BPE8 SPDEF-overexpressing and shSPDEF cells compared to respective controls. ....	42
Figure 22: Gene expression-based stratification of CTC223 SPDEF cell lines.....	44
Figure 23: Gene Set Enrichment Analysis of CTC223 shSPDEF cells compared to pTRIPZ non-silencing control.....	45
Figure 24: Top variant gene stratification of pTRIPZ non-silencing and shSPDEF samples of CTC288, CTC223 and BPE8 cell lines.....	48
Figure 25: Differentially expressed genes between shSPDEF and control cells of BPE8, CTC223 and CTC288 models. ....	49
Figure 26: AR-associated curated gene sets (C2) are negatively enriched in shSPDEF cells of BPE8, CTC223 and CTC288 relative to controls. ....	49
Figure 27: Metabolic gene sets enriched in shSPDEF cells relative to control of BPE8, CTC223 and CTC288 cell models. ....	50
Figure 28: Gene expression-based stratification of BPE7 SPDEF cell lines. ....	52
Figure 29: AR-associated curated gene sets are negatively enriched in BPE7 shSPDEF cells relative to non-silencing control.....	53
Figure 30: Gene Set Enrichment Analysis of BPE7 shSPDEF cells relative to non-silencing control.....	54
Figure 31: Gene Set Enrichment Analysis of BPE8 shSPDEF tumors relative to controls.....	56
Figure 32: Metabolic gene sets enriched in BPE7 shSPDEF tumors relative to controls.....	57
Figure 33: AR target genes validation in BPE8, CTC223 and BPE7 SPDEF overexpression and knockdown cell models. ....	59
Figure 34: AR and associated target genes are upregulated upon SPDEF knock-out. ....	60
Figure 35: AR agonist activation regulates AR gene and targets expression in AR <sup>+</sup> breast cancer cells.....	61
Figure 36: CRIPSR/Cas9-mediated AR knock-out in AR <sup>+</sup> breast cancer cells. ....	62
Figure 37: AR knock-out does not impair <i>in vivo</i> tumor growth of BPE8 AR <sup>+</sup> cells.....	63
Figure 38: Glycolytic target genes validation in BPE8, CTC223 and BPE7 SPDEF overexpression and knockdown cell models. ....	65

---

Figure 39: Glycolysis/gluconeogenesis-associated genes are deregulated upon SPDEF knock-out.....	66
Figure 40: Glycolytic genes are upregulated in AR <sup>-</sup> BPE7 shSPDEF tumors relative to controls. ....	67
Figure 41: SPDEF and FBP1 protein are co-expressed in AR <sup>+</sup> breast cancer cell models.. ...	68
Figure 42: Glycolysis/gluconeogenesis-associated genes are downregulated in FBP1 knock-out cells.....	70
Figure 43: FBP1 knock-out does not impair <i>in vivo</i> tumor growth of BPE8 AR <sup>+</sup> cells. (A) ...	71
Figure 44: <i>SPDEF</i> and <i>FBP1</i> are co-expressed in human breast cancers and FBP1 expression predicts survival. ....	72
Figure 45: Fatty acid metabolism target genes validation in BPE8, CTC223 and BPE7 SPDEF overexpression and knockdown cell models. ....	74
Figure 46: Fatty acid metabolic genes are deregulated upon SPDEF knock-out. ....	75
Figure 47: Fatty acid synthesis genes are downregulated in AR <sup>+</sup> BPE8 shSPDEF tumors relative to the controls. ....	76
Figure 48: SPDEF regulates <i>ACLY</i> , <i>ACC</i> , <i>FASN</i> and <i>CD36</i> protein expression. ....	77
Figure 49: Isotope tracing experiment scheme.....	78
Figure 50: Isotopologues distribution in BPE8 shSPDEF and pTRIPZ NS control cells. ....	80
Figure 51: Evidence for decreased fatty acid synthesis in BPE8 shSPDEF cells compared to control.....	81
Figure 52: Fatty acid uptake is increased in BPE8 shSPDEF cells compared to control. ....	81
Figure 53: <i>CD36</i> expression confers growth advantage to SPDEF knockdown cells. ....	83
Figure 54: <i>CD36</i> <sup>+</sup> cells grow out faster in BPE8 shSPDEF cells. ....	84
Figure 55: Pharmacological <i>CD36</i> inhibition in shSPDEF cells significantly inhibits cell growth.....	85
Figure 56: shSPDEF cells exhibit a growth disadvantage when cultured in HPLM. ....	86
Figure 57: Fatty acid metabolism target genes are deregulated in BPE8 SPDEF overexpression and knockdown cells cultured in HPLM.....	87
Figure 58: Fatty acid synthase is enriched in AR <sup>+</sup> breast cancers.....	89

---

Figure 59: SPDEF controls mitochondrial respiration activity in AR <sup>+</sup> BPE8 cells. ....	91
Figure 60: SPDEF controls mitochondrial respiration activity in AR <sup>+</sup> CTC223 cells.....	92
Figure 61: Pharmacological activation of AR controls mitochondrial respiration activity in AR <sup>+</sup> MDA-MB-453 cells. ....	94
Figure 62: Pharmacological activation of AR increases mitochondrial respiration activity in AR <sup>+</sup> CTC223 cells but does not restore the decrease in mitochondrial respiration in shSPDEF cells.....	95
Figure 63: Mitochondrial marker expression in SPDEF KO cells. ....	97
Figure 64: LeGO iT2 plasmid map. ....	125
Figure 65: pTRIPZ plasmid map.....	127
Figure 66: Overview of Seahorse XF Mito Stress Assay.....	133

## 10 List of Tables

Table 1: Cancer stem cell breast cancer medium. ....	113
Table 2: Cancer stem cell mastermix. ....	114
Table 3: Cell culture conditions. Medium was purchased from Gibco, Life Technologies... ..	115
Table 4: Human plasma-like medium recipe. ....	116
Table 5: Primary antibodies used for western blot analysis. ....	119
Table 6: TaqMan gene expression assays used for RT-qPCR analysis. ....	121
Table 7: CRISPR-Cas9 guideRNAs used for knock-out experiments. ....	130
Table 8: Primer used for DNA amplification and sanger sequencing. ....	131

## 11 List of Supplement

Supplementary Figure 1: <i>SPDEF</i> and <i>ER</i> association in breast cancer patients. ....	138
Supplementary Figure 2: Heatmap of breast cancer patients for <i>ESR1</i> , <i>SPDEF</i> and <i>AR</i> gene expression. ....	139
Supplementary Figure 3: Characterization of PDX tumors and cell lines. ....	140
Supplementary Figure 4: Validation of <i>SPDEF</i> gene expression by RT-qPCR analysis. ....	141
Supplementary Figure 5: <i>SPDEF</i> overexpression reduces <i>in vivo</i> tumor growth of AR <sup>+</sup> ER <sup>+</sup> CTC223 cells. ....	142
Supplementary Figure 6: <i>SPDEF</i> up- and downregulation reduces <i>in vivo</i> tumor-initiating capacity in AR <sup>-</sup> ER <sup>+</sup> CTC288 cells. ....	142
Supplementary Figure 7: Gene expression-based stratification of BPE8 <i>SPDEF</i> -overexpressing and iT2 control samples. ....	143
Supplementary Figure 8: Gene expression-based stratification of CTC288 <i>SPDEF</i> cell lines. ....	144
Supplementary Figure 9: Top variant gene stratification in BPE7 sh <i>SPDEF</i> cells. ....	145
Supplementary Figure 10: Gene Enrichment Analysis of BPE8 sh <i>SPDEF</i> cells compared to respective control. ....	146
Supplementary Figure 11: Gene Set Enrichment Analysis of CTC223 <i>SPDEF</i> -overexpressing and sh <i>SPDEF</i> cells compared to respective controls. ....	147
Supplementary Figure 12: Gene Set Enrichment Analysis for Hallmark gene sets of CTC288 <i>SPDEF</i> -overexpressing and iT2 control cells. ....	148
Supplementary Figure 13: Gene Set Enrichment Analysis for C2 curated gene sets of CTC288 sh <i>SPDEF</i> and pTRIPZ non-silencing control cells. ....	148
Supplementary Figure 14: Gene Set Enrichment Analysis of CTC288 sh <i>SPDEF</i> and pTRIPZ non-silencing control cells. ....	149
Supplementary Figure 15: Gene Set Enrichment Analysis of sh <i>SPDEF</i> cells of BPE8, CTC223 and CTC288 lines relative to respective controls. ....	150



---

Supplementary Figure 16: Gene Set Enrichment Analysis of BPE7 SPDEF-overexpressing compared to iT2 control cells. ....	151
Supplementary Figure 17: Top variant gene stratification in AR <sup>+</sup> and AR <sup>-</sup> shSPDEF tumors relative to controls. ....	152
Supplementary Figure 18: Target genes validation in MDA-MB-453 shSPDEF cells. ....	153
Supplementary Figure 19: Target genes validation in BPE8 AR KO cells.....	154
Supplementary Figure 20: Target genes validation in CTC288 SPDEF-overexpressing and shSPDEF cells. ....	155
Supplementary Figure 21: Isotope tracing experiments.....	156
Supplementary Figure 22: CRIPSR/Cas9-mediated CD36 disruption in BPE8 shSPDEF and control cells. ....	157
Supplementary Figure 23: Glycolytic and AR-associated target genes are deregulated in BPE8 SPDEF overexpression and knockdown cells cultured in HPLM.....	158
Supplementary Figure 24: <i>CD36</i> expression is not associated with <i>SPDEF</i> expression in human breast cancers. ....	159
Supplementary Figure 25: SPDEF controls mitochondrial respiration activity in AR <sup>+</sup> MDA-MB-453 cells. ....	160
Supplementary Table 1: Correlation Scores in ER positive (ER <sup>+</sup> ) and negative (ER <sup>-</sup> ) breast cancer patients. ....	137
Supplementary Table 2: Hormone receptor status in PDX breast cancer patients.....	140

## 12 Contributions

The following people contributed to the work presented in this inaugural dissertation:

The presented PhD thesis was supervised by Prof. Dr. Andreas Trumpp and Dr. Martin R. Sprick. This project was partly funded by the Bosch Research Foundation from June 2017 to December 2021. The patient-derived xenograft cell lines and respective cancer stem cell breast cancer medium utilized within this thesis were established and optimized by Dr. Massimo Saini and Dr. Roberto Würth. Dr. Massimo Saini found SPDEF to be highly expressed in EpCAM<sup>high</sup>-expressing circulating tumor cells capable of initiating a tumor *in vivo*. Dr. Franziska M. Zickgraf investigated the role of SPDEF in high grade serous ovarian cancer and found that SPDEF acts pro-tumorigenic in this tumor entity. Based on these findings, I generated the hypothesis that SPDEF might be involved in the tumorigenic process in breast cancer.

Ornella Kossi, Corinna Klein and Vanessa Vogel provided essential technical and experimental support. In detail, Ornella Kossi conducted cDNA syntheses and subsequent RT-qPCR analyses illustrated in this study. Corinna Klein performed the injection of cancer cells into the mammary fat pad of NSG mice within the *in vivo* limiting dilution assay (Figure 15). Vanessa Vogel performed embedding of tumor tissue and immunohistochemistry staining. SPDEF-overexpressing plasmid was cloned by Dr. Franziska M. Zickgraf. Further, she tested shRNAs targeting SPDEF in ovarian cancer cell lines within the frame of her dissertation. Based on her findings, SPDEF-overexpression and shSPDEF vectors were used within this study. Virus production was performed in co-work with Dr. Franziska M. Zickgraf. Dr. Roberto Würth was greatly supportive in cell culture handling and advice on PDX cell lines. Cells were sorted at the Flow Cytometry Core Facility, DKFZ Heidelberg. Fluorescent activated cell sorting (FACS) was partially assisted by Tobias, Markus, Klaus and Flo. Tumor and xenograft images were acquired using the AxioScan slide scanner provided by the Light Microscopy Core Facility, DKFZ Heidelberg. Mammary fat pad surgeries were partially conducted in co-work with Vera Thiel. In addition, Vera Thiel and Jonas Schwickert were great help in monitoring *in vivo* tumor growth and harvesting tumors and organs when analyzing tumorigenesis of CRISPR-Cas9 KO cells. Thanks to Anja Rathgeb and her team of the Animal Facility, DKFZ Heidelberg for monitoring animal welfare and taking care of the animals. Dr. Felix Geist was a crucial support for the patient data analysis using R-Studio. Microarray analysis were performed at the Genomics and Proteomics Core Facility, DKFZ Heidelberg. Dr. Manuel Reitberger was very supportive in analyzing the microarray data and differential gene

expression analysis using R-Studio. Andreas Narr provided important initial support when performing the CRISPR-Cas9 mediated knock-out experiments. Further, he was a great help in designing and analyzing FACS experiments and data. Dr. Mattia Falcone initiated the start of performing Seahorse Mito Stress metabolic measurements. Subsequent experiments were performed in co-work with Dr. Andrea Geist. Thanks to Dr. Guoliang Cui for providing the Agilent Seahorse XFe 96 machine at DKFZ Heidelberg. Isotope tracing experiments were performed in collaboration with Dr. Marteinn T. Snaebjörnsson, Schulze Lab, DKFZ Heidelberg. *In vitro* tracing experiments were performed in parts by Ornella Kossi. After harvesting the samples, they were handed over to Dr. Marteinn T. Snaebjörnsson who conducted LC/MS measurements and data analysis. Thanks to Prof. Dr. Almut Schulze who provided initial input and feedback for performing the tracing experiments. Pharmacological inhibition experiments targeting CD36 were conducted and analyzed by Corinna Schumacher within her medical doctoral thesis supervised by me.

At the end, I would like to thank especially Dr. Kristin Decker, Vera Thiel, Michael Berlin and Dr. Martin R. Sprick for proofreading this doctoral thesis.

## 13 Acknowledgements

First and foremost, I would like to thank **Dr. Martin Sprick**. I am very grateful for your support and help throughout my doctoral studies. I really enjoyed our meetings, which usually ended in endless scientific discussions – now and then up to four hours. I enjoyed coming up with the wildest hypotheses and convincing you at the end how cool cellular metabolism is. In addition, your intellectual and technical expertise and experience helped me to develop as a scientist and raise my awareness of critical thinking. Thank you for trusting me to make my own project successful and giving me the freedom to develop this project independently. This has made me the scientist I am today, and I am proud to be able to write this dissertation on my own project. Thank you for the mentoring and the great time in the METICS group.

I would like to thank **Prof. Dr. Andreas Trumpp** for giving me the great opportunity to do a PhD in your lab. When I applied for the DKFZ PhD selection, I was determined to get a PhD position in your lab to work on breast cancer. During my PhD at HI-STEM, I had the unique opportunity to develop my project independently, which has shaped me professionally and personally. Thank you for your support throughout my doctoral studies and creating this great environment at HI-STEM. I am also grateful for having had the opportunity to present my work at international conferences, especially at the AACR 2022 in New Orleans, USA - the most beautiful end to my PhD I could have imagined.

I would also like to thank the **Bosch Research Foundation** for funding this project from June 2017 to December 2021. I am grateful for this opportunity to receive a fellowship from the Bosch Research Foundation - this was a special experience in this PhD program that I would not want to miss. Special thanks in this regard to **Dr. Jürgen Steigert** and **Dr. Klaus Dieterich**.

Thank you, **Prof. Dr. Holger Sültmann**, for being a member of my thesis advisory committee and your role as second examiner of my dissertation. I appreciate your support, input and contributions from the beginning of my PhD journey. Thank you, **Prof. Dr. Ingrid Lohmann** and **Dr. Karin Müller-Decker**, for being members of my defense committee. I appreciate your interest in my work and that you took the time to evaluate this study. Many thanks to my further TAC member **Dr. Martin Jechlinger**. I appreciate your support, input and feedback to this project.

I would like to thank **Prof. Dr. Almut Schulze** for her contribution and sharing her expertise on tumor metabolism with us. Many thanks to **Dr. Marteinn T. Snaebjörnsson**. I have enjoyed

working with you and greatly appreciate your contributions to this work. Thank you for making it possible to produce and analyze the latest results on short notice so that I could still include them in this PhD thesis.

A special thank you to all the current and former members of the **METICS** group. It was great to have each and every one of you in the group and it was a lot of fun working with you. Thank you for your help, crucial input, critical feedback and motivation: **Dr. Massimo Saini, Dr. Franziska Zickgraf, Dr. Felix Geist, Dr. Manuel Reitberger, Dr. Elisa Espinet, Ornella Kossi, Vera Thiel, Jonas Schwickert, Dr. Jennifer Wischhusen, Tim Vorberg and Corinna Schumacher**. Thanks to **Dr. Roberto Würth, Dr. Lisa Becker, Tasneem Cheytan and Paul Schwerd-Kleine** for the great team work in our CTC team. It was a pleasure to work with you guys. **Corinna Klein and Vanessa Vogel**, thank you for all your help with mouse work and immunohistochemistry. I am grateful for your help.

**Corinna S.**, thank you for joining my project. You did a great job during your time at HI-STEM and I really appreciate your contributions driving this project.

**Ornella**, I deeply thank you for your support and cooperation, especially in the last few months. You have encouraged me to keep going and helped me get through the most difficult times. I have no idea how we managed to do so many experiments in such a short time, all of which ended up with great results. You are an inspiring person and I am glad we got to know each other better and became friends.

**Roberto**, I would like to thank you for your continuous support during my time at HI-STEM. You are a great scientist from whom I learned a lot and I enjoyed working with you. Thank you for your advice, especially on cell culture. I am glad to have met you and hope to stay in touch.

**Felix**, you are the best colleague anyone could wish for. I could always rely on you and you taught me everything I know about bioinformatics analysis. Before, I could never have imagined that bioinformatic analyses with R could be so much fun. Thank you for your support to my project even after you stopped working in our lab. You are a great person and I am happy to call you a friend.

**Jonas**, thank you so much for your help in the lab, especially with the large mouse experiments. It was a lot of fun working with you. I am glad that you also discovered the interest in metabolism and will now take over the role of the metabolism expert in the METICS group. It has been a pleasure to get to know you and I am glad to have you as a friend.

**Vera**, thank you for all the fun moments we had together in and outside of the lab. Thank you for your scientific support, whether it was helping with mouse experiments or your feedback and input for my project. Thank you for the cell culture parties, the 90s dance sessions and well-deserved coffee breaks. I couldn't imagine my time as a PhD at HI-STEM without you. I am grateful to have found such a good friend in you.

Thanks to all the present and past members of the out lunch/coffee/milk club: **Dr. Manuel Reitberger, Dr. Pia Sommerkamp, Dr. Andrea Geist, Vera Thiel, Andreas Narr, Jonas Schwickert, Maija Leppä, Manuel Mastel, Tim Vorberg, Tasneem Cheytan, and many more...** Thanks for the fun conversations and non-scientific discussions. I have enjoyed having lunch with you guys every day promptly at 11:30.

**Andrea**, my Metabolism buddy, it was very nice to work with you and share the interest in metabolism with you. Thank you for numerous interesting scientific discussions and your support. It was great riding the seahorse with you. Thanks for the great moments we had together in and outside of the lab. After you left, there was a missing part in the lab. I found a true friend in you and I hope we never lose sight of each other.

**Pia and Petra**, it was a pleasure to share an office with you. Thanks **Petra**, for all the delicious chocolate and nice conversations we had. **Pia**, thank you for spending time together in the office and all the funny moments we had together. I couldn't have wished for anyone better next to me and with whom I enjoyed the Kinderschokolade-break. You are an exemplary scientist and I have never met such a well-organized person in my life. I could learn so much from you and have become much more organized. Thank you for the great moments and your friendship! I hope we never lose track of each other.

**Andi**, it was a pleasure to meet you at HI-STEM. Thank you for your scientific advice and support especially in FACS experiments. Thank you for all the scientific discussion, nice talks, coffee breaks and great moments we had in and outside the lab. You became a very good friend in a short period of time and I am very grateful for that. And of course, you are also among my metabolism buddies.

Special thanks to our '**Thanksgiving group**': **Lisa, Sam, Pia, Alex, Felix, Andrea, Kristin, Ronny, Vera and Michi**. I am very grateful that we met and found each other partly at HI-STEM. We are a great group and even though some of us might live a few kilometers away, I am sure we will at least keep our annual Thanksgiving meal as a tradition. I am thankful for each past meal and look forward too many more nice dinner parties. You have all become good

friends of mine and I have taken you to my heart. **Kristin**, thank you for proofreading my thesis also for your critical comments. I am very happy that we will work together soon again.

Liebe **Sabrina**, liebe **Julia**, danke, dass ich euch meine besten Freundinnen nennen kann. Ihr seid immer für mich da gewesen und habt mich unterstützt. **Sabrina**, du warst ein wesentlicher Teil meiner Promotionszeit und hast meist alles live über zahlreiche Sprachnachrichten miterlebt. Du kanntest sogar die Zeiten meiner wöchentlichen Meetings und warst gefühlt bei allem dabei. Ich weiß, dass ich mich immer auf dich verlassen kann und ich bin froh, dass du in meinem Leben bist. **Julia**, du bist eine großartige Freundin, und obwohl wir ein Stück voneinander entfernt wohnen, sind wir uns immer nah und werden uns nie aus den Augen verlieren. Ihr seid die besten Freundinnen, die man sich wünschen kann. Ich bin dankbar für all die Unterstützung während dieser doch sehr anstrengenden Zeit in meinem Leben.

**Thomas**, **Conny** und **Elly**, ihr seid meine zweite Familie und ich bin froh, euch in meinem Leben zu haben. Ihr seid immer für uns da und ich schätze eure Unterstützung und euer Verständnis sehr. Ich genieße jeden Besuch bei euch und jeder Spieleabend war eine kleine Auszeit in dieser manchmal stressigen Lebensphase. **Conny**, danke, dass du uns immer so verwöhnst, es fühlt sich jedes Mal wie ein kleiner Urlaub an.

Von ganzen Herzen möchte ich meiner Familie danken: meinen Eltern **Isolde** und **Rolf**, meinen Geschwistern **Sebastian** und **Nathalie**, meiner Schwägerin **Melanie**, meiner Nichte **Freya** und **Danylo**. Vielen Dank für die endlose Unterstützung, die ihr mir während meines Studiums und meiner Promotionszeit gegeben habt. Diese Doktorarbeit wäre ohne euch nicht möglich gewesen. Ihr hattet immer Vertrauen in mich, dass ich es schaffen würde, habt immer an mich geglaubt, und habt mich ermutigt, mein Bestes zu geben. Ich bin euch zutiefst dankbar für die Liebe und das Verständnis, das ihr mir entgegengebracht habt. Außerdem möchte ich meiner **Oma** danken, die nicht mehr bei uns sein kann. Sie war eine starke Frau und ich bin dankbar für ihre Unterstützung und Liebe.

**Michi**, du bist die Liebe meines Lebens und mein bester Freund #nieohnemeinTeam. Ich habe dich im Laborkittel kennengelernt und bin froh, dass du einen ähnlichen (verrückten) Weg eingeschlagen hast wie ich. Ich bin dankbar, dass wir diesen Weg gemeinsam gegangen sind. Danke für dein unendliches Verständnis, fürs Zuhören, dass du immer für mich da bist und deine unendliche Liebe. Ohne dich hätte ich das nie geschafft. Du hast immer an mich geglaubt und mich ermutigt weiterzumachen. Ich bin zutiefst dankbar, dich in meinem Leben zu haben und liebe dich von ganzem Herzen.

